

UNIVERSITÀ DEGLI STUDI DI MILANO  
PHD IN MOLECULAR AND CELLULAR BIOLOGY, XXXIII CYCLE  
DIPARTIMENTO DI BIOSCIENZE

DRUG-MEDIATED NFIX INHIBITION AS A NEW THERAPY FOR MUSCULAR DYSTROPHIES

BIO/17 - ISTOLOGIA

GIUSEPPE ANGELINI

PROF.SSA GRAZIELLA MESSINA

PROF. MARTIN KATER

A.A. 2019/2020

**UNIVERSITÀ DEGLI STUDI DI MILANO**

*PHD IN MOLECULAR AND CELLULAR BIOLOGY, XXXIII CYCLE*

DIPARTIMENTO DI BIOSCIENZE

**DRUG-MEDIATED NFκB INHIBITION AS A NEW  
THERAPY FOR MUSCULAR DYSTROPHIES**

BIO/17 - ISTOLOGIA

GIUSEPPE ANGELINI

PROF.SSA GRAZIELLA MESSINA

PROF. MARTIN KATER

A.A. 2019/2020

## ABSTRACT (ITALIAN)

Le distrofie muscolari (DM) sono un gruppo di miopatie monogeniche ancora incurabili, caratterizzate da una progressiva degenerazione del muscolo scheletrico, da complicazioni respiratorie e cardiache, e morte prematura. Le miofibre distrofiche sono molto fragili a causa di mutazioni nel Complesso Distrofina-Glicoproteina (DGC), che fornisce un supporto fisico alla contrazione muscolare. Per via di queste mutazioni, nei muscoli distrofici si verificano cicli continui di degenerazione/rigenerazione delle miofibre, i quali causano progressivamente un esaurimento delle cellule satelliti, le cellule staminali muscolari scheletriche, e la perdita del tessuto muscolare scheletrico.

I topi distrofici geneticamente privi del fattore di trascrizione Nfix, cruciale per il passaggio dalla miogenesi embrionale a quella fetale, presentano miglioramenti morfologici e funzionali della malattia. Ciò è dovuto al rallentamento della rigenerazione muscolare e ad un cambiamento fenotipico delle miofibre verso un metabolismo più ossidativo in assenza di Nfix.

Recentemente, nel nostro laboratorio abbiamo dimostrato che la via di segnalazione delle MAPK (MEK/ERK) modula positivamente i livelli di Nfix sia nei mioblasti fetali in vitro che nei feti in vivo, suggerendo una possibile via verso un'inibizione farmacologica indiretta di Nfix in un contesto distrofico.

In questo progetto di ricerca, abbiamo dimostrato che tale regolazione è conservata anche nei mioblasti postnatali. Infatti, il trattamento cronico di topi *Sgca* null adulti con due MEK-inibitori usati in clinica, Trametinib e Selumetinib, ogni giorno per 14 giorni tramite sonda gastrica orale, provoca una diminuzione dei livelli delle proteine pERK e Nfix nei muscoli scheletrici distrofici. L'espressione del gene *Nfix* nel muscolo trattato non cambia, indicando il coinvolgimento di meccanismi di regolazione post-traduzionali piuttosto che trascrizionali. Questa riduzione di Nfix non è ancora sufficiente tuttavia a garantire un miglioramento morfologico dei muscoli distrofici, i quali presentano miofibre più piccole, necrosi più alta e, inaspettatamente, delle calcificazioni in seguito a trattamento con alte dosi dei farmaci. Ciononostante, i muscoli trattati con Trametinib e Selumetinib presentano un numero più alto di miofibre con un metabolismo ossidativo, il quale protegge dai danni distrofici.

Il nostro studio dimostra che Nfix è modulato dal pathway di MEK/ERK nei muscoli distrofici postnatali in vivo, facendo luce sulla rete di regolazione alla base di questo fattore di trascrizione così importante nelle MD. Combinare la somministrazione dei MEK-inibitori con altri farmaci e/o un approccio di nutrigenomica da poco sviluppato nel nostro laboratorio, che agisce sulle calcificazioni, potrebbe portare a miglioramenti nel protocollo di trattamento, ponendo le basi ad un approccio combinato per affrontare tali malattie così eterogenee.

## ABSTRACT (ENGLISH)

Muscular Dystrophies (MDs) are still incurable monogenic myopathies characterized by progressive degeneration of skeletal muscle, respiratory and cardiac complications, and premature death. Dystrophic myofibers are highly fragile, due to mutations in the Dystrophin-Glycoprotein Complex (DGC), which provides a physical support to muscle contraction. In dystrophic muscles, chronic cycles of degeneration/regeneration of myofibers occur, progressively leading to an exhaustion of satellite cells, the skeletal muscle stem cells (MuSCs), and to the loss of skeletal muscle tissue.

Dystrophic mice lacking the transcription factor Nfix, crucial for the switch from embryonic to fetal myogenesis, display morphological and functional improvements of the disease, due to the slowing down of muscle regeneration and to a shift towards more oxidative myofibers.

Recently, we demonstrated that the MAPK (MEK/ERK) signaling pathway positively regulates the Nfix protein levels both in fetal myoblasts *in vitro* and in fetuses *in vivo*, bringing out the idea of an indirect pharmacological inhibition of Nfix in a dystrophic context.

In this research project, we demonstrate that this regulation is also conserved in postnatal myoblasts. Chronic treatment of adult *Sgca* null mice with two FDA-approved MEK-inhibitors, Trametinib and Selumetinib, every day for 14 days by oral gavage, causes a decrease of pERK and Nfix protein levels in dystrophic skeletal muscles. The *Nfix* gene expression in treated muscle does not change, indicating the involvement of post-translational rather than transcriptional mechanisms of regulation. This reduction of Nfix is nevertheless not sufficient to improve the histology of dystrophic muscles, which display smaller myofibers, higher necrosis, and, unexpectedly, calcification at high drugs dosages. However, Trametinib- and Selumetinib-treated muscles exhibit more myofibers with an oxidative metabolism, which is known to protect from dystrophic damage.

Our study provides a proof-of-concept that Nfix is modulated by the MEK/ERK pathway in postnatal dystrophic muscles *in vivo*, unraveling the regulatory network behind this crucial transcription factor in MDs. Combining the MEK-inhibitor administration with other drugs and/or a type of diet acting on calcifications might improve the treatment, setting the stage for a combined approach to face such heterogeneous diseases.

# TABLE OF CONTENTS

<b>1. AIM OF THE THESIS</b> .....	<b>1</b>
<b>2. INTRODUCTION</b> .....	<b>3</b>
2.1. MYOGENESIS .....	3
2.1.1. SATELLITE CELLS AND ADULT MYOGENESIS.....	3
2.1.2. MUSCLE REGENERATION.....	4
2.2. MUSCULAR DYSTROPHIES .....	8
2.2.1. MOLECULAR PATHOGENESIS OF MDs .....	8
2.2.2. CHRONIC CYCLES OF MUSCLE DEGENERATION/REGENERATION .....	10
2.2.3. THERAPEUTIC STRATEGIES FOR MDs .....	11
2.3. NUCLEAR FACTOR-1X (NFIX).....	16
2.3.1. NFIX IN MUSCLE DEVELOPMENT.....	18
2.3.2. NFIX IN MUSCLE REGENERATION.....	19
2.3.3. NFIX IN MUSCULAR DYSTROPHIES .....	20
2.3.4. REGULATION OF NFIX EXPRESSION.....	21
<b>3. RESULTS AND DISCUSSION</b> .....	<b>23</b>
3.1. MEK/ERK SIGNALING MODULATES NFIX POSTNATALLY .....	23
3.2. EVALUATION OF TRAMETINIB EFFICACY IN DECREASING NFIX LEVELS IN MUSCULAR DYSTROPHY.....	26
3.2.1. TRAMETINIB DECREASES THE NFIX PROTEIN IN POSTNATAL MYOBLASTS IN VITRO..	26
3.2.2. CHRONIC TREATMENT WITH TRAMETINIB CAUSES A REDUCTION OF pERK AND NFIX IN DYSTROPHIC MUSCLE.....	30
3.2.3. TRAMETINIB-TREATED MUSCLES DISPLAY CALCIFICATIONS AND MORE OXIDATIVE MYOFIBERS.....	35
3.3. EFFICACY OF SELUMETINIB, A MEK-INHIBITOR ALREADY USED FOR MUSCULAR DYSTROPHY, IN DECREASING NFIX LEVELS .....	40
3.3.1. SELUMETINIB DECREASES pERK AND NFIX IN DYSTROPHIC MUSCLES.....	40
3.3.2. CHRONIC TREATMENT WITH SELUMETINIB HAS DIFFERENT EFFECTS ON THE HISTOLOGY OF DYSTROPHIC MUSCLES THAN TRAMETINIB .....	42
<b>4. CONCLUSIONS AND FUTURE PERSPECTIVES</b> .....	<b>47</b>
<b>5. MATERIALS AND METHODS</b> .....	<b>51</b>
5.1. CELL ISOLATION AND CULTURES .....	51
5.1.1. IN VITRO TREATMENT.....	52

5.2. ANIMAL MODELS.....	52
5.2.1. <i>IN VIVO TREATMENT</i> .....	52
5.3. PROTEIN EXTRACTION.....	53
5.3.1. <i>SDS-PAGE AND WESTERN BLOT</i> .....	53
5.4. RNA EXTRACTION.....	54
5.4.1. <i>RETROTRANSCRIPTION</i> .....	54
5.4.2. <i>QUANTITATIVE REAL-TIME PCR (qRT-PCR)</i> .....	54
5.5. ISOLATION, INCLUSION AND CRYO-SECTIONING OF MUSCLES.....	55
5.5.1. <i>IMMUNOFLUORESCENCE</i> .....	55
5.5.2. <i>HEMATOXYLIN &amp; EOSIN</i> .....	55
5.5.3. <i>MILLIGAN'S TRICHROME STAINING</i> .....	56
5.5.4. <i>SUCCINATE DEHYDROGENASE (SDH) ASSAY</i> .....	56
5.5.5. <i>IMAGE ACQUISITION AND CROSS-SECTIONAL AREA (CSA) ANALYSIS</i> .....	57
5.6. STATISTICAL ANALYSIS AND GRAPHS.....	57
<b>BIBLIOGRAPHY.....</b>	<b>58</b>

## 1. AIM OF THE THESIS

Few years ago, our lab demonstrated that the transcription factor Nfix has a negative role in the progression of Muscular Dystrophy (Rossi et al. 2017). After this study, we focused our research on developing different biological tools to target Nfix in adult dystrophic muscle. Indeed, decreasing the expression of Nfix might represent an innovative method to improve the quality of dystrophic muscle tissue for further therapeutic interventions. To this aim, we are following different approaches.

Firstly, a genetic approach. Indeed, we demonstrated that silencing *Nfix* through the RNA interference *in vivo* leads to evident morphological ameliorations of muscular dystrophy (Rossi et al. 2017). Hence, we are developing a non-viral system to specifically carry a short hairpin RNA against Nfix (shNfix) towards myoblasts and myofibers *in vivo*.

Secondly, a nutrigenomic approach. Last year, I contributed to provide experimental evidence about the beneficial effects of a cyanidin-rich diet on the morphology and functionality of dystrophic muscles (M. Saclier et al. 2020). The molecular mechanisms behind these cyanidin-mediated improvements are not completely known, however we have some cues that cyanidin intake causes a decrease in the Nfix levels in dystrophic muscles.

Thirdly, a pharmacological approach. This might be reached by performing a drug design approach based on the structure of the Nfix protein. Within this aim, we started a collaboration with a group of structural biochemists to define the structure of Nfix, which is still unknown. Although this approach would be preferable and the most specific, it will take time as the structure of the protein is not known yet. Therefore, a parallel approach consists in understanding how this transcription factor is transcriptionally and post-transcriptionally regulated to interfere with its expression and/or its activity on target genes. Therefore, we are analyzing the regulatory network underlying the expression and the protein stability of Nfix in both prenatal and postnatal myoblasts. Recently, I contributed to demonstrate that the MAPK (MEK/ERK) pathway positively regulate Nfix in fetal myoblasts. Particularly, the inhibition of this signaling cascade through a specific MEK-inhibitor causes a decrease in Nfix protein levels delaying the differentiation of myogenic cells (Taglietti et al. 2018). From these data, we thought about a pharmacological way to indirectly target Nfix in dystrophic muscles *in vivo*. To this aim, we selected two different MEK-inhibitors, Trametinib (GSK) and Selumetinib (Merck), which are already used in clinic as anti-cancer drugs. Moreover, Selumetinib was tested in a murine model of Emery-Dreifuss Muscular Dystrophy (EDMD) with promising results.

The main aim of this PhD thesis is to verify whether the inhibition of the MEK/ERK pathway by Trametinib or Selumetinib can decrease the expression of Nfix also in postnatal myoblasts *in vitro*

and in dystrophic muscle *in vivo*, as observed in fetal myogenic cells, leading to histological improvements of the disease. The results obtained from this proof-of-principle study will be extremely important for a future pharmacological repurposing of these drugs for the treatment of muscular dystrophy.

## 2. INTRODUCTION

### 2.1. MYOGENESIS

Myogenesis is the biological process that generates differentiated muscular tissue from undifferentiated cells. There are two types of myogenesis: prenatal and postnatal myogenesis (Bentzinger et al. 2012).

Prenatal myogenesis is a continuous process which occurs during the development and is divided into embryonic and fetal myogenesis. Embryonic/fetal progenitors proliferate, migrate, and differentiate to build the muscular tissue *de novo*, following a specific, temporally-defined pattern of extracellular signals and intracellular transcription factors (Asfour, Allouh, and Said 2018).

Postnatal myogenesis takes place in a full-developed muscle upon both homeostatic turnover and damage, with the aim to regenerate the muscular tissue and restore its functions. Like in muscular development, adult muscle progenitors proliferate and differentiate into newly formed myofibers recapitulating many molecular mechanisms of prenatal myogenesis (Yin, Price, and Rudnicki 2013). In both cases, myogenic progenitors (cells with a being acquired fate) derive from a specific stem cells population (not acquired fate). Embryonic/fetal myogenic progenitors originate from the ventral part of somites (called dermomyotome), which are temporary metameric structures of paraxial mesoderm; a subpopulation of these cells in the central part of dermomyotome persist in undifferentiated state after birth, giving rise to postnatal satellite cells (Tajbakhsh 2009).

#### 2.1.1. SATELLITE CELLS AND ADULT MYOGENESIS

Satellite cells are the *bona fide* skeletal muscle stem cells (MuSCs), namely the postnatal undifferentiated cells responsible for physiological turnover and regeneration after damages of the adult muscular tissues. MuSCs are adult, self-renewing cells that potentially generate different mesodermal lineages, like muscle, bone, and brown fat (Asakura, Komaki, and Rudnicki 2001; Shefer, Wleklinski-Lee, and Yablonka-Reuveni 2004; Seale et al. 2008). However, under physiological conditions MuSCs give rise to a muscular lineage, in which cells are organized in a heterogeneous hierarchy with several grades of myogenic differentiation (Collins et al. 2005; Sambasivan et al. 2011; Lepper, Partridge, and Fan 2011).

During normal skeletal muscle homeostasis, satellite cells are located at the periphery of myofibers, between the sarcolemma and the basal lamina, close to capillaries, in an undifferentiated and quiescent state (Mauro 1961; Schultz, Gibson, and Champion 1978; Christov et al. 2007; Bentzinger et al. 2012). In this context, they express the unique marker Pax7 (paired box protein 7), which

exclusively identifies this type of cells (Seale et al. 2000, 2004). Enwrapped by the basal lamina, Pax7<sup>+</sup> cells are extremely controlled by intrinsic and extrinsic signals. Indeed, extracellular molecules and MuSC-surrounding cells constitute the so called “stem cell niche”, a molecular and cellular environment which transcriptionally and metabolically control the satellite cell behavior (Cheung and Rando 2013).

Several extracellular ligands (like laminin, Collagen VI, collagen V etc) and cell-cell interactions in the niche regulate important intracellular molecular pathways (Notch, Wnt, Yap signaling), maintaining satellite cells in quiescence (QSCs) (Mourikis et al. 2012; Rozo, Li, and Fan 2016; Mohassel, Reghan Foley, and Bönnemann 2018; Goel et al. 2017; Zhang et al. 2016). Interestingly, QSCs are not just passive hosts of the niche, but they actively secrete some of the quiescence-associated ligands that act in autocrine signaling, like collagen V (Baghdadi, Castel, et al. 2018).

Satellite cells can integrate all these external signals together with their own genetic and epigenetic background, assuming two different quiescence states: “dormant” QSCs are in a deeper quiescence, with very low proliferation rate and high expression of Pax7 (Pax7<sup>Hi</sup> cells); “poised” QSCs are still quiescent but more primed for myogenic commitment, with a low expression of Pax7 (Pax7<sup>Low</sup> cells) and a higher proliferation rate than the dormant ones (Rocheteau et al. 2012; Pala et al. 2018).

Serial transplantations and lineage-tracing experiments in rodents demonstrate that MuSCs give rise to both differentiated myofibers and undifferentiated stem compartments (Rocheteau et al. 2012; Keefe et al. 2015). Moreover, specific deletion of this stem cell population cause the inability of muscular tissue to regenerate upon injury (Relaix and Zammit 2012). Therefore, MuSCs display all the features and the functionality attributed to adult stem cells, allowing the homeostatic turnover and injury-induced regeneration of postnatal muscular tissue.

The efficiency and proper timing of the regeneration process are determined by both intrinsic features of myogenic cells and extrinsic support from non-myogenic cells (macrophages, FAPs, endothelial cells, etc.) (Wosczyzna and Rando 2018).

### **2.1.2. MUSCLE REGENERATION**

Despite common assumptions, the muscular tissue is constantly renewed even without any damages or exercise: in resting state, MuSCs supply myonuclei for 20-50% of hindlimb and diaphragm myofibers, respectively (Pawlikowski et al. 2015). However, MuSCs express their fully regenerative potential in response to muscle damages.

Upon injury or exercise, damaged myofibers release defined pro-inflammatory and intracellular molecules in the interstitial space. These damaged myofiber-derived factors (DMDFs) or damage-associated molecular patterns (DAMPs) stimulate both muscular and non-muscular cells to activate

an acute inflammatory response, which is the starting point of a temporally coordinated regeneration process. It represents a “sterile inflammation” due to the absence of exogen pathogens (Rodgers et al. 2017; Tsuchiya et al. 2020).

DMDFs attract circulating immune cells (like neutrophils, monocytes/macrophages, T lymphocytes) inside the degenerative milieu. The infiltrating cells start to remove cellular debris, and secrete pro-inflammatory cytokines that stimulate muscle regeneration (Wosczyzna and Rando 2018; Helmbacher and Stricker 2020). Macrophages play a key role in this context, assuming two different phenotypes. The M1 macrophages are present in the early phase of muscle damage, acting as cellular scavengers by phagocytosis and producing pro-inflammatory cytokines that trigger acute inflammation and MuSC activation. Once degeneration has been contained, M1 macrophages switch to M2 anti-inflammatory phenotype, supporting the resolution of inflammation, wound healing, and myoblasts differentiation into newly formed myofibers (Chazaud et al. 2009; Brigitte et al. 2010; Arnold et al. 2007). Such phenotypical switch from M1 to M2 macrophages is induced by phagocytosis and ensures the proper timing of regeneration. Preventing macrophages infiltration or phenotypical switch impairs the regeneration of injured muscles (Perdiguero et al. 2011; Marielle Saclier et al. 2013; Johann et al. 2007; Lemke 2019).

Stimulated by acute inflammation and disruption of basal lamina following muscle injury, QSCs (Pax7<sup>Low</sup> cells, mainly) change their metabolic and transcriptional status into activated satellite cells (ASCs). MuSCs detect the damages inside the tissue, migrate towards the site of injury, exit from quiescence, proliferate in myoblasts and differentiate in myocytes (Baghdadi, Firmino, et al. 2018). The activation of MuSCs is mediated by the expression of a specific family of transcription factors, called myogenic-regulatory factors (MRFs): Myf5, MyoD, myogenin (MyoG), MRF4 (Myf6). Each of these basic helix-loop-helix factors can individually induce myogenic commitment when transfected into non-myogenic cells (like fibroblasts), and their temporally orchestrated expression is at the basis of muscle regeneration (Braun et al. 1989; Edmondson and Olson 1989; Beauchamp et al. 2000; Bentzinger et al. 2012).

MyoD and Myf5 are the first MRFs to be expressed in activated satellite cells. MyoD is a determinant factor for the myogenic commitment and its genetic absence strongly impairs myoblasts differentiation; instead, *Myf5*<sup>-/-</sup> myoblasts display delayed proliferation and are more prone to differentiate. However, *MyoD*- or *Myf5*-deficient mice exhibit mild defects in muscle regeneration and satellite cells activity, indicating that these MRFs share compensatory but non overlapping functions (Yablonka-Reuveni et al. 1999; Cornelison et al. 2000; Ustanina et al. 2007; Yamamoto et al. 2018).

Most of the activated satellite cells express both *Myf5* and *MyoD*, while *Pax7*<sup>+</sup>/*Myf5*<sup>-</sup>/*MyoD*<sup>+</sup> myoblasts are less present (Zammit et al. 2002). The balance between *Pax7*, *Myf5* and *MyoD* is crucial for the satellite cell-fate decision. Thanks to *Myf5* and *Pax7*, activated satellite cells generate undifferentiated transient-amplifying cells that proliferate and sustain regeneration; if *MyoD* expression predominates, MuSC-derived myoblasts downregulate *Pax7* and start to express *MyoG* and *MRF4*, exiting from cell cycle and acquiring a complete commitment into terminal differentiated myocytes (Rudnicki et al. 2008; Almada and Wagers 2016; H. Olguin and Olwin 2012).

Importantly, a group of transient-amplifying cells can downregulate *MyoD* expression and return to quiescence, restoring the QSCs compartment for subsequent rounds of regeneration (self-renewal). *Myf5* expression represents an imprint of previous activations in self-renewing MuSCs. *Pax7*<sup>+</sup>/*Myf5*<sup>+</sup> satellite cells are more prone to differentiate than the *Pax7*<sup>+</sup>/*Myf5*<sup>-</sup> counterpart (~10% of the total QSCs pool), which instead exhibits a more robust self-renewal ability (Kuang et al. 2007).

Moreover, the MuSC compartment is preserved by the asymmetric division of satellite cells. Asymmetric division leads a stem cell to divide into two daughter cells with different cell fates: a stem cell and a committed cell. Beside the proliferative symmetric division, both *Pax7*<sup>+</sup>/*Myf5*<sup>-</sup> and *Pax7*<sup>Hi</sup> satellite cells more frequently undergo asymmetric division in apical-basal orientation: the daughter stem cell is close to basal lamina, while the daughter committed cell is in contact with the myofiber plasmalemma.

In addition, MuSCs can asymmetrically segregate the DNA between daughter cells. Daughter stem cell maintains the same DNA template strands, while daughter committed cell inherits the newly synthesized DNA strands (Rocheteau et al. 2012). All these cellular and molecular mechanisms allow the MuSC preservation and self-renewal throughout life, fulfilling myoblasts demand after each cycle of regeneration.

Differentiating myoblasts progressively accumulate *MyoD*, which creates a protein complex in the nucleus, binding to transcriptional coactivators, inhibitors, and epigenetic modifiers. The *MyoD* complex induces the expression of *MyoG* and *MRF4*, the early-differentiation MRFs.

*MyoG* plays a crucial role in this phase, inhibiting *Pax7* transcription and inducing the expression of late-differentiation genes, like the *Myocyte Enhancer Factor-2* family (*MEF2s*) (H. C. Olguin et al. 2007; Gillespie et al. 2009; Taylor and Hughes 2017). *MyoD* and *MyoG* heterodimerize with different myogenic regulators, like E-proteins and *MEF2s*, broadening the plethora of target genes involved in this process. Such feed-forward mechanism drives myoblasts towards the irreversible differentiation into myocytes, which ultimately fuse with each other (hyperplasia) or with pre-existing myofibers (hypertrophy), repairing the muscular damage.

There are an early and a late fusion of myocyte. The early fusion is a myocyte-myocyte fusion, guided by  $\beta 1$ -integrin and forming an immature myotubes. The late fusion drives myocytes towards fusing into immature myotubes, whose caliber gradually increase with maturation into myofibers. This latter phase is regulated by Filamin C and NFATc/IL-4 signaling (Schwander et al. 2003; Dalkilic et al. 2006; Horsley et al. 2003).

Myofibers are elongated cellular syncytia, whose myonuclei are negative for MRFs and express muscular differentiation markers, like Myosin Light Chain (MyLC), different isoforms of Myosin Heavy Chain (MyHC), muscle creatine kinase (MCK) etc. (Berkes and Tapscott 2005; Meadows et al. 2008). Regenerating immature myofibers have a small caliber, are centrally nucleated and express developmental MyHC (dMyHC), which is rapidly substituted by adult isoforms following maturation and fiber type specification (D'Albis et al. 1988; Schiaffino et al. 2015).

Nascent myofibers also produce myostatin (Mstn), a secreted protein belonging to the TGF- $\beta$  family. Myostatin is a paracrine molecule that highly inhibits muscle growth, blocking the protein synthesis of myofibers, hampering proliferation and differentiation of myoblasts, and preventing MuSC activation and self-renewal. Genetic knock-out mutations in the *Mstn* gene leads to an evident muscular phenotype with high hyperplasia and hypertrophy of skeletal muscles (Kostyunina, Ivanova, and Smirnova 2018).

Extension and stiffness of the connective tissue strongly impact on MuSC differentiation and myofiber maturation (Grounds 2008). Therefore, muscle resident non-myogenic cells have a crucial role in supporting regeneration. Fibro-adipogenic progenitors (FAPs) are involved in the extracellular matrix (ECM) remodeling. During early regeneration phases, FAPs highly proliferate following MuSC activation, but their number is controlled by M1-secreted TNF- $\alpha$ , which induces apoptosis in FAPs. During late regeneration phases, M2-secreted TGF- $\beta$  stimulates FAPs to differentiate and to produce collagen and other ECM components, which act as a temporary scaffold for the myofiber formation. Moreover, FAPs secrete IL-6 and IGF-1, that stimulate myoblasts to differentiate and sustain the myogenic progression (Joe et al. 2010; Lemos et al. 2015; M. T. Webster et al. 2016).

The regeneration process is usually completed in about 1-month post-injury, when muscle has completely restored its functionality. However, the timing of regeneration strongly depends on type and degree of injury. The more serious and wider injured area is, the more unbalanced towards fibrosis (fibrotic scarring) regeneration occurs. In such multistep and time-defined biological process, each phase is finely tuned to have a proportional regeneration according to the degeneration entity. Defects in one of the involved cells or genes could lead to unbalanced and chronic histological impairments (Mann et al. 2011).

## **2.2. MUSCULAR DYSTROPHIES**

Muscular Dystrophies (MDs) are a highly heterogeneous group of inherited diseases affecting skeletal muscles. Although classified as neuromuscular disorders (like Multiple Sclerosis or Amyotrophic Lateral Sclerosis), they are monogenic myopathies with no effects on motor neurons: the primary biological defects in MDs are related to muscular tissue.

All different types of MDs are characterized by one main clinical feature: a progressive and increasing weakness in the voluntary muscular contraction. Dystrophic patients experience gradual difficulties in using arms and legs, impaired mobility until the wheel-chair dependency, respiratory complications, cardiac involvement, and premature death.

The incapacity to generate sufficient muscular force is due to high fragility of dystrophic myofibers, which undergoes a relentless degeneration and necrosis upon muscular contraction, followed by an impaired regeneration process. This results in an extensive wasting of skeletal muscle tissue, which is replaced by fibrotic and fatty tissue without contractile capacity (fibrosis).

These histological and clinical traits are common in all types of MDs. However, the degree of severity, the age of onset, the distribution of affected skeletal muscles, and the involvement of other organs (central nervous system, cardiac tissue, etc.) extremely differ between MDs, influencing prognosis and lifespan of patients (Emery 2002).

### **2.2.1. MOLECULAR PATHOGENESIS OF MDs**

Modern genetic tools have allowed the identification of mutated genes in dystrophies: there are more than 40 genes involved, each of which have several types of mutations and modes of inheritance (Benarroch et al. 2019).

Despite such further heterogeneous aspect in MDs group, the identification of dystrophic genes has provided a more logic classification of the different clinical manifestations that are commonly associated to the disease. Therefore, MDs are now classified according to the sub-cellular localization and function of the causative mutated proteins (Mercuri, Bönnemann, and Muntoni 2019).

Mutated proteins in dystrophies are subdivided in four main classes:

- Cellular matrix and extracellular proteins = like Laminin-2, Collagen VI,  $\alpha$ -dystroglicans, etc.
- Sarcolemmal and sarcomeric proteins = e.g. dystrophin, sarcoglycans, titin, etc.
- Nuclear proteins = Lamin A and Emerin
- Enzymes = catalyzing post-translational modifications of the above-mentioned proteins.

The most common types of MDs are caused by mutations in genes belonging to the first and the second group (Mah et al. 2015). These proteins physically interact with each other in a protein complex that is crucial for muscular contraction: the dystrophin-glycoprotein complex (DGC).

DGC is located at the sarcolemma of muscular fibers and acts as a bridge between the inner sarcomeric cytoskeleton (actin and myosin) and the outer basal lamina that envelops each myofiber. The role of this molecular scaffold consists in the transmission of the produced lateral force to ECM, and in the equal allocation of the contractile tension to the other myofibers. Thus, DGC provide a physical support to muscle contraction, preventing the sarcolemma and the whole muscular tissue from contraction-associated injuries (Petrof et al. 1993). The DGC proteins are sequentially bound together, thereby structural mutations or post-translational defects in one of them result in impairment or even disruption of the entire complex (Peter, Marshall, and Crosbie 2008).

Dystrophin is the key component of DGC. The *Dystrophin* gene is located on chromosome X and is the longest gene in the mammalian genome. Its 427-kDa protein interacts with both sarcomeric filaments at N-terminus and the sarcolemmal protein  $\beta$ -dystroglycan at C-terminus.  $\beta$ -dystroglycan is in turn associated with the extracellular protein  $\alpha$ -dystroglycan, which binds laminin-2 of the extracellular matrix. The actin-dystrophin-dystroglycans-laminin interaction is the main backbone of DGC, which mechanically supports muscular contraction (Ervasti and Campbell 1993; Muntoni, Torelli, and Ferlini 2003).

Duchenne Muscular Dystrophy (DMD) is the most frequent neuromuscular disease in male children, and it is caused by mutations in the *dystrophin* gene leading to non-functional or completely absent protein. Interestingly, mutation in the *dystrophin* gene generating a semi-functional protein are causative for the milder and less frequent Becker Muscular Dystrophy (BMD) (Crisafulli et al. 2020).

Sarcoglycans are a group of four transmembrane glycoproteins ( $\alpha$ -,  $\beta$ -,  $\gamma$ -,  $\delta$ -sarcoglycan) that are combined in a tetrameric complex in muscle. The sarcoglycan isoforms can selectively bind dystroglycans and dystrophin, supporting the mechanical role of the other DGC components.

As a matter of fact, mutations in the sarcoglycan isoforms cause sarcoglycanopathies, a subgroup of Limb Girdle Muscular Dystrophies (LGMD). Defects in one of sarcoglycans severely affect the entire sarcoglycan complex and, in some cases, also the DGC abundance on sarcolemma (F. Duclos et al. 1998; Fanin and Angelini 1999; Durbeej and Campbell 2002; Sandonà and Betto 2009) (with the exception of  $\gamma$ -sarcoglycan, whose genetic absence does not influence the amount of dystrophin (Bönnemann et al. 2002; Higuchi et al. 1998)).

Besides its mechanical and physical function, DGC also plays an important role in the modulation of intracellular signaling pathways. Several data demonstrate that mutations in this complex cause impairments in molecular signaling underlying proliferation, differentiation, oxidative metabolism,

and apoptosis of muscle cells (Bhatnagar and Kumar 2010; Shin et al. 2013). Most of the DGC proteins have extracellular ligand-binding domains and intracellular docking motifs for kinases/phosphatases involved in essential physiological processes (Yoshida et al. 1998; James et al. 2000).

Some of the altered intracellular signaling pathways in dystrophy are secondary responses to the DGC mechanical defects. Indeed, the loss of the sarcolemma integrity in dystrophic myofibers leads to a great increase in  $\text{Ca}^{2+}$  influx, activating calcium-related proteins, like calmodulin and calcineurin, that affect mitochondria activity and cause myofibers apoptosis (Culligan and Ohlendieck 2002; Goll et al. 2003; Chakkalakal et al. 2004; Rahimov and Kunkel 2013).

However, some signaling pathways are activated in dystrophic muscles without any signs of mechanical stress (Hack et al. 1999; Goldberg et al. 1998) or before the onset of myofiber necrosis. For example, the NF- $\kappa$ B activity (the master regulator of inflammation) is increased in several types of MDs and precedes muscular degeneration (Kumar and Boriek 2003; S. Messina et al. 2006).

Likely, mechanical stress and altered signaling pathways mutually occur and synergistically lead to the degeneration of dystrophic myofibers. The expression and the physiological role of the mutated DGC protein in other non-skeletal muscle tissues strongly influence the clinical manifestations of the different MDs (Rando 2001).

Understanding the proper biochemical and gene regulatory network inside the dystrophic muscular cells is crucial for finding new molecular targets and developing novel therapeutic approaches to slow down the disease progression (Rahimov and Kunkel 2013).

### **2.2.2. CHRONIC CYCLES OF MUSCLE DEGENERATION/REGENERATION**

Unlike what happens in the injured muscle, where all the involved myofibers are synchronously first damaged and then healed or newly formed, in the dystrophic muscle degenerating and regenerating areas coexist. The typical histology of MD-affected muscle display clusters of regenerating myofibers (small caliber and centrally nucleated) close to both hypertrophic myofibers and degenerating zones. The latter consist in necrotic myofibers, infiltrating cells, fat depositions, and fibrosis, indicating chronic inflammation and impaired regeneration (Mercuri, Bönnemann, and Muntoni 2019).

This asynchronous degeneration/regeneration dynamic in dystrophic myofibers might be related to the non-sequential motor unit recruitment during muscle contraction, the different susceptibility to necrosis of fast than slow myofibers (C. Webster et al. 1988; Ljubcic et al. 2011), and intrinsic defects in the regenerative potential of dystrophic MuSCs.

Indeed, MuSCs lacking dystrophin display impaired proliferating capacity and reduction in asymmetric division. The DGC acts as a scaffold for post-translational modifications and the

cytoplasmatic retention of proteins involved in the asymmetric division. Therefore, despite the general number of MuSCs is higher in dystrophic muscle than wild-type one, the asymmetric-dividing MuSCs are less present in a dystrophic context (Dumont et al. 2015; N. C. Chang et al. 2018). Moreover, dystrophic MuSC-derived myoblasts present shorter telomeres and are more prone to differentiate than wild-type myoblasts (Sacco et al. 2010).

All the newly-formed myofibers share the same mutation of dystrophic MuSCs and in turn exhibit structural fragility. Hence, the persistence of a degenerative milieu in dystrophic muscle continuously stimulates infiltrating leukocytes to produce pro-inflammatory cytokines, which exacerbate the regeneration defect. While the acute inflammation is necessary for the regeneration process, the chronic inflammation in dystrophy cause imbalances between all the cellular players involved in regenerating/degenerating muscles (Lagrotta-Candido et al. 2002).

For example, the phenotypical switch from M1 to M2 macrophages is temporally impaired in MDs. In dystrophic muscle, macrophages assume a hybrid phenotype that produces both pro-inflammatory and anti-inflammatory cytokines at the same time (Villalta et al. 2009). The constant presence of these different cues results in altered MuSC activation and differentiation without an appropriate self-renewal. Progressively, these vicious degeneration/regeneration cycles lead to an exhaustion of the satellite cells compartment and a complete loss of the muscle regenerative capacity (Madarò et al. 2019; Forcina, Cosentino, and Musarò 2020).

In this context of chronic inflammation, high levels of TGF- $\beta$  stimulate FAPs to proliferate and prematurely differentiate into fibro-adipocytes. Differentiated FAPs produce the ECM components (like collagen I), contributing to the pathological fibrosis and fat deposition (Lemos et al. 2015; Perandini et al. 2018; Wosczyzna and Rando 2018). Fibrotic and adipose tissues replace degenerated myofibers but are completely unfunctional, reducing the muscle contractile capacity and the area of available tissue for cell or gene therapy.

### **2.2.3. THERAPEUTIC STRATEGIES FOR MDs**

Muscular Dystrophies are still incurable diseases and the approved therapies mostly slow down the disease progression. As mentioned above, MDs are heterogenous pathologies characterized by genetic mutations, muscle degeneration/regeneration, and inflammation. All current preclinical and clinical trials are trying to mainly target these features of dystrophic muscles. However, the timing of treatment and the quality of muscular tissue are two important aspects that highly affect the therapeutic efficiency.

### Anti-inflammatory drugs

Current therapeutic approaches mainly target the chronic inflammation that highly perturbs the dystrophic milieu. Corticosteroids are the gold standard anti-inflammatory drugs for MD treatment and are administered to patient early before other medical care interventions.

Several clinical trials have demonstrated that the daily treatment with glucocorticoids (e.g. prednisone, deflazacort) has beneficial effects on dystrophic muscles, reducing myofiber necrosis, fibrosis, and stimulating regeneration. Upon chronic treatment with prednisone, DMD boys display improved muscle strength and a general delay in the disease progression (Waldrop and Flanigan 2019). However, the protracted administration of corticosteroids raises several and serious side effects (e.g. Cushing syndrome), requiring different dosing regimens to balance beneficial and adverse effects (McDonald et al. 2018).

Therefore, recent pre-clinical and clinical studies are directed to test innovative anti-inflammatory compounds with a molecular mechanism comparable to corticosteroids, but without or with limited side effects. Many of these drugs target mediators of the inflammation, acting in a more specific way than the broad effects of glucocorticoids.

Vamorolone (glucocorticoid analogue) and Edasalonexent are two inhibitors of Nf-kB, the master regulator of the inflammation. Pre-clinical studies have reported promising results of these two Nf-kB inhibitors on *dystrophin*-deficient (*mdx*) mouse, and Phase II clinical trials on DMD boys are ongoing (Hammers et al. 2016; Donovan et al. 2017; Smith et al. 2020).

TNF- $\alpha$  is another pro-inflammatory cytokine that have detrimental effects in some inflammatory diseases, like rheumatoid arthritis and psoriasis. In dystrophic muscles, TNF- $\alpha$  mediates inflammation and induces necrosis of myofibers. From these assumptions, the soluble TNF- $\alpha$  receptor (etanercept) and the anti-TNF $\alpha$  antibody were tested in *mdx* mice, displaying reduced necrosis and improvements in the histology after the treatment (Pierno et al. 2007; Piers et al. 2011).

### Enhancing the muscle regeneration

Other experimental therapies for MDs are based on boosting the myofiber regeneration to compensate the pathological degeneration. Indeed, several myostatin inhibitors were successfully used in young and aged *mdx* mice, displaying improvements of the disease, increased myofiber hypertrophy, and reduced fibrosis (Bogdanovich et al. 2002; Philip, Lu, and Gao 2005).

Unfortunately, preclinical studies on larger animals and clinical trials on DMD patients did not obtain positive results. Upon treatment with myostatin inhibitors or follistatin (natural myostatin antagonist), DMD boys presented a slight increase in muscle size, but no enhance in muscle strength. Nonetheless,

myostatin inhibitors cause also a reduction of fibrosis in dystrophic muscles, emerging the possibility to use these compounds in combination with gene and cell therapy approaches (Wagner 2020).

The HDAC inhibitor Givinostat acts on myostatin/follistatin pathway and is showing promising results in a Phase II clinical trial on DMD patients. This inhibitor induces hypertrophy of myofibers and reduces necrosis, fibrosis, and fat deposition, improving the quality of muscular tissue for further therapeutic interventions (Bettica et al. 2016).

### Gene correction and gene replacement

All the therapies mentioned so far are not resolutive for MDs, since the genetic defect is still present, albeit improvements in general muscle histology after the treatment. Innovative gene therapies were recently developed to treat MDs, directly targeting the causative mutations by approaches of gene correction or gene replacement.

Gene correction tools fix a mutation that disrupts the open reading frame of a gene. These types of mutations are present in the *dystrophin* gene of about 70% of DMD patients, and cause the generation of a truncated and non-functional dystrophin protein (Muntoni, Torelli, and Ferlini 2003).

Several molecular strategies are tested to overcome the nonsense mutation. Gentamicin and Ataluren are two drugs that induce read-through of the nonsense mutation, forcing ribosomes to translate the premature stop codon with an amino acid and generate the full-length dystrophin protein. These drugs are well-tolerated by the organism, but a Phase III clinical trial has revealed a modest therapeutic efficacy on patient (McDonald et al. 2017).

Antisense oligonucleotides (AONs) and snRNAs can induce the exon skipping, namely the exclusion of mutated exon in the mature dystrophin mRNA, producing a shorter but functional dystrophin protein. While AONs are systemically administered as chemical compounds, snRNAs are carried by a plasmid and require a vector-based delivery system. AONs and snRNAs were preclinically tested for the treatment of different types of MDs, however they have a modest efficacy *in vivo* on DMD patient (Goemans et al. 2011).

The CRISPR-Cas9 system might be a ground-breaking genetic tool to induce gene correction *in vivo*. CRISPR-Cas9 induces a double-strand break into a specific DNA sequence, stimulating the DNA repair system to perform a non-homologous end joining (deletion of mutated exon) or a homologous recombination with a donor sequence (the non-mutated exon). The CRISPR-Cas9 and donor sequences are encoded by a single plasmid and delivered by a viral vector. Up to now, preclinical trials on *mdx* mice and dystrophic canine models have demonstrated the feasibility of this therapeutic strategy. However, some limits about the CRISPR-Cas9 gene toxicity and immunoreactivity should be further analyzed (Nelson et al. 2019; Amoasii et al. 2018).

Unlike gene correction, gene replacement is a mutation-independent strategy. In that case, an additional copy of the non-mutated gene is delivered into the nucleus of target cells, restoring the protein functionality.

According to the loading capacity of viral vectors, the excessive length of the dystrophin gene strongly limits its delivery. Therefore, mini-dystrophin sequences were synthesized, packed into adeno associated vectors (AAVs) and intravenously administered to patients, trying to convert the DMD into the milder BMD. Phase III clinical trials based on this technology are ongoing and these results will also provide important insights about safety and efficacy of this strategy (Chamberlain and Chamberlain 2017). For example, mini-dystrophins might be immunogenic in DMD patients like the full-length isoform, eliciting auto-immune reaction against the “gene corrected” muscles (Mendell et al. 2010).

The vector delivery is another crucial issue of these plasmid-based approaches. The main therapeutic goal for MDs is reaching all the muscles inside the organism, in particular diaphragm and heart which are affected in the late stages of the pathology.

AAVs represent the most suitable viral vectors for gene therapy of MDs, because of their high muscle tropism. Indeed, there are two AAV serotypes with a tropism for skeletal and cardiac muscles: AAV2 and AAV9. To increase the therapeutic efficiency, multiple doses of minidystrophin-AAV are administered to patient. AAVs are non-integrating viral vectors, but this is not a limiting-feature for the postmitotic myofibers, in which exogenous DNA is stably maintained. Immune reaction against the viral vector, the presence of pre-existing neutralizing antibodies anti-AAVs (upon natural infection) and the necessity of multiple doses strongly limit the feasibility of this therapy, excluding patients to use one or both AAV serotypes (Galli et al. 2018).

Thanks to their high loading capacity and less immunogenicity, non-viral vectors (like nanocarriers, liposomes, etc.) might overcome the AAV-associated limits. Different research groups are trying to improve the non-viral vectors production, decreasing their toxicity, and increasing their muscle tropism. *In vitro* and *in vivo* preclinical studies on that are promising for future application in the therapy of MDs (Nance et al. 2017; Emami et al. 2019; Mitchell et al. 2020).

### Cell therapy

Regenerative medicine is based on using cells as therapeutic agent and might be applied to treat MDs. Indeed, myogenic cells can be isolated from a healthy donor (heterologous cells) or from the patient (autologous cells). In this latter case, autologous myogenic cells are first gene-edited *ex vivo*, then

transplanted into patient to regenerate a non-mutated and healthy tissue. The therapeutic efficiency of this approach highly depends on the type and the engraftment of cells used.

MuSCs would be the perfect cells for the cell therapy of MDs, because of their stemness and their regenerative capacity. However, these cells strongly rely on the extrinsic signals from the niche and they rapidly lose their stemness when manipulated *in vitro*, differentiating in committed myoblasts (Boonen and Post 2008). Moreover, MuSCs display very limited engraftment upon intramuscular injection, as well as scant homing capacity upon systemic administration, namely their migration from the circulatory system to muscles (Tedesco et al. 2010). For these reasons, transplantations of autologous, unaffected MuSC-derived myoblasts are tested in clinical trials for defined types of dystrophy, like oculo-pharyngeal MD where affected muscles are localized in a confined and accessible region of the body (Périé et al. 2014).

Embryonic stem cells (ES) and induced-pluripotent stem cells (iPS) can be successfully differentiated into myogenic progenitor *in vitro*. Their high stemness and proliferative capacity might be useful to overcome MuSC intrinsic limits mentioned above. Although, the delivery issue, as well as ethical and safety concerns, are still present about using these cells in regenerative medicine (Verhaart and Aartsma-Rus 2019).

Mesoangioblasts are muscle vasculature-associated progenitor cells. These cells are related to human pericytes and have myogenic potential *in vitro* and *in vivo*. Indeed, although MuSCs are essential for the muscle regeneration, mesoangioblasts contribute to adult myogenesis to some extent. Importantly, mesoangioblasts can cross the vessel wall, demonstrating remarkable migration ability into regenerating muscles through the circulatory system (Sampaolesi et al. 2006). These features make mesoangioblasts suitable for cell therapy of MDs. In a Phase II clinical trial, HLA-matched mesoangioblasts were intra-arterially injected in DMD boys. After the treatment, DMD patients did not display clinical improvements due to very low engraftment of transplanted cells (Cossu et al. 2016).

All the data from preclinical and clinical studies have demonstrated that the efficiency of a therapy against MDs is directly correlated to the quality of muscle tissue. Consequently, the timing of the medical intervention is crucial for the therapeutic outcome. Therefore, gene or cell therapy for MDs should start before the dystrophic alterations irreversibly compromise the muscle tissue. Alternatively, any pharmacological treatments that slow down disease progression and improve

muscle histology should be combined with the gene and cell therapy. A multilevel therapy, which restore protein functionality but also the tissue integrity at the same time, should be useful to treat such degenerating and heterogeneous diseases like MDs.

### **2.3. NUCLEAR FACTOR-1X (NFI1X)**

Nuclear Factor-1X (Nfix) is a transcription factor belonging to the Nuclear Factor-1 (NFI) protein family, which consists in 4 members: Nfia, Nfib, Nfic, and Nfix.

These transcription factors are encoded by four homologous genes in all mammals and arose from a unique common ancestor during chordate evolution. Each *Nfi* gene generates a high number of transcript variants by an extensive alternative splicing on immature mRNA. Moreover, the NFI proteins have several isoforms thanks to different post-translational modifications (Gronostajski 2000).

All the NFIs are mainly characterized by two protein regions: a highly conserved DNA binding and dimerization N-terminal domain; a highly variable transactivation/repression C-terminal domain. NFIs can reciprocally hetero- or homodimerize binding the DNA consensus sequence TTGGC(N5)GCCAA, which is present in the adenovirus type 4 replication origins and in the promoters/enhancers of different tissue-specific genes (K. S. Chen et al. 2017).

These transcription factors are expressed by several tissues during both specific developmental stages and the postnatal period. Thanks to their double nature of activators and repressors of the gene expression, NFIs can modulate the gene regulatory network underlying crucial cellular processes, like proliferation and differentiation.

*In vivo* and *in vitro* studies revealed that NFIs are particularly involved in the stem cell biology of different tissues, inducing activation of stem cells and differentiation into committed cells. This function is especially evident in embryonic/fetal period, while in adult stem cells NFIs have different roles according to the kind of tissue (Harris et al. 2015).

Knockout animal models for each NFI display high mortality at birth or few weeks postnatal, because of serious development defects. For example, *Nfic* is crucial for the development of mammary glands (Murtagh, Martin, and Gronostajski 2003), *Nfib* for brain and lung development (Hsu et al. 2011), *Nfia* for brain and urinary tract formation (Lu et al. 2007).

*Nfix* null mice usually die at 3 weeks after birth, exhibiting serious defects in skeleton (kyphosis), intestine malformations, and brain deformations (Driller et al. 2007). Indeed, Nfix plays crucial roles in endochondral ossification, as well as in developing cerebral cortex and cerebellum. The *Nfix* deficiency impairs neuronal and glial differentiation, with concomitant high expansion of radial glia

cells, namely the embryonic neuronal stem cells (Heng et al. 2014). Thereby, *Nfix* null mice exhibit hydrocephalous and megalencephaly, that is enlarged cerebral cortex due to a high amount of neuronal progenitor cells with delayed differentiation (Driller et al. 2007). Interestingly, *NFIX* haploinsufficiency is the genetic cause for Malan Syndrome, a human genetic disorder characterized by cognitive deficit, skeletal defects, and macrocephaly (Malan et al. 2010).

*Nfix* promotes the radial glia differentiation thanks to its transactivation/repressor C-terminal domain. On the one hand, *Nfix* activates the expression of target genes involved in astrocyte differentiation (like *Gfap*); on the other, *Nfix* inhibits the expression of self-renewal factors in neuronal stem cells (like *Sox9*). Moreover, *Nfix* influences the cell-fate decision, stimulating radial glia cells to generate astrocytes rather than oligodendrocytes (Heng et al. 2014; Zhou et al. 2015).

Depending on the type of tissue, postnatally NFIs either promote cell differentiation as they do in the prenatal period or have an opposite function.

*Nfic* has maintained its developmental role also in the postnatal formation of tooth and bone, modulating the osteoblast differentiation and maturation (X. Chen et al. 2014; Lee et al. 2014). Instead, *Nfib* and *Nfix* are crucial transcription factors regulating the proliferation, self-renewal, and cell-fate of hair follicle stem cells (HFSCs). *Nfib*-lacking hair follicle displays normal HFSC behavior, but increased differentiation of melanocytes. Moreover, the double *Nfib/Nfix* null HFSCs are more prone to assume a lineage infidelity state and mainly differentiate into epidermal cells upon injury, leading to a premature exhaustion of HFSC compartment (C. Y. Chang et al. 2013; Adam et al. 2020).

*NFIX* also regulates the survival and the lineage specification of hematopoietic stem cells (HSCs). In these cells, *NFIX* activates the expression of survival genes and blocks early stages of lymphoid differentiation into B cells in favor of the myeloid lineage. The genetic absence of *Nfix* impairs colony-forming potential and engraftment ability of transplanted HSCs (Holmfeldt et al. 2013; Riddell et al. 2014).

Generally, the stem cell biology is based on molecular mechanisms that strongly correlate with cancer. Here too, NFIs have been identified as oncogenes or tumor-suppressor genes in different kinds of cancer. In some developmental-based cancers, which affect children, NFIs have tumor-suppressor functions (like *Nfix* in medulloblastoma), inducing differentiation of tumor cells and reducing the frequency of metastasis (Łastowska et al. 2014). While, in adult cancers NFIs usually act as oncogenes (like *Nfib* and *Nfix* in prostatic cancer or *Nfia* in glioblastoma), because they maintain

tumor cells in an undifferentiated and malignant state (Grabowska et al. 2016; Glasgow et al. 2013; Piper, Gronostajski, and Messina 2018).

To sum up, NFIs have a double function: modulators of cell differentiation during development, and cell-fate determinants or self-renewal regulators in adult tissue. *Nfix* in skeletal muscle tissue represents an exception to this general rule.

### 2.3.1. NFIX IN MUSCLE DEVELOPMENT

Skeletal muscle development is characterized by two consecutive waves of prenatal myogenesis: embryonic and fetal myogenesis.

Embryonic myogenesis takes place between day 10 and 12 of the murine embryo development (E10-E12) and leads to the generation of primary or embryonic myofibers. Embryonic myoblasts migrate from dermomyotome and differentiate in primary myofibers, which constitute the scaffold of emerging skeletal muscle tissue. Between E12.5 and E17, a transcriptional and phenotypical switch occurs in the undifferentiated muscle progenitors, from which fetal myoblasts arise and differentiate into fetal or secondary myofibers (Chal and Pourquié 2017).

Embryonic and fetal myoblasts are two distinct populations of progenitor cells with different transcriptional regulation, susceptibility to external cues, and types of myofibers they generate. Indeed, embryonic myoblasts originate from Pax3<sup>+</sup>/Pax7<sup>-</sup> progenitors, are insensitive to both TGF- $\beta$  and  $\beta$ -catenin signaling and differentiate into myofibers expressing both embryonic and slow Myosin Heavy Chain (*Myh7*). Conversely, fetal myoblasts arise from Pax3-derived Pax7<sup>+</sup> cells, are sensible to TGF- $\beta$  and  $\beta$ -catenin signaling, and differentiate in secondary myofibers, which express some fetal markers, like MCK,  $\beta$ -enolase, PKC $\theta$ , and fast-MyHC (Hutcheson et al. 2009).

*Nfix* is a key regulator of this embryonic-to-fetal switch of prenatal myoblasts. It was demonstrated that NFIX is more expressed by fetal than embryonic myoblasts, in which the *Nfix* transcript is almost absent (Biressi et al. 2007). Gain-of-function experiments have demonstrated that *Nfix* induces embryonic myoblasts to assume a fetal phenotype. Indeed, *Nfix*-expressing embryonic myoblasts differentiate into fetal-like myotubes, in which the expression of the fetal marker  $\beta$ -enolase is activated, while the slow-MyHC expression is inhibited (G. Messina et al. 2010).

Likewise, silencing *Nfix* in fetal myoblasts strongly impairs their differentiation, generating few and short embryonic-like myotubes. In si*Nfix*-myotubes, the *Myh7* transcript is higher than the control, while the expression of fetal markers, like MCK and  $\beta$ -enolase, is completely abolished.

Similar results were obtained also *in vivo* by the analysis of MyoD-Cre/*Nfix*<sup>c/-</sup> mice (Campbell et al. 2008), in which *Nfix* is specifically deleted in muscles. Skeletal muscle-specific *Nfix* null fetuses are

smaller than the WT, indicating a delay in the development. Moreover, *Nfix* null fetal muscles display an embryo-like phenotype: myofibers with a small caliber, high expression of slow-MyHC, absence of fetal markers (MCK and  $\beta$ -enolase), and a general disorganization of sarcomeres. On the other side, over-expressing *Nfix* in embryonic skeletal muscles (Mlc1f-*Nfix2* embryo) cause a morphological and transcriptional switch towards fetal phenotype (G. Messina et al. 2010).

Like the other NFIs, NFIX can modulate the embryonal-to-fetal switch of myoblasts thanks to its double activity as activator/repressor of the target genes, directly or indirectly. Specifically, NFIX can bind both the MCK (*Ckm*) and the  $\beta$ -enolase (*Eno3*) promoters (fetal markers), activating their expressions; at the same time, NFIX indirectly causes a reduction of the slow-MyHC levels in fetal myoblasts, inhibiting the expression of *Nfatc4*, an activator of the *Myh7* gene.

Likely, NFIX heterodimerizes with other coactivators or corepressors (like MEF2C or SOX6), broadening the pool of its target genes (Taglietti et al. 2016). The identification of these coactivators/corepressors might be useful for the modulation of the NFIX activity.

### 2.3.2. NFIX IN MUSCLE REGENERATION

As said above, the adult muscle regeneration recapitulates molecular mechanisms that govern prenatal myogenesis. In fact, in postnatal myogenesis, *Nfix* acts as inducer of myoblasts differentiation similarly to its function during prenatal myogenesis.

Recently, our research group demonstrated that also postnatal *Nfix* null muscles display some morphological and molecular differences than the WT counterpart. *Nfix* null myofibers present a reduced cross-sectional area (CSA) and an increased expression of slow-MyHC in both slow and fast muscles (Rossi et al. 2016).

Upon cardiotoxin-induced injury, muscles lacking *Nfix* exhibit a delay in the regeneration process, with a prolonged expression of early-differentiation markers (like dMyHC and MyoG) at 10 and 14 days after injury when the regeneration process is supposed to be almost completed. Moreover, due to the absence of *Nfix*, regenerating muscles have higher amount of Myostatin (Mstn), a well-known inhibitor of muscular regeneration and growth (Rossi et al. 2016).

The slowing-down of regeneration is not correlated to the *Nfix* null developmental defects, but rather it is cell-autonomously dependent to the *Nfix* absence in adult MuSCs. Precisely, the conditional genetic deletion of *Nfix* in Pax7<sup>+</sup> cells (Pax7-Cre<sup>ERT2</sup>:*Nfix*<sup>fl/-</sup> mice) leads to a regeneration delay upon muscle injury similar to what observed in *Nfix* null mice.

Despite *Nfix* is expressed *in vivo* by MuSCs, proliferating myoblasts, and differentiated myonuclei, *ex vivo* experiments on single fibers demonstrated that myoblasts lacking *Nfix* have a delay in early

differentiation (from MyoD<sup>+</sup> to MyoD<sup>+</sup>/MyoG<sup>+</sup> cells) but not in MuSCs activation (from Pax7<sup>+</sup> to Pax7<sup>+</sup>/MyoD<sup>+</sup> cells).

Likely, the enhanced Myostatin signaling in *Nfix* null muscles is the main cause of the regeneration and differentiation delay. Specifically, Nfix can bind the promoter and inhibit the expression of the *Mstn* gene in differentiated C2C12 cell line. Furthermore, silencing *Mstn* in regenerating *Nfix* null muscles leads to a rescue of the delayed regeneration (Rossi et al. 2016).

All these data demonstrate that Nfix control the proper timing of postnatal muscle regeneration modulating myoblast early differentiation through the inhibition of Myostatin gene.

Last year, in our lab was demonstrated that Nfix is also crucial for the M1-to-M2 switch in macrophages (Marielle Saclier et al. 2020). Macrophages are a non-myogenic cell population that are essential for the timing regulation of muscular regeneration upon injury (see Section 2.1.2).

Like for embryonic and fetal myoblasts, M2 anti-inflammatory macrophages express higher level of *Nfix* than M1 pro-inflammatory macrophages. *In vivo* conditional knocking-out and *in vitro* silencing of *Nfix* in infiltrating monocytes (LysM<sup>Cre</sup>:*Nfix*<sup>fl/fl</sup>), from which macrophages originate, revealed that M2 macrophages lacking *Nfix* are less present than M1 counterpart and display a M1-like phenotype. Interestingly, impaired M1-to-M2 switching due to the absence of *Nfix* in macrophages alters muscle regeneration. Indeed, upon injury, regenerating LysM<sup>Cre</sup>:*Nfix*<sup>fl/fl</sup> muscles display a similar delay in regeneration like the *Nfix* null and Pax7-Cre<sup>ERT2</sup>:*Nfix*<sup>fl/-</sup> models, in which *Nfix* is genetically absent in either the whole organism or specifically in MuSCs (Marielle Saclier et al. 2020).

Owing to the *Nfix* deletion, M1 macrophages are defective in their switch towards the M2 phenotype, maintaining a M1-like phenotype and stimulating myoblasts to proliferate rather than differentiate. Together with the reduced differentiation of *Nfix* null myoblasts, this results in a slowing down of muscular regeneration, highlighting the relevance of crosstalk between myogenic and non-myogenic cells for the proper muscle homeostasis.

### 2.3.3. NFIX IN MUSCULAR DYSTROPHIES

In the field of Muscular Dystrophies, it is well-known that slow myofibers are more protected from dystrophy than fast myofibers (C. Webster et al. 1988; Danieli-Betto et al. 2005). Driving myogenic cells towards preferentially differentiating into slow rather than fast myofibers might be a good strategy to improve the quality of regenerated muscles after dystrophic damages.

Since *Nfix* promotes myoblasts differentiation and inhibits the slow MyHC expression in muscle, three years ago, our research group cross *Nfix* null mouse with *dystrophin*-deficient (*mdx*) or  $\alpha$ -*sarcoglycan* (*Sgca*) null mice, analyzing the resulting phenotype. This demonstrated that the

dystrophic muscles lacking *Nfix* display morphological and functional improvements of the disease (Rossi et al. 2017).

Specifically, adult *Sgca* null and *mdx* mice without *Nfix* present skeletal muscles with less necrotic myofibers, less infiltrating macrophages, reduced fibrosis, decreased number of centrally nucleated myofibers (regenerating myofibers) and higher fiber caliber (CSA). Moreover, *Nfix* deletion in dystrophic context leads to a switch of myofibers towards the oxidative, slow-twitch phenotype. Thanks to these histological improvements of muscles, *Nfix* null:*Sgca* null mice run longer than *Sgca* null mice, demonstrating higher resistance to fatigue.

Instead, the specific overexpression of *Nfix* in *Sgca* null muscles (*Sgca* null:*Mlc1f-Nfix2*) causes a worsening in all histological hallmarks, confirming the detrimental role of *Nfix* in muscular dystrophy (Rossi et al. 2017).

Interestingly, similar histological rescue of dystrophic muscles was obtained thanks to the silencing of *Nfix* in adult *Sgca* null mice by RNA interference. Electroporating a short-hairpin for *Nfix* (sh*Nfix*) in dystrophic *Tibialis anterior* causes a general amelioration of muscular histology and a switch towards oxidative myofibers (Rossi et al. 2017).

Enhancing the muscle regeneration by myostatin inhibitors did not lead to positive clinical results on dystrophic large animals and DMD boys (excluding the reduced fibrosis, see Section 2.2.3). Thereby, we propose a novel therapeutic approach for MDs, based on delaying rather than promoting muscle regeneration in dystrophy.

Our experiments clearly demonstrate that silencing *Nfix* in dystrophic muscle might be a therapeutic strategy for muscular dystrophy, slowing down the muscle regeneration and guiding myofibers to assume an oxidative, more protected phenotype.

#### **2.3.4. REGULATION OF NFIX EXPRESSION**

Knowing how a transcription factor is transcriptionally and post-transcriptionally regulated is essential to inhibit its activity on target genes. Therefore, we analyzed the transcriptional regulation of *Nfix* in embryonic, fetal, and MuSC-derived myoblasts (Taglietti et al. 2018).

We demonstrated that *Nfix* expression is induced by JunB in fetal myoblasts. Indeed, JunB is more present in fetal than embryonic myoblasts and its expression correlates with *Nfix*. Gain and Loss-of-function experiments in embryonic and fetal myoblasts displayed that JunB, binding the *Nfix* promoter, is essential for *Nfix* expression in fetal myoblasts. Activating the *Nfix* gene, JunB indirectly promotes the switch from embryonic to fetal myogenesis (Taglietti et al. 2018).

Moreover, RhoA/ROCK and MAPK (MEK/ERK) signaling pathways regulate the JunB and Nfix protein levels between embryonic and fetal myoblasts. RhoA/ROCK pathway is particularly active during embryonic myogenesis and inhibits the MEK/ERK pathway, leading to a decrease in JunB and Nfix proteins. In fetal myoblasts, RhoA/ROCK signaling is inactive, while MAPK pathway is activated, increasing the JunB and Nfix protein amounts. By treating embryonic and fetal myoblasts *in vitro* with specific inhibitors for RhoA/ROCK and MEK/ERK pathways, we have shown that RhoA/ROCK is an upstream inhibiting pathway of MEK/ERK and that these two signaling pathways specifically modulate JunB and Nfix proteins in prenatal myogenesis. Interestingly, treating fetuses *in vivo* with the specific MEK/ERK inhibitor (PD98059) causes a strong decrease in JunB and Nfix proteins in muscle and a reduction in CSA of fetal myofibers (Taglietti et al. 2018).

These data provide novel important insights on the regulation network underlying the *Nfix* expression, rising the opportunity to inhibit Nfix in dystrophic muscle through the pharmacological modulation of MAPK pathways.

### 3. RESULTS AND DISCUSSION

#### 3.1. MEK/ERK SIGNALING MODULATES NFIX POSTNATALLY

As mentioned above (see Section 2.3.4), the Nfix protein is regulated by both the MAPK (MEK/ERK) and RhoA/ROCK pathways in prenatal myoblasts. However, *in vitro* treatments with specific inhibitors of these signaling cascades (PD98059 to inhibit ERK phosphorylation; Y27632 to block RhoA/ROCK signaling) on postnatal MuSC-derived myoblasts led to different results (Taglietti et al. 2018).

Firstly, we noticed that the ERK protein was highly phosphorylated (pERK) during proliferation and early differentiation of myoblasts (1 day in differentiation medium, 1dDM), indicating the activation of MEK/ERK pathway in these conditions. On the contrary, RhoA/ROCK pathway was particularly active during differentiation of postnatal myoblasts, from 2dDM onward. JunB was present only in proliferating myoblasts, whereas the Nfix protein increased in differentiating myoblasts at 1dDM and its expression was maintained throughout differentiation (**Fig. 1A**).

To verify whether Nfix was regulated by MEK/ERK and RhoA/ROCK pathways also postnatally, we treated juvenile MuSC-derived myoblasts, isolated from CD1 pups at 10 days (P10), with two specific inhibitors of the pathways. Juvenile myoblasts were exposed to 50  $\mu$ M of PD98059 (MEK/ERK inhibitor) during proliferation, when MEK/ERK signaling is active, and to 10  $\mu$ g/ml of Y27632 (RhoA/ROCK inhibitor) at 2 dDM when the ROCK kinase signaling reaches its peak. Differentiating Y27632-treated postnatal myoblasts displayed a huge decrease of phosphorylated Myosin Phosphatase Target Subunit 1 (pMYPT1) but no difference in the Nfix protein level than vehicle (DMSO)-treated cells (**Fig. 1B,D**). Conversely, the treatment with PD98059 of proliferating juvenile myoblasts caused a decrease of both phosphorylated-ERK (pERK) and Nfix proteins compared to the control (**Fig. 1C,E**).

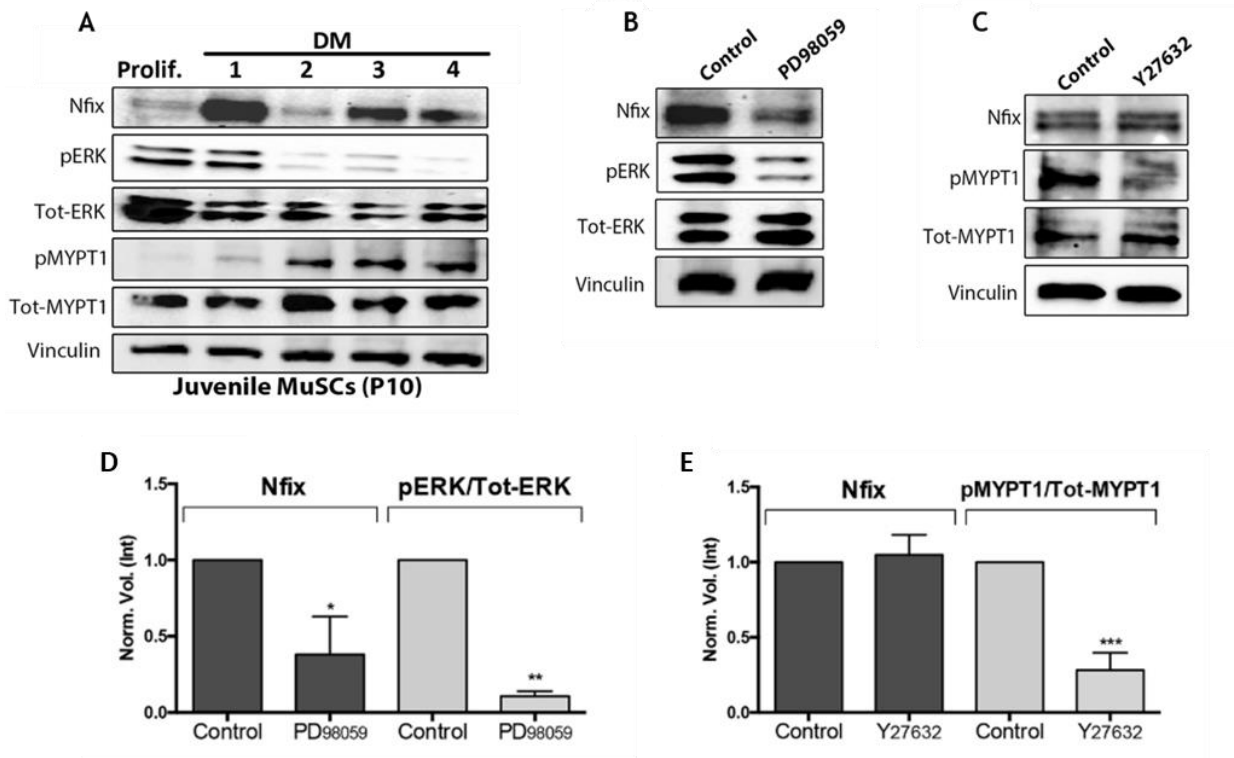


**Figure 1. Inhibition of MEK/ERK signaling pathway leads a decrease in Nfix protein level.**

(A) Representative western blots of juvenile MuSC-derived myoblasts in proliferation (Prolif.) and at different days in differentiation medium (DM), revealing protein levels of Nfix, ERK (pERK, tot-ERK), Myosin Phosphatase Target Subunit 1 (pMYPT1, tot-MYPT1) and Vinculin. (B-E) Western blots and quantification of juvenile myoblasts displaying levels of Nfix, ERK, MYPT1 and Vinculin upon treatment with PD98059 (B-D), Y27632 (C-E) and DMSO (control).

We then asked whether these drugs impinged on the normal behavior of treated-myogenic cells. Therefore, upon the *in vitro* treatments we analyzed apoptosis, proliferation, differentiation, and the expression of myogenic markers in postnatal myoblasts. As shown in **Fig. 2A**, the degree of apoptosis, evaluated through the activated caspase 3 (aCasp3) and caspase 9 (aCasp9) protein levels, was not increased by the inhibitors. While inhibition of RhoA/ROCK signaling by Y27632 slightly increased the fusion index of myogenic cells, differentiating PD98059-treated myoblasts had less fusion potential than the control, as seen for fetal myoblasts (**Fig. 2C-G**). This reduced fusion ability upon the MEK/ERK inhibition is not correlated to proliferative defects. Indeed, the amount of proliferating BrdU<sup>+</sup> cells did not change upon PD98059 or Y27632 treatment (**Fig. 2H**). Moreover, expression of the main myogenic markers (Pax7, Myogenin, MyHC) was not altered in treated myoblasts during proliferation and differentiation (**Fig. 2B**).

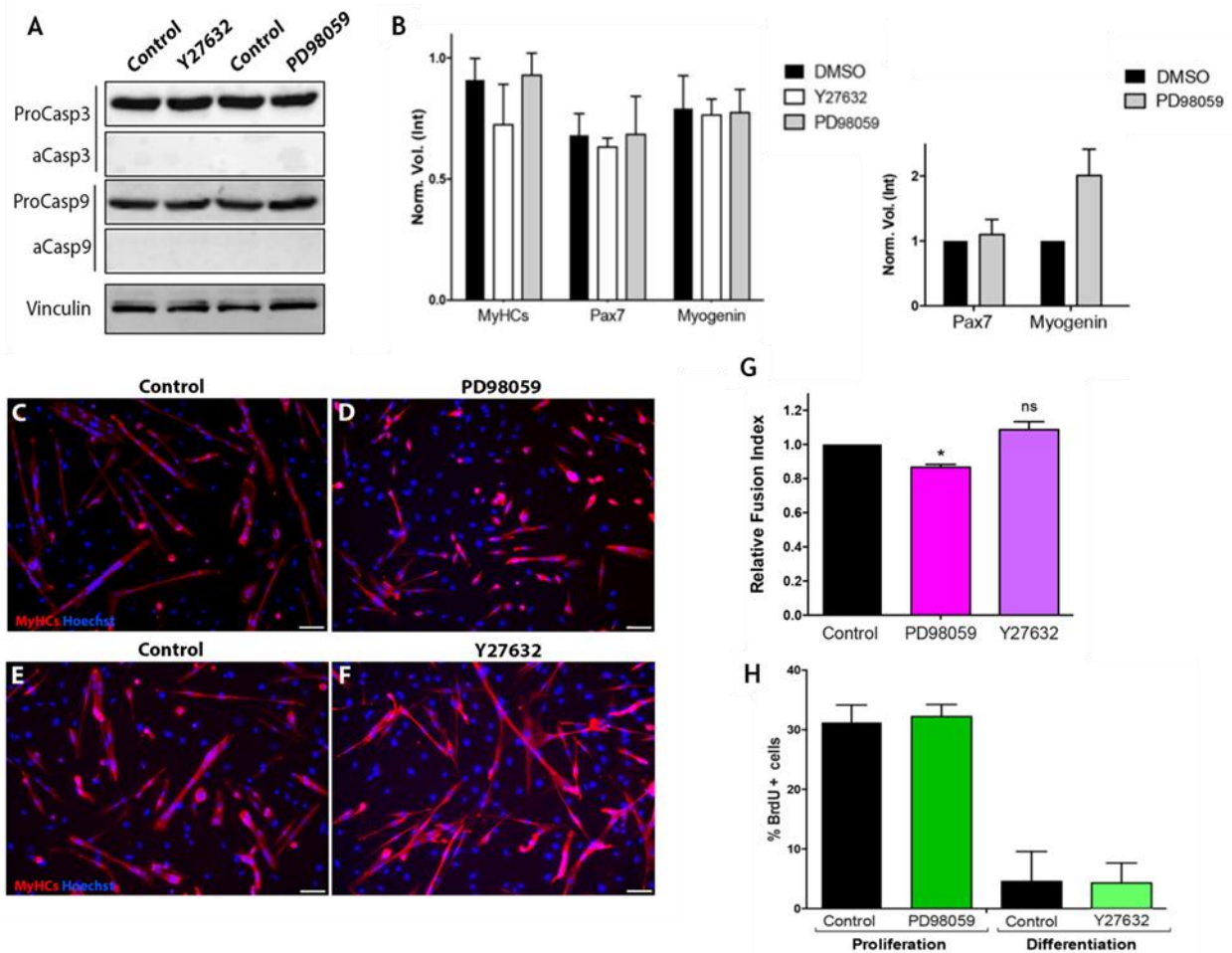


**Figure 2. Effects of treatment with MEK/ERK and RhoA/ROCK inhibitors on apoptosis, proliferation, and differentiation of juvenile MuSC-derived myoblasts.**

(A) Western blots of protein extracts from control, PD98059 and Y27632-treated juvenile myoblasts, displaying levels of caspase 3 (ProCasp3, aCasp3), caspase 9 (ProCasp9, aCasp9) and Vinculin. (B) Protein levels of the main myogenic markers (MyHCs, Pax7, Myogenin) in proliferating (*graph on the right*) and differentiating (*graph on the left*) postnatal myoblasts upon treatment with PD98059 and Y27632 (one-way ANOVA test, n=5). (C-F) Representative immunofluorescence pictures of MyHCs (red) and nuclei (blue) on differentiating MuSC-derived myoblasts treated with DMSO (control), PD98059 and Y27632, with (G) quantification of the fusion index (\*P<0.05; one-way ANOVA test, n=5). (H) Graph of BrdU<sup>+</sup> myoblasts treated with DMSO (control), PD98059 and Y27632 in proliferation and differentiation (ANOV test, n=5).

These data indicate that the positive modulation of the Nfix protein by MEK/ERK pathway is also conserved in postnatal MuSC-derived myoblasts, as in the fetal period. By the PD98059-induced inhibition of ERK phosphorylation, the Nfix protein levels decreased in proliferating myoblasts causing a delay in myogenic differentiation, as confirmed by the reduced fusion ability of treated-cells than the control. Otherwise, RhoA/ROCK pathway does not modulate the Nfix protein in postnatal myogenic cells during differentiation, when this pathway is particularly active (Taglietti et al. 2018).

These results have brought out the idea that Nfix protein might be modulated through a pharmacological inhibition of the MEK/ERK signaling pathway in a dystrophic context.

### **3.2. EVALUATION OF TRAMETINIB EFFICACY IN DECREASING NFIX LEVELS IN MUSCULAR DYSTROPHY**

To decrease the Nfix expression by a pharmacological inhibition of the MEK/ERK pathway, we identified a class of drugs, called MEK-inhibitors, that were suitable for our goal. Specifically, we chose Trametinib (GSK1120212 or Mekinist®), an allosteric, ATP noncompetitive inhibitor of MEK1/2 in the MAPK pathway. Trametinib shares the same molecular mechanism of PD98059 but has better pharmacological features for preclinical studies and clinical trials as anti-cancer drug (Montagut and Settleman 2009). Indeed, the hyperactivation of MAPK pathway is responsible for the development of several cancer types, like melanoma, thyroid cancer, colon cancer. In 2014, both FDA (NDA204114, NCT01682083) and EMA (EMEA/H/C/002643) have approved the oral treatment with Trametinib alone or in combination with BRAF-inhibitors (dabrafenib) of patients with unresectable melanoma, metastatic non-small cell lung cancer, or anaplastic thyroid cancer (Zeiser, Andrlová, and Meiss 2018).

#### **3.2.1. TRAMETINIB DECREASES THE NFIX PROTEIN IN POSTNATAL MYOBLASTS *IN VITRO***

Firstly, we tested the capacity of Trametinib to decrease Nfix through MEK/ERK-inhibition in myogenic cells *in vitro*, as observed with PD98059. Therefore, juvenile MuSC-derived myoblasts were treated for 14 h with different concentrations of Trametinib with the aim of selecting the proper dosage of MEK-inhibitor to decrease both pERK and Nfix protein levels. As expected, Trametinib-treated cells displayed a concentration-dependent inhibition of the ERK phosphorylation; moreover, 100 nM of Trametinib caused a concomitant decrease in the Nfix protein levels of about 40% than the vehicle-treated cells (**Fig. 3A-B**). Myoblasts treating with higher dosages (1 and 10  $\mu$ M) of Trametinib also revealed a decrease in Nfix protein, although not statistically significant.

To understand whether this ERK-dependent modulation of Nfix is at either transcriptional or post-transcriptional level, we quantified the *Nfix* mRNA between 100 nM Trametinib and DMSO-treated myoblasts. As displayed in **Figure 3C**, the *Nfix* specific transcript did not change after treatment with 100 nM Trametinib, revealing that the inhibition of MEK might affect the Nfix protein stability rather than its gene expression.

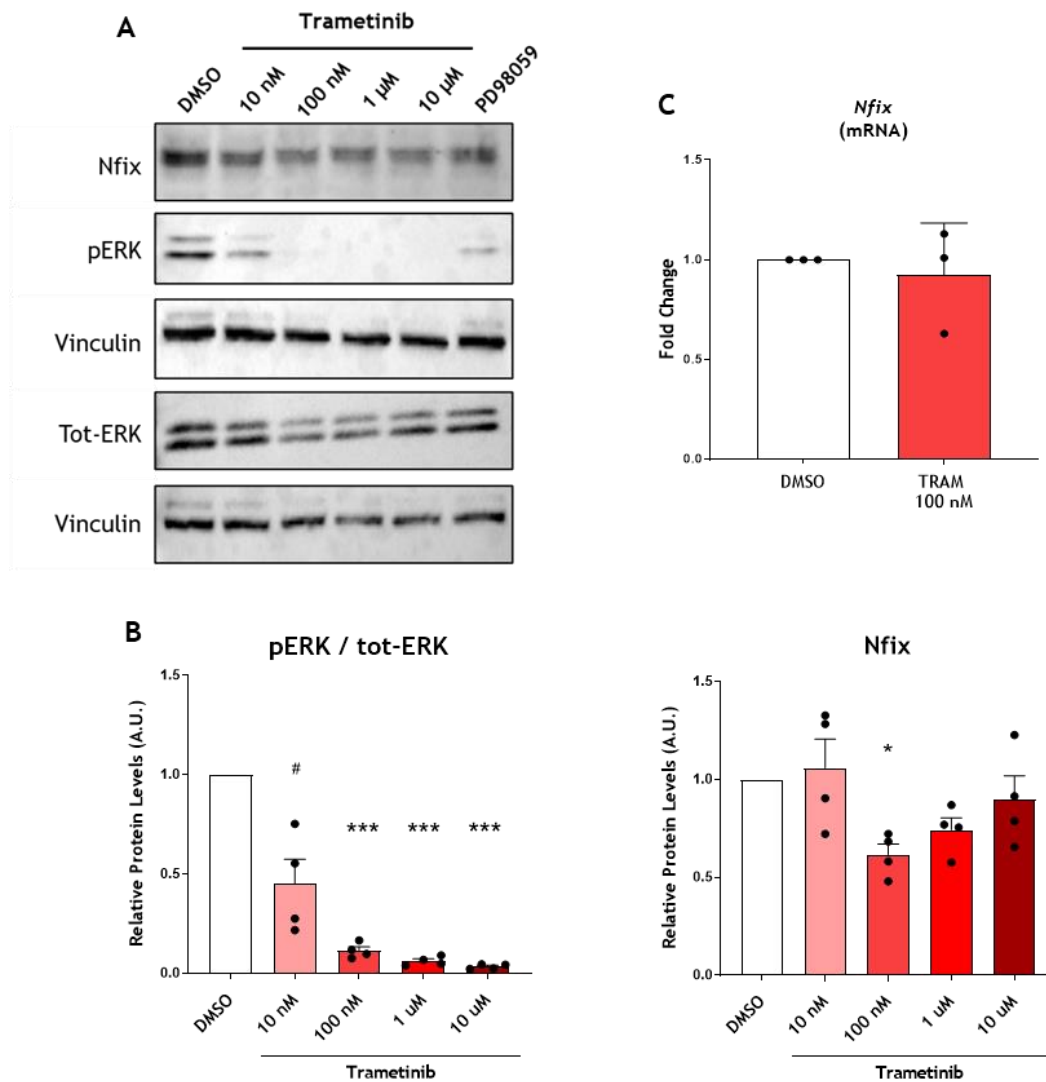


**Figure 3. *In vitro* treatment with Trametinib leads to a decrease in pERK and Nfix protein in juvenile MuSC-derived myoblasts.**

(A) Representative western blots of juvenile myoblasts treated with DMSO and different concentration of Trametinib *in vitro*, revealing protein levels of Nfix, ERK (pERK, tot-ERK), and Vinculin used as housekeeping protein. PD98059-treated myoblasts were used as positive control. (B) Quantitative densitometry of pERK/tot-ERK (graph on the left) and Nfix (graph on the right) protein levels in juvenile myoblasts treated with DMSO or Trametinib at different concentrations (\*  $P < 0.05$ , \*\*\*  $P < 0.001$ , #  $P = 0.0538$ , paired one-way ANOVA test,  $n = 4$ ). (C) qRT-PCR for expression of *Nfix* in juvenile MuSC-derived myoblasts treated with vehicle (DMSO) or 100 nM Trametinib for 14 h.  $\beta$ -actin was used as housekeeping gene (paired t-test with Welch's correction,  $n = 3$ ).

Juvenile myoblasts used for these experiments were isolated through the Magnetic-Activated Cell Sorting (MACS) with the satellite cell isolation kit (Miltenyi®). MACS-isolated myoblast cultures were not completely pure, and few Nfix-expressing fibroblasts were still present in dishes (not shown). Therefore, we decided to treat NIH3T3 cells (a cell line of immortalized murine fibroblasts) with different concentrations of Trametinib to exclude potential interference in the results. Trametinib-treated NIH3T3 presented concentration-dependent decrease of pERK but comparable

Nfix protein levels to the control (**Fig. 4A-B**). Hence, the MEK/ERK pathway does not positively modulate the Nfix protein in fibroblasts like what it occurs in myogenic cells. Further analysis on NIH3T3 and primary fibroblast culture might reveal the presence of cell-specific signaling pathways underlying the Nfix expression and/or post-translational regulation.

Concerning this aspect, recent results from our lab demonstrated that the negative regulation of Nfix by the RhoA/ROCK pathway, that is present in fetal but not in juvenile myoblasts, is postnatally conserved in macrophages. Indeed, Y27632-treated macrophages displayed an upregulation of the Nfix protein and, consequently, a higher frequency in the switch from M1 to M2 than vehicle-treated cells (Marielle Saclier et al. 2020). Due to the crucial role of macrophages in regenerating and dystrophic muscle, we evaluated whether the MEK/ERK signaling cascade might regulate Nfix also in macrophages. Specifically, *in vitro*-polarizing M2 macrophages, which express higher level of Nfix than M1, were treated with similar dosages of Trametinib used for myoblasts and fibroblasts. Despite a huge inhibition of the ERK phosphorylation, treatment with Trametinib did not result in a concomitant reduction of the Nfix protein in M2 macrophages (**Fig. 4C-D**). Interestingly, comparing the quantification of pERK/tot-ERK ratio between all the experiments, macrophages appeared to be more sensitive to lower concentration of Trametinib than myoblasts and fibroblasts. Moreover, using the same antibody and experimental conditions, protein extract from macrophages displayed a single band for the Nfix signal on Western Blot rather than the classical doublet present in myogenic cells and fibroblasts (**Fig. 3A; Fig. 4A,C**). Deeper molecular analyses are performed in the lab to understand these divergences.

These data revealed that the MEK/ERK pathway positively regulates Nfix in juvenile MuSC-derived myoblasts. This regulation occurs at post-translational level and is cell-type specific. Inhibiting the MEK/ERK pathway through Trametinib causes a reduction of the Nfix protein in myogenic cells *in vitro*, setting the stage for an indirect, pharmacological inhibition of Nfix in muscle *in vivo*.

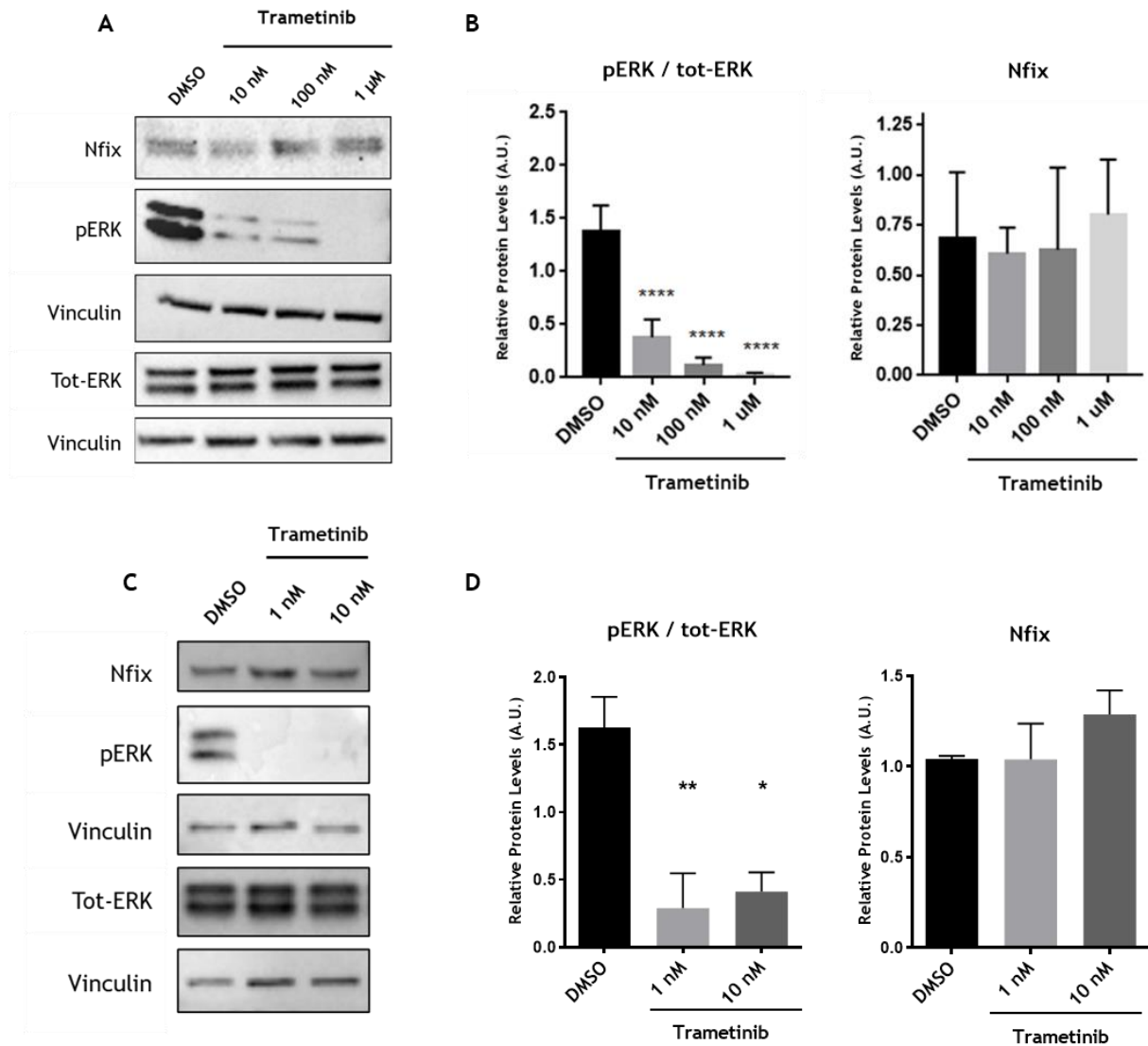


**Figure 4.** *In vitro* treatment with Trametinib did not affect the Nfix protein in fibroblasts and M2 macrophages.

Representative Western Blots of protein extracts from NIH3T3 (**A**, **B**) and M2 macrophages (**C**, **D**) treated with DMSO or Trametinib at different concentrations *in vitro*. The protein levels of Nfix, ERK (pERK, tot-ERK), and Vinculin as housekeeping protein were quantified by densitometry (\*\*\*\*  $P < 0.0001$ , \*\*  $P < 0.001$ , \*  $P < 0.05$ , one-way ANOVA test,  $n=3$ ).

### 3.3.2. CHRONIC TREATMENT WITH TRAMETINIB CAUSES A REDUCTION OF pERK AND NFIX IN DYSTROPHIC MUSCLE

As described before, Trametinib is a MEK-inhibitor that was recently approved by FDA and EMA for the treatment of different types of human cancer. Thereby, Trametinib was extensively tested in preclinical animal models of cancer (rodents). Particularly, we focused on preclinical studies in which Trametinib was administered to mice by oral gavage, that is a more feasible and less stressful route of administration. Despite many differences between all the treatment protocols described in literature, two features are constants about the oral administration of Trametinib *in vivo*: firstly, drug or vehicle are dissolved in a viscous solvent which improves the uptake by the intestinal mucosa (in our case, 0.5% hydroxypropylmethylcellulose and 0.2% Tween-80 in distilled water); secondly, a daily administration of the drug for at least 2 weeks is necessary to stably decrease pERK. Moreover, since the MEK/ERK pathway has an ubiquitous and crucial role in all the tissues, the chronic administration of low doses of Trametinib is essential to maintain a systemic short-circulating half-life of the drug and potentially avoiding toxicities (Dumble et al. 2014; King et al. 2013; Qiu et al. 2015; Cowan and Keiser 2015). Specifically, we followed the treatment protocol described by Gilmartin et al., which provided a wide analysis about efficiency and distribution of this MEK-inhibitor *in vivo* in rats (Gilmartin et al. 2011). We decided to administer the FDA-approved MEK-inhibitors Trametinib to *Sgca* null mice by oral gavage. The *Sgca* null mouse model displays a muscular dystrophy that is more severe than the *mdx* mouse, better resembling the human Duchenne Muscular Dystrophy (DMD) pathology (Franck Duclos et al. 1998).

To analyze the pharmacokinetic of Trametinib in dystrophic muscle, we treated adult *Sgca* null mice (5 weeks old) with 3 mg/kg of Trametinib or DMSO by oral gavage and we collected *Tibialis anterior* and Diaphragms, which are the most affected muscles by the disease, after 2-, 8-, 12- and 24-hours post dose (**Fig. 5A**). Protein extracts from Trametinib-treated muscles have revealed that pERK was very low at 2- and 8-hours post-dose than the control, indicating a strong inhibition of MEK by Trametinib in *Tibialis anterior* muscles at these timepoints. The Trametinib-induced MEK inhibition was abolished at 12- and 24-hours post treatment, when the ratio pERK/tot-ERK was comparable between drug and vehicle-treated muscles (**Fig. 5A**). Protein extracts from Diaphragms displayed a similar trend for both Nfix and pERK levels (data not shown). These results confirmed what Gilmartin and colleagues have observed in Nude mouse and rat models with tumor xenografts. A single oral dose of Trametinib strongly reduces the MEK activity and the ERK phosphorylation for more than 8 hours in adult *Sgca* null muscles. However, acute treatment with Trametinib is not sufficient to also decrease the Nfix protein in dystrophic muscles, except for a slight but not significant reduction at 8 hs post dose (**Fig. 5A**).

To verify whether a stable inhibition of the ERK phosphorylation in dystrophic muscle might lead to a reduction of the Nfix protein, we decided to treat adult *Sgca* null mice (5 weeks old) with three different concentrations of Trametinib (0.3, 3 and 6 mg/kg) daily for 14 consecutive days, by oral gavage (**Fig. 5B**). Daily weight of each mouse was measured with the aim of dosing the proper amount of Trametinib and checking for general toxic effects of the treatment (20% weight loss). As observed in graphs (**Fig. 5C**), there were no significant differences in weight between treated and control group of mice for all the three doses. Moreover, Trametinib-treated mice did not present any evident phenotypical alterations than control. Therefore, the oral administration of Trametinib at these concentrations, every day for 14 days, was not apparently toxic for dystrophic mice. Analyzing the total protein extracts of *Tibialis anterior* from treated mice at day 14, we have observed that 0.3 mg/kg Trametinib was not sufficient to have a reduction of pERK than DMSO-treated muscle. Conversely, higher drug dosages (3 and 6 mg/kg) caused a statistically significant reduction of pERK/tot-ERK ratio (more than 70% for 3 mg/kg) demonstrating that Trametinib properly inhibited the MEK/ERK pathway at these conditions. In addition, treated muscles with 3 and 6 mg/kg of Trametinib also displayed a decreasing trend of the Nfix protein. The reduction of Nfix is more evident at 6 than 3 mg/kg of Trametinib, although not statistically significant due to high variability of the Nfix protein levels in control and to different cell types in the whole muscle lysates, such as fibroblasts and macrophages, that we demonstrated not to be linked to ERK in terms of Nfix expression and that might alter the final result (**Fig. 5D**).

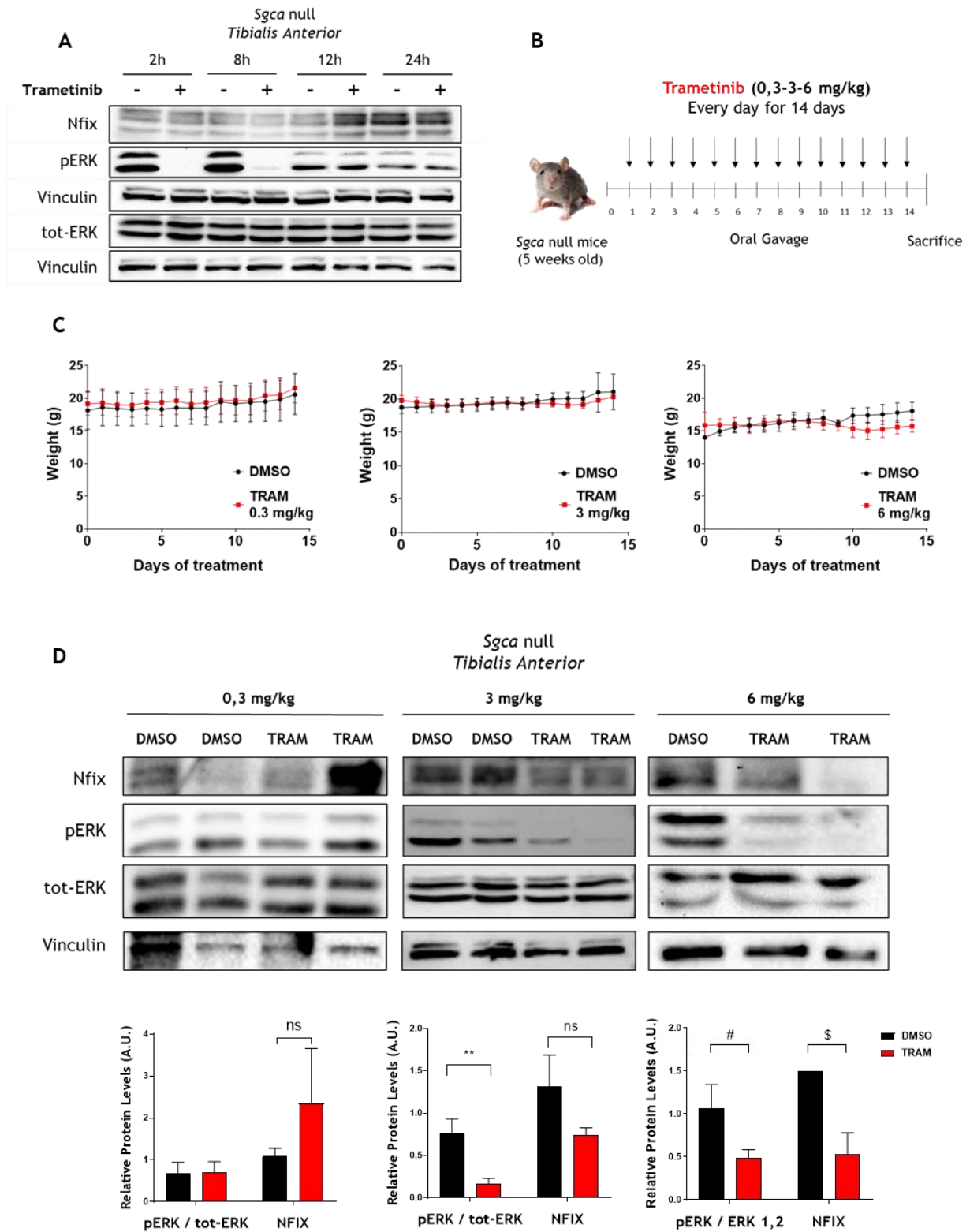


**Figure 5. Acute and chronic administration of Trametinib to adult *Sgca* null mice by oral gavage.**

(A) Representative Western Blots of protein extracts from *Sgca* null *Tibialis anterior* muscles treated with DMSO (-) or 3 mg/kg of Trametinib (+) after 2-, 8-, 12- and 24-hours, displaying protein levels of Nfix, pERK, tot-ERK, and Vinculin as housekeeping gene (n=3). (B) Visual scheme of the chronic treatment protocol used to treat dystrophic animals. 0.3, 3 and 6 mg/kg of Trametinib was administered to adult *Sgca* null mice (5 weeks old) by oral gavage, every day for 14 days. (C) Graphs of variations in weight between *Sgca* null mice orally treated with Trametinib (0.3, 3 and 6 mg/kg) and DMSO as control, every day for 14 days. (D)

Representative Western Blots of protein extracts from *Tibialis anterior* muscles of *Sgca* null mice treated with 0.3, 3 and 6 mg/kg of Trametinib every day for 14 days, by oral gavage. Quantifications by densitometric analysis of Nfix and pERK/tot-ERK protein levels are depicted in the graphs below. Vinculin was used as housekeeping gene (\*\* P<0,001, # P=0.0595, \$ P=0.581; 3 mg/kg: Mann Whitney test; 0.3 mg/kg and 6 mg/kg: unpaired t-test, n=4 for DMSO and each concentration of Trametinib).

These data were also confirmed by immunofluorescence on *Tibialis anterior*. Notably, by immunofluorescence, indeed, we managed to identify Nfix+ nuclei *in situ* in muscle cells, where Nfix was less expressed in dystrophic *Tibialis anterior* upon treatment with 3 and 6 mg/kg of Trametinib than the control, with a statistically significant reduction of about 10% of Nfix+ nuclei (**Fig. 6A-B**). Interestingly, the *Nfix* expression did not change between Trametinib and DMSO-treated muscles, supporting the idea of a post-translational modulation of the Nfix protein by the MEK/ERK pathway as observed *in vitro* (**Fig. 6C, Fig. 3C**).

These experiments demonstrated that the chronic administration of Trametinib (3 and 6 mg/kg), every day for 14 days by oral gavage, leads to a constant inhibition of pERK and, consequently, a decrease in the Nfix protein in skeletal muscles of adult *Sgca* null mice. This treatment is not toxic for animals that displayed normal weight and behavior upon chronic administration of the drug.

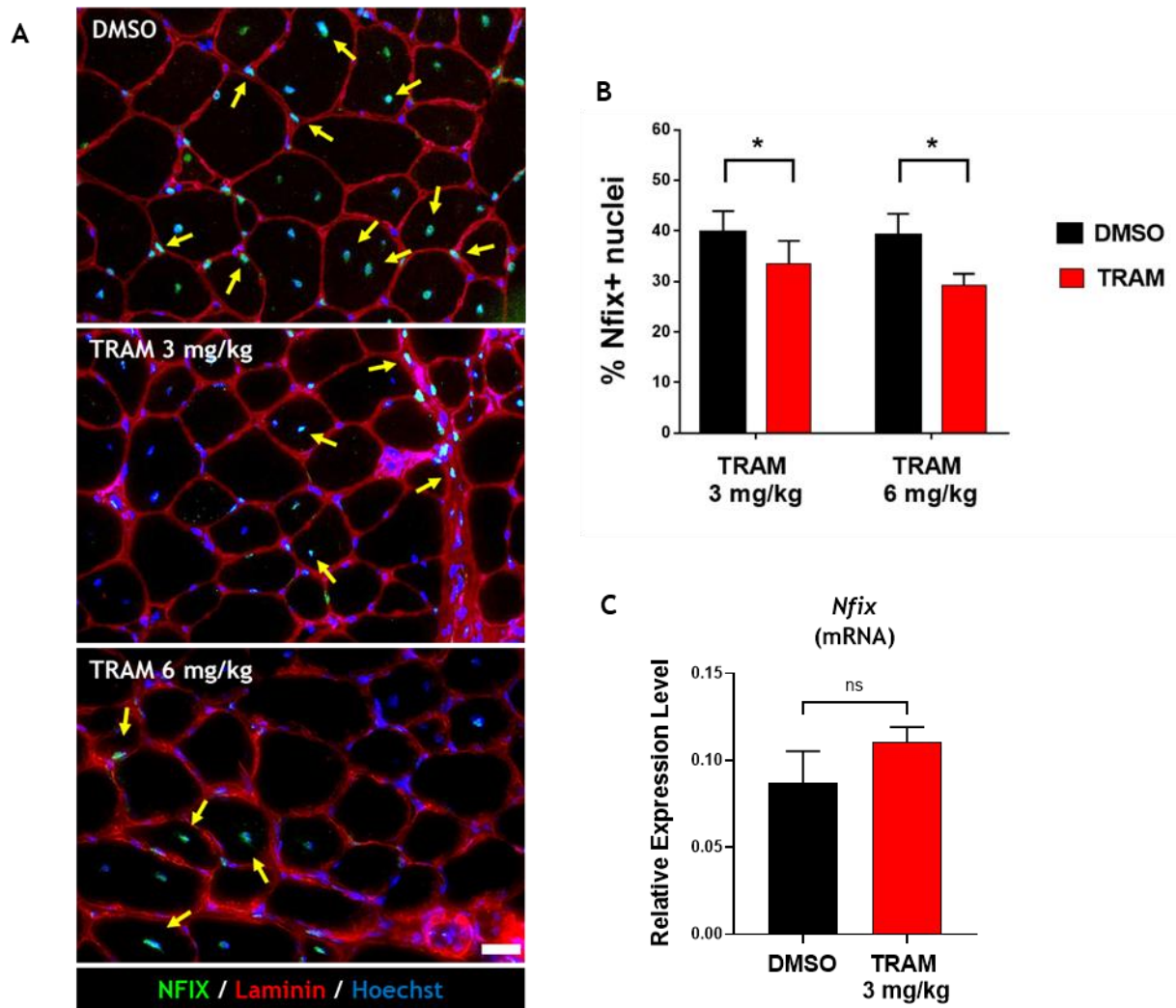


**Figure 6. Chronic treatment with Trametinib induces a reduction of Nfix+ cells in dystrophic muscles.** (A) Representative immunofluorescence images of *Tibialis anterior* muscles isolated from adult *Sgca* null mice treated with DMSO, 3 and 6 mg/kg Trametinib. Nfix+ nuclei are in green, Laminin is red, Hoechst staining for all the nuclei is in blue. (B) Graph depicting the percentage of Nfix+ nuclei on the total number of nuclei per section in 3 and 6 mg/kg Trametinib than DMSO (vehicle)-treated muscles (\*  $P < 0.05$ , Unpaired t-test with Welch's correction,  $n = 4$ ). (C) qRT-PCR for expression of *Nfix* in *Tibialis anterior* treated with vehicle (DMSO) or 3 mg/kg Trametinib every day for 14 days by oral gavage.  $\beta$ -actin was used as housekeeping gene (Unpaired t-test with Welch's correction,  $n = 3$ ).

### 3.2.3. TRAMETINIB-TREATED MUSCLES DISPLAY CALCIFICATIONS AND MORE OXIDATIVE MYOFIBERS

We demonstrated that the silencing of *Nfix* in *Sgca* null mice by a specific short-hairpin (shNfix) leads to histological improvements of dystrophy with reduced CSA of myofibers, increased centrally nucleated myofibers, decreased Collagen-I area, and a switch towards more oxidative myofibers. Muscles were analyzed 2 weeks after electroporation, suggesting that the genetic absence of Nfix in this time-window affects morphological parameters of *Sgca null* muscles (Rossi et al. 2017).

Therefore, we analyzed all the main histological markers of Trametinib-treated dystrophic muscles after 14 days of treatment to verify whether the reduction of Nfix upon MEK inhibition resulted in the amelioration of the disease.

Firstly, we evaluated the general histology of *Tibialis anterior* and Diaphragm after treatment with 3 and 6 mg/kg of Trametinib, which are the two dosages that allowed a good inhibition of both pERK and Nfix. Hematoxylin and Eosin (H&E) staining revealed that Trametinib-treated muscles exhibited a dystrophic phenotype like the control with infiltrating areas, necrotic myofibers, regenerating fibers. Furthermore, 6 mg/kg-treated muscles and 3 mg/kg-treated *Diaphragm* displayed visible histological alterations, like thick calcified myofibers that distinctly impaired muscle histology (**Figure 7A**). To attest whether calcifications are related to either the treatment or the *Sgca* null background, we treated age-matched WT mice with 3 mg/kg of Trametinib with the same protocol (every day for 14 days, by oral gavage). Interestingly, WT Diaphragm did not display calcified myofibers after the treatment with Trametinib, suggesting that a chronic MEK inhibition might lead to calcification only in dystrophic muscles (**Figure 7B**).

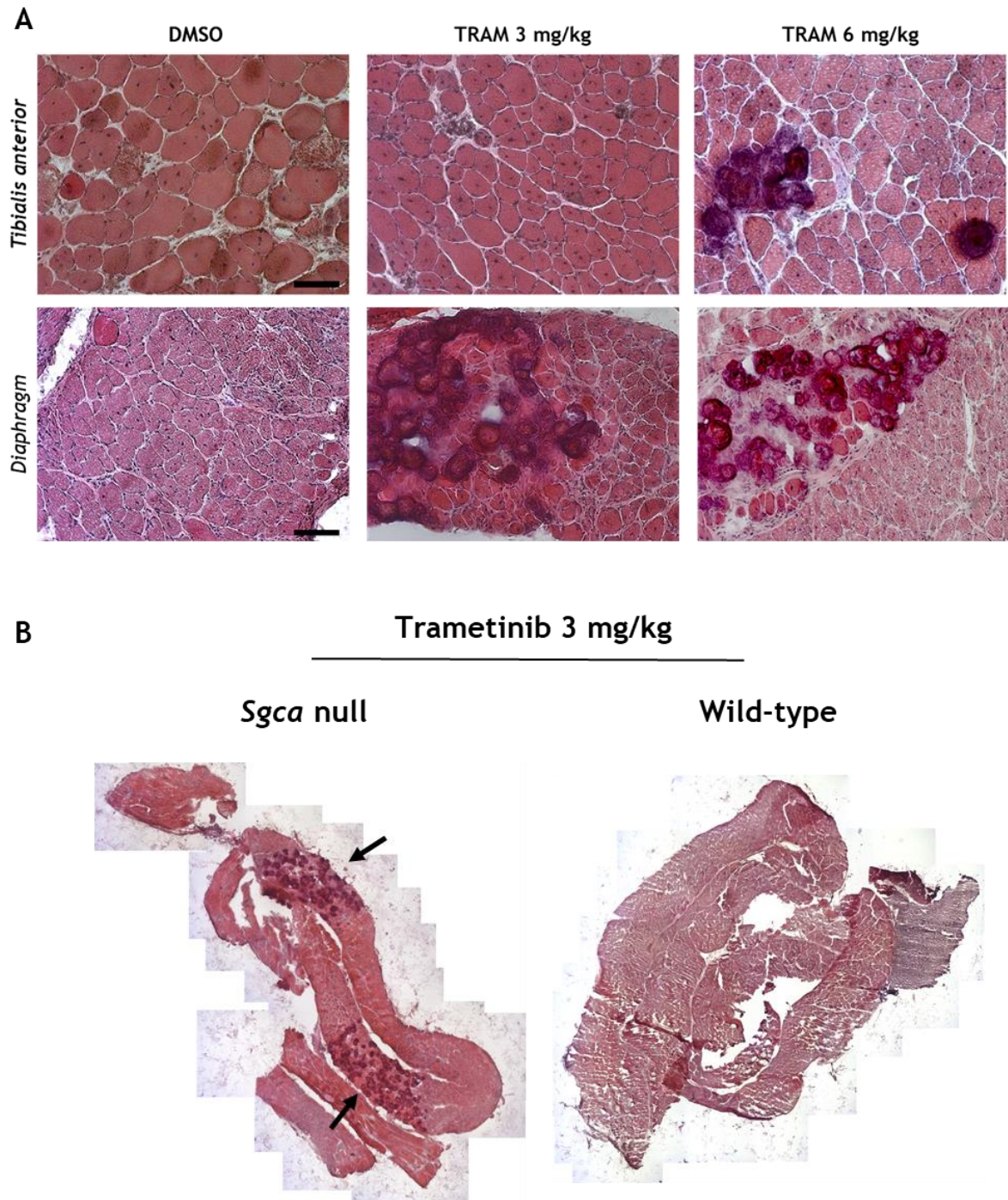


**Figure 7. Chronic treatment with Trametinib causes calcified myofibers in dystrophic muscles.**

(A) Hematoxylin and eosin (H&E) staining of *Tibialis anterior* (top) and Diaphragm (down) muscles treated with DMSO, 3 and 6 mg/kg of Trametinib every day for 14 days by oral gavage. Scale bar 100  $\mu$ m for *Tibialis anterior*, 200  $\mu$ m for Diaphragm (n=4 for each condition). (B) Entire Diaphragm muscle sections isolated from adult *Sgca* null and WT mice (5 weeks old) after oral treatment with 3 mg/kg of Trametinib every day for 14 days by oral gavage. Black arrows indicate areas with calcified myofibers (n=4 *Sgca* null mice and n=3 WT mice).

Since calcified myofibers highly altered the histology of treated muscle, we decided to focus on 3 mg/kg Trametinib-treated *Tibialis anterior* muscles, which had fewer calcified myofibers and a more analyzable histology. Fibrotic depositions, evaluated by Milligan's trichrome staining and Immunofluorescence for Collagen-I, was comparable with Trametinib and DMSO group. Therefore, Trametinib treatment did not improve fibrosis in dystrophic muscles (**Fig. 8**).

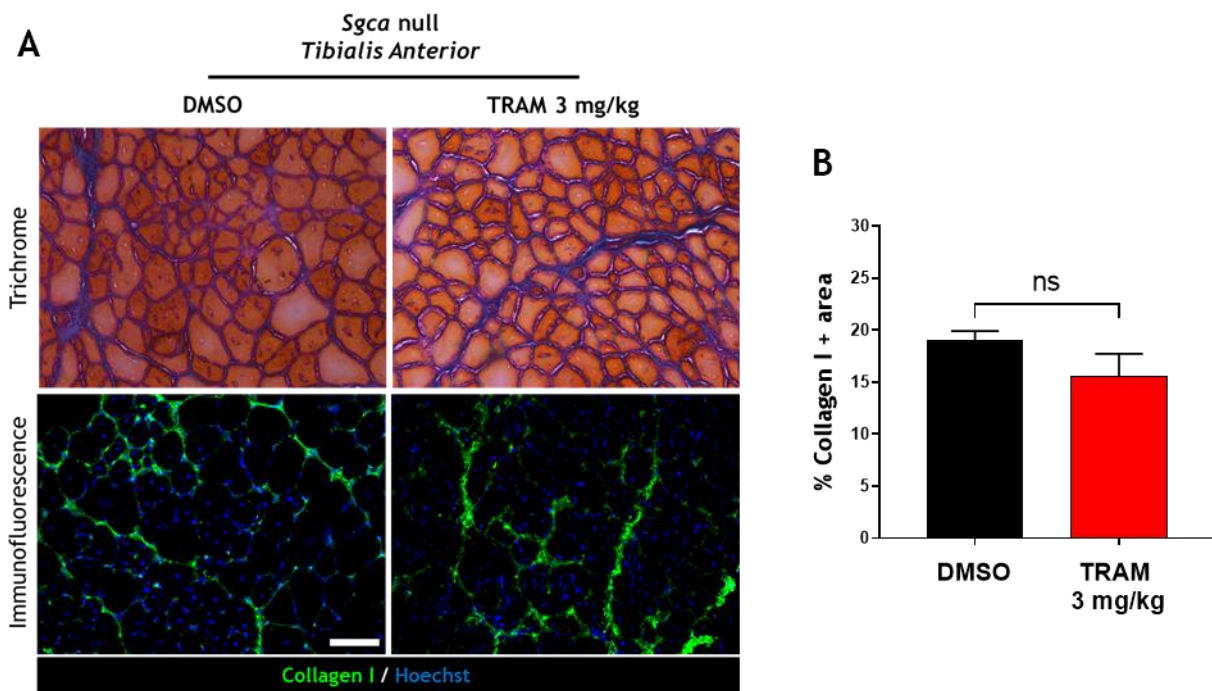


**Figure 8. Trametinib did not reduce fibrotic depositions in dystrophic muscle.**

(A) Milligan's trichrome staining and Immunofluorescence of Collagen I on *Tibialis anterior* muscles treated with DMSO and 3 mg/kg of Trametinib every day for 14 days by oral gavage. Scale bar 100  $\mu$ m (n=4 for each condition). (B) Quantification of Collagen-I<sup>+</sup> area of *Tibialis anterior* muscles chronically treated with DMSO and 3 mg/kg of Trametinib (Unpaired t-test with Welch's correction, n=4 for each condition).

Although *Nfix* null myofibers have smaller caliber than WT ones, *Sgca* null:*Nfix* null muscles present an increased cross-sectional area (CSA) and less centrally nucleated myofibers, indicating a delay in the regeneration process (Rossi et al. 2017). By contrast, dystrophic *Tibialis anterior* muscles chronically treated with 3 mg/kg Trametinib did not display changes in CSA, with a slight increase in small myofibers. A similar amount of centrally nucleated myofibers was measured in Trametinib-treated muscles compared to the control (**Fig. 9A-B**). Accumulation of Immunoglobulin G (IgG) inside dystrophic myofibers indicates inflammation, damages of the sarcolemma, and necrosis (Forcina, Cosentino, and Musarò 2020). We observed a higher number of IgG<sup>+</sup> myofibers in dystrophic muscles after treatment with Trametinib than DMSO, indicating high necrosis and

inflammation of treated muscle (**Fig. 9D**). Conversely, the number of infiltrating macrophages (F4/80+ cells) was similar between Trametinib and DMSO-treated muscles (**Fig. 9E**).

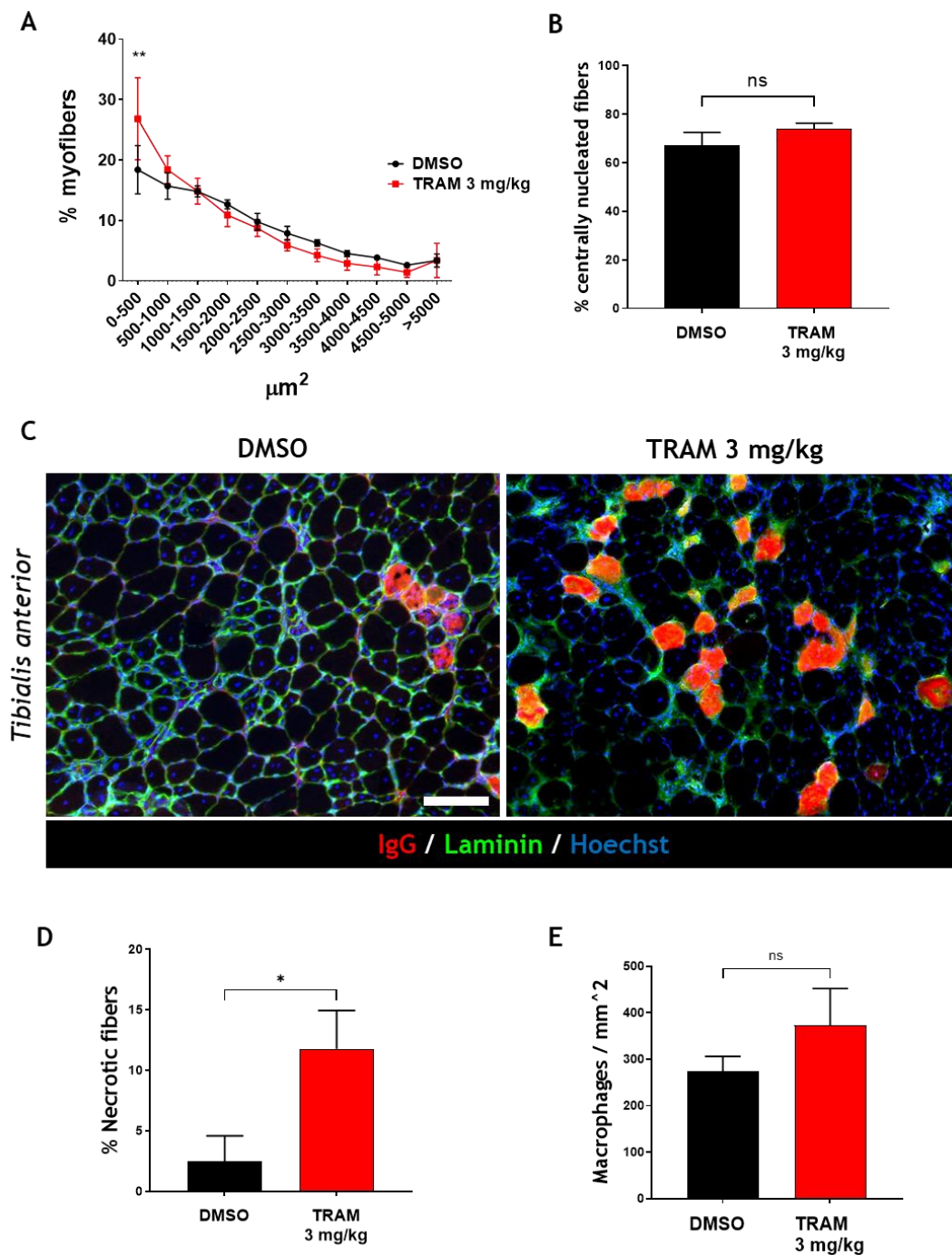


**Figure 9. Effect of Trametinib on caliber, regeneration, necrosis, and inflammation of dystrophic myofibers.**

Quantifications of (A) cross-sectional area distribution, (B) centrally nucleated myofibers, (D) IgG<sup>+</sup> or necrotic fibers, and (E) macrophages infiltration (F4/80+ cells) of *Sgca* null *Tibialis anterior* treated with DMSO (black line) and 3 mg/kg Trametinib (red bar/line) (\*\* P<0,001, one-way ANOVA test for CSA, Unpaired t-test with Welch's correction for B, D, E; n=4 for each condition). (C) Immunofluorescence against murine IgG (red)

and Laminin (green) of *Tibialis anterior* muscles chronically treated with DMSO and 3 mg/kg of Trametinib. Hoechst staining for all the nuclei is in blue (Scale bar 200  $\mu$ m; n=4 for each condition).

Dystrophic muscles lacking or being silenced for *Nfix* presented a more oxidative metabolism of myofibers (G. Messina et al. 2010; Rossi et al. 2017). To verify if Trametinib might have induced a similar phenotypical modulation, we performed the Succinate Dehydrogenase staining (SDH staining) by which oxidative myofibers are stained in blue. SDH staining revealed that chronic administration of 3 mg/kg Trametinib caused a slight switch towards oxidative phenotype of dystrophic myofibers. This was also confirmed by the expression levels of genes associated to oxidative metabolism. Indeed, there was an increasing trend of the *Sdha*, *Sdhb*, and *Cox5* expression in Trametinib-treated dystrophic *Tibialis anterior* than the control, although not statistically significant (**Fig. 10**).

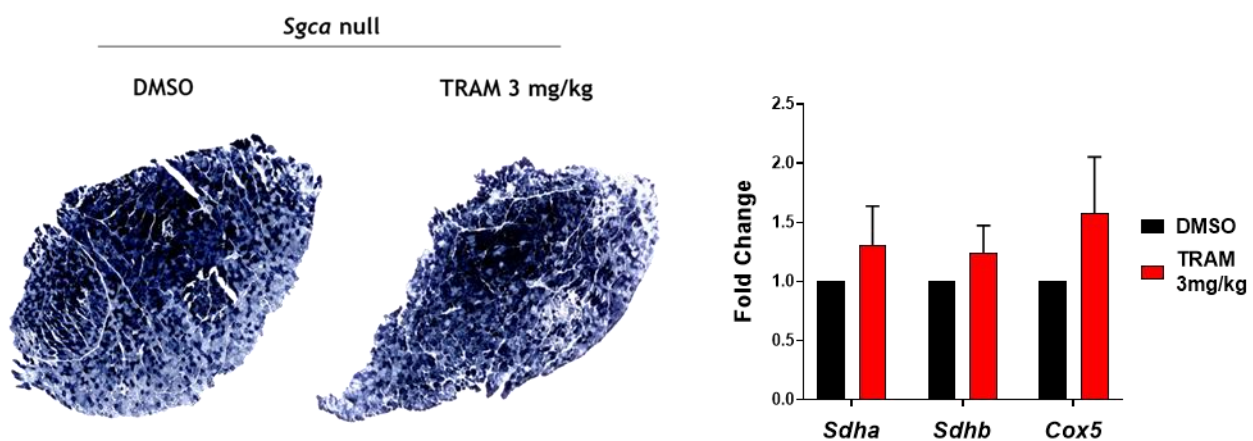


**Figure 10. Oxidative metabolism of dystrophic muscles upon treatment with Trametinib.**

On the left, SDH staining on entire *Sgca* null *Tibialis anterior* muscle sections upon chronic treatment with Trametinib or DMSO. On the right, qRT-PCR for expression of *Sdha*, *Sdhb*, *Cox5* in *Tibialis anterior* treated with DMSO or 3 mg/kg Trametinib every day for 14 days by oral gavage.  $\beta$ -actin was used as housekeeping gene (Unpaired t-test with Welch's correction, n=3)

In conclusion, these experiments provided a proof-of-concept about *Nfix* modulation by the MEK/ERK pathway in postnatal dystrophic muscles *in vivo*. Chronic administration of Trametinib, every day for 14 days by oral gavage, to adult *Sgca* null mice reduces the *Nfix* protein levels in skeletal muscles. However, this reduction is not sufficient to improve the histology of dystrophic muscles, which display smaller myofibers, higher necrosis, and unexpectedly, calcification at high dosages of the drug. Nevertheless, Trametinib-treated myofibers seems to be more prone to the

phenotypical switch towards oxidative metabolism, which is known to be more protected from dystrophic damages (see Section 2.2.3).

Further analyses are necessary to understand the nature and the origin of calcified myofibers, with the aim of avoiding their generation. The development of alternative protocol of administration or combining Trametinib with other drugs, even by changing the type of MEK-inhibitor, might be useful to reduce both Nfix levels and calcified myofibers upon treatment in dystrophic muscle.

### **3.3. EVALUATION OF SELUMETINIB, A MEK-INHIBITOR ALREADY USED FOR MUSCULAR DYSTROPHY, IN DECREASING NFIX LEVELS**

Selumetinib is a MEK-inhibitor used in preclinical studies as a potential treatment for cancer and cachexia (Li et al. 2016). In a phase II clinical trial (NCT02407405), Selumetinib was tested against Neurofibromatosis Type 1 thanks to its ability to inhibit the MEK/ERK pathway which is particularly active in this type of cancer.

Recently, Selumetinib was tested in a murine model of Emery-Dreifuss Muscular Dystrophy (EDMD) with promising results. EDMD is caused by mutation in the lamin A/C gene (*Lmna*), encoding the A-type nuclear lamins in the internal side of nuclear envelope. Muchir et al. observed that murine EDMD muscles have higher amount of pERK than WT ones, indicating that MEK/ERK pathway is active in this type of dystrophy. After a chronic treatment with Selumetinib, murine EDMD muscles displayed improvements in histology and increased CSA, indicating a general rescue of normal muscle morphology (Muchir et al. 2013).

Therefore, we decided to treat *Sgca* null mice with Selumetinib which have a beneficial role in EDMD muscles. We followed a similar treatment protocol used for Trametinib and in a mouse model of cancer cachexia (Yang et al. 2017), administrating 25 mg/kg of Selumetinib or DMSO every day for 14 days by oral gavage.

#### **3.3.1. SELUMETINIB DECREASES pERK AND NFIX IN DYSTROPHIC MUSCLES**

As done for Trametinib, Selumetinib-treated mice were daily checked, and their weight measured to evaluate the general health of animals. We did not observe loss nor differences of weight with respect to control group (DMSO) during the treatment (**Fig. 11A**). Moreover, chronic treatment with Selumetinib caused a significant decrease of both pERK protein and Nfix-positive nuclei in *Tibialis anterior* muscles as much as Trametinib-treated muscles (**Fig. 11B-D**). Thereby, the oral administration of Selumetinib, every day for 14 days, decreased the Nfix protein levels in muscle at the same extent of Trametinib, without affecting the general health of dystrophic mice. These results

further confirm the Nfix modulation by MEK/ERK pathways in postnatal dystrophic muscles, regardless the MEK-inhibitor used.

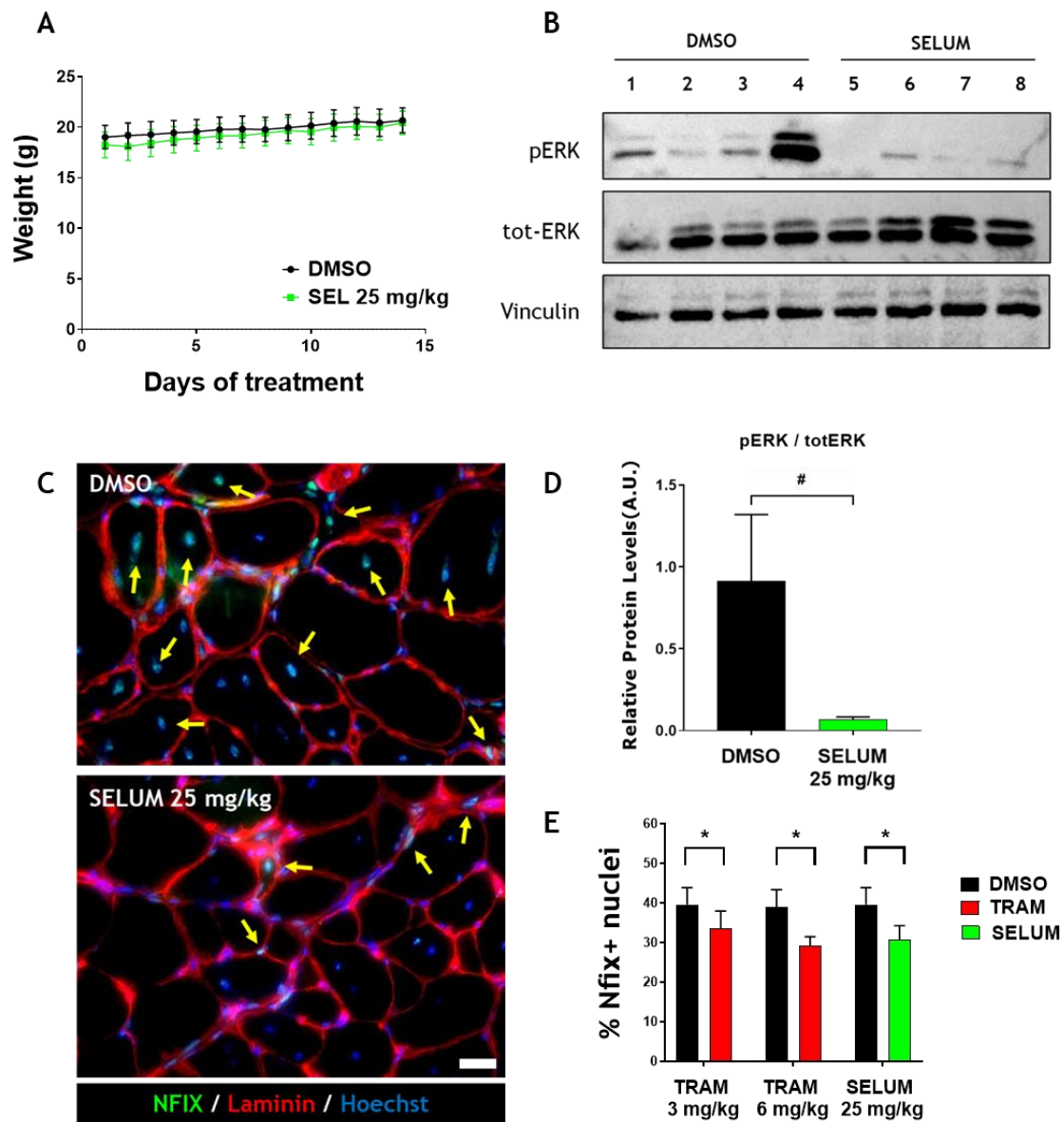


**Figure 11. Effect of chronic treatment with Selumetinib on mouse weight, pERK and Nfix.**

(A) Graphs of variations in weight between *Sgca* null mice orally treated with Selumetinib (25 mg/kg) and DMSO as control, every day for 14 days (n=4 for Selumetinib and DMSO group). (B) Representative Western Blots and relative quantification (D) of protein extracts from Selumetinib (SELUM) and DMSO treated *Tibialis anterior* muscles, displaying protein levels of Nfix, pERK, tot-ERK, and Vinculin as housekeeping gene (# P=0.061, Unpaired t-test with Welch's correction, n=4). (C) Representative immunofluorescence images of *Tibialis anterior* muscles treated with DMSO or 25 mg/kg Selumetinib. Nfix+ nuclei are in green, Laminin is red, Hoechst staining for all the nuclei is in blue. (D) Graphs depicting the percentage of Nfix+ nuclei on the total number of nuclei per section in 25 mg/kg Selumetinib than DMSO (vehicle)-treated muscles (top) and Trametinib-treated muscles (down) (\* P<0.05, Unpaired t-test with Welch's correction, n=4).

### 3.3.2. CHRONIC TREATMENT WITH SELUMETINIB HAS DIFFERENT EFFECTS ON THE HISTOLOGY OF DYSTROPHIC MUSCLES THAN TRAMETINIB

Despite the effect, although partial, on Nfix protein levels, as observed for Trametinib the chronic treatment with Selumetinib in dystrophic muscles did not display general morphological improvements. Selumetinib-treated muscles exhibited histological hallmarks typical of muscular dystrophy: necrotic fibers, infiltrating areas, heterogeneous caliber of myofibers. As what we observed for 3 mg/kg Trametinib, calcified myofibers are very few in *Tibialis anterior* but abundant in Diaphragm muscles upon Selumetinib administration (**Fig. 12**). Therefore, we have focused on *Tibialis anterior* to perform further histological analysis.

Milligan's trichrome staining and Immunofluorescence of Collagen-I revealed no differences in fibrotic depositions between the Selumetinib and DMSO group, confirming that Selumetinib did not improve fibrosis in muscular dystrophy (**Fig. 13**).

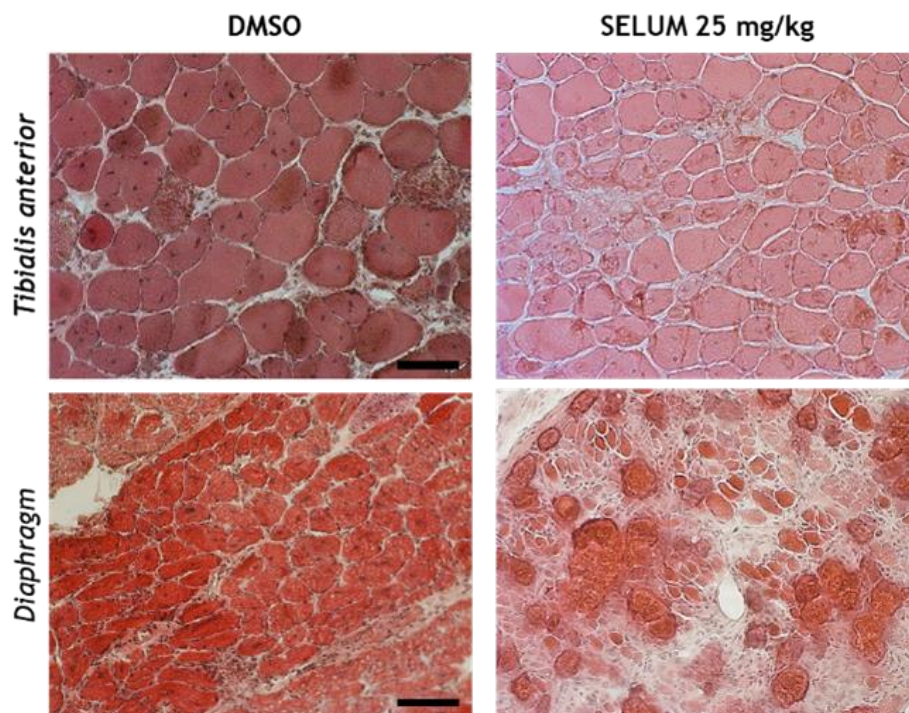


**Figure 12. Chronic treatment with Selumetinib causes calcified myofibers in dystrophic Diaphragm.** Hematoxylin and eosin (H&E) staining of *Sgca* null *Tibialis anterior* (top) and Diaphragm (down) muscles treated with DMSO and 25 mg/kg of Selumetinib every day for 14 days by oral gavage. Scale bar 100  $\mu$ m for *Tibialis anterior*, 200  $\mu$ m for Diaphragm (n=4 for each condition).

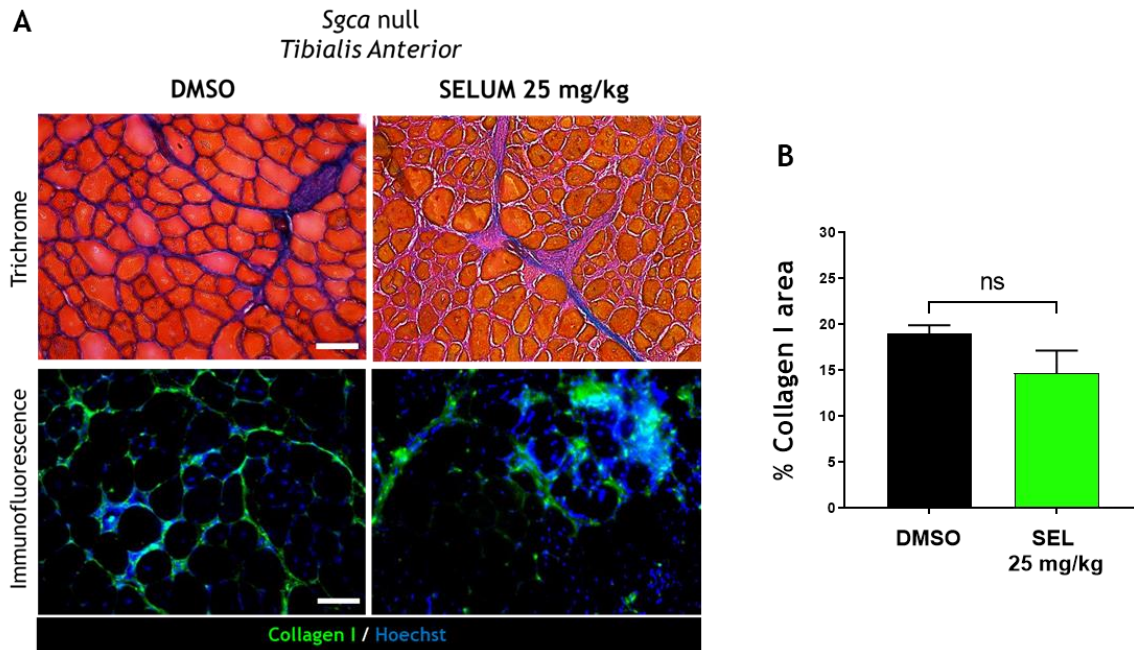


**Figure 13. Selumetinib did not reduce fibrosis in dystrophic *Tibialis anterior* muscles.**

(A) Milligan's trichrome staining and Immunofluorescence of Collagen I on *Tibialis anterior* muscles treated with DMSO and 25 mg/kg of Selumetinib every day for 14 days by oral gavage. Scale bar 100  $\mu$ m (n=4 for each condition). (B) Quantification of Collagen-I<sup>+</sup> area of *Tibialis anterior* muscles chronically treated with DMSO and 25 mg/kg of Selumetinib (Unpaired t-test with Welch's correction, n=4 for each condition).

As observed for Trametinib, Selumetinib-treated animals did not show any improvements in CSA distribution and necrosis of myofibers. After the treatment with Selumetinib, dystrophic *Tibialis anterior* exhibited no remarkable changes in fiber caliber (Fig. 14A) and a higher amount of IgG-positive myofibers than the control (Fig. 14C-D). However, centrally nucleated myofibers were significantly less in Selumetinib-treated muscles than the DMSO group (Fig. 14B), resembling the delay in regeneration observed in *Sgca* null:*Nfix* null phenotype (Rossi et al. 2017).

Despite the treatment with Trametinib did not lead to a significant increase of macrophages in dystrophic muscles (Fig. 9E), Selumetinib-treated *Tibialis anterior* displayed higher number of infiltrated macrophages (F4/80+ cells) than the control, indicating a worsening of inflammation inside the treated muscles (Fig. 14E).

Concerning the metabolism of myofibers, we noticed a slight increase of SDH-positive myofibers in dystrophic muscles after the chronic treatment with Selumetinib. Like what we observed with Trametinib, the chronic inhibition of the MEK/ERK pathway in a dystrophic context leads to a slight switch towards oxidative phenotype of dystrophic myofibers (Fig. 10, Fig.15).

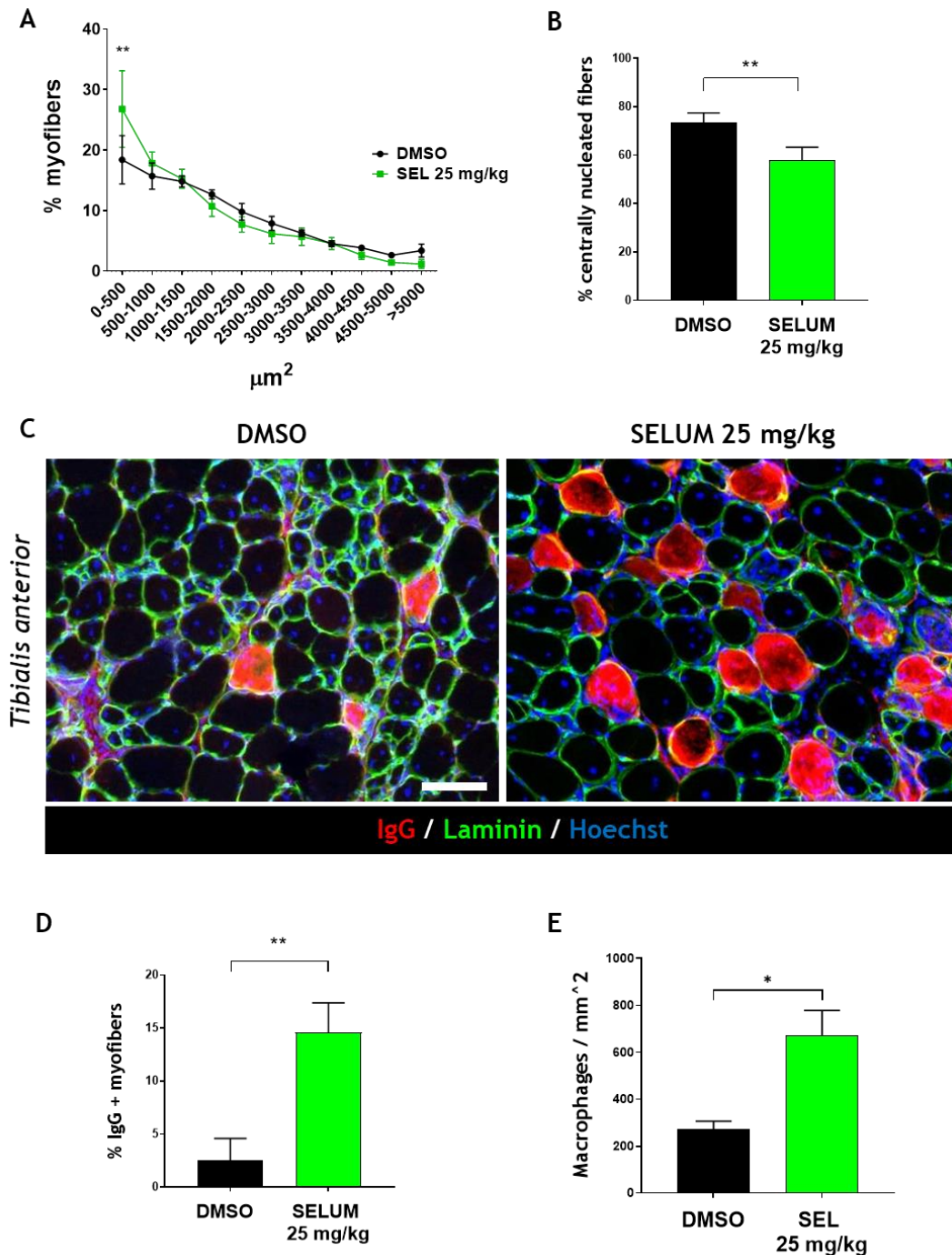


**Figure 14. Effect of Selumetinib on caliber, regeneration, necrosis, and inflammation of dystrophic myofibers.**

Quantifications of (A) cross-sectional area distribution, (B) centrally nucleated myofibers, (D) IgG<sup>+</sup> or necrotic fibers, and (E) macrophages infiltration (F4/80+ cells) of *Sgca* null *Tibialis anterior* treated with DMSO (black line) and 25 mg/kg Selumetinib (green bar/line) (\* P<0.05, \*\* P<0,001, one-way ANOVA test for CSA, Unpaired t-test with Welch's correction for B, D, E; n=4 for each condition). (C) Immunofluorescence against murine IgG (red) and Laminin (green) of *Tibialis anterior* muscles chronically treated with DMSO and 25 mg/kg of Selumetinib. Hoechst staining for all the nuclei is in blue (Scale bar 100 µm; n=4 for each condition).

## *Sgca* null

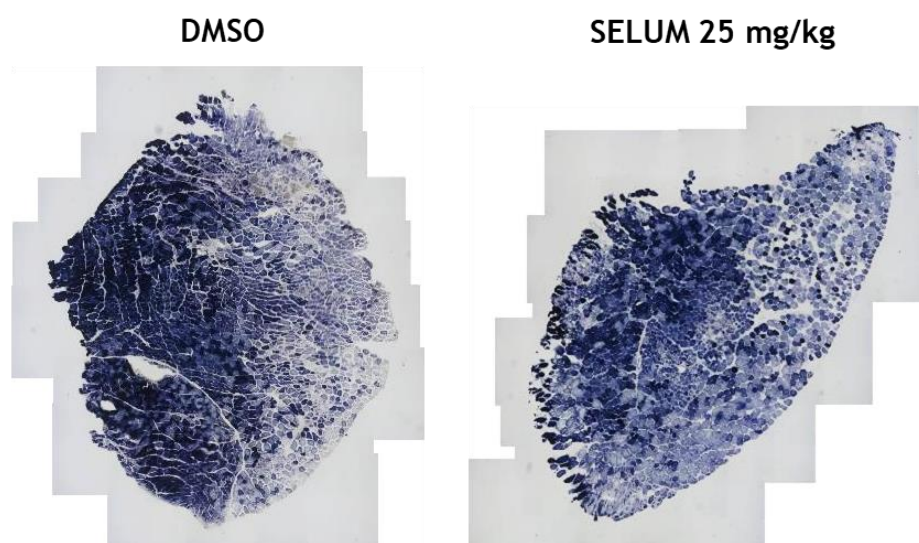


**Figure 15. Oxidative metabolism of dystrophic muscles upon treatment with Selumetinib.** SDH staining on entire *Sgca* null *Tibialis anterior* muscle sections upon chronic treatment with 25 mg/kg Selumetinib or DMSO (n=4).

To sum up, we have demonstrated that the transcription factor Nfix is regulated by the MEK/ERK signaling pathway in muscle cells during both fetal and postnatal period. Indeed, the inhibition of MEK through two different MEK-inhibitors, Trametinib and Selumetinib, leads to a decrease in the Nfix protein levels in myoblasts *in vitro* and in dystrophic muscles *in vivo*. The reduction of the Nfix protein upon MEK inhibition is not caused by a decrease in the *Nfix* gene expression, indicating the involvement of post-translational rather than transcriptional mechanisms of regulation.

However, the reduction of Nfix in treated dystrophic muscles was not sufficient to have ameliorations of muscular histology, as observed in *Sgca* null:*Nfix* null mice and in *Sgca* null muscles after the silencing of *Nfix*. On the contrary, the chronic treatment with both Trametinib and Selumetinib causes a slight decrease in cross-sectional area and an increase of necrotic myofibers in dystrophic muscles, which are negative histological hallmarks in muscular dystrophy. Moreover, the chronic inhibition of MEK/ERK pathway in dystrophic muscles causes the generation of calcified myofibers, which alter the muscular histology of Diaphragm, in particular. Further analyses are necessary to understand whether these histological alterations are related to either the *Sgca* null genetic background or the dystrophic context *per se*.

On the other hand, the pharmacological inhibition of MEK leads to a slight switch towards oxidative metabolism of dystrophic myofibers, which are more protected from damages than glycolytic fibers.

These results support the idea that a small reduction in the Nfix protein through the MEK/ERK inhibition is sufficient to affect the muscle metabolism.

To make the puzzle even more complicated, Selumetinib also induces an increase of infiltrated macrophages and a reduction in centrally nucleated myofibers. Therefore, despite a common molecular mechanism (MEK inhibition), Trametinib and Selumetinib might affect alternative signaling pathways, leading to different effects on muscular dystrophy.

#### 4. CONCLUSIONS AND FUTURE PERSPECTIVES

The transcription factor Nfix is involved in both prenatal development (G. Messina et al. 2010) and postnatal regeneration (Rossi et al. 2016) of skeletal muscle tissue. In embryonic and adult myoblasts, Nfix acts as modulator of cell differentiation, supporting the progression of prenatal and adult myogenesis. This role is particularly detrimental in the dystrophic context, where vicious cycles of degeneration/regeneration of myofibers lead to a premature exhaustion of MuSC pool and loss of muscle regenerative capacity. Indeed, we demonstrated that delaying rather than boosting muscle regeneration by decreasing *Nfix* expression is beneficial for dystrophic muscle, resulting in functional and histological ameliorations (Rossi et al. 2017).

Our efforts in these years were focused on delineating the regulatory network underlying Nfix at both transcriptional and post-translational levels in muscle cells. Recently, we provided experimental evidence that the RhoA/ROCK and the MEK/ERK pathways modulate the Nfix levels during embryo and fetal myogenesis, both *in vitro* and *in vivo* (Taglietti et al. 2018). In particular, the RhoA/ROCK pathway inhibits Nfix expression in embryonic myoblasts, while the MEK/ERK pathway positively modulates Nfix in fetal myoblasts. In postnatal myoblasts, only the Nfix modulation by the MEK/ERK pathway is conserved, revealing that the signaling network underlying Nfix in myoblasts is different between prenatal and postnatal period. The specific inhibition of MEK by PD98059 leads to a decrease of the Nfix protein levels in MuSC-derived myoblasts. This inhibition does not impinge on proliferation or apoptosis of treated cells, which display a delayed myogenic differentiation because of decreased Nfix levels. Interestingly, the *Nfix* mRNA is not reduced after the MEK inhibition, suggesting a post-translational rather than transcriptional regulation of Nfix protein by the MEK/ERK pathway in myoblasts. Specific analyses on post-translational modifications of the Nfix protein might provide numerous insights about its regulation and function.

These promising *in vitro* experiments encouraged us to develop a pharmacological approach to inhibit Nfix also *in vivo*, particularly in adult dystrophic mice where Nfix plays a deleterious role in the progression of the pathology. The MAPK pathway mediates several signals for cell survival and proliferation. Indeed, the MEK/ERK signaling cascade is highly activated in cancer, where gain-of-function mutations in the RAS GTPase and RAF kinase (the starting point of the MAPK pathway) are the main cause of oncogenic transformation (Nickols et al. 2019). Basing on preclinical and clinical trials, we selected two FDA-approved MEK-inhibitors, Trametinib and Selumetinib, which have more suitable pharmacological features for preclinical and clinical trials than PD98059 (Montagut and Settleman 2009). Moreover, several studies confirmed the inability of these MEK-inhibitors to target the brain (where Nfix has a crucial function in regulating differentiation of

neuronal stem cells), making these drugs suited for a pharmacological repurposing in muscular dystrophy (Gilmartin et al. 2011).

By chronic treatment with Trametinib and Selumetinib of *Sgca* null mice, we provided the proof-of-concept that Nfix is modulated by the MEK/ERK pathway in adult dystrophic muscles, as in the fetal period. Specifically, chronic treatment with MEK-inhibitors caused the decrease of Nfix protein levels and Nfix+ nuclei in *Sgca* null muscles. Specific IF double-staining with anti-Nfix and anti-Pax7, -MyoD, or -MyoG antibodies might be useful to identify in which muscle cells the MAPK pathway mainly modulates Nfix *in vivo*. This modulation occurs at post-translational levels, confirming what we observed after the treatment with the MEK-inhibitor of myoblasts *in vitro*. The regulation of Nfix by the MEK/ERK pathway might be also useful in other pathological contexts. Specifically, a recent Phase II clinical trial (NCT02881242) has revealed the efficacy of Trametinib as monotherapy in patients affected by untreatable prostate cancer (Nickols et al. 2019). Intriguingly, Nfix, together with Nfib, has an oncogenic activity in the stroma of prostatic cancer, acting on the chromatin access of specific target genes that promote tumor proliferation (Grabowska et al. 2016). Analyzing the pERK-Nfix interaction in cancer or other cell types might help to unveil similar molecular mechanism also in myoblasts.

The resulting reduction of the Nfix protein upon the treatment with Selumetinib and Trametinib was not sufficient to improve the histology of dystrophic muscles, which display no evident ameliorations of the main histological hallmarks. These results might be explained by different aspects.

Firstly, two weeks of drug administration might be not sufficient, and a longer period of treatment might progressively decrease the Nfix protein levels. Indeed, the kinetic of pERK activity is very rapid as well as the phosphorylation dynamics of its substrates (Ahmed et al. 2014). Therefore, a constant and longer inhibition of MEK activity might be directly or indirectly affect the Nfix protein stability.

Secondly, the reduction of Nfix protein might be not sufficient to lead changes in expression of its target genes. While some target genes of Nfix in prenatal myoblasts are known, only myostatin (*Mstn*) was identified as a direct target gene of Nfix by ChIP analysis in postnatal myoblasts, so far. Over-expressing Nfix in adult myoblasts leads to a reduced expression of *myostatin*, indicating a trans-repression activity of Nfix on this gene (Rossi et al., 2016). Therefore, it would be interesting to verify any changes in myostatin expression in untreated (DMSO) and treated (MEK-inhibitor) muscles.

Thirdly, the adult dystrophic mice might have a too compromised muscle tissue, hiding the ameliorations related to reduction of Nfix by the inhibition of the MEK/ERK cascade. Thereby, an early MEK inhibition in neonatal mice (P10) might be helpful to have a higher decrease of Nfix in muscles and more evident histological ameliorations of the disease.

Fourthly, the group of MEK-inhibitors is very heterogenous and it is composed by a variety of drugs which, despite a common molecular mechanism on inhibiting MEK1/2 activity, differ in their indirect action on other parallel signaling pathways and in pharmacokinetic properties (Santos and Crespo 2018; Yuan et al. 2020). Whereby, the MEK inhibition in dystrophic muscles might stimulate alternative/compensatory signaling pathways that counteract the decrease of Nfix, acting on other NFIs and/or cell types (FAPs, macrophages, endothelial cells, etc.). Further analyses on parallel MAPK pathways (like JNK and p38 signaling pathways), that have numerous overlaps with the MEK/ERK pathway, might be useful to address this point.

This hypothesis is supported by the arising of calcified myofibers after MEK inhibition in a dystrophic context only, revealing a correlation between this signaling pathway and muscular dystrophy. Interestingly, similar calcified myofibers were observed in a mouse model of muscular dystrophy, called *mdx* <sup>$\beta$ geo</sup>, in which all the *dystrophin* isoforms (short and long isoforms) are completely deleted (Young et al. 2020). Together with the well-known role of dystrophin as scaffold for the MEK/ERK pathway (Spence et al. 2004), the treatment with MEK-inhibitors of *mdx* mice might provide important insights on the origin of these calcifications. Furthermore, the treatment of juvenile *Sgca* null myoblasts *in vitro* might be important to verify whether the genetic dystrophic background affects the link between pERK and Nfix.

Notably, chronic treatment with both Trametinib and Selumetinib caused a slight increase of myofibers with an oxidative metabolism. In our lab a similar but more evident result was observed in two models of muscular dystrophy in which Nfix is genetic ablated or silenced (*Sgca* null:*Nfix* null and *Sgca* null electroporated with shNfix, respectively) (Rossi et al. 2017). These data might suggest a concentration-dependent effect of Nfix on target genes that regulate the metabolic switch of myofibers towards oxidative metabolism. Several transcription factors, particularly those involved in the regulation of chromatin access, exert a concentration-dependent effects on gene expression (Lundgren et al. 2000). This might reveal a role of Nfix as chromatin modifier also in myoblasts and/or myofibers, as observed in stem cells of the hair follicle (Adam et al. 2020).

Myofibers with an oxidative metabolism express a higher amount of antioxidant enzymes (like catalase, glutathione peroxidase, superoxide dismutase) to balance the redox environment. Thanks to their expression profile, slow-twitch oxidized myofibers are more protected from oxidative-stress induced damages which cause necrosis in muscular dystrophy (Danieli-Betto et al. 2005; Kozakowska et al. 2015). Last year, we demonstrated that a cyanidin-rich diet, provided at weaning for 5 weeks, is beneficial to reduce inflammation and oxidative stress in muscles of adult *Sgca* null mice. Cyanidin belongs to the group of anthocyanins, which are well-known anti-inflammatory and antioxidant compounds produced by red-pigmented plants and fruits. Thanks to the cyanidin intake

through the diet, dystrophic muscles displayed morphological and functional improvements of the disease, and a switch towards more oxidative phenotype of myofibers (M. Saclier et al. 2020). A little is known about the molecular mechanism at the basis of cyanidin effects on skeletal muscles, however we observed an enhanced mitochondria biogenesis, reduced macrophage inflammation and increased MyHC-I expression after dietary supplementation with cyanidin (M. Saclier et al. 2020). Intriguingly, cyanidin-rich diet also caused a reduction in Nfix<sup>+</sup> nuclei in skeletal muscles (data not shown) which might explain the histological ameliorations observed.

In mice, a purple corn diet for 5 weeks was sufficient to avoid cardiotoxic toxicity of doxorubicin, a chemotherapeutic agent used for the treatment of breast cancer (Petroni et al. 2017). Since chronic treatment with MEK-inhibitors of *Sgca* null mice caused high inflammation and macrophage infiltration in myofibers (particularly with Selumetinib), combining this treatment with the cyanidin-rich diet, acting on the redox environment and chronic inflammation, might be a rational method to overcome these issues. It would be interesting to verify whether the combination between cyanidin and Trametinib/Selumetinib might also prevent genesis of calcified myofibers.

As said above, our gold-standards are two models of *Sgca* null mice in which Nfix is genetic deleted or silenced (*Sgca* null:*Nfix* null and *Sgca* null with shNfix, respectively). Therefore, delivering the shNfix to dystrophic muscles by a non-viral system might be a parallel and/or alternative therapeutic strategy (Baltusnikas et al. 2017). Due to the scant availability of AAV serotypes with a muscle tropism for the gene therapy of muscular dystrophy (Galli et al. 2018), we are trying to develop non-viral nanocarriers (cationic liposomes) carrying a plasmid with the shNfix expression cassette and a reporter gene. Thanks to a collaboration with University of Padua, we would like to add some muscle receptor-binding ligands on the surface of liposomes to improve their tropism on muscle. *In vitro* experiments are ongoing with encouraging results.

The silencing of *Nfix* is not resolutive for muscular dystrophy because it does not replace or correct the mutation underlying the disease. However, decreasing the Nfix levels improves the quality of muscle tissue, which is critical for further therapeutic interventions. Therefore, a multi-disciplinary and multi-level approach seems to be the most promising therapeutic strategy for such heterogeneous diseases.

## 5. MATERIALS AND METHODS

### 5.1. CELL ISOLATION AND CULTURES

Juvenile MuSC-derived myoblasts were isolated from WT (CD1) pups at postnatal day 10 (P10). All hindlimb muscles were collected from each mouse and placed into 5 ml of DF50 medium (Dulbecco's Modified Eagle Medium, 50% Fetal Bovine Serum Gibco 10270-106, 1% Penicillin/Streptomycin Euroclone ECB3001D). Non-muscular tissues were removed from muscles under a stereomicroscope, in sterile conditions. Then, muscles were mechanically and enzymatically digested for 20 min at 37°C under strong agitation with 1.5 mg/ml Dispase (Gibco 17105041), 0.15 mg/ml Collagenase (Sigma C9263), and 0.1 mg/ml DNase I (Roche 11284932001) in PBS 1X (EuroClone ECB4004L). After every digestion cycle, dissociated cells were collected in DF10 (DMEM, 10% FBS, 1% P/S, 1% L-Glutamine EuroClone ECB30000D) at 4°C to inactivate the enzymes. Once all the digestion cycles have finished and all cells have been gathered in the same tubes, they were centrifuged at 300 rcf for 5 minutes at 4°C. The pellet was resuspended in 10 ml of DF10 and filtered using the 70- $\mu$ m filter first, then the 40- $\mu$ m filter. Filtered cells were centrifuged at 300 rcf for 5 minutes at 4°C, and the supernatant was discarded.

Cell pellet was resuspended in 80  $\mu$ l per gram of tissue of MACS Buffer (phosphate-buffered saline, pH 7.2, 0.5% bovine serum albumin, 2 mM EDTA) and 20  $\mu$ l of Satellite Cell Isolation Kit per gram of tissue (Miltenyi Biotec, 130-104-268). The mixture was incubated at 4°C, for 15 minutes and then magnetically separated follow the specific protocol. The flow-through, which contains the myogenic cells, was collected and centrifuged at 300 rcf for 5 minutes.

Then, the cell pellet was resuspended in proliferation medium for satellite cells (DMEM, 20% FBS, 10% Horse Serum Euroclone ECS0090L, 1% P/S, 1% L-Glutamine, 0.1% Gentamycin Sigma G1397, 2,5 ng/ml  $\beta$ -FGF Peprotech 100-18B) and counted using a Burker chamber. 30.000 cells were plated on collagen-coated  $\varnothing$ =90 mm dishes (about 8 ml per dish) and incubated at 37°C for 48 h. The proliferation medium was completely replaced after 24 h.

After two days (48h), cells were washed twice with Dulbecco's Phosphate Buffered Saline 1X (PBS, EuroClone ECB4004L). 1 ml of diluted Trypsin (1:1 with PBS 1X, Sigma T4174) was added to allow detachment of MuSC-derived myoblasts. The cells were incubated for 1-2 minutes at 37°C. The trypsinization was then quickly blocked by addition of 5 ml of FBS-containing medium, which were used to collect all the cells. The gathered cells were then centrifuged at 300 rcf for 5 minutes, the pellet was resuspended in an adequate volume of proliferation medium, and then counted using a Burker chamber. Cells were plated in collagen-coated  $\varnothing$ =35mm petri dishes at about 5000 cells/cm<sup>2</sup> in 2 ml of proliferation medium and incubated at 37°C.

### **5.1.1. *IN VITRO* TREATMENT**

PD98059 (Cell signaling) and Y27632 (Calbiochem) were dissolved in dimethyl sulfoxide (DMSO) and added to myoblasts at 50  $\mu$ M and 10  $\mu$ g/ml, respectively, for 16 h, at 37°C, 5% CO<sub>2</sub>.

Trametinib (GSK1120212, Mekinist®) and Selumetinib (AZD6244) were purchased from Selleckchem and dissolved in DMSO at stock dilutions of 12 mg/ml and 30 mg/ml, respectively, under sterile conditions. Trametinib was added at different concentrations to juvenile MuSC-derived myoblasts, for 14 h. For each experimental condition, cells treated with 0.1% DMSO were the control. After the treatment, the cells allocated for molecular biology studies (protein or RNA extraction) were washed twice with cold PBS 1X and frozen at -20°C. For immunofluorescence assays, cells were briefly washed with PBS 1X at room temperature (RT) and immediately fixed (see immunofluorescence protocol).

## **5.2. ANIMAL MODELS**

For the *in vivo* experiments, we used the  $\alpha$ -sarcoglycan-deficient dystrophic mouse model (*Sgca* null mice) generated by Duclos et al. in 1998 as a model of muscular dystrophy.

All mice were maintained under pathogen-free conditions with a 12h/12-h light/dark cycles. All the experimental procedures were carried out in accordance with the Italian law (D. Lgs n. 2014/26, implementation of 2010/63/UE) and approved by the University of Milan Animal Welfare Body and by the Italian Health Ministry.

### **5.2.1. *IN VIVO* TREATMENT**

Concerning the *in vivo* studies, Trametinib and Selumetinib were dissolved at a dose volume of 0.2 mL/20 g body weight in 0.5% hydroxypropylmethylcellulose (Sigma-Aldrich H7509), 0.2% Tween-80 (Sigma-Aldrich P1754) in distilled water (pH 8.0). Adult *Sgca* null mice (5-weeks old) were treated 0,3-3-6 mg/kg of Trametinib or 25 mg/kg of Selumetinib by oral gavage, every day for 14 days, and then sacrificed at 4 h post dose. Control mice were treated with vehicle only (DMSO). Sacrifice was performed through cervical dislocation, according to the directions of the European directive.

### **5.3. PROTEIN EXTRACTION**

Protein extracts were obtained from cultured myoblasts lysed with RIPA buffer (10mM Tris-HCl pH 8.0, 1mM EDTA, 1% Triton-X, 0.1% sodium deoxycholate, 0.1% SDS, 150mM NaCl in deionized water) for 30 min on ice, while total protein extracts from adult muscles were obtained from homogenized tissues in Tissue extraction Buffer (50mM Tris-HCl, 1mM EDTA, 1% Triton-X, 150mM NaCl). Protease and phosphatase inhibitors were always added to both RIPA and Tissue extraction Buffer. After lysis, samples were centrifugated at 4°C for 10 min at 10000 rcf and the supernatants were collected and quantified using the DC Protein Assay (Bio-Rad).

#### **5.3.1. SDS-PAGE AND WESTERN BLOT**

40 µg of total protein extract was denatured with SDS Page Loading sample buffer (100 mM Tris pH 6.8, 4% SDS, 0.2% Bromophenol blue, 20% Glycerol and 10 mM dithiothreitol) and heated at 95°C for 5 minutes. Then, denatured protein samples were loaded on 8-10% SDS (Sigma-Aldrich) acrylamide gel to perform electrophoresis running and then blotted to nitrocellulose membrane (Whatman, Protran Nitrocellulose Transfer Membrane). Afterwards, the membrane was blocked in 5% Milk TBST 1X for 1 hour and then primary antibodies dissolved in 5% Milk TBST 1X or Signal Boost (Calbiochem 407207) were incubated O/N at 4°C in agitation. We used the following primary antibodies and dilutions: rabbit anti-Nfix (1:2500, Genetech), mouse anti-Vinculin (1:2500, Sigma-Aldrich), rabbit anti-pERK (1:1000, Cell Signaling), rabbit anti-totERK (1:1000, Cell Signaling), rabbit anti-JunB (1:500; SantaCruz Biotechnology, 210), rabbit anti-MYPT1 phosphorylated in Thr696 (1:500; SantaCruz Biotechnology, sc-17556-R), rabbit anti-Tot MYPT1 (1:500; SantaCruz Biotechnology, H-130), mouse anti-caspase 9 (1:1000; Cell Signalling Technology, 9508), rabbit anti-caspase 3 (1:1000; Cell Signalling Technology, 9662), mouse anti-total MyHC (hybridoma MF20; 1:5; DSHB), mouse anti-Pax7 (hybridoma; 1:5; DSHB), mouse anti-Myogenin (hybridoma; 1:5; DSHB). The day after blots were washed with TBST 1X and incubated with secondary antibodies (anti-mouse or anti-rabbit, 1:10000, IgG-HRP, Bio-Rad) for 45 min at RT in 5% Milk TBST 1X. Protein bands were revealed through ECL detection reagent (GeneSpin) and images were acquired using the ChemiDoc MP System (Biorad). The Image Lab software was used to measure and quantify the bands of independent western blot experiments. The obtained absolute quantity was compared with the reference band and expressed in the graphs as normalized volume (Norm. Vol. Int.). All the values are presented as mean±sem.

## 5.4. RNA EXTRACTION

Total RNA was isolated from muscle sections and myogenic cultures through the TRIzol™ Reagent protocol (Invitrogen). The sample was homogenized in 1 mL TRIzol™ Reagent and then incubated at RT for 5 minutes. Subsequently, 0,2 mL of chloroform was added to the tubes which were shaken and incubated for 3 minutes at RT. Then, a centrifuge at 12000 g for 15' at 4°C was performed. The upper aqueous phase with the RNA was carefully collected in a new tube. Then, 0,5 mL of Isopropanol was added to the aqueous phase and incubated for 10 minutes to permit the precipitation of the RNA and 5–10 µg of RNase-free glycogen was added to make the pellet more visible. The RNA pellet was resuspended in 1 mL of 75% ethanol, vortexed and centrifugated at 7500 g at 4°C discarding the supernatant; the wash in ethanol was performed twice. The RNA pellet was let air dry for about 10 minutes avoiding its complete dryness and then resuspended in 10-15 µL of RNase-free water. RNA samples were quantified through NanoDrop Spectrophotometer (Implen) and stored at -80°C.

### 5.4.1. RETROTRANSCRIPTION

Total RNA was retrotranscribed to complementary DNA (cDNA) with iScript™ Reverse Transcription Supermix (Bio-Rad). For each sample, a reaction mixture with a final volume of 20 µL was prepared containing 0.5 µg of RNA, 4 µL of 5X iScript RT Supermix and nuclease-free water to reach the volume. The reaction mixture was put in the PCR thermocycler and retrotranscribed following this thermal protocol: 25°C for 5 minutes, 42°C for 30 minutes, 85°C for 5 minutes. Finally, cDNA was stored at -20°C.

### 5.4.2. QUANTITATIVE REAL-TIME PCR (qRT-PCR)

The cDNA obtained was diluted 1:10 in sterile water and 5 µl of the diluted cDNA was used for qRT-PCR. The real-time PCR was performed using SYBR Green Supermix (Bio-Rad). Relative mRNA expression levels were normalised on *β-actin* expression levels. We used the following primers: *Nfix* fwd CACTGGGGCGACTTGTAGAG; *Nfix* rev AGGCTGACAAGGTGTGGC; *SdhA* fwd AGAGATGTTGTGTCTCGATCCAT; *SdhA* rev CTGCAGGTAGACGTGATCTTTCT; *SdhB* fwd AGCAAAGTCTCCAAAATCTACCC; *SdhB* rev TCAATGGATTTGTATTGTGCGTA; *Cox5* fwd TTGCGTAAAGGGATGAATACT; *Cox5* rev TTTGTCCTTAACAACCTCCAAGA; *β-actin* fwd CTCTGGCTCCTAGCACCATGAAGA; *β-actin* rev GTAAAACGCAGCTCAGTAACAGTCCG.

## **5.5. ISOLATION, INCLUSION AND CRYO-SECTIONING OF MUSCLES**

Left and right *Tibialis Anterior*, *Quadriceps femoris*, *Soleus*, *Extensor Digitorum Longus*, *Gastrocnemius* and Diaphragm muscles were collected from each mouse and vertically placed on a cork support with a small amount of inclusion gum (Tragacanth Gum Sigma G1128). Then, muscles were put in Isopentane (Carlo Erba, 524391), which was precooled in liquid nitrogen. After 2-5 mins in isopentane, the muscles were immersed in liquid nitrogen and conserved at -80°C.

Muscles were serially cut with the cryostat (Leica, CM1850) at -25°C. The width of each muscle slice was fixed at 7 µm, and they were collected on Super frost Microscope slides (Thermo-Fisher Scientific, 10123560WCUT). For each muscle, representative transverse sections were cut.

### **5.5.1. IMMUNOFLUORESCENCE**

Cell cultures and muscle slides were fixed for 10 min at 4°C with 4% paraformaldehyde (PFA) in PBS 1X and then were permeabilized with 0.2% Triton X-100 (Sigma-Aldrich), 1% BSA (Sigma-Aldrich) in PBS 1X for 30 min at room temperature (RT). After permeabilization, the samples were treated with a blocking solution composed by 4% BSA for 45 min at RT and incubated O/N at 4°C in darkness with primary antibody diluted in PBS. The primary antibodies used are: rabbit anti-Nfix (1:200, Novus Biologicals), mouse anti-total MyHC (hybridoma MF20, 1:1, Developmental Studies Hybridoma Bank, DSHB), and mouse anti-Pax7 (hybridoma Pax7; 1:1; DSHB), goat anti-collagen I (1:200, Southern Biotech), rat anti-F4/80 (1:400, Clone CI-A3-1, Novusbio), rat anti-laminin (1:300, Sigma-Aldrich). After two washes with PBS, 1% BSA and 0.2% Triton, the samples were incubated for 45 min at RT in darkness with secondary antibodies (Alexa Fluor 488, 594 nm; 1:500; Invitrogen | Thermo Fisher Scientific) and Hoechst (1:500, Sigma-Aldrich). Finally, the cells or muscle slices were washed twice with PBS 1X and mounted with Fluorescence Mounting Medium (Dako S3023) and mounting slides (Prestige).

### **5.5.2. HEMATOXYLIN & EOSIN**

Hematoxylin and Eosin staining allows histological analysis of muscle sections at the microscope in bright field. First, muscle slides were dipped in distilled water for 1 minute, then stained with Hematoxylin of Meyer (Sigma, HHS32) for 4 minutes in darkness. Subsequently, muscle sections were rinsed in distilled water and put under running water for at least 15 minutes. Next, slides were rinsed again in distilled water and dehydrated in ethanol 70% (1 minute) and in ethanol 90% (2 minutes). Then, sections were stained in a solution of 0,5% eosin (Sigma, E4382) in ethanol in darkness for 7 minutes. Subsequently, slides were dehydrated with passages in ethanol 90% (1

minute), 95% (2 minutes) and 100% (5 minutes). Finally, sections were cleaned in xylene (VWR, BHD Prolabo), and mounted with cover glasses and Eukitt mounting medium (Bio Optica, 09-00250). They were let dry overnight under a chemical hood and conserved at room temperature (RT) protected from the sunlight.

### **5.5.3. MILLIGAN'S TRICHROME STAINING**

Milligan's trichrome staining is aimed to analyze fibrotic deposition and extracellular matrix. Firstly, muscle sections were fixed with Bouin solution (Sigma, HT10132) for 1 hour at RT and then washed under the running water for 1 hour. Afterwards, slides were dipped in distilled water for 1 minute and then in a mordant solution constituted by 3 parts of solution A (3g of Potassium dichromate; Sigma, 7778-50-9 and 100ml of MilliQ water) and 1 part of solution B (10ml of HCl; VWR, BHD Pablo, 87003-253 and 100ml of ethanol 95% in MilliQ water) for 5 minutes. Then, sections were washed in distilled water for 2 minutes to remove the excess of mordant and stained with Acid Fuchsin (0.1ml of Acid fuchsin, Sigma, 3244-88-0 in 100ml of MilliQ water) for 30 seconds. After a rapid wash in distilled water, the stain was fixed with Phosphomolybdic acid 1% (Sigma, 51429-74-4) for 3 minutes. The following passage was the stain with Orange G dye (2g of Orange G, Sigma, 1936-15-8 and 100ml of Phosphomolybdic acid 1%) for 5 minutes followed by a wash in distilled water for 2 minutes. Afterwards, sections were dipped in Acetic acid 1% (VWR, BDH Pablo, 87003-212) for 2 minutes and stained with Fast Green (10ml of mother solution [1g of Fast Green FCF, Sigma, 2353-45-9; 100ml of Acetic acid 2% in MilliQ water] and 90ml of MilliQ water) for 5 minutes and with Acetic acid 1% for 2 minutes. Subsequently, slides were dehydrated with serially passages in ethanol 95% (2 minutes) and ethanol 100% (5 minutes). Finally, sections were cleaned in xylene and mounted with cover glasses and Eukitt mounting solution. Mounted glasses were let dry overnight under a chemical hood and stored at RT protected from the sunlight.

### **5.5.4. SUCCINATE DEHYDROGENASE (SDH) ASSAY**

SDH staining allows to distinguish between oxidative and less oxidative myofibers; indeed, succinate dehydrogenase (SDH) is a mitochondrial enzyme responsible for the oxidation of succinate to fumarate in the citric acid cycle. This histochemical assay allows to evaluate the relative SDH activity of individual muscle fiber: the more one contains SDH, the more intense the color is.

For SDH staining, muscle slices 8-10  $\mu\text{m}$ -thick were freshly cut. Sections were incubated in SDH incubating solution (one tablet of nitrobluetetrazolium (Sigma N5514) dissolved in 0.2 M sodium succinate-0.2 M phosphate buffer, pH 7.4,) for 1 hour at 37°C, rinsed in distilled water, rapidly dipped

in 30%, 60%, 30% acetone and rinsed again in distilled water. Next, slides were dehydrated with rapidly passages in ethanol 70%-90%-95%-100% and again in a cleaned 100%. Then, sections were cleared in xylene, and mounted with cover glasses and Eukitt mounting medium.

#### **5.5.5. IMAGE ACQUISITION AND CROSS-SECTIONAL AREA (CSA) ANALYSIS**

Images were acquired with an inverted microscope (Leica-DMI6000B) equipped with Leica DFC365FX and DFC400 cameras and  $\times 10$ ,  $\times 20$ ,  $\times 40$  magnification objectives. The Leica Application Suite software was used for acquisition, while Photoshop was used to generate merged images.

The cross-sectional area (CSA) was evaluated on Immunofluorescence anti-Laminin staining of *Tibialis anterior* sections. Images of the entire section were split into two half and separately analyzed with Open-CSAM tool for ImageJ software (Chazaud et al. 2019).

#### **5.6. STATISTICAL ANALYSIS AND GRAPHS**

All data are expressed as mean $\pm$ SEM. Graphs were obtained using GraphPad Prism software and analyzed with Normalization test and the appropriate two-tailed statistical test (Unpaired t-test with Welch's correction or one-way ANOVA test). \*  $P < 0.05$ , \*\*  $P < 0.01$ , \*\*\*  $P < 0.001$ , confidence interval 95%, alpha level 0.05.

## BIBLIOGRAPHY

- Adam, Rene C., Hanseul Yang, Yejing Ge, Nicole R. Infarinato, Shiri Gur-Cohen, Yuxuan Miao, Ping Wang, et al. 2020. *NFI Transcription Factors Provide Chromatin Access to Maintain Stem Cell Identity While Preventing Unintended Lineage Fate Choices*. *Nature Cell Biology*. Vol. 22. Springer US. <https://doi.org/10.1038/s41556-020-0513-0>.
- Ahmed, Shoeb, Kyle G. Grant, Laura E. Edwards, Anisur Rahman, Murat Cirit, Michael B. Goshe, and Jason M. Haugh. 2014. "Data-Driven Modeling Reconciles Kinetics of ERK Phosphorylation, Localization, and Activity States." *Molecular Systems Biology* 10 (1): 1-14. <https://doi.org/10.1002/msb.134708>.
- Almada, Albert E., and Amy J. Wagers. 2016. "Molecular Circuitry of Stem Cell Fate in Skeletal Muscle Regeneration, Ageing and Disease." *Nature Reviews Molecular Cell Biology* 17 (5): 267-79. <https://doi.org/10.1038/nrm.2016.7>.
- Amoasii, Leonela, John C.W. Hildyard, Hui Li, Efrain Sanchez-Ortiz, Alex Mireault, Daniel Caballero, Rachel Harron, et al. 2018. "Gene Editing Restores Dystrophin Expression in a Canine Model of Duchenne Muscular Dystrophy." *Science*. <https://doi.org/10.1126/science.aau1549>.
- Arnold, Ludovic, Adeline Henry, Françoise Poron, Yasmine Baba-Amer, Nico Van Rooijen, Anne Plonquet, Romain K. Gherardi, and Bénédicte Chazaud. 2007. "Inflammatory Monocytes Recruited after Skeletal Muscle Injury Switch into Antiinflammatory Macrophages to Support Myogenesis." *Journal of Experimental Medicine*. <https://doi.org/10.1084/jem.20070075>.
- Asakura, Atsushi, Motohiro Komaki, and Michael A. Rudnicki. 2001. "Muscle Satellite Cells Are Multipotential Stem Cells That Exhibit Myogenic, Osteogenic, and Adipogenic Differentiation." *Differentiation* 68 (4-5): 245-53. <https://doi.org/10.1046/j.1432-0436.2001.680412.x>.
- Asfour, Hasan A., Mohammed Z. Allouh, and Raed S. Said. 2018. "Myogenic Regulatory Factors: The Orchestrators of Myogenesis after 30 Years of Discovery." *Experimental Biology and Medicine* 243 (2): 118-28. <https://doi.org/10.1177/1535370217749494>.
- Baghdadi, Meryem B., David Castel, Léo Machado, So-ichiro Fukada, David E. Birk, Frederic Relaix, Shahragim Tajbakhsh, Philippos Mourikis, and The. 2018. "Reciprocal Signalling by Notch-Collagen V-CALCR Retains Muscle Stem Cells in Their Niche." *Nature* 557: 714-18.

- Baghdadi, Meryem B., Joao Firmino, Kartik Soni, Brendan Evano, Daniela Di Girolamo, Philippos Mourikis, David Castel, and Shahragim Tajbakhsh. 2018. "Notch-Induced MiR-708 Antagonizes Satellite Cell Migration and Maintains Quiescence." *Cell Stem Cell* 23 (6): 859-868.e5. <https://doi.org/10.1016/j.stem.2018.09.017>.
- Baltusnikas, Juozas, Andrej Fokin, Johannes Winkler, and Julius Liobikas. 2017. "Long-Term Regulation of Gene Expression in Muscle Cells by Systemically Delivered SiRNA." *Journal of Controlled Release* 256: 101-13. <https://doi.org/10.1016/j.jconrel.2017.04.037>.
- Beauchamp, Jonathan R., Louise Heslop, David S.W. Yu, Shahragim Tajbakhsh, Robert G. Kelly, Anton Wernig, Margaret E. Buckingham, Terence A. Partridge, and Peter S. Zammit. 2000. "Expression of CD34 and Myf5 Defines the Majority of Quiescent Adult Skeletal Muscle Satellite Cells." *Journal of Cell Biology* 151 (6): 1221-33. <https://doi.org/10.1083/jcb.151.6.1221>.
- Benarroch, Louise, Gisèle Bonne, François Rivier, and Dalil Hamroun. 2019. "The 2020 Version of the Gene Table of Neuromuscular Disorders (Nuclear Genome)." *Neuromuscular Disorders*. <https://doi.org/10.1016/j.nmd.2019.10.010>.
- Bentzinger, C Florian, Yu Xin Wang, Michael A Rudnicki, C Florian Bentzinger, Yu Xin Wang, and Michael A Rudnicki. 2012. "Building Muscle : Molecular Regulation of Myogenesis Building Muscle : Molecular Regulation of Myogenesis." <https://doi.org/10.1101/cshperspect.a008342>.
- Berkes, Charlotte A., and Stephen J. Tapscott. 2005. "MyoD and the Transcriptional Control of Myogenesis." *Seminars in Cell and Developmental Biology*. <https://doi.org/10.1016/j.semcdb.2005.07.006>.
- Bettica, Paolo, Stefania Petrini, Valentina D'Oria, Adele D'Amico, Michela Catteruccia, Marika Pane, Serena Sivo, et al. 2016. "Histological Effects of Givinostat in Boys with Duchenne Muscular Dystrophy." *Neuromuscular Disorders*. <https://doi.org/10.1016/j.nmd.2016.07.002>.
- Bhatnagar, Shephali, and Ashok Kumar. 2010. "Therapeutic Targeting of Signaling Pathways in Muscular Dystrophy." *Journal of Molecular Medicine* 88 (2): 155-66. <https://doi.org/10.1007/s00109-009-0550-4>.
- Biressi, Stefano, Enrico Tagliafico, Giuseppe Lamorte, Stefania Monteverde, Elena Tenedini, Enrica Roncaglia, Sergio Ferrari, et al. 2007. "Intrinsic Phenotypic Diversity of Embryonic and Fetal Myoblasts Is Revealed by Genome-Wide Gene Expression Analysis on Purified Cells." *Developmental Biology* 304 (2): 633-51.

<https://doi.org/10.1016/j.ydbio.2007.01.016>.

- Bogdanovich, Sasha, Thomas O.B. Krag, Elisabeth R. Barton, Linda D. Morris, Lisa Anne Whittemore, Rexford S. Ahima, and Tejvir S. Khurana. 2002. "Functional Improvement of Dystrophic Muscle by Myostatin Blockade." *Nature*. <https://doi.org/10.1038/nature01154>.
- Bönnemann, C. G., J. Wong, K. J. Jones, H. G.W. Lidov, C. A. Feener, F. Shapiro, B. T. Darras, L. M. Kunkel, and K. N. North. 2002. "Primary  $\gamma$ -Sarcoglycanopathy (LGMD 2C): Broadening of the Mutational Spectrum Guided by the Immunohistochemical Profile." *Neuromuscular Disorders*. [https://doi.org/10.1016/S0960-8966\(01\)00276-0](https://doi.org/10.1016/S0960-8966(01)00276-0).
- Boonen, Kristel J M, and Mark J Post. 2008. "The Muscle Stem Cell Niche: Regulation of Satellite Cells during Regeneration." *Tissue Engineering. Part B, Reviews* 14 (4): 419-31. <https://doi.org/10.1089/ten.teb.2008.0045>.
- Braun, T., G. Buschhausen-Denker, E. Bober, E. Tannich, and H. H. Arnold. 1989. "A Novel Human Muscle Factor Related to but Distinct from MyoD1 Induces Myogenic Conversion in 10T1/2 Fibroblasts." *EMBO Journal*. <https://doi.org/10.1002/j.1460-2075.1989.tb03429.x>.
- Brigitte, Madly, Clementine Schilte, Anne Plonquet, Yasmine Baba-Amer, Adeline Henri, Caroline Charlier, Shahrugim Tajbakhsh, Matthew Albert, Romain K. Gherardi, and Fabrice Chrétien. 2010. "Muscle Resident Macrophages Control the Immune Cell Reaction in a Mouse Model of Notexin-Induced Myoinjury." *Arthritis and Rheumatism*. <https://doi.org/10.1002/art.27183>.
- Campbell, Christine E., Michael Piper, Céline Plachez, Yu Ting Yeh, Joan S. Baizer, Jason M. Osinski, E. David Litwack, Linda J. Richards, and Richard M. Gronostajski. 2008. "The Transcription Factor Nfix Is Essential for Normal Brain Development." *BMC Developmental Biology* 8: 1-18. <https://doi.org/10.1186/1471-213X-8-52>.
- Chakkalakal, Joe V., Mary Ann Harrison, Salvatore Carbonetto, Eva Chin, Robin N. Michel, and Bernard J. Jasmin. 2004. "Stimulation of Calcineurin Signaling Attenuates the Dystrophic Pathology in Mdx Mice." *Human Molecular Genetics*. <https://doi.org/10.1093/hmg/ddh037>.
- Chal, Jérôme, and Olivier Pourquié. 2017. "Making Muscle: Skeletal Myogenesis in Vivo and in Vitro." *Development (Cambridge)* 144 (12): 2104-22. <https://doi.org/10.1242/dev.151035>.
- Chamberlain, Joel R., and Jeffrey S. Chamberlain. 2017. "Progress toward Gene Therapy for Duchenne Muscular Dystrophy." *Molecular Therapy*.

<https://doi.org/10.1016/j.ymthe.2017.02.019>.

- Chang, Chiung Ying, H. Amalia Pasolli, Eugenia G. Giannopoulou, Géraldine Guasch, Richard M. Gronostajski, Olivier Elemento, and Elaine Fuchs. 2013. "NFIB Is a Governor of Epithelial-Melanocyte Stem Cell Behaviour in a Shared Niche." *Nature* 495 (7439): 98-102. <https://doi.org/10.1038/nature11847>.
- Chang, Natasha C., Marie Claude Sincennes, Fabien P. Chevalier, Caroline E. Brun, Melanie Lacaria, Jessica Segalés, Pura Muñoz-Cánoves, Hong Ming, and Michael A. Rudnicki. 2018. "The Dystrophin Glycoprotein Complex Regulates the Epigenetic Activation of Muscle Stem Cell Commitment." *Cell Stem Cell* 22 (5): 755-768.e6. <https://doi.org/10.1016/j.stem.2018.03.022>.
- Chazaud, Bénédicte, Madly Brigitte, Houda Yacoub-Youssef, Ludovic Arnold, Romain Gherardi, Corinne Sonnet, Peggy Lafuste, and Fabrice Chretien. 2009. "Dual and Beneficial Roles of Macrophages during Skeletal Muscle Regeneration." *Exercise and Sport Sciences Reviews*. <https://doi.org/10.1097/JES.0b013e318190ebdb>.
- Chazaud, Bénédicte, Aurélie Trignol, Rémi Mounier, Thibaut Desgeorges, Solene Lyon, Bruno Chapuis, Julien Gondin, et al. 2019. "Open-CSAM, a New Tool for Semi-Automated Analysis of Myofiber Cross-Sectional Area in Regenerating Adult Skeletal Muscle." *Skeletal Muscle* 9 (1): 1-12. <https://doi.org/10.1186/s13395-018-0186-6>.
- Chen, Kok Siong, Jonathan W.C. Lim, Linda J. Richards, and Jens Bunt. 2017. "The Convergent Roles of the Nuclear Factor I Transcription Factors in Development and Cancer." *Cancer Letters* 410: 124-38. <https://doi.org/10.1016/j.canlet.2017.09.015>.
- Chen, Xiang, Guoqing Chen, Lian Feng, Zongting Jiang, Weihua Guo, Mei Yu, and Weidong Tian. 2014. "Expression of Nfic during Root Formation in First Mandibular Molar of Rat." *Journal of Molecular Histology*. <https://doi.org/10.1007/s10735-014-9588-x>.
- Cheung, Tom H., and Thomas A. Rando. 2013. "Molecular Regulation of Stem Cell Quiescence." *Nature Reviews Molecular Cell Biology*. <https://doi.org/10.1038/nrm3591>.
- Christov, Christo, Fabrice Chretien, Rana Abou-Khalil, Guillaume Bassez, Grégoire Vallet, François-Jérôme Authier, Yann Bassaglia, et al. 2007. "Muscle Satellite Cells and Endothelial Cells: Close Neighbors and Privileged Partners." *Molecular Biology of the Cell* 18 (December): 986-94. <https://doi.org/10.1091/mbc.E06>.
- Collins, Charlotte A., Irwin Olsen, Peter S. Zammit, Louise Heslop, Aviva Petrie, Terence A. Partridge, and Jennifer E. Morgan. 2005. "Stem Cell Function, Self-Renewal, and Behavioral Heterogeneity of Cells from the Adult Muscle Satellite Cell Niche." *Cell*

122 (2): 289-301. <https://doi.org/10.1016/j.cell.2005.05.010>.

- Cornelison, D. D.W., Bradley B. Olwin, Michael A. Rudnicki, and Barbara J. Wold. 2000. "MyoD(-/-) Satellite Cells in Single-Fiber Culture Are Differentiation Defective and MRF4 Deficient." *Developmental Biology*. <https://doi.org/10.1006/dbio.2000.9682>.
- Cossu, Giulio, Stefano C Previtali, Sara Napolitano, Maria Pia Cicalese, Francesco Saverio Tedesco, Francesca Nicastro, Maddalena Noviello, et al. 2016. "Intra-arterial Transplantation of HLA-matched Donor Mesoangioblasts in Duchenne Muscular Dystrophy." *EMBO Molecular Medicine*. <https://doi.org/10.15252/emmm.201607129>.
- Cowan, Noemi, and Jennifer Keiser. 2015. "Repurposing of Anticancer Drugs: In Vitro and in Vivo Activities against *Schistosoma Mansoni*." *Parasites and Vectors*. <https://doi.org/10.1186/s13071-015-1023-y>.
- Crisafulli, Salvatore, Janet Sultana, Andrea Fontana, Francesco Salvo, Sonia Messina, Sonia Messina, and Gianluca Trifirò. 2020. "Global Epidemiology of Duchenne Muscular Dystrophy: An Updated Systematic Review and Meta-Analysis." *Orphanet Journal of Rare Diseases*. <https://doi.org/10.1186/s13023-020-01430-8>.
- Culligan, Kevin G, and Kay Ohlendieck. 2002. "Abnormal Calcium Handling in Muscular Dystrophy." *Basic Applied Myology*.
- D'Albis, Anne, René Couteaux, Chantal Janmot, Agnès Roulet, and Jean-Claude -C Mira. 1988. "Regeneration after Cardiotoxin Injury of Innervated and Denervated Slow and Fast Muscles of Mammals: Myosin Isoform Analysis." *European Journal of Biochemistry*. <https://doi.org/10.1111/j.1432-1033.1988.tb14068.x>.
- Dalkilic, I., J. Schienda, T. G. Thompson, and L. M. Kunkel. 2006. "Loss of FilaminC (FLNc) Results in Severe Defects in Myogenesis and Myotube Structure." *Molecular and Cellular Biology*. <https://doi.org/10.1128/mcb.00243-06>.
- Danieli-Betto, Daniela, Alessandra Esposito, Elena Germinario, Dorianna Sandonà, Tiziana Martinello, Anna Jakubiec-Puka, Donatella Biral, and Romeo Betto. 2005. "Deficiency of  $\alpha$ -Sarcoglycan Differently Affects Fast- and Slow-Twitch Skeletal Muscles." *American Journal of Physiology - Regulatory Integrative and Comparative Physiology*. <https://doi.org/10.1152/ajpregu.00673.2004>.
- Donovan, Joanne M., Michael Zimmer, Elliot Offman, Toni Grant, and Michael Jirousek. 2017. "A Novel NF-KB Inhibitor, Edasalonexent (CAT-1004), in Development as a Disease-Modifying Treatment for Patients With Duchenne Muscular Dystrophy: Phase 1 Safety, Pharmacokinetics, and Pharmacodynamics in Adult Subjects." *Journal of*

*Clinical Pharmacology*. <https://doi.org/10.1002/jcph.842>.

- Driller, K., A. Pagenstecher, M. Uhl, H. Omran, A. Berlis, A. Grunder, and A. E. Sippel. 2007. "Nuclear Factor I X Deficiency Causes Brain Malformation and Severe Skeletal Defects." *Molecular and Cellular Biology* 27 (10): 3855-67. <https://doi.org/10.1128/MCB.02293-06>.
- Duclos, F., O. Broux, N. Bourg, V. Straub, G. L. Feldman, Y. Sunada, L. E. Lim, et al. 1998. "B-Sarcoglycan: Genomic Analysis and Identification of a Novel Missense Mutation in the LGMD2E Amish Isolate." *Neuromuscular Disorders*. [https://doi.org/10.1016/S0960-8966\(97\)00135-1](https://doi.org/10.1016/S0960-8966(97)00135-1).
- Duclos, Franck, Volker Straub, Steven A. Moore, David P. Venzke, Ron F. Hrstka, Rachelle H. Crosbie, Madeleine Durbeej, et al. 1998. "Progressive Muscular Dystrophy in  $\alpha$ -Sarcoglycan-Deficient Mice." *Journal of Cell Biology* 142 (6): 1461-71. <https://doi.org/10.1083/jcb.142.6.1461>.
- Dumble, Melissa, Ming Chih Crouthamel, Shu Yun Zhang, Michael Schaber, Dana Levy, Kimberly Robell, Qi Liu, et al. 2014. "Discovery of Novel AKT Inhibitors with Enhanced Anti-Tumor Effects in Combination with the MEK Inhibitor." *PLoS ONE*. <https://doi.org/10.1371/journal.pone.0100880>.
- Dumont, Nicolas A., Yu Xin Wang, Julia Von Maltzahn, Alessandra Pasut, C. Florian Bentzinger, Caroline E. Brun, and Michael A. Rudnicki. 2015. "Dystrophin Expression in Muscle Stem Cells Regulates Their Polarity and Asymmetric Division." *Nature Medicine* 21 (12): 1455-63. <https://doi.org/10.1038/nm.3990>.
- Durbeej, Madeleine, and Kevin P. Campbell. 2002. "Muscular Dystrophies Involving the Dystrophin-Glycoprotein Complex: An Overview of Current Mouse Models." *Current Opinion in Genetics and Development* 12 (3): 349-61. [https://doi.org/10.1016/S0959-437X\(02\)00309-X](https://doi.org/10.1016/S0959-437X(02)00309-X).
- Edmondson, D. G., and E. N. Olson. 1989. "A Gene with Homology to the Myc Similarity Region of MyoD1 Is Expressed during Myogenesis and Is Sufficient to Activate the Muscle Differentiation Program." *Genes & Development*. <https://doi.org/10.1101/gad.3.5.628>.
- Emami, Michael R., Courtney S. Young, Ying Ji, Xiangsheng Liu, Ekaterina Mokhonova, April D. Pyle, Huan Meng, and Melissa J. Spencer. 2019. "Polyrotaxane Nanocarriers Can Deliver CRISPR/Cas9 Plasmid to Dystrophic Muscle Cells to Successfully Edit the DMD Gene." *Advanced Therapeutics* 1900061: 1900061. <https://doi.org/10.1002/adtp.201900061>.

- Emery, Alan E.H. 2002. "The Muscular Dystrophies." *Lancet* 359 (9307): 687-95. [https://doi.org/10.1016/S0140-6736\(02\)07815-7](https://doi.org/10.1016/S0140-6736(02)07815-7).
- Ervasti, J. M., and K. P. Campbell. 1993. "A Role for the Dystrophin-Glycoprotein Complex as a Transmembrane Linker between Laminin and Actin." *Journal of Cell Biology*. <https://doi.org/10.1083/jcb.122.4.809>.
- Fanin, Marina, and Corrado Angelini. 1999. "Regeneration in Sarcoglycanopathies: Expression Studies of Sarcoglycans and Other Muscle Proteins." *Journal of the Neurological Sciences*. [https://doi.org/10.1016/S0022-510X\(99\)00102-1](https://doi.org/10.1016/S0022-510X(99)00102-1).
- Forcina, Laura, Marianna Cosentino, and Antonio Musarò. 2020. "Mechanisms Regulating Muscle Regeneration: Insights into the Interrelated and Time-Dependent Phases of Tissue Healing." *Cells* 9 (5). <https://doi.org/10.3390/cells9051297>.
- Galli, Francesco, Laricia Bragg, Linda Meggiolaro, Maira Rossi, Miriam Caffarini, Naila Naz, Sabrina Santoleri, and Giulio Cossu. 2018. "Gene and Cell Therapy for Muscular Dystrophies: Are We Getting There?" *Human Gene Therapy* 29 (10): 1098-1105. <https://doi.org/10.1089/hum.2018.151>.
- Gillespie, Mark A., Fabien Le Grand, Anthony Scimè, Shihuan Kuang, Julia Von Maltzahn, Vanessa Seale, Ana Cuenda, Jeffrey A. Ranish, and Michael A. Rudnicki. 2009. "P38- $\Gamma$ -Dependent Gene Silencing Restricts Entry Into the Myogenic Differentiation Program." *Journal of Cell Biology* 187 (7): 991-1005. <https://doi.org/10.1083/jcb.200907037>.
- Gilmartin, Aidan G., Maureen R. Bleam, Arthur Groy, Katherine G. Moss, Elisabeth A. Minthorn, Swarupa G. Kulkarni, Cynthia M. Rominger, et al. 2011. "GSK1120212 (JTP-74057) Is an Inhibitor of MEK Activity and Activation with Favorable Pharmacokinetic Properties for Sustained in Vivo Pathway Inhibition." *Clinical Cancer Research* 17 (5): 989-1000. <https://doi.org/10.1158/1078-0432.CCR-10-2200>.
- Glasgow, Stacey M., Dylan Laug, Vita S. Brawley, Zhiyuan Zhang, Amanda Corder, Zheng Yin, Stephen T.C. Wong, et al. 2013. "The MiR-223/Nuclear Factor I-A Axis Regulates Glial Precursor Proliferation and Tumorigenesis in the CNS." *Journal of Neuroscience*. <https://doi.org/10.1523/JNEUROSCI.0321-13.2013>.
- Goel, Aviva J., Marysia Kolbe Rieder, Hans Henning Arnold, Glenn L. Radice, and Robert S. Krauss. 2017. "Niche Cadherins Control the Quiescence-to-Activation Transition in Muscle Stem Cells." *Cell Reports*. <https://doi.org/10.1016/j.celrep.2017.10.102>.
- Goemans, Nathalie M., Mar Tulinius, Johanna T. van den Akker, Brigitte E. Burm, Peter F. Ekhart, Niki Heuvelmans, Tjadine Holling, et al. 2011. "Systemic Administration of

PRO051 in Duchenne's Muscular Dystrophy." *New England Journal of Medicine*.  
<https://doi.org/10.1056/nejmoa1011367>.

Goldberg, Laura R., Irena Hausmanowa-Petrusewicz, Anna Fidzianska, David J. Duggan, Lisa S. Steinberg, and Eric P. Hoffman. 1998. "A Dystrophin Missense Mutation Showing Persistence of Dystrophin and Dystrophin-Associated Proteins yet a Severe Phenotype." *Annals of Neurology*. <https://doi.org/10.1002/ana.410440619>.

Goll, Darrel E., Valery F. Thompson, Hongqi Li, Wei Wei, and Jinyang Cong. 2003. "The Calpain System." *Physiological Reviews*.  
<https://doi.org/10.1152/physrev.00029.2002>.

Grabowska, Magdalena M., Stephen M. Kelly, Amy L. Reese, Justin M. Cates, Tom C. Case, Jianghong Zhang, David J. Degraff, et al. 2016. "NFIB Regulates Transcriptional Networks That Control the Development of Prostatic Hyperplasia." *Endocrinology*.  
<https://doi.org/10.1210/en.2015-1312>.

Gronostajski, Richard M. 2000. "Roles of the NFI/CTF Gene Family in Transcription and Development." *Gene*. [https://doi.org/10.1016/S0378-1119\(00\)00140-2](https://doi.org/10.1016/S0378-1119(00)00140-2).

Grounds, Miranda D. 2008. "Complexity of Extracellular Matrix and Skeletal Muscle Regeneration." In *Skeletal Muscle Repair and Regeneration*.  
[https://doi.org/10.1007/978-1-4020-6768-6\\_13](https://doi.org/10.1007/978-1-4020-6768-6_13).

Hack, A. A., L. Cordier, D. I. Shoturma, M. Y. Lam, H. L. Sweeney, and E. M. McNally. 1999. "Muscle Degeneration without Mechanical Injury in Sarcoglycan Deficiency." *Proceedings of the National Academy of Sciences of the United States of America*.  
<https://doi.org/10.1073/pnas.96.19.10723>.

Hammers, David W., Margaret M. Sleeper, Sean C. Forbes, Cora C. Coker, Michael R. Jirousek, Michael Zimmer, Glenn A. Walter, and H. Lee Sweeney. 2016. "Disease-Modifying Effects of Orally Bioavailable NF-KB Inhibitors in Dystrophin-Deficient Muscle." *JCI Insight*. <https://doi.org/10.1172/jci.insight.90341>.

Harris, Lachlan, Laura A. Genovesi, Richard M. Gronostajski, Brandon J. Wainwright, and Michael Piper. 2015. "Nuclear Factor One Transcription Factors: Divergent Functions in Developmental versus Adult Stem Cell Populations." *Developmental Dynamics* 244 (3): 227-38. <https://doi.org/10.1002/dvdy.24182>.

Helmbacher, Françoise, and Sigmar Stricker. 2020. "Tissue Cross Talks Governing Limb Muscle Development and Regeneration." *Seminars in Cell and Developmental Biology* 104 (February): 14-30. <https://doi.org/10.1016/j.semcd.2020.05.005>.

Heng, Yee Hsieh Evelyn, Robert C. McLeay, Tracey J. Harvey, Aaron G. Smith, Guy Barry,

- Kathleen Cato, Céline Plachez, et al. 2014. "NFIx Regulates Neural Progenitor Cell Differentiation during Hippocampal Morphogenesis." *Cerebral Cortex*. <https://doi.org/10.1093/cercor/bhs307>.
- Higuchi, Itsuro, Hisaomi Kawai, Yoshifumi Umaki, Masakazu Kawajiri, Katsuhito Adachi, Hidetoshi Fukunaga, Masanori Nakagawa, Kimiyoshi Arimura, and Mitsuhiro Osame. 1998. "Different Manners of Sarcoglycan Expression in Genetically Proven  $\alpha$ -Sarcoglycan Deficiency and  $\gamma$ -Sarcoglycan Deficiency." *Acta Neuropathologica*. <https://doi.org/10.1007/s004010050882>.
- Holmfeldt, Per, Jennifer Pardieck, Anjelica C. Saulsberry, Satish Kumar Nandakumar, David Finkelstein, John T. Gray, Derek A. Persons, and Shannon McKinney-Freeman. 2013. "Nfix Is a Novel Regulator of Murine Hematopoietic Stem and Progenitor Cell Survival." *Blood*. <https://doi.org/10.1182/blood-2013-04-493973>.
- Horsley, Valerie, Katie M. Jansen, Stephen T. Mills, and Grace K. Pavlath. 2003. "IL-4 Acts as a Myoblast Recruitment Factor during Mammalian Muscle Growth." *Cell*. [https://doi.org/10.1016/S0092-8674\(03\)00319-2](https://doi.org/10.1016/S0092-8674(03)00319-2).
- Hsu, Yu Chih, Jason Osinski, Christine E. Campbell, E. David Litwack, Dan Wang, Song Liu, Cindy J. Bachurski, and Richard M. Gronostajski. 2011. "Mesenchymal Nuclear Factor I B Regulates Cell Proliferation and Epithelial Differentiation during Lung Maturation." *Developmental Biology*. <https://doi.org/10.1016/j.ydbio.2011.04.002>.
- Hutcheson, David A., Jia Zhao, Allyson Merrell, Malay Haldar, and Gabrielle Kardon. 2009. "Embryonic and Fetal Limb Myogenic Cells Are Derived from Developmentally Distinct Progenitors and Have Different Requirements for  $\beta$ -Catenin." *Genes and Development* 23 (8): 997-1013. <https://doi.org/10.1101/gad.1769009>.
- James, M., A. Nuttall, J. L. Ilsley, K. Ottersbach, J. M. Tinsley, M. Sudol, and S. J. Winder. 2000. "Adhesion-Dependent Tyrosine Phosphorylation of  $\beta$ -Dystroglycan Regulates Its Interaction with Utrophin." *Journal of Cell Science*.
- Joe, Aaron W.B., Lin Yi, Anuradha Natarajan, Fabien Le Grand, Leslie So, Joy Wang, Michael A. Rudnicki, and Fabio M.V. Rossi. 2010. "Muscle Injury Activates Resident Fibro/Adipogenic Progenitors That Facilitate Myogenesis." *Nature Cell Biology*. <https://doi.org/10.1038/ncb2015>.
- Johann, Axel M., Vera Barra, Anne-Marie Kuhn, Andreas Weigert, Andreas Knethen, and Bernhard Brüne. 2007. "Apoptotic Cells Induce Arginase II in Macrophages, Thereby Attenuating NO Production." *The FASEB Journal*. <https://doi.org/10.1096/fj.06-7815com>.

- Keefe, Alexandra C., Jennifer A. Lawson, Steven D. Flygare, Zachary D. Fox, Mary P. Colasanto, Sam J. Mathew, Mark Yandell, and Gabrielle Kardon. 2015. "Muscle Stem Cells Contribute to Myofibres in Sedentary Adult Mice." *Nature Communications* 6 (May). <https://doi.org/10.1038/ncomms8087>.
- King, Alastair J., Marc R. Arnone, Maureen R. Bleam, Katherine G. Moss, Jingsong Yang, Kelly E. Fedorowicz, Kimberly N. Smitheman, et al. 2013. "Dabrafenib; Preclinical Characterization, Increased Efficacy When Combined with Trametinib, While BRAF/MEK Tool Combination Reduced Skin Lesions." *PLoS ONE*. <https://doi.org/10.1371/journal.pone.0067583>.
- Kostyunina, D. S., A. D. Ivanova, and O. V. Smirnova. 2018. "Myostatin: Twenty Years Later." *Human Physiology* 44 (1): 88-101. <https://doi.org/10.1134/S0362119718010127>.
- Kozakowska, Magdalena, Katarzyna Pietraszek-Gremplewicz, Alicja Jozkowicz, and Jozef Dulak. 2015. "The Role of Oxidative Stress in Skeletal Muscle Injury and Regeneration: Focus on Antioxidant Enzymes." *Journal of Muscle Research and Cell Motility* 36 (6): 377-93. <https://doi.org/10.1007/s10974-015-9438-9>.
- Kuang, Shihuan, Kazuki Kuroda, Fabien Le Grand, and Michael A. Rudnicki. 2007. "Asymmetric Self-Renewal and Commitment of Satellite Stem Cells in Muscle." *Cell* 129 (5): 999-1010. <https://doi.org/10.1016/j.cell.2007.03.044>.
- Kumar, Ashok, and Aladin M. Boriek. 2003. "Mechanical Stress Activates the Nuclear Factor-kappaB Pathway in Skeletal Muscle Fibers: A Possible Role in Duchenne Muscular Dystrophy." *The FASEB Journal*. <https://doi.org/10.1096/fj.02-0542com>.
- Lagrotta-Candido, Jussara, Rita Vasconcellos, Marta Cavalcanti, Marcelo Bozza, Wilson Savino, and Thereza Quirico-Santos. 2002. "Resolution of Skeletal Muscle Inflammation in Mdx Dystrophic Mouse Is Accompanied by Increased Immunoglobulin and Interferon- $\gamma$  Production." *International Journal of Experimental Pathology*. <https://doi.org/10.1046/j.1365-2613.2002.00221.x>.
- Łastowska, Maria, Hani Al-Afghani, Haya H. Al-Balool, Harsh Sheth, Emma Mercer, Jonathan M. Coxhead, Chris P.F. Redfern, et al. 2014. "Identification of a Neuronal Transcription Factor Network Involved in Medulloblastoma Development." *Acta Neuropathologica Communications*. <https://doi.org/10.1186/2051-5960-1-35>.
- Lee, Dong Seol, Han Wool Choung, Heung Joong Kim, Richard M. Gronostajski, Young Il Yang, Hyun Mo Ryoo, Zang Hee Lee, Hong Hee Kim, Eui Sic Cho, and Joo Cheol Park. 2014. "NFI-C Regulates Osteoblast Differentiation via Control of Osterix Expression."

- Stem Cells*. <https://doi.org/10.1002/stem.1733>.
- Lemke, Greg. 2019. "How Macrophages Deal with Death." *Nature Reviews Immunology*. <https://doi.org/10.1038/s41577-019-0167-y>.
- Lemos, Dario R., Farshad Babaeijandaghi, Marcela Low, Chih Kai Chang, Sunny T. Lee, Daniela Fiore, Regan Heng Zhang, Anuradha Natarajan, Sergei A. Nedospasov, and Fabio M.V. Rossi. 2015. "Nilotinib Reduces Muscle Fibrosis in Chronic Muscle Injury by Promoting TNF-Mediated Apoptosis of Fibro/Adipogenic Progenitors." *Nature Medicine*. <https://doi.org/10.1038/nm.3869>.
- Lepper, Christoph, Terence A. Partridge, and Chen Ming Fan. 2011. "An Absolute Requirement for Pax7-Positive Satellite Cells in Acute Injury-Induced Skeletal Muscle Regeneration." *Development*. <https://doi.org/10.1242/dev.067595>.
- Li, Chen, Zhongxiu Chen, Hao Yang, Fangbo Luo, Lihong Chen, Huawei Cai, Yajiao Li, et al. 2016. "Selumetinib, an Oral Anti-Neoplastic Drug, May Attenuate Cardiac Hypertrophy via Targeting the ERK Pathway." *PLoS ONE* 11 (7): 1-17. <https://doi.org/10.1371/journal.pone.0159079>.
- Ljubcic, Vladimir, Pedro Miura, Matthew Burt, Louise Boudreault, Shiema Khogali, John A. Lunde, Jean Marc Renaud, and Bernard J. Jasmin. 2011. "Chronic AMPK Activation Evokes the Slow, Oxidative Myogenic Program and Triggers Beneficial Adaptations in Mdx Mouse Skeletal Muscle." *Human Molecular Genetics*. <https://doi.org/10.1093/hmg/ddr265>.
- Lu, Weining, Fabiola Quintero-Rivera, Yanli Fan, Fowzan S. Alkuraya, Diana J. Donovan, Qiongchao Xi, Annick Turbe-Doan, et al. 2007. "NFIA Haploinsufficiency Is Associated with a CNS Malformation Syndrome and Urinary Tract Defects." *PLoS Genetics*. <https://doi.org/10.1371/journal.pgen.0030080>.
- Lundgren, Mats, Cheok Man Chow, Pierangela Sabbattini, Andrew Georgiou, Sophie Minaee, and Niall Dillon. 2000. "Transcription Factor Dosage Affects Changes in Higher Order Chromatin Structure Associated with Activation of a Heterochromatic Gene." *Cell* 103 (5): 733-43. [https://doi.org/10.1016/S0092-8674\(00\)00177-X](https://doi.org/10.1016/S0092-8674(00)00177-X).
- Madaro, Luca, Alessio Torcinaro, Marco de Bardi, Federica F. Contino, Mattia Pelizzola, Giuseppe R. Diaferia, Giulia Imeneo, Marina Bouchè, Pier Lorenzo Puri, and Francesca de Santa. 2019. "Macrophages Fine Tune Satellite Cell Fate in Dystrophic Skeletal Muscle of Mdx Mice." *PLoS Genetics*. <https://doi.org/10.1371/journal.pgen.1008408>.
- Mah, Jean K., Lawrence Korngut, Kirsten M. Fiest, Jonathan Dykeman, Lundy J. Day, Tamara Pringsheim, and Nathalie Jette. 2015. "A Systematic Review and Meta-

- Analysis on the Epidemiology of the Muscular Dystrophies.” *Canadian Journal of Neurological Sciences*. <https://doi.org/10.1017/cjn.2015.311>.
- Malan, Valérie, Diana Rajan, Sophie Thomas, Adam C. Shaw, Hélène Louis Dit Picard, Valérie Layet, Marianne Till, et al. 2010. “Distinct Effects of Allelic NFIX Mutations on Nonsense-Mediated mRNA Decay Engender Either a Sotos-like or a Marshall-Smith Syndrome.” *American Journal of Human Genetics*. <https://doi.org/10.1016/j.ajhg.2010.07.001>.
- Mann, Christopher J., Eusebio Perdiguero, Yacine Kharraz, Susana Aguilar, Patrizia Pessina, Antonio L. Serrano, and Pura Muñoz-Cánoves. 2011. “Aberrant Repair and Fibrosis Development in Skeletal Muscle.” *Skeletal Muscle* 1 (1): 21. <https://doi.org/10.1186/2044-5040-1-21>.
- Mauro, A. 1961. “Satellite Cell of Skeletal Muscle Fibers.” *The Journal of Biophysical and Biochemical Cytology* 9: 493-95. <https://doi.org/10.1083/jcb.9.2.493>.
- McDonald, Craig M., Craig Campbell, Ricardo Erazo Torricelli, Richard S. Finkel, Kevin M. Flanigan, Nathalie Goemans, Peter Heydemann, et al. 2017. “Ataluren in Patients with Nonsense Mutation Duchenne Muscular Dystrophy (ACT DMD): A Multicentre, Randomised, Double-Blind, Placebo-Controlled, Phase 3 Trial.” *The Lancet*. [https://doi.org/10.1016/S0140-6736\(17\)31611-2](https://doi.org/10.1016/S0140-6736(17)31611-2).
- McDonald, Craig M., Erik K. Henricson, Richard T. Abresch, Tina Duong, Nanette C. Joyce, Fengming Hu, Paula R. Clemens, et al. 2018. “Long-Term Effects of Glucocorticoids on Function, Quality of Life, and Survival in Patients with Duchenne Muscular Dystrophy: A Prospective Cohort Study.” *The Lancet*. [https://doi.org/10.1016/S0140-6736\(17\)32160-8](https://doi.org/10.1016/S0140-6736(17)32160-8).
- Meadows, Eric, Jang Hyeon Cho, Jesse M. Flynn, and William H. Klein. 2008. “Myogenin Regulates a Distinct Genetic Program in Adult Muscle Stem Cells.” *Developmental Biology* 322 (2): 406-14. <https://doi.org/10.1016/j.ydbio.2008.07.024>.
- Mendell, Jerry R., Katherine Campbell, Louise Rodino-Klapac, Zarife Sahenk, Chris Shilling, Sarah Lewis, Dawn Bowles, et al. 2010. “Dystrophin Immunity in Duchenne’s Muscular Dystrophy.” *New England Journal of Medicine*. <https://doi.org/10.1056/nejmoa1000228>.
- Mercuri, Eugenio, Carsten G. Bönnemann, and Francesco Muntoni. 2019. “Muscular Dystrophies.” *The Lancet* 394 (10213): 2025-38. [https://doi.org/10.1016/S0140-6736\(19\)32910-1](https://doi.org/10.1016/S0140-6736(19)32910-1).
- Messina, Graziella, Stefano Biressi, Stefania Monteverde, Alessandro Magli, Marco

- Cassano, Laura Perani, Elena Roncaglia, et al. 2010. "Nfix Regulates Fetal-Specific Transcription in Developing Skeletal Muscle." *Cell* 140 (4): 554-66. <https://doi.org/10.1016/j.cell.2010.01.027>.
- Messina, Sonia, Alessandra Bitto, M'hammed Aguenouz, Letteria Minutoli, Maria C. Monici, Domenica Altavilla, Francesco Squadrito, and Giuseppe Vita. 2006. "Nuclear Factor Kappa-B Blockade Reduces Skeletal Muscle Degeneration and Enhances Muscle Function in Mdx Mice." *Experimental Neurology*. <https://doi.org/10.1016/j.expneurol.2005.11.021>.
- Mitchell, Michael J, Margaret M Billingsley, Rebecca M Haley, Robert Langer, Marissa E Wechsler, and Nicholas A Peppas. 2020. "Engineering Precision Nanoparticles." *Nature Reviews Drug Discovery*. <https://doi.org/10.1038/s41573-020-0090-8>.
- Mohassel, Payam, A. Reghan Foley, and Carsten G. Bönnemann. 2018. "Extracellular Matrix-Driven Congenital Muscular Dystrophies." *Matrix Biology*. <https://doi.org/10.1016/j.matbio.2018.06.005>.
- Montagut, Clara, and Jeff Settleman. 2009. "Targeting the RAF-MEK-ERK Pathway in Cancer Therapy." *Cancer Letters* 283 (2): 125-34. <https://doi.org/10.1016/j.canlet.2009.01.022>.
- Mourikis, Philippos, Ramkumar Sambasivan, David Castel, Pierre Rocheteau, Valentina Bizzarro, and Shahragim Tajbakhsh. 2012. "A Critical Requirement for Notch Signaling in Maintenance of the Quiescent Skeletal Muscle Stem Cell State." *Stem Cells* 30 (2): 243-52. <https://doi.org/10.1002/stem.775>.
- Muchir, Antoine, Young J. Kim, Sarah A. Reilly, Wei Wu, Jason C. Choi, and Howard J. Worman. 2013. "Inhibition of Extracellular Signal-Regulated Kinase 1/2 Signaling Has Beneficial Effects on Skeletal Muscle in a Mouse Model of Emery-Dreifuss Muscular Dystrophy Caused by Lamin A/C Gene Mutation." *Skeletal Muscle* 3 (1): 1-10. <https://doi.org/10.1186/2044-5040-3-17>.
- Muntoni, Francesco, Silvia Torelli, and Alessandra Ferlini. 2003. "Dystrophin and Mutations: One Gene, Several Proteins, Multiple Phenotypes." *Lancet Neurology* 2 (12): 731-40. [https://doi.org/10.1016/S1474-4422\(03\)00585-4](https://doi.org/10.1016/S1474-4422(03)00585-4).
- Murtagh, Janice, Finian Martin, and Richard M. Gronostajski. 2003. "The Nuclear Factor I (NFI) Gene Family in Mammary Gland Development and Function." *Journal of Mammary Gland Biology and Neoplasia*. <https://doi.org/10.1023/A:1025909109843>.
- Nance, Michael E., Chady H. Hakim, N. Nora Yang, and Dongsheng Duan. 2017. "Nanotherapy for Duchenne Muscular Dystrophy: Nanotherapy for Duchenne Muscular

Dystrophy.” *Wiley Interdisciplinary Reviews: Nanomedicine and Nanobiotechnology*, 1472. <https://doi.org/10.1002/wnan.1472>.

- Nelson, Christopher E., Yaoying Wu, Matthew P. Gemberling, Matthew L. Oliver, Matthew A. Waller, Joel D. Bohning, Jacqueline N. Robinson-Hamm, et al. 2019. “Long-Term Evaluation of AAV-CRISPR Genome Editing for Duchenne Muscular Dystrophy.” *Nature Medicine*. <https://doi.org/10.1038/s41591-019-0344-3>.
- Nickols, Nicholas G., Ramin Nazarian, Shuang G. Zhao, Victor Tan, Vladislav Uzunangelov, Zheng Xia, Robert Baertsch, et al. 2019. “MEK-ERK Signaling Is a Therapeutic Target in Metastatic Castration Resistant Prostate Cancer.” *Prostate Cancer and Prostatic Diseases* 22 (4): 531-38. <https://doi.org/10.1038/s41391-019-0134-5>.
- Olguin, HC, and BB Olwin. 2012. “Pax-7 up-Regulation Inhibits Myogenesis and Cell Cycle Progression in Satellite Cells: A Potential Mechanism for Self- Renewal.” *Developmental Biology* 275 (2): 375-88. <https://doi.org/10.1016/j.ydbio.2004.08.015.Pax-7>.
- Olguin, Hugo C., Zhihong Yang, Stephen J. Tapscott, and Bradley B. Olwin. 2007. “Reciprocal Inhibition between Pax7 and Muscle Regulatory Factors Modulates Myogenic Cell Fate Determination.” *Journal of Cell Biology* 177 (5): 769-79. <https://doi.org/10.1083/jcb.200608122>.
- Pala, Francesca, Daniela Di Girolamo, Sébastien Mella, Siham Yennek, Laurent Chatre, Miria Ricchetti, and Shahragim Tajbakhsh. 2018. “Distinct Metabolic States Govern Skeletal Muscle Stem Cell Fates during Prenatal and Postnatal Myogenesis.” *Journal of Cell Science* 131 (14): jcs212977. <https://doi.org/10.1242/jcs.212977>.
- Pawlikowski, Bradley, Crystal Pulliam, Nicole Dalla Betta, Gabrielle Kardon, and Bradley B Olwin. 2015. “Pervasive Satellite Cell Contribution to Uninjured Adult Muscle Fibers.” *Skeletal Muscle*, 1-13. <https://doi.org/10.1186/s13395-015-0067-1>.
- Perandini, Luiz Augusto, Patricia Chimin, Diego da Silva Lutkemeyer, and Niels Olsen Saraiva Câmara. 2018. “Chronic Inflammation in Skeletal Muscle Impairs Satellite Cells Function during Regeneration: Can Physical Exercise Restore the Satellite Cell Niche?” *FEBS Journal*. <https://doi.org/10.1111/febs.14417>.
- Perdiguerro, Eusebio, Pedro Sousa-Victor, Vanessa Ruiz-Bonilla, Mercè Jardí, Carme Caelles, Antonio L. Serrano, and Pura Muñoz-Cánoves. 2011. “P38/MKP-1-Regulated AKT Coordinates Macrophage Transitions and Resolution of Inflammation during Tissue Repair.” *Journal of Cell Biology*. <https://doi.org/10.1083/jcb.201104053>.
- Périé, Sophie, Capucine Trollet, Vincent Mouly, Valérie Vanneaux, Kamel Mamchaoui,

- Belaïd Bouazza, Jean Pierre Marolleau, et al. 2014. "Autologous Myoblast Transplantation for Oculopharyngeal Muscular Dystrophy: A Phase I/IIa Clinical Study." *Molecular Therapy*. <https://doi.org/10.1038/mt.2013.155>.
- Peter, Angela K., Jamie L. Marshall, and Rachelle H. Crosbie. 2008. "Sarcospan Reduces Dystrophic Pathology: Stabilization of the Utrophin-Glycoprotein Complex." *Journal of Cell Biology* 183 (3): 419-27. <https://doi.org/10.1083/jcb.200808027>.
- Petrof, Basil J., Joseph B. Shrager, Hansell H. Stedman, Alan M. Kelly, and H. Lee Sweeney. 1993. "Dystrophin Protects the Sarcolemma from Stresses Developed during Muscle Contraction." *Proceedings of the National Academy of Sciences of the United States of America*. <https://doi.org/10.1073/pnas.90.8.3710>.
- Petroni, K., M. Trinei, M. Fornari, V. Calvenzani, A. Marinelli, L.A. Micheli, R. Pilu, et al. 2017. "Dietary Cyanidin 3-Glucoside from Purple Corn Ameliorates Doxorubicin-Induced Cardiotoxicity in Mice." *Nutrition, Metabolism and Cardiovascular Diseases* 27 (5): 462-69. <https://doi.org/10.1016/j.numecd.2017.02.002>.
- Philip, Bevin, Zhijian Lu, and Yijie Gao. 2005. "Regulation of GDF-8 Signaling by the P38 MAPK." *Cellular Signalling*. <https://doi.org/10.1016/j.cellsig.2004.08.003>.
- Pierno, S., B. Nico, R. Burdi, A. Liantonio, M. P. Didonna, V. Cippone, B. Fraysse, et al. 2007. "Role of Tumour Necrosis Factor  $\alpha$ , but Not of Cyclo-Oxygenase-2-Derived Eicosanoids, on Functional and Morphological Indices of Dystrophic Progression in Mdx Mice: A Pharmacological Approach." *Neuropathology and Applied Neurobiology*. <https://doi.org/10.1111/j.1365-2990.2007.00798.x>.
- Piers, A. T., T. Lavin, H. G. Radley-Crabb, A. J. Bakker, M. D. Grounds, and G. J. Pinniger. 2011. "Blockade of TNF in Vivo Using CV1q Antibody Reduces Contractile Dysfunction of Skeletal Muscle in Response to Eccentric Exercise in Dystrophic Mdx and Normal Mice." *Neuromuscular Disorders*. <https://doi.org/10.1016/j.nmd.2010.09.013>.
- Piper, Michael, Richard Gronostajski, and Graziella Messina. 2018. "Nuclear Factor One X in Development and Disease." *Trends in Cell Biology* 29 (1): 20-30. <https://doi.org/10.1016/j.tcb.2018.09.003>.
- Qiu, Jian Ge, Yao Jun Zhang, Yong Li, Jin Ming Zhao, Wen Ji Zhang, Qi Wei Jiang, Xiao Long Mei, et al. 2015. "Trametinib Modulates Cancer Multidrug Resistance by Targeting ABCB1 Transporter." *Oncotarget*. <https://doi.org/10.18632/oncotarget.3820>.
- Rahimov, Fedik, and Louis M. Kunkel. 2013. "Cellular and Molecular Mechanisms Underlying Muscular Dystrophy." *Journal of Cell Biology* 201 (4): 499-510.

<https://doi.org/10.1083/jcb.201212142>.

- Rando, Thomas A. 2001. "The Dystrophin-Glycoprotein Complex, Cellular Signaling, and the Regulation of Cell Survival in the Muscular Dystrophies." *Muscle and Nerve* 24 (12): 1575-94. <https://doi.org/10.1002/mus.1192>.
- Relaix, F., and P. S. Zammit. 2012. "Satellite Cells Are Essential for Skeletal Muscle Regeneration: The Cell on the Edge Returns Centre Stage." *Development* 139 (16): 2845-56. <https://doi.org/10.1242/dev.069088>.
- Riddell, Jonah, Roi Gazit, Brian S. Garrison, Guoji Guo, Assieh Saadatpour, Pankaj K. Mandal, Wataru Ebina, et al. 2014. "Reprogramming Committed Murine Blood Cells to Induced Hematopoietic Stem Cells with Defined Factors." *Cell*. <https://doi.org/10.1016/j.cell.2014.04.006>.
- Rocheteau, Pierre, Barbara Gayraud-Morel, Irene Siegl-Cachedenier, Maria A. Blasco, and Shahragim Tajbakhsh. 2012. "A Subpopulation of Adult Skeletal Muscle Stem Cells Retains All Template DNA Strands after Cell Division." *Cell* 148 (1-2): 112-25. <https://doi.org/10.1016/j.cell.2011.11.049>.
- Rodgers, Joseph T., Matthew D. Schroeder, Chanthia Ma, and Thomas A. Rando. 2017. "HGFA Is an Injury-Regulated Systemic Factor That Induces the Transition of Stem Cells into GAlert." *Cell Reports* 19 (3): 479-86. <https://doi.org/10.1016/j.celrep.2017.03.066>.
- Rossi, Giuliana, Stefania Antonini, Chiara Bonfanti, Stefania Monteverde, Chiara Vezzali, Shahragim Tajbakhsh, Giulio Cossu, and Graziella Messina. 2016. "Nfix Regulates Temporal Progression of Muscle Regeneration through Modulation of Myostatin Expression." *Cell Reports* 14 (9): 2238-49. <https://doi.org/10.1016/j.celrep.2016.02.014>.
- Rossi, Giuliana, Chiara Bonfanti, Stefania Antonini, Mattia Bastoni, Stefania Monteverde, Anna Innocenzi, Marielle Saclier, Valentina Taglietti, and Graziella Messina. 2017. "Silencing Nfix Rescues Muscular Dystrophy by Delaying Muscle Regeneration." *Nature Communications* 8 (1): 1-12. <https://doi.org/10.1038/s41467-017-01098-y>.
- Rozo, Michelle, Liangji Li, and Chen Ming Fan. 2016. "Targeting B1-Integrin Signaling Enhances Regeneration in Aged and Dystrophic Muscle in Mice." *Nature Medicine*. <https://doi.org/10.1038/nm.4116>.
- Rudnicki, M. A., F. Le Grand, I. McKinnell, and S. Kuang. 2008. "The Molecular Regulation of Muscle Stem Cell Function." In *Cold Spring Harbor Symposia on Quantitative Biology*. <https://doi.org/10.1101/sqb.2008.73.064>.

- Sacco, Alessandra, Foteini Mourkioti, Rose Tran, Jinkuk Choi, Michael Llewellyn, Peggy Kraft, Marina Shkreli, et al. 2010. "Short Telomeres and Stem Cell Exhaustion Model in Mdx Mice." *Cell* 143 (7): 1059-71. <https://doi.org/10.1016/j.cell.2010.11.039.Short>.
- Saclier, M., C. Bonfanti, S. Antonini, G. Angelini, G. Mura, F. Zanaglio, V. Taglietti, et al. 2020. "Nutritional Intervention with Cyanidin Hinders the Progression of Muscular Dystrophy." *Cell Death and Disease* 11 (2). <https://doi.org/10.1038/s41419-020-2332-4>.
- Saclier, Marielle, Michela Lapi, Chiara Bonfanti, Giuliana Rossi, Stefania Antonini, and Graziella Messina. 2020. "The Transcription Factor Nfix Requires RhoA-ROCK1 Dependent Phagocytosis to Mediate Macrophage Skewing during Skeletal Muscle Regeneration." *Cells* 9 (3): 708. <https://doi.org/10.3390/cells9030708>.
- Saclier, Marielle, Houda Yacoub-Youssef, Abigail L. Mackey, Ludovic Arnold, Hamida Ardjoune, Melanie Magnan, Frederic Sailhan, et al. 2013. "Differentially Activated Macrophages Orchestrate Myogenic Precursor Cell Fate during Human Skeletal Muscle Regeneration." *Stem Cells*. <https://doi.org/10.1002/stem.1288>.
- Sambasivan, Ramkumar, Roseline Yao, Adrien Kissenpfennig, Laetitia van Wittenberghe, Andràs Paldi, Barbara Gayraud-Morel, Hind Guenou, Bernard Malissen, Shahragim Tajbakhsh, and Anne Galy. 2011. "Pax7-Expressing Satellite Cells Are Indispensable for Adult Skeletal Muscle Regeneration." *Development*. <https://doi.org/10.1242/dev.067587>.
- Sampaolesi, Maurilio, Stephane Blot, Giuseppe D'Antona, Nicolas Granger, Rossana Tonlorenzi, Anna Innocenzi, Paolo Mognol, et al. 2006. "Mesoangioblast Stem Cells Ameliorate Muscle Function in Dystrophic Dogs." *Nature* 444 (7119): 574-79. <https://doi.org/10.1038/nature05282>.
- Sandonà, Dorianna, and Romeo Betto. 2009. "Sarcoglycanopathies: Molecular Pathogenesis and Therapeutic Prospects." *Expert Reviews in Molecular Medicine* 11 (September): 1-27. <https://doi.org/10.1017/S1462399409001203>.
- Santos, Eugenio, and Piero Crespo. 2018. "The RAS-ERK Pathway: A Route for Couples." *Science Signaling* 11 (554): 1-3. <https://doi.org/10.1126/scisignal.aav0917>.
- Schiaffino, Stefano, Alberto C. Rossi, Vika Smerdu, Leslie A. Leinwand, and Carlo Reggiani. 2015. "Developmental Myosins: Expression Patterns and Functional Significance." *Skeletal Muscle*. <https://doi.org/10.1186/s13395-015-0046-6>.
- Schultz, Edward, Marcia C. Gibson, and Thomas Champion. 1978. "Satellite Cells Are

- Mitotically Quiescent in Mature Mouse Muscle: An EM and Radioautographic Study.” *Journal of Experimental Zoology*. <https://doi.org/10.1002/jez.1402060314>.
- Schwander, Martin, Marco Leu, Michael Stumm, Olivier M. Dorchies, Urs T. Rugg, Johannes Schittny, and Ulrich Müller. 2003. “B1 Integrins Regulate Myoblast Fusion and Sarcomere Assembly.” *Developmental Cell*. [https://doi.org/10.1016/S1534-5807\(03\)00118-7](https://doi.org/10.1016/S1534-5807(03)00118-7).
- Seale, Patrick, Bryan Bjork, Wenli Yang, Shingo Kajimura, Sherry Chin, Shihuan Kuang, Anthony Scimè, et al. 2008. “PRDM16 Controls a Brown Fat/Skeletal Muscle Switch.” *Nature*. <https://doi.org/10.1038/nature07182>.
- Seale, Patrick, Jeff Ishibashi, Anthony Scimè, and Michael A. Rudnicki. 2004. “Pax7 Is Necessary and Sufficient for the Myogenic Specification of CD45+:Sca1+ Stem Cells from Injured Muscle.” *PLoS Biology*. <https://doi.org/10.1371/journal.pbio.0020130>.
- Seale, Patrick, Luc A Sabourin, Adele Girgis-Gabardo, Ahmed Mansouri, Peter Gruss, and Michael A Rudnicki. 2000. “Pax7 Is Required for the Specification of Myogenic Satellite Cells Skeletal Muscle Are Mitotically Quiescent and Are Activated in Response to Diverse Stimuli, Including Stretching, Exercise, Injury, and Electrical Stimulation (Schultz.” *Cell* 102: 777-86. [https://doi.org/10.1016/S0092-8674\(00\)00066-0](https://doi.org/10.1016/S0092-8674(00)00066-0).
- Shefer, Gabi, Monika Wleklinski-Lee, and Zipora Yablonka-Reuveni. 2004. “Skeletal Muscle Satellite Cells Can Spontaneously Enter an Alternative Mesenchymal Pathway.” *Journal of Cell Science*. <https://doi.org/10.1242/jcs.01419>.
- Shin, Jonghyun, Marjan M. Tajrishi, Yuji Ogura, and Ashok Kumar. 2013. “Wasting Mechanisms in Muscular Dystrophy.” *International Journal of Biochemistry and Cell Biology* 45 (10): 2266-79. <https://doi.org/10.1016/j.biocel.2013.05.001>.
- Smith, Edward C., Laurie S. Conklin, Eric P. Hoffman, Paula R. Clemens, Jean K. Mah, Richard S. Finkel, Michela Guglieri, et al. 2020. “Efficacy and Safety of Vamorolone in Duchenne Muscular Dystrophy: An 18-Month Interim Analysis of a Non-Randomized Open-Label Extension Study.” *PLoS Medicine*. <https://doi.org/10.1371/journal.pmed.1003222>.
- Spence, Heather J., Amardeep S. Dhillon, Marian James, and Steven J. Winder. 2004. “Dystroglycan, a Scaffold for the ERK-MAP Kinase Cascade.” *EMBO Reports* 5 (5): 484-89. <https://doi.org/10.1038/sj.embor.7400140>.
- Taglietti, Valentina, Giuseppe Angelini, Giada Mura, Chiara Bonfanti, Enrico Caruso, Stefania Monteverde, Gilles Le Carrou, Shhragim Tajbakhsh, Frédéric Relaix, and Graziella Messina. 2018. “RhoA and ERK Signalling Regulate the Expression of the

- Transcription Factor Nfix in Myogenic Cells.” *Development* 145 (21): dev163956. <https://doi.org/10.1242/dev.163956>.
- Taglietti, Valentina, Giovanni Maroli, Solei Cermenati, Stefania Monteverde, Andrea Ferrante, Giuliana Rossi, Giulio Cossu, Monica Beltrame, and Graziella Messina. 2016. “Nfix Induces a Switch in Sox6 Transcriptional Activity to Regulate MyHC-I Expression in Fetal Muscle.” *Cell Reports* 17 (9): 2354-66. <https://doi.org/10.1016/j.celrep.2016.10.082>.
- Tajbakhsh, S. 2009. “Skeletal Muscle Stem Cells in Developmental versus Regenerative Myogenesis.” *Journal of Internal Medicine* 266 (4): 372-89. <https://doi.org/10.1111/j.1365-2796.2009.02158.x>.
- Taylor, Michael V., and Simon M. Hughes. 2017. “Mef2 and the Skeletal Muscle Differentiation Program.” *Seminars in Cell and Developmental Biology* 72: 33-44. <https://doi.org/10.1016/j.semcdb.2017.11.020>.
- Tedesco, Francesco Saverio, Arianna Dellavalle, Jordi Diaz-Manera, Graziella Messina, and Giulio Cossu. 2010. “Repairing Skeletal Muscle: Regenerative Potential of Skeletal Muscle Stem Cells.” *Journal of Clinical Investigation*. <https://doi.org/10.1172/JCI40373>.
- Tsuchiya, Yoshifumi, Yasuo Kitajima, Hiroshi Masumoto, and Yusuke Ono. 2020. “Damaged Myofiber-Derived Metabolic Enzymes Act as Activators of Muscle Satellite Cells.” *Stem Cell Reports*, September. <https://doi.org/10.1016/j.stemcr.2020.08.002>.
- Ustanina, Svetlana, Jaime Carvajal, Peter Rigby, and Thomas Braun. 2007. “The Myogenic Factor Myf5 Supports Efficient Skeletal Muscle Regeneration by Enabling Transient Myoblast Amplification.” *STEM CELLS*. <https://doi.org/10.1634/stemcells.2006-0736>.
- Verhaart, Ingrid E. C., and Annemieke Aartsma-Rus. 2019. “Therapeutic Developments for Duchenne Muscular Dystrophy.” *Nature Reviews Neurology*. <https://doi.org/10.1038/s41582-019-0203-3>.
- Villalta, S. Armando, Hal X. Nguyen, Bo Deng, Tomomi Gotoh, and James G. Tidbal. 2009. “Shifts in Macrophage Phenotypes and Macrophage Competition for Arginine Metabolism Affect the Severity of Muscle Pathology in Muscular Dystrophy.” *Human Molecular Genetics*. <https://doi.org/10.1093/hmg/ddn376>.
- Wagner, Kathryn R. 2020. “The Elusive Promise of Myostatin Inhibition for Muscular Dystrophy.” *Current Opinion in Neurology* 33 (5): 621-28. <https://doi.org/10.1097/WCO.0000000000000853>.
- Waldrop, Megan A., and Kevin M. Flanigan. 2019. “Update in Duchenne and Becker

- Muscular Dystrophy.” *Current Opinion in Neurology* 32 (5): 722-27. <https://doi.org/10.1097/WCO.0000000000000739>.
- Webster, Cecelia, Laura Silberstein, Arthur P. Hays, and Helen M. Blau. 1988. “Fast Muscle Fibers Are Preferentially Affected in Duchenne Muscular Dystrophy.” *Cell*. [https://doi.org/10.1016/0092-8674\(88\)90463-1](https://doi.org/10.1016/0092-8674(88)90463-1).
- Webster, Micah T., Uri Manor, Jennifer Lippincott-Schwartz, and Chen Ming Fan. 2016. “Intravital Imaging Reveals Ghost Fibers as Architectural Units Guiding Myogenic Progenitors during Regeneration.” *Cell Stem Cell* 18 (2): 243-52. <https://doi.org/10.1016/j.stem.2015.11.005>.
- Wosczyzna, Michael N., and Thomas A. Rando. 2018. “A Muscle Stem Cell Support Group: Coordinated Cellular Responses in Muscle Regeneration.” *Developmental Cell* 46 (2): 135-43. <https://doi.org/10.1016/j.devcel.2018.06.018>.
- Yablonka-Reuveni, Zipora, Michael A. Rudnicki, Anthony J. Rivera, Michael Primig, Judy E. Anderson, and Priscilla Natanson. 1999. “The Transition from Proliferation to Differentiation Is Delayed in Satellite Cells from Mice Lacking MyoD.” *Developmental Biology*. <https://doi.org/10.1006/dbio.1999.9284>.
- Yamamoto, Masakazu, Nicholas P. Legendre, Arpita A. Biswas, Alexander Lawton, Shoko Yamamoto, Shahragim Tajbakhsh, Gabrielle Kardon, and David J. Goldhamer. 2018. “Loss of MyoD and Myf5 in Skeletal Muscle Stem Cells Results in Altered Myogenic Programming and Failed Regeneration.” *Stem Cell Reports* 10 (3): 956-69. <https://doi.org/10.1016/j.stemcr.2018.01.027>.
- Yang, Quan Jun, Huo Yan, Yong Long Han, Li Li Wan, Li Jie, Jin Lu Huang, Jin Lu, Peng Guo Chen, Gan Run, and Guo Cheng. 2017. “Selumetinib Attenuates Skeletal Muscle Wasting in Murine Cachexia Model through ERK Inhibition and AKT Activation.” *Molecular Cancer Therapeutics* 16 (2): 334-43. <https://doi.org/10.1158/1535-7163.MCT-16-0324>.
- Yin, Hang, Feodor Price, and Michael A. Rudnicki. 2013. “Satellite Cells and the Muscle Stem Cell Niche.” *Physiological Reviews* 93 (1): 23-67. <https://doi.org/10.1152/physrev.00043.2011>.
- Yoshida, Tomokazu, Yan Pan, Hironori Hanada, Yuko Iwata, and Munekazu Shigekawa. 1998. “Bidirectional Signaling between Sarcoglycans and the Integrin Adhesion System in Cultured L6 Myocytes.” *Journal of Biological Chemistry*. <https://doi.org/10.1074/jbc.273.3.1583>.
- Young, Christopher N.J., Maxime R.F. Gosselin, Robin Rumney, Aleksandra Oksiejuk,

- Natalia Chira, Lukasz Bozycki, Paweł Matryba, et al. 2020. "Total Absence of Dystrophin Expression Exacerbates Ectopic Myofiber Calcification and Fibrosis and Alters Macrophage Infiltration Patterns." *American Journal of Pathology* 190 (1): 190-205. <https://doi.org/10.1016/j.ajpath.2019.09.021>.
- Yuan, Jimin, Xiaoduo Dong, Jiajun Yap, and Jiancheng Hu. 2020. "The MAPK and AMPK Signalings: Interplay and Implication in Targeted Cancer Therapy." *Journal of Hematology and Oncology* 13 (1): 1-19. <https://doi.org/10.1186/s13045-020-00949-4>.
- Zammit, Peter S., Louise Heslop, Valérie Hudon, J. David Rosenblatt, Shahragim Tajbakhsh, Margaret E. Buckingham, Jonathan R. Beauchamp, and Terence A. Partridge. 2002. "Kinetics of Myoblast Proliferation Show That Resident Satellite Cells Are Competent to Fully Regenerate Skeletal Muscle Fibers." *Experimental Cell Research* 281 (1): 39-49. <https://doi.org/10.1006/excr.2002.5653>.
- Zeiser, Robert, Hana Andrlová, and Frank Meiss. 2018. "Trametinib (GSK1120212)." *Recent Results Cancer Res.* 211: 91-100. [https://doi.org/10.1007/978-3-319-91442-8\\_7](https://doi.org/10.1007/978-3-319-91442-8_7).
- Zhang, Hongbo, Dongryeol Ryu, Yibo Wu, Karim Gariani, Xu Wang, Peiling Luan, Davide D'Amico, et al. 2016. "NAD<sup>+</sup> Repletion Improves Mitochondrial and Stem Cell Function and Enhances Life Span in Mice." *Science*. <https://doi.org/10.1126/science.aaf2693>.
- Zhou, Bo, Jason M. Osinski, Juan L. Mateo, Ben Martynoga, Fraser J. Sim, Christine E. Campbell, Francois Guillemot, Michael Piper, and Richard M. Gronostajski. 2015. "Loss of NFIX Transcription Factor Biases Postnatal Neural Stem/Progenitor Cells Toward Oligodendrogenesis." *Stem Cells and Development*. <https://doi.org/10.1089/scd.2015.0136>.

## LIST OF PAPERS

- “RhoA and ERK Signalling Regulate the Expression of the Transcription Factor Nfix in Myogenic Cells.” *Development* 145 (21): dev163956. <https://doi.org/10.1242/dev.163956>  
Taglietti V., **Angelini G.**, Mura G., Bonfanti C., Caruso E., Monteverde S., Le Carrou G., Tajbakhsh S., Relaix F., and Messina G. 2018.
- “Nutritional Intervention with Cyanidin Hinders the Progression of Muscular Dystrophy.” *Cell Death and Disease* 11 (2). <https://doi.org/10.1038/s41419-020-2332-4>  
Saclier M., C. Bonfanti, S. Antonini, **G. Angelini**, G. Mura, F. Zanaglio, V. Taglietti, V. Romanello, M. Sandri, C. Tonelli, K. Petroni, M. Cassano and G. Messina. 2020.

## RESEARCH ARTICLE

# RhoA and ERK signalling regulate the expression of the transcription factor Nfix in myogenic cells

Valentina Taglietti<sup>1,2</sup>, Giuseppe Angelini<sup>1</sup>, Giada Mura<sup>1</sup>, Chiara Bonfanti<sup>1</sup>, Enrico Caruso<sup>1</sup>, Stefania Monteverde<sup>1</sup>, Gilles Le Carrou<sup>3</sup>, Shahragim Tajbakhsh<sup>3,4</sup>, Frédéric Relaix<sup>2</sup> and Graziella Messina<sup>1,\*</sup>

## ABSTRACT

The transcription factor Nfix belongs to the nuclear factor one family and has an essential role in prenatal skeletal muscle development, where it is a master regulator of the transition from embryonic to foetal myogenesis. Recently, Nfix was shown to be involved in adult muscle regeneration and in muscular dystrophies. Here, we have investigated the signalling that regulates Nfix expression, and show that JunB, a member of the AP-1 family, is an activator of Nfix, which then leads to foetal myogenesis. Moreover, we demonstrate that their expression is regulated through the RhoA/ROCK axis, which maintains embryonic myogenesis. Specifically, RhoA and ROCK repress ERK kinase activity, which promotes JunB and Nfix expression. Notably, the role of ERK in the activation of Nfix is conserved postnatally in satellite cells, which represent the canonical myogenic stem cells of adult muscle. As lack of Nfix in muscular dystrophies rescues the dystrophic phenotype, the identification of this pathway provides an opportunity to pharmacologically target Nfix in muscular dystrophies.

**KEY WORDS:** ERK kinases, Nfix, RhoA, Skeletal muscle, Signalling

## INTRODUCTION

Nuclear factor one X (Nfix) belongs to the nuclear factor one (Nfi) family of transcription factors, which consists of four closely related genes in vertebrates: *Nfia*, *Nfib*, *Nfic* and *Nfix* (Gronostajski, 2000). We demonstrated previously that Nfix plays an essential role in prenatal skeletal muscle development, where it is responsible for the crucial checkpoint: the transcriptional switch from embryonic to foetal myogenesis (Messina et al., 2010; Pistocchi et al., 2013; Taglietti et al., 2016). Moreover, we reported that Nfix also regulates postnatal muscle homeostasis and the correct timing of muscle regeneration following injury (Rossi et al., 2016). Indeed, in the absence of Nfix, muscle regeneration is strongly delayed, indicating that Nfix is crucial for maintenance of the correct timing of skeletal muscle regeneration (Rossi et al., 2016).

Based on this evidence, we suggested that slower regenerating and twitching dystrophic musculature might be more protected from progression of the pathology through the silencing of *Nfix*, as in both  $\alpha$ -sarcoglycan-deficient (*Sgca* null) (Duclos et al., 1998) and dystrophin-deficient (*mdx*) mice (Chapman et al., 1989). Indeed, lack of *Nfix* provides morphological and functional

protection from degenerative processes through promotion of a more oxidative musculature and by slowing down muscle regeneration, which is in contrast to previous studies that were aimed at promoting of muscle regeneration (Rossi et al., 2017a). We thus provided the proof of principle to propose a new therapeutic approach to delay the progression of such pathologies that is based on slowing down the degeneration-regeneration cycle, instead of increasing the rate of regeneration. It is thus necessary to identify the molecular signalling pathways that regulates Nfix expression. Therefore, we focused on this signalling in the prenatal period, which is characterised by a defined temporal window of *Nfix* expression.

Prenatal skeletal muscle development is a biphasic process that involves differentiation of two distinct populations of muscle progenitors, known as the embryonic and foetal myoblasts (Biressi et al., 2007b; Hutcheson et al., 2009). In mouse, the process of embryonic myogenesis takes place around embryonic day (E) 10.5–12.5. During this phase, embryonic myoblasts are committed to differentiate into primary slow-twitch fibres, which establishes the primitive architecture of the prenatal muscles. Then, foetal myogenesis occurs between E14.5 and E17.5, when foetal myoblasts give rise to fast-twitching secondary fibres. This allows complete maturation of the prenatal muscles and confers fibre type diversification, which fulfil different functional demands of adult skeletal muscle (Schiaffino and Reggiani, 2011). *Nfix* expression is low during embryonic myogenesis and is strongly increased specifically during foetal myogenesis (Messina et al., 2010; Taglietti et al., 2016; Biressi et al., 2007b).

Embryonic and foetal myoblasts differ in terms of their morphology, extracellular signalling responses and gene expression profiles (Biressi et al., 2007a,b). These differences indicate that a transcriptional change is needed to switch from embryonic to foetal myogenesis. Nfix activates foetal-specific genes, such as muscle creatine kinase (*Ckm*) and  $\beta$ -enolase (*Eno3*), and represses embryonic-specific genes, such as *Myh7* (Messina et al., 2010; Taglietti et al., 2016), underscoring its crucial role as a regulator of this temporal switch.

To investigate the signalling that regulates *Nfix* expression, we examined JunB, the second most highly expressed transcription factor during foetal myogenesis (Biressi et al., 2007b). JunB is a member of the activator protein 1 (AP1) family, which is involved in maintenance of muscle mass and prevention of atrophy in adult muscles (Raffaello et al., 2010). However, the role of JunB during prenatal development is unknown. Here, we demonstrate that JunB is necessary for *Nfix* activation, which leads, in turn, to establishment of the foetal genetic programme. We also investigated the Rho GTPase RhoA because of its important roles in many intracellular signalling pathways (Amano et al., 1996; Kimura et al., 1996), which are mediated through activation of its major effector, the Rho-kinase ROCK. The interplay between the RhoA/ROCK pathway and various signalling molecules, such as the ERK kinases

<sup>1</sup>Department of Biosciences, University of Milan, 20133 Milan, Italy. <sup>2</sup>Biology of the Neuromuscular System, INSERM IMRB U955-E10, UPEC, ENVA, EFS, Creteil 94000, France. <sup>3</sup>Stem Cells and Development, Department of Developmental and Stem Cell Biology, Institut Pasteur, Paris 75015 France. <sup>4</sup>CNRS UMR 3738, Institut Pasteur, Paris 75015 France.

\*Author for correspondence (graziella.messina@unimi.it)

 V.T., 0000-0001-7166-6748; G.M., 0000-0001-8189-0727

(Zuckerbraun et al., 2003; Li et al., 2013), is known to promote the correct transduction of extracellular signals, and thus to condition the gene expression networks. Here, we report that the RhoA/ROCK axis defines the identity of embryonic myoblasts through repression of the activation of the ERK kinases and, as a consequence, of *JunB* and *Nfix*. Conversely, during foetal myogenesis, ERK activity is necessary for expression of *JunB*, which activates *Nfix*, to promote the beginning of the foetal myogenesis programme, and hence complete the maturation of prenatal muscle. Of particular interest, ERK activity is also necessary for *Nfix* expression in juvenile satellite cell-derived myoblasts, demonstrating that the ERK pathway is conserved from prenatal to postnatal myogenesis.

## RESULTS

### JunB regulates the expression of Nfix, which is then self-maintained

Although it has been demonstrated that *Nfix* and *JunB* are expressed at high levels specifically during foetal myogenesis (Biressi et al., 2007b), the temporal aspects of their expression profiles have not been defined in detail. We first used fluorescence-activated cell sorting (FACS) to analyse the transcript levels of *Nfix* and *JunB* in

freshly isolated purified myoblasts from *Myf5<sup>GFP-P/+</sup>* embryonic muscle (Kassar-Duchossoy et al., 2004) at E11.5, E12.5 and E13.5, and from foetal muscle at E14.5, E15.5, E16.5 and E17.5. Both *Nfix* and *JunB* started to be expressed around E14.5, and their expression then increased at E15.5, remaining high up to E17.5 (Fig. S1A,B). Western blotting of total skeletal muscle lysates at these different stages showed similar profiles of *Nfix* and *JunB* expression, as also revealed by qRT-PCR (Fig. 1A, Fig. S1C,D). These data confirmed that *Nfix* and *JunB* expression occurs only during the foetal stages of muscle development, specifically from E14.5.

To better characterise the patterns of expression of *Nfix* and *JunB* in foetal muscle progenitors, we carried out immunostaining on *Myf5<sup>GFP-P/+</sup>*-purified myoblasts obtained from fetuses at E14.5, E15.5 and E16.5. Freshly isolated myoblasts were maintained in culture for 2 h, to allow their adhesion, and then *Nfix* and *JunB* expression was monitored (Fig. 1B-C, Fig. S1E-F). At all time points analysed, a large proportion of the foetal myoblasts co-expressed *Nfix* and *JunB* (E14.5, 77.2%±2.52%; E15.5, 85%±4.14%; E16.5, 82%±3.91%), and at E14.5 and E15.5 there were some myoblasts positive for only *JunB* (E14.5, 10.3%±0.65%; E15.5, 10.2%±1.02%). Conversely, at E16.5, some myoblasts were positive for *Nfix* but not for *JunB* (13.9%±1.79%), and the

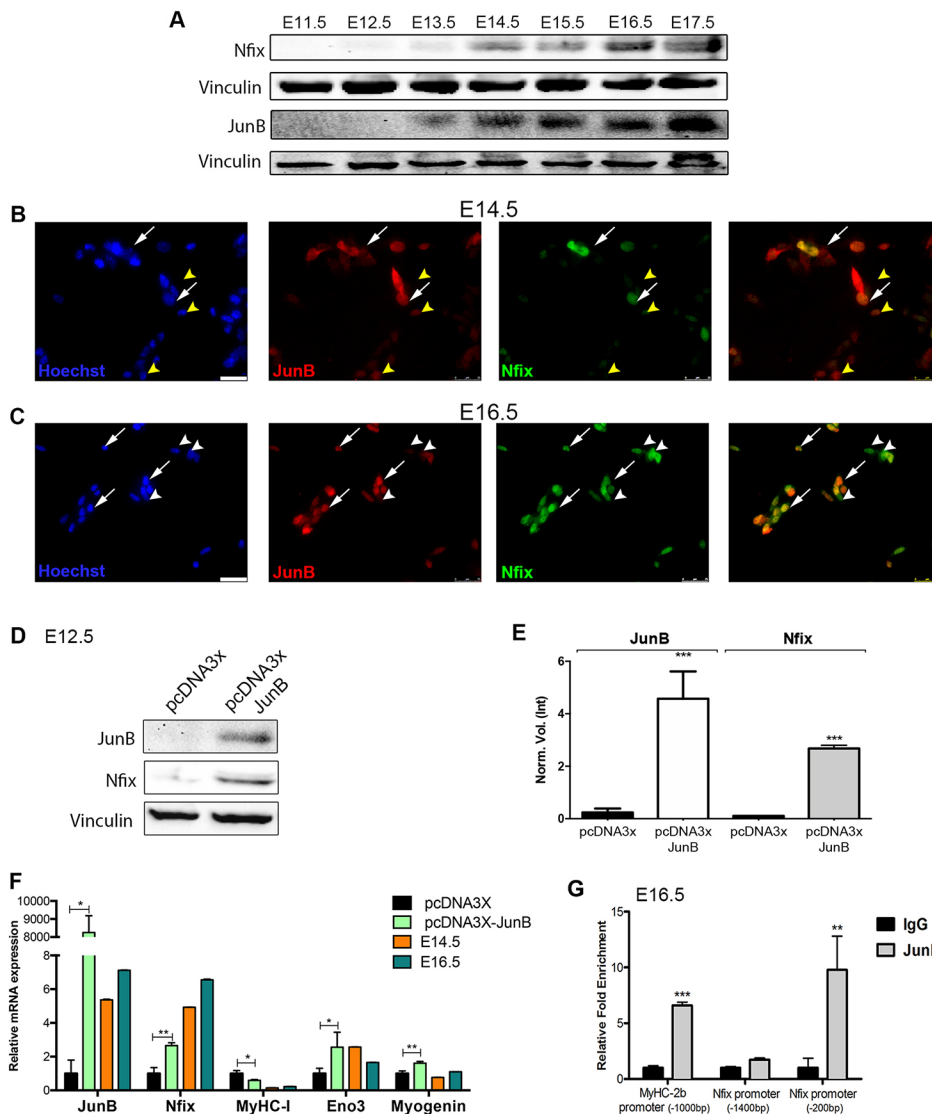


**Fig. 1. Developmental timing of *Nfix* and *JunB*, and direct activation of *Nfix*.**

(A) Representative western blots for *Nfix* and *JunB* for purified *Myf5<sup>GFP-P/+</sup>* myoblasts isolated from E11.5 to E17.5 muscle. Vinculin was used to normalise the total amount of loaded protein (*JunB* and *Nfix* were analysed on two separate gels, with data normalised to the respective vinculin). (B,C) Representative immunofluorescence for *JunB* (red) and *Nfix* (green) with freshly isolated *Myf5<sup>GFP-P/+</sup>*-purified myoblasts at E14.5 (B) and E16.5 (C). Nuclei were counterstained with Hoechst. White arrows, myoblasts co-expressing *JunB* and *Nfix*; yellow arrowheads in B, nuclei positive for *JunB* and negative for *Nfix*; white arrowheads in C, myoblasts positive for *Nfix* but not for *JunB*. Scale bars: 25  $\mu$ m. (D) Representative western blots of lysates from embryonic (E12.5) myoblasts overexpressing *JunB* (pcDNA3.1x-*JunB*) compared with control myoblasts (pcDNA3.1x). Vinculin was used to normalise the total amount of loaded protein. (E) Quantitative densitometry of *Nfix* and *JunB* in independent western blot experiments ( $***P<0.001$ ;  $n=5$ ). (F) qRT-PCR from *Myf5<sup>GFP-P/+</sup>*-purified embryonic myoblasts (E12.5) transfected with the pcDNA3x-*JunB* overexpressing vector or with pcDNA3x. The data are compared with the endogenous levels at E14.5 and E16.5 muscles ( $*P<0.05$ ;  $**P<0.01$ ;  $n=5$ ). (G) ChIP assay with anti-*JunB* antibodies for foetal myotubes (E16.5) on the positive control region (MyHC-2B promoter), the distal *Nfix* promoter region (1400 bp upstream of *Nfix* transcription start site) and the proximal *Nfix* promoter (–200 bp upstream of *Nfix* transcription start site). IgG was used as the unrelated antibody ( $**P<0.01$ ;  $***P<0.001$ ;  $n=5$ ).

increased number of Nfix-positive myoblasts at E16.5 is statistically significant compared with E14.5 (Fig. S1G).

As JunB appeared to be expressed earlier than Nfix, the interplay between Nfix and JunB was investigated. Embryonic myoblasts were transfected with the pcDNA3.1x-JunB expressing vector and the expression of Nfix then analysed by western blotting. Nfix was activated earlier in the embryonic myoblasts overexpressing JunB, compared with those with the only control vector (Fig. 1D,E). To further support this observation, *Myf5<sup>GFP-P/+</sup>*-purified embryonic myoblasts were induced to express JunB upon pcDNA3.1x-JunB transfection, and the transcript levels of *Nfix* were examined by qRT-PCR. The population of embryonic myoblasts expressing JunB also expressed Nfix, whereas Nfix was essentially absent in the control myoblasts (Fig. 1F), suggesting that JunB was responsible for the activation of Nfix. As a consequence, JunB-positive embryonic myoblasts (and therefore Nfix) show earlier downregulation of the typical embryonic marker MyHC-I (Myh7) and upregulation of the foetal marker  $\beta$ -enolase. Indeed, Nfix has been shown to inhibit MyHC-I (Messina et al., 2010; Taglietti et al., 2016) and activate  $\beta$ -enolase (Messina et al., 2010). These data indicate that the induction of JunB in embryonic myoblasts promotes the expression of Nfix and, therefore, the activation of the foetal genetic programme.

To determine whether JunB can bind Nfix regulatory regions, *in silico* sequence analysis was performed for the *Nfix* promoter.

The two AP-1 consensus sites [i.e. 5'-TGA(G/C)TCA-3'; Chinenov and Kerppola, 2001; Eferl and Wagner, 2003] were identified about 200 base pairs (bp) and 1400 bp upstream of the *Nfix* gene transcription start site. To determine whether JunB could bind these two sites, chromatin immunoprecipitation (ChIP) assays were carried out for JunB on differentiated foetal myoblasts (E16.5). As shown in Fig. 1G, JunB was directly bound to the *Nfix* promoter in the region that was proximal to the transcription start site (-200 bp), but not to the distal region (-1400 bp). The *MyHC-2b* promoter was used as the positive control sequence for the ChIP assays with JunB (Raffaello et al., 2010). Taken together, these data show that JunB therefore binds the Nfix promoter and, through an unknown mechanism, is able to regulate Nfix expression.

Similarly, we investigated whether the expression of Nfix in embryonic muscles can promote *JunB* expression in embryonic myoblasts transfected with the pCH-Nfix2 vector. However, the expression of *Nfix* did not induce *JunB* expression in the embryonic myoblasts (Fig. 2A). To support this observation, protein levels of JunB were determined in embryonic myoblasts purified from transgenic mice that overexpressed Nfix (i.e. *Tg:Mlc1f-Nfix2*) under the transcriptional control of the myosin light chain 1F promoter and enhancer (Jiang et al., 2002; Messina et al., 2010). JunB was essentially absent at E12.5 in the *Tg:Mlc1f-Nfix2* embryonic myoblasts, as in the wild-type littermates (Fig. 2B, Fig. S2A). As expected, JunB was also

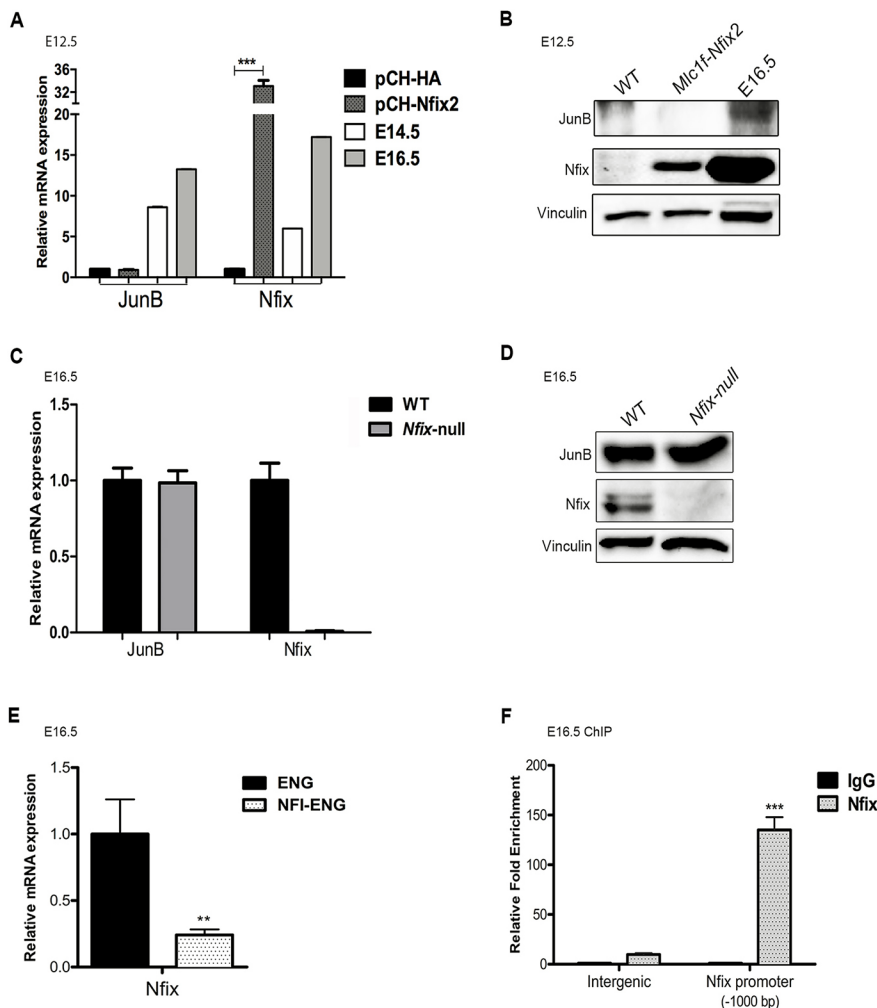


**Fig. 2. Nfix does not regulate JunB, but promotes its own expression.** (A) qRT-PCR for JunB and Nfix for embryonic (E12.5) myoblasts transfected with the Nfix-overexpressing vector (pCH-Nfix2) or the control vector (pCH-HA). The data are compared with the endogenous levels at E14.5 and E16.5 muscles ( $***P < 0.01$ ;  $n = 5$ ). (B) Representative western blots for Nfix and JunB of protein extracts from wild-type and *Tg:Mlc1f-Nfix2* embryonic muscle (E12.5) with foetal muscle (E16.5) as positive control. Vinculin was used to normalise the total amount of loaded protein. (C) qRT-PCR for JunB and Nfix on wild-type and *Nfix*-null foetal muscle (E16.5). (D) Representative western blots for Nfix and JunB on lysates from wild-type and *Nfix*-null foetal muscle (E16.5). Vinculin was used to normalise the total amount of loaded protein. (E) qRT-PCR for Nfix on foetal myoblasts transfected with the dominant-negative NFI-engrailed (NFI-ENG) compared with foetal myoblasts expressing engrailed domain (ENG) ( $**P < 0.01$ ;  $n = 5$ ). (F) ChIP assay using anti-Nfix antibodies on foetal myotubes to test Nfix binding to its own promoter (-1000 bp; Nfix promoter). An intergenic region was used as the negative control and IgG as the unrelated antibody ( $***P < 0.01$ ).

expressed normally in *Nfix*-null foetal myoblasts (Campbell et al., 2008) (Fig. 2C-D, Fig. S2B), indicating that *Nfix* does not control *JunB* expression.

To determine whether once expressed, *Nfix* can maintain its own expression, foetal myoblasts were transduced with a lentiviral vector that expressed a dominant-negative Nfi-engrailed (NFI-ENG) fusion protein composed of the *Drosophila* ENG transcriptional repression domain fused with the *Nfia* DNA-binding and dimerisation domain (Bachurski et al., 2003). Overexpression of NFI-ENG resulted in inhibition of Nfi factor transactivation activity, as NFI-ENG acts as a dominant-negative form (Messina et al., 2010). The NFI-ENG foetal myoblasts showed strong downregulation of *Nfix* compared with the control foetal myoblasts that expressed only the engrailed domain (ENG) (Fig. 2E). This indicated that Nfi factors can activate the transcription of *Nfix*.

To further support these data, ChIP assays were carried out for *Nfix* in differentiated foetal myoblasts. These showed direct binding of *Nfix* to its own promoter at an NFI consensus binding site located 1000 bp upstream of the *Nfix* gene transcription start site (Fig. 2F). Taken together, these data demonstrate that *Nfix*, once activated by a mechanism that in part involves JunB, is able in turn to promote its own expression.

### JunB is necessary for *Nfix* induction, but not for the direct activation of the foetal myogenic programme

As we showed that JunB promotes the expression of *Nfix* in embryonic myoblasts, we then investigated whether JunB is necessary to activate the myogenic foetal programme (Messina et al., 2010). For this reason, cell sorting was used to isolate foetal myoblasts from E16.5 *Myf5*<sup>GFP-P/+</sup> muscles, and JunB was silenced using a small-hairpin RNA (shJunB, foetal myoblasts). As control, *Myf5*<sup>GFP-P/+</sup>-purified foetal myoblasts were transduced with a scrambled lentiviral vector that targeted a non-related sequence. When cultured under conditions that promote differentiation, the purified foetal myoblasts silenced for JunB showed the standard embryonic phenotype, which was characterised by mononucleated myocytes and multinucleated myotubes that contained only a few nuclei (Biressi et al., 2007b). This specific inhibition of JunB decreased the expression of *Nfix* (Fig. 3A,B), whereas the typical embryonic marker MyHC-I was greatly induced (Fig. 3C).

As the foetal programme was affected, we investigated whether in shJunB foetal myoblasts, the effects on foetal myogenesis were specifically due to the lack of JunB, or were the consequence of downregulation of *Nfix*. Purified shJunB foetal myoblasts were transduced with an HA-tagged *Nfix2* expression vector

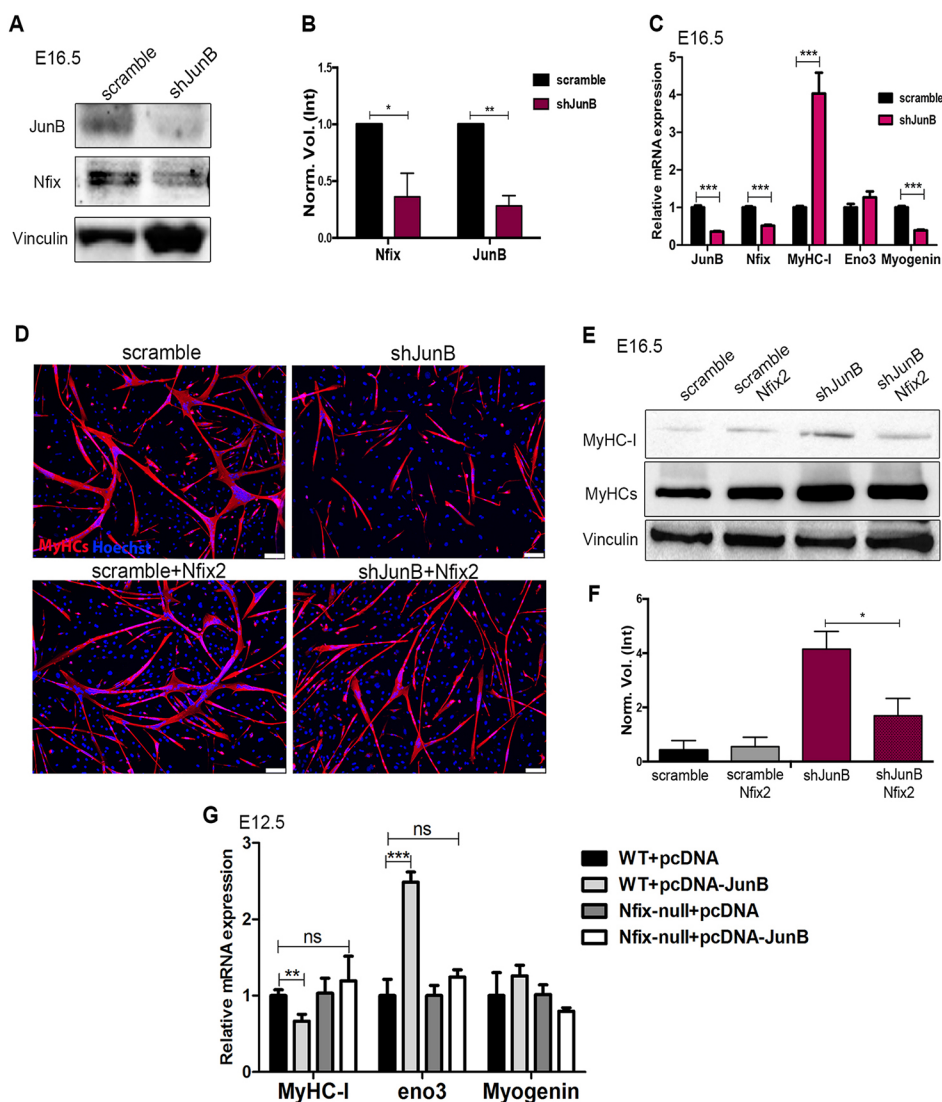


**Fig. 3. Silencing of JunB leads to the acquisition of embryonic features as a consequence of downregulation of *Nfix*.**

(A) Representative western blots of shJunB and control (scramble) foetal differentiated myoblasts. Vinculin was used to normalise the total amount of loaded protein. (B) Quantitative densitometry of *Nfix* and JunB of five independent western blot assays (\* $P < 0.05$ ; \*\* $P < 0.01$ ; n=5). (C) qRT-PCR of *Myf5*<sup>GFP-P/+</sup>-purified foetal myoblasts infected with lenti-shJunB or the scramble vector, for analysis of expression of *Nfix* and MyHC-I (\*\* $P < 0.001$ ). (D) Representative immunofluorescence images of differentiated *Myf5*<sup>GFP-P/+</sup>-purified foetal myoblasts co-transduced with the shJunB and HA-*Nfix2* lentivectors (shJunB+Nfix2) or the single and non-targeting (scramble) vectors as controls, showing MyHCs (MF20; red) and Hoechst (blue). Scale bars: 100  $\mu$ m. (E) Representative western blots of differentiated foetal myoblasts (scramble+pCH-HA, scramble+Nfix2, shJunB+pCH-HA and shJunB+Nfix2) showing MyHC-I expression. MyHCs (MF20) and vinculin were used to normalise the total amount of loaded protein. (F) Densitometric quantification of MyHC-I protein versus vinculin (\* $P < 0.05$ ; n=5). (G) qRT-PCR of wild-type and *Nfix*-null embryonic myoblasts transfected with the JunB-overexpressing vector or with the control vector (pcDNA) (\*\* $P < 0.01$ ; \*\*\* $P < 0.001$ ; n=5).

(shJunB+Nfix2) (Fig. S2C) and cultured under differentiating conditions. After 3 days *in vitro*, silencing of JunB reduced the number of nuclei per myotube (Fig. S2D), the fusion index (Fig. S2E) and the area of each myotube (Fig. S2F), which indicated impaired foetal myoblast differentiation and fusion. More importantly, the foetal shJunB+Nfix2 cultures contained larger myotubes than the foetal shJunB cultures, with more nuclei in clusters in the centres of the myotubes (Fig. 3D). Furthermore, the morphology of the shJunB+Nfix2 myotubes was similar to those for both scrambled and Nfix2-transduced cultures, showing a significant rescue of the analysed morphological parameters (Fig. 3D, Fig. S2D-F), which indicated that the rescue of Nfix function in shJunB foetal myoblasts was sufficient to reactivate the foetal programme. To determine whether this rescue was associated with a phenotypic change, western blotting was used to examine the expression of the typical embryonic marker MyHC-I. As shown in Fig. 3E,F, the shJunB foetal myoblasts expressed high levels of slow MyHC-I after differentiation, whereas this upregulation of MyHC-I was not seen for the differentiated shJunB+Nfix2 foetal myoblasts, with downregulation of MyHC-I seen instead, as expected. Moreover, wild-type embryonic myoblasts overexpressing JunB showed downregulated MyHC-I and activated  $\beta$ -enolase as a consequence of the Nfix upregulation. In contrast, in the *Nfix*-null embryonic myoblasts, overexpression of JunB did not lead to any changes in MyHC-I and  $\beta$ -enolase, as the markers of embryonic and foetal myogenesis, respectively (Fig. 3G, Fig. S2G). These data demonstrate that, although JunB is required for *Nfix* induction, it is not sufficient to activate the foetal myogenic programme. Hence, Nfix acts downstream of JunB and is strictly required for activation of the foetal myogenic programme.

### The RhoA/ROCK axis negatively regulates ERK activity

We next aimed to identify the upstream signalling necessary for *JunB* induction, and therefore for *Nfix* expression. The Rho GTPase RhoA is required for the myogenic process, and its activity must be finely regulated in time for correct muscle differentiation (Castellani et al., 2006). To determine whether RhoA activity is regulated temporally during prenatal muscle development, GST-Rhotekin pull-down assays were performed on lysates of E12.5, E14.5 and E16.5 myoblasts, with active Rho GTPases quantified by western blotting. As shown in Fig. 4A, GTP-bound activated Rho was increased at E12.5 and E14.5, whereas at E16.5 it decreased. Thus, the Rho GTPases were selectively activated during embryonic myogenesis and shut down at the foetal stage. Five independent pull-down experiments were quantified through the normalisation of the relative amount of pixel intensity (Int) on the reference band, showing a statistically significant decrease in RhoA activity at E16.5 compared with both E12.5 and E14.5 (Fig. S2H).

RhoA is an upstream activator of ROCK kinases and requires ROCK activity for its effects, which also impinge upon myogenesis (Nishiyama et al., 2004; Pelosi et al., 2007). Thus, to support the activation of RhoA signalling during embryonic myogenesis, phosphorylation of the specific ROCK substrate MYPT1 on Thr 696 was examined during prenatal skeletal muscle development (Seko et al., 2003; Murányi et al., 2005). As shown in Fig. 4B and quantified in Fig. S3A, MYPT1 phosphorylation was seen only during the early phase of myogenesis, between E11.5 and E12.5, which confirmed that RhoA and ROCK are both active during primary myogenesis.

The RhoA/ROCK axis is known to regulate the signalling of many intracellular substrates, such as the ERK kinases (Zuckerbraun et al., 2003; Li et al., 2013). The activities of the

ERK kinases were therefore examined during prenatal development, as determined by their phosphorylation. Indeed, the phosphorylated ERKs were seen only during foetal myogenesis, from E14.5 to E17.5 (Fig. 4C, Fig. S3B). Given that RhoA/ROCK signalling might be involved in embryonic to foetal transition, embryonic myoblasts were treated with the ROCK inhibitor Y27632 (Uehata et al., 1997). Proliferation, differentiation and apoptosis were assessed after 3 days of Y27632 or vehicle treatment (Fig. 4D-I). EdU incorporation, after a single 2 h pulse, and the apoptosis (quantification of embryonic myoblasts expressing the cleaved and active form of caspase 3) did not show significant changes between Y27632-treated and control cells (Fig. 4D-F). Conversely, the morphology of Y27632-exposed embryonic myotubes resembled the typical feature of foetal differentiated fibres with a tendency for increased fusion index (Fig. 4G-I), suggesting a precocious switch toward the foetal phase. To better elucidate the changes induced by ROCK inhibition, we evaluated ERK activity by immunoblotting and showed that embryonic myoblasts treated with Y27632 had greatly increased ERK activity (Fig. 4J). Conversely, activated phospho-ERK (pERK) decreased in foetal myoblasts expressing the activated RhoA (RhoV14), compared with control cells (Fig. 4J). Densitometric quantification of embryonic myoblasts treated with Y27632 or vehicle and of foetal myoblasts expressing RhoV14 or a control plasmid revealed a significant increase of pERK in embryonic cells treated with ROCK inhibitor, expressed as a ratio of the total amount of ERK kinases. In contrast, foetal myoblasts expressing RHOV14 showed a statistically significant decrease in the content of activated ERK (Fig. 4K). Taken together, these data indicate that ROCK mediates the negative regulation that RhoA signalling has on ERK kinase activity.

### The ERK kinases are modulated upon RhoA/ROCK misregulation in muscle progenitors

To determine whether the RhoA/ROCK axis has a role in regulation of *JunB* and *Nfix*, the effects of the ROCK inhibitor Y27632 on *Myf5*<sup>GFP-P/+</sup>-purified embryonic myoblasts were analysed. Here, ROCK inhibition led to increased *Junb* and *Nfix* expression, but did not affect myogenin and MyHC-emb expression (Fig. 5A). As expected, genes specifically expressed during embryonic myogenesis, such as *Myh7*, *Smad6* and *Tcf15* (Biressi et al., 2007a,b), were decreased and an earlier expression of a panel of foetal genes, such as  $\beta$ -enolase (*Eno3*), *Nfia*, *Ckm* and *Prkcq* was observed (Figs 5A, S3C).

The effects of ROCK inhibition on the early expression of *Junb* and *Nfix* and on the downregulation of slow MyHC were also investigated by western blotting (Fig. 5B), and quantified in Fig. S3D. *Myf5*<sup>GFP-P/+</sup>-purified foetal myoblasts that were transduced with a lentiviral vector expressing the constitutively active form of RhoA (RHOV14) showed a dramatic decrease in *JunB* and *Nfix* mRNA levels. Instead, MyHC-I was highly expressed, rather than being repressed, which indicated that RHOV14-expressing foetal myoblasts acquired a more embryonic-like gene transcription profile (Fig. 5C). Western blotting confirmed that the *JunB* and *Nfix* transcription factors were downregulated in the RHOV14 foetal myoblasts, whereas MyHC-I was significantly induced (Fig. 5D and Fig. S3E).

As the RhoA and ROCK axis is able to block the activation of ERK (Li et al., 2013), we hypothesised that the ERK kinases might regulate *Junb* and *Nfix* expression. Thus, foetal myoblasts were treated with the ERK antagonist PD98059, which selectively inhibits MEK kinases, preventing the activation of ERK signalling. First, we analysed the effects of ERK inhibition on foetal myoblasts

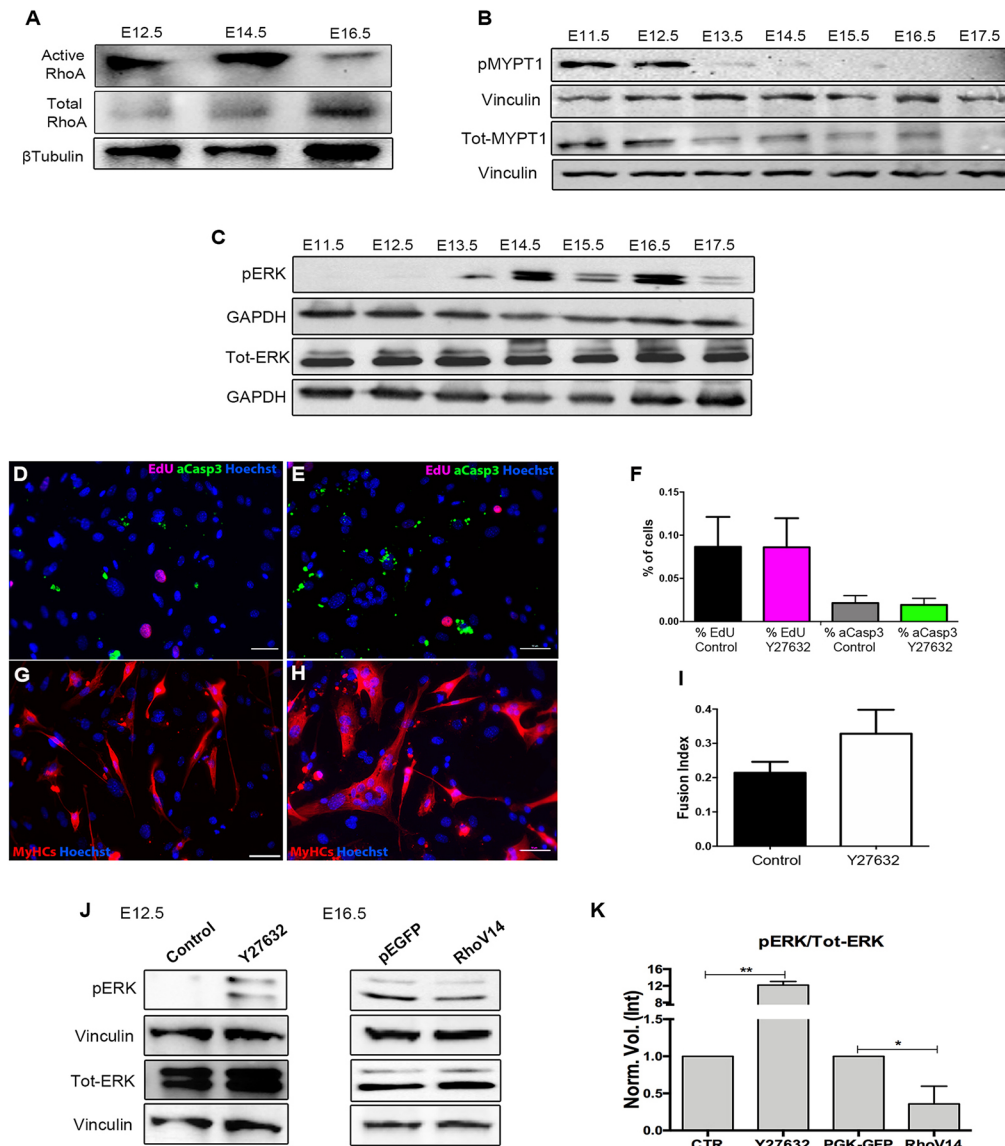


**Fig. 4. The RhoA/ROCK axis inhibits ERK kinase activity during embryonic myogenesis.** (A) Representative pull-down assay of lysates of myoblasts at E12.5, E14.5 and E16.5. Active Rho GTPases were detected using western blotting, and the amount of input is shown in the lower panel (total RhoA).  $\beta$ -Tubulin was used to normalise the total input. (B,C) Representative western blots of E11.5 to E17.5 muscle for MYPT1 phosphorylated at Thr696 by ROCK (B) and for phosphorylated ERK (pERK) and total ERK (Tot-ERK) (C). In B, total MYPT1 (Tot-MYPT1) and vinculin were used to normalise the loaded protein; to avoid cross-reactions between the antibodies, the same samples were analysed on separate gels. In C, GAPDH was used to normalise the loaded protein, and although the antibodies against tot-ERK and pERK were raised in different species, the same samples were analysed on separate gels. (D,E) Immunofluorescence for cleaved caspase 3 (active caspase, aCasp3) and EdU detection on embryonic (E12.5) myotubes treated with vehicle (D) or Y27632 (E) for 3 days until the differentiation. (F) Quantification of the percentage of cells positive for EdU, upon 2 h EdU pulse, and of the percentage of cells expressing cleaved caspase 3 (aCasp3) at the nuclear and/or perinuclear level. The quantification was performed on differentiated embryonic myotubes after the daily treatment with Y27632. No significant changes were observed between control and Y27632-treated cells ( $n=5$ ). (G,H) Immunofluorescence for sarcomeric myosins (MyHCs) and Hoechst of control (G) and Y27632-treated (H) embryonic myotubes. (I) Graph illustrating the fusion index, calculated as ratio of nuclei number in myocytes/myotubes on the total number of nuclei ( $n=5$ ). (J) Representative western blots of: embryonic myoblasts (E12.5) treated with the ROCK inhibitor Y27632 or with vehicle (left); and foetal myoblasts (E16.5) transduced with the lentivirus expressing constitutively activated RhoA (RHOV14) or the control (PEGK-GFP) (right). Vinculin was used to normalise the amount of loaded protein. (K) Quantitative densitometry of phosphorylated (p)ERK normalised according to the ratio between total ERK and vinculin ( $*P<0.05$ ;  $**P<0.01$ ;  $n=5$ ).

by examining proliferation, apoptosis, differentiation and the fusion index. Both proliferation, after an EdU pulse of 2 h, and apoptosis were not affected by ERK inhibition (Fig. 5E-G), whereas only incubation for 12 h with PD98059 delayed the differentiation of foetal myoblasts, as demonstrated by the decrease of the fusion index compared with the control cells (Fig. 5H-J), and changed the expression of some genes specifically expressed during embryonic or foetal myogenesis (Fig. S3F).

Western blot was used to examine JunB and Nfix protein levels. The immunoblot in Fig. 5K and the densitometric analysis in Fig. S3G show that expression of JunB and Nfix was indeed reduced in these PD98059-treated foetal myoblasts. These results indicate that activation of ERK kinases can promote foetal myogenesis through the activation of JunB and Nfix.

We then examined whether the ERKs are the RhoA/ROCK signalling downstream targets during myogenesis. As shown

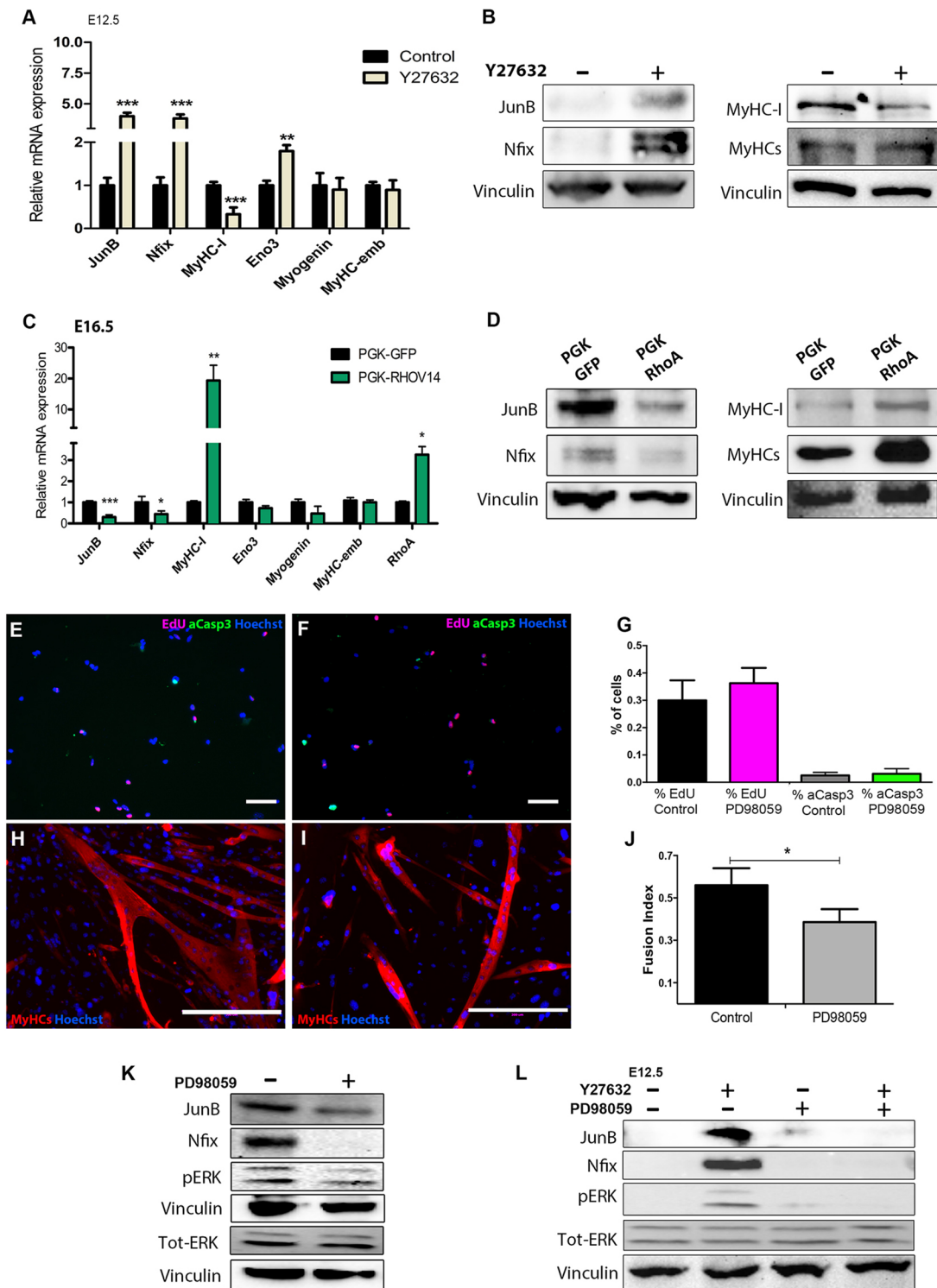


**Fig. 5. RhoA and ROCK activities inhibit foetal myogenesis through inhibition of JunB and Nfix, while ERK activity promotes JunB and Nfix expression.** (A) qRT-PCR for expression of embryonic and foetal markers of Myf5<sup>GFP-P/+</sup>-purified embryonic myoblasts treated with the ROCK inhibitor Y27632 or vehicle (\*\* $P < 0.01$ ; \*\*\* $P < 0.001$ ;  $n = 5$ ). (B) Representative western blot of embryonic myoblasts treated with the ROCK inhibitor Y27632 or not treated. MyHCs (MF20) and vinculin were used to normalise the total amount of loaded protein. (C) qRT-PCR for expression of embryonic and foetal markers of Myf5<sup>GFP-P/+</sup>-purified foetal myoblasts transduced with constitutively activated RhoA (PGK-RhoV14) or control (PGK-GFP) lentivectors (\* $P < 0.05$ ; \*\* $P < 0.01$ ). (D) Representative western blots for JunB, Nfix and MyHC-I of foetal myoblasts overexpressing constitutively activated RhoA (PGK-RHOV14) or control (PGK-GFP). MyHCs (MF20) and vinculin were used to normalise the total amount of loaded protein. (E, F) EdU detection and immunofluorescence for active and cleaved caspase 3 (aCasp3) on control (E) and PD98059-treated (F) foetal myoblasts ( $n = 5$ ). (G) Quantification of the percentage of EdU- or aCasp3-positive cells ( $n = 5$ ). (H, I) Immunofluorescence for sarcomeric myosins (MyHCs) and Hoechst of control (H) and PD98059-treated (I) foetal myotubes. (J) Graph illustrating the fusion index of foetal myotubes treated with vehicle only (control) or with the ERK inhibitor PD98059 (\* $P < 0.05$ ;  $n = 5$ ). (K) Representative western blots of foetal myoblasts treated with the ERK inhibitor PD98059 or vehicle. Vinculin was used to normalise the total amount of loaded protein. (L) Representative western blots of embryonic myoblasts treated with the ROCK inhibitor Y27632 and/or the ERK inhibitor PD98059 or vehicle.

in Fig. 5L and in Fig. S3H-J, ROCK inhibition in embryonic myoblasts enhanced ERK phosphorylation and activation, which led to upregulation of JunB and Nfix. Furthermore, treatment with Y27632 (ROCK inhibitor) and PD98059 (ERK antagonist) led to reductions in JunB and Nfix expression, as in the control embryonic myoblasts. These data indicate that the ERK kinases are downstream effectors of RhoA/ROCK during prenatal myogenesis, and that ERK activity is necessary for activation of JunB and Nfix.

### ERK kinases regulate Nfix expression *in vivo*

To determine whether ERK inhibition can also modify Nfix regulation *in vivo*, foetuses were exposed to PD98059. Pregnant mice were treated on day 15.5 of gestation (E15.5) with a single systemic injection of either vehicle (dimethylsulfoxide) or 10 mg/kg PD98059, and the foetuses were harvested the day after (Fig. 6A). Western blotting of myoblasts isolated from these foetuses demonstrated that PD98059 treatment decreased the phosphorylation of the ERK kinases (pERK), which was associated with downregulation of Nfix and of JunB (Fig. 6B). The reduction of Nfix, JunB and pERK protein levels were also measured by densitometric quantification (Fig. 6C). Morphologically, the PD98059-exposed foetal muscles showed a shift in myofibre area distribution towards smaller values compared with the control

(Fig. 6D-F), which correlates with the reduction in the fusion index observed *in vitro* (Fig. 5H-J).

Furthermore, immunofluorescence analysis of foetal cross-sections with antibodies directed against all of the sarcomeric myosins and Nfix (Fig. 6G-L) clearly showed a reduction of Nfix in foetal muscle. Consistent with this observation, we noted a significant decrease in the percentage of myonuclei expressing Nfix upon PD98059 treatment compared with the control (Fig. 6O). In addition, Nfix expression was not altered in the extra-muscular tissues of these PD98059-exposed foetuses, which indicated that the ERK kinases regulate Nfix specifically in developing skeletal muscle. To validate the finding that the downregulation of Nfix specifically occurred in myogenic foetal progenitors, we performed immunofluorescence for Pax7, a marker of the myogenic lineage, and Nfix on muscle sections of control and PD98059-exposed foetuses. As shown in Fig. 6M,N and quantified in Fig. 6P, upon PD98059 treatment, there was a lower number of cells co-expressing Pax7 and Nfix, indicating that systemic injection of PD98059 suppresses Nfix expression in foetal muscle *in vivo*.

### ERK kinases also control Nfix postnatally

Recently, we demonstrated that Nfix is expressed also in adult muscle satellite (stem) cells (Rossi et al., 2016), and that its

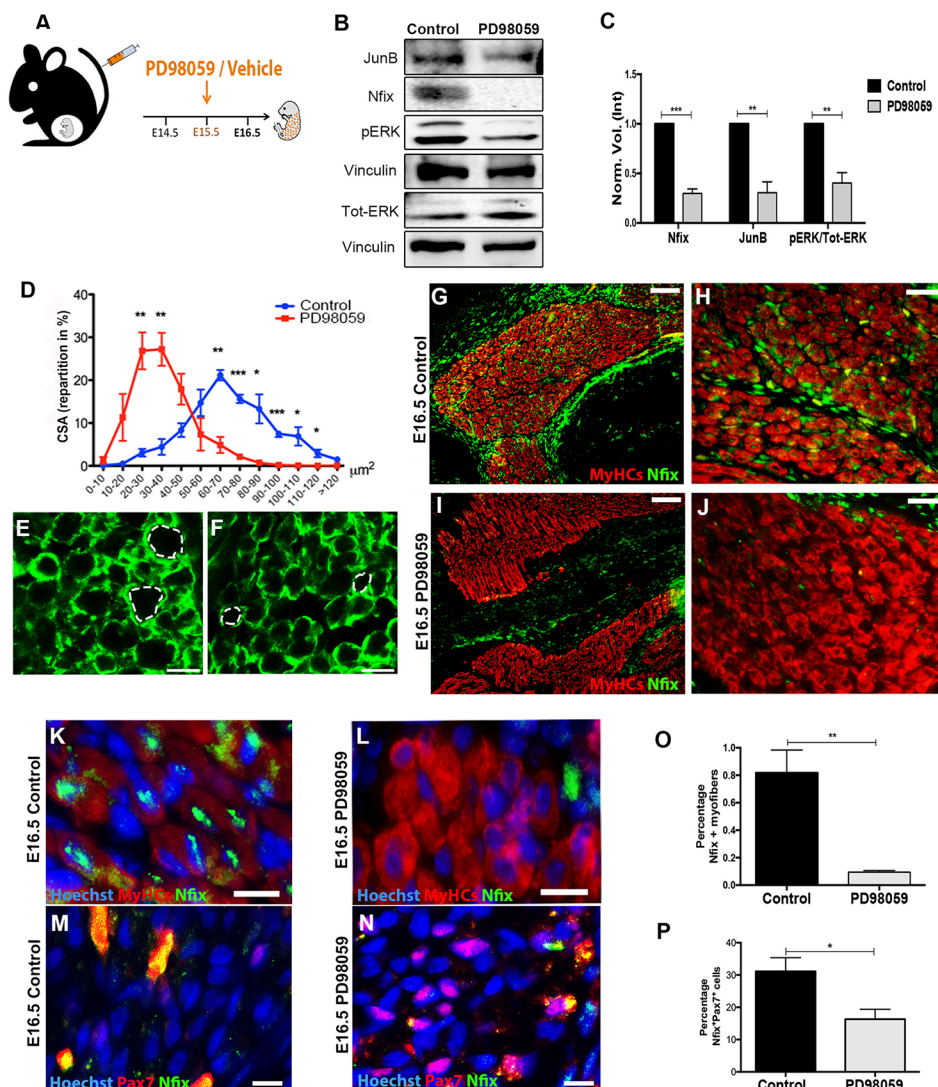


**Fig. 6. Inhibition of ERK activity blocks Nfix expression *in vivo*.** (A) Experimental scheme of PD98059 administration to pregnant mice at E15.5. (B) Representative western blots of foetal myoblasts isolated from PD98059-treated or control (vehicle) foetuses. Vinculin was used to normalise the total amount of loaded protein. (C) Quantitative densitometry of Nfix, JunB and the ratio of pERK to total ERK. (\*\* $P < 0.01$ ; \*\*\* $P < 0.001$ ;  $n = 5$ ). (D) Myofibre cross-sectional area (CSA) distribution in foetal muscles treated with vehicle only or PD98059 (\* $P < 0.05$ ; \*\* $P < 0.01$ ; \*\*\* $P < 0.001$ ;  $n = 5$ ). (E,F) Representative immunofluorescence images of control (E) or PD98059-treated (F) foetal muscles using anti-laminin antibody. The dotted lines highlight the CSA of the foetal fibres. Scale bars: 25  $\mu\text{m}$ . (G-J) Representative immunofluorescence images of muscle sections from E16.5 control (G,H) and PD98059-treated (I,J) foetuses using anti-MyHCs (red) and Nfix (green) antibodies. Scale bars: 50  $\mu\text{m}$ , in G,I; 25  $\mu\text{m}$  in H,J. (K,L) High magnification of the immunofluorescence on control and PD98059-exposed foetal muscle sections with anti-MyHCs (red) and Nfix (green) antibodies. Scale bars: 10  $\mu\text{m}$ . (M,N) High magnification of the immunofluorescence on control and PD98059-exposed foetal muscle sections with Pax7 (red) and Nfix (green) antibodies. Scale bars: 10  $\mu\text{m}$ . (O) Quantification of the percentage of Nfix-positive myonuclei in foetuses treated with PD98059 or vehicle (\*\* $P < 0.01$ ;  $n = 5$ ). (P) Quantification of the percentage of Pax7-positive cells expressing Nfix in PD98059-treated or control foetuses (\* $P < 0.05$ ;  $n = 5$ ).

silencing appears to be a promising approach to ameliorate dystrophic phenotypes and to slow down the progression of these pathologies (Rossi et al., 2017b). To determine whether RhoA/ROCK-ERK signalling is also involved in *Nfix* regulation in skeletal muscle stem cells (MuSCs), we first characterised the timing of RhoA/ROCK and ERK expression and activation in juvenile MuSC-derived myoblasts, isolated at postnatal day 10 (P10), from their proliferation to 4 days in differentiation media (dDM). Western blotting revealed transient activation of the ERK kinases (Fig. 7A and Fig. S4A, pERK) during proliferation and in the early phase of differentiation (1dDM). Conversely, ROCK kinase was specifically active during the later phases of differentiation, as seen by specific phosphorylation of the ROCK substrate (Fig. 7A and Fig. S4B, pMYPT1). However, JunB was specifically expressed only during the proliferation phase (Fig. S4C), whereas *Nfix* showed higher expression at 1dDM, but its expression was maintained throughout differentiation (Fig. 7A and Fig. S4D), when there was little or no ERK activity.

We then asked whether this ERK-independent expression of *Nfix* in the later phases of differentiation is due to *Nfix*-mediated

activation of its own expression. Juvenile MuSCs (P10) were transduced with lentiviral vectors that expressed dominant-negative *Nfi*-engrailed (NFI-ENG) or the control (ENG), and the cells were differentiated for 3 and 4 days (i.e. 3dDM, 4dDM). As shown in Fig. S4E,F, expression of NFI-ENG was associated with decreased expression of *Nfix*, which indicated that *Nfix* was necessary for maintaining its own expression.

To determine whether the ERK and RhoA/ROCK pathways are also conserved in the regulation of *Nfix* expression in postnatal myogenesis, RhoA/ROCK and ERK activities were inhibited in MuSCs. Isolated juvenile MuSC-derived myoblasts were treated during proliferation with PD98059, to inhibit ERK signalling in the phase of its highest activation, whereas they were exposed to a ROCK inhibitor, Y27632, during differentiation (2dDM), when the ROCK kinases are active.

First, we tested the effect of PD98059 and Y27632 on MuSC behaviour, analysing by western blot the expression of Pax7, myogenin and sarcomeric myosins after the differentiation (2dDM) (Fig. S4G-H) or during the proliferation phase (PD98059 treatment, Fig. S4J,K); we did not observe any significant difference between

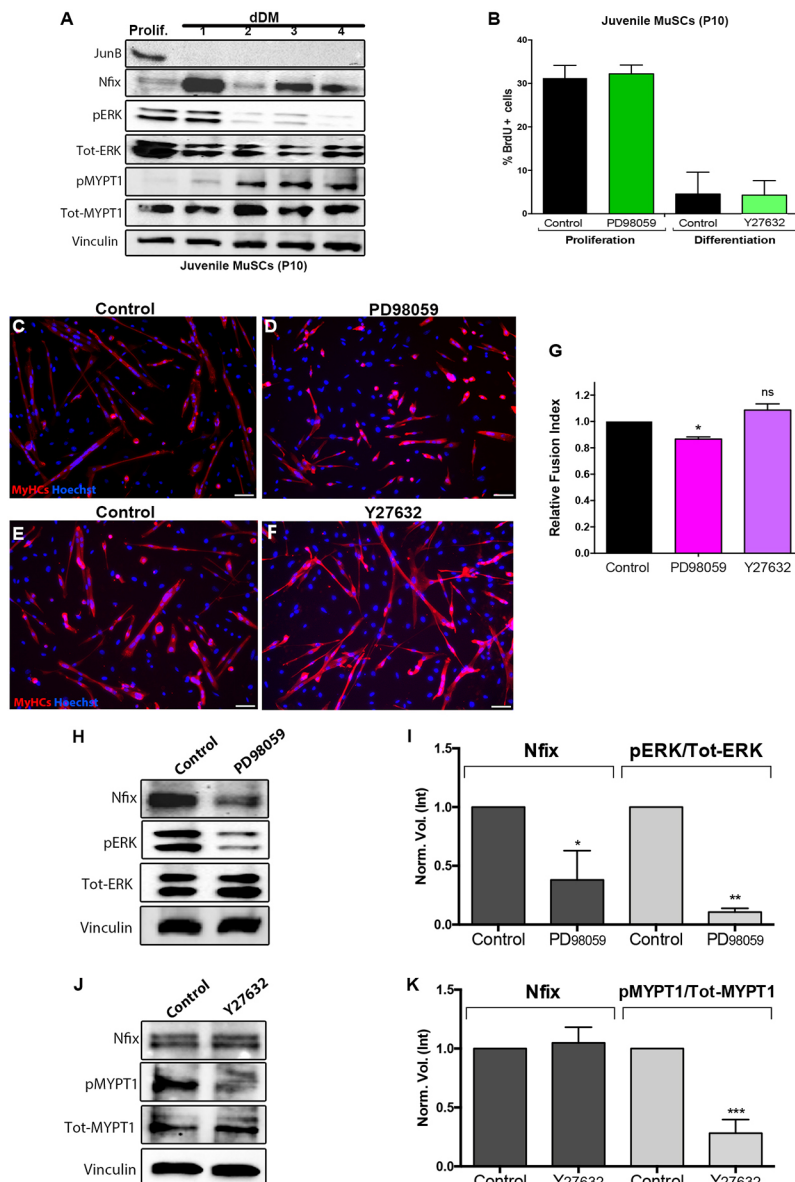


**Fig. 7. ERK activity promotes *Nfix* expression in juvenile MuSCs.** (A) Representative western blots of juvenile MuSCs isolated at postnatal day 10 (P10), revealing *Nfix*, ERK (pERK, totERK) and MyPT1 (pMYPT1, totMyPT1) during proliferation and differentiation (day in differentiation medium, dDM). (B) Quantification of the percentage of proliferative juvenile MuSCs (% BrdU-positive cells) following overnight ERK treatment (proliferation) or 2 days ROCK inhibition, until differentiation ( $n=5$ ). (C-F) Immunofluorescence of sarcomeric myosins (MyHCs) after PD98059 treatment (C,D) or Y27632 exposure (E,F). The juvenile MuSCs were treated overnight with PD98059 and then allowed to differentiate, whereas the treatment with Y27632 was performed every day until differentiation. Scale bars: 50  $\mu\text{m}$ . (G) Graph of the fusion index relative to control of differentiated satellite cells, treated with PD98059 or Y27632 ( $*P<0.05$ ;  $n=5$ ). (H) Western blots of juvenile MuSCs after treatment with the ERK inhibitor PD98059 or vehicle, showing *Nfix* and ERK (pERK, totERK) during proliferation. (I) Graph showing the densitometric quantification of *Nfix* and the ratio of pERK on Tot-ERK in juvenile MuSCs treated with PD98059 ( $*P<0.05$ ;  $**P<0.01$ ;  $n=5$ ). (J) Western blots showing *Nfix* and MyPT1 (pMYPT1, totMyPT1) in juvenile and differentiated MuSCs after daily treatment with the ROCK inhibitor Y27632 or vehicle. Vinculin was used to normalise the amount of loaded protein. (K) Quantification of the densitometry data from western blots of *Nfix* and the ratio of pMYPT1 on Tot-MYPT1 upon Y27632 treatment in juvenile MuSCs ( $***P<0.001$ ;  $n=5$ ).

control and treated cells for all the analysed myogenic markers. Moreover, we assessed whether the treatments might influence the degree of apoptosis, proliferation and differentiation. As shown in Fig. S4I,L, the level of apoptosis through the activation of caspase 3 (aCasp3) and caspase 9 (aCasp9) was not altered by the inhibitors. Treatment with either PD98059 during the proliferative phase or with Y27632 from the start of differentiation (1dDM) did not impinge on the proliferative rate (Fig. 7B), whereas the fusion potential of myogenic cells was reduced after the exposure to PD98059 (Fig. 7C,D,G), as seen for foetal myoblasts. Conversely, the treatment with Y27632 induced only a slight increase in the fusion index of myogenic cells (Fig. 7E-G). Finally, we showed that the inhibition of phosphorylation and activation of the ERK kinases correlated with an impairment of Nfix expression (Fig. 7H,I). In contrast, juvenile MuSCs treated with the ROCK inhibitor during differentiation did not lead to any effects on Nfix expression (Fig. 7J-K, 3dDM).

Taken together, these data suggest that only ERK activity is necessary for the early expression of *Nfix* in juvenile MuSCs, thus confirming that the ERK pathway is conserved from prenatal to postnatal myogenesis. Conversely, the role of RhoA/ROCK in Nfix expression does not appear to be conserved.

## DISCUSSION

*Nfix* plays a crucial role in the transition from embryonic to foetal myogenesis, and thus in the activation of the foetal genetic programme, as well as during muscle regeneration (Messina et al., 2010; Rossi et al., 2016). Therefore, a major objective has been to investigate the mechanism of activation of *Nfix* with the goal to design pharmacological approaches as a therapeutic strategy for treatment of muscular dystrophies (Rossi et al., 2017a,b). Here, we expose a signalling pathway involving RhoA/ERK/JunB that is crucial for the regulation of *Nfix* expression.

We initially looked at JunB, as it is the second most expressed transcription factor in foetal myoblasts (Biressi et al., 2007b), and it has been described as an important factor in the physiology of skeletal muscle (Raffaello et al., 2010). We show that JunB and *Nfix* are co-expressed in foetal progenitor cells, and that JunB modulates *Nfix* expression, thus defining JunB as an activator of *Nfix* at the onset of foetal myogenesis. Moreover, these data demonstrate that the foetal genetic programme is fully governed by *Nfix*, as *Nfix* expression is essential for the switch between these two phases of prenatal muscle development. We also demonstrate that JunB alone does not regulate this transition from embryonic to foetal myogenesis, although it is necessary for *Nfix* expression. Of note, a lack of JunB in adult muscle results in atrophic myofibres, owing to the inhibitory effects of JunB on myostatin expression (Raffaello et al., 2010), which represents the same phenotype that we described in the *Nfix*-null mouse (Rossi et al., 2016). Collectively, these observations suggest that JunB may function through its activation of *Nfix* in adult skeletal muscle. Whether the effect of JunB on *Nfix* expression is direct or is mediated by other co-factor remains to be investigated.

Given that both JunB and *Nfix* are necessary for the maintenance of adult skeletal muscle mass, and to further define the signalling involved in the temporal regulation of myogenic progression, we focused on the RhoA GTPases and the ERK kinases. RhoA GTPases and ERK kinases have both been suggested to impact on myofibre size, whereby inhibition of RhoA signalling leads to increased myofibre size (Coque et al., 2014), and inhibition of the ERK cascade leads to muscle atrophy that is associated with reduced myofibre diameters (Haddad and Adams, 2004; Shi et al., 2009).

Interestingly, it has also been shown that RhoA activates the Rho kinase ROCK, which in turn inhibits ERK activity (Khatiwala et al., 2009; Li et al., 2013).

Although the relationship between the RhoA and ERK kinase activities had not been characterised in prenatal skeletal muscle development, we speculated that they are involved in the control of JunB and *Nfix* expression. Indeed, we show increased RhoA and ROCK activities at specific time points throughout embryonic myogenesis, whereas the ERK kinases were activated only during foetal myogenesis. We also demonstrate that the RhoA/ROCK pathway modulates ERK function, the activation of which is essential for promotion of the foetal programme through activation of JunB and *Nfix*. Therefore, *in vivo* dysfunction of ERK activation during development results in decreased *Nfix* expression in foetal skeletal muscle. Thus, we show that the RhoA/ROCK-ERK signalling is at least one of the major signalling pathways that regulates the temporal progression of prenatal myogenesis through the promotion of *Nfix* expression. However, at present, the upstream inputs that orchestrate the modulation of these signalling pathways remain unknown.

In summary, we have defined the RhoA/ROCK pathway as an important regulator of embryonic myogenesis, where it maintains the repression of JunB and *Nfix* expression through inhibition of ERK activity. However, this role of RhoA/ROCK in the inhibition of *Nfix* expression is not conserved in juvenile MuSCs. This is not unexpected, as foetal myoblasts and satellite cells are distinct populations of muscle progenitors that differ in terms of their transcriptional expression (Alonso-Martin et al., 2016). Thus, at the onset of foetal myogenesis, RhoA/ROCK signalling progressively decreases, thereby promoting the activation of the ERK kinases, which is in turn necessary for *JunB* and *Nfix* expression. Finally, we demonstrate that the transition from embryonic to foetal muscle is dependent on *Nfix*, the expression of which is mediated by JunB.

From a biological perspective, our findings represent an important step towards understanding the molecular regulation of *Nfix* expression, and therefore the definition of embryonic and foetal myogenic identities. Moreover, although significant progress has been made in deriving myogenic cells from pluripotent stem cells (Chal et al., 2015; Chal and Pourquié, 2017), methods that can promote robust myogenic differentiation are lacking. Indeed, protocols that allow successful generation of contractile myofibres can only partially reproduce prenatal muscle development, as they do not consider the key step of transition from embryonic to foetal myogenesis. Thus, to generate mature myofibres, in contrast to the thin and short myotubes that are typical of embryonic myofibres, the induction of foetal myogenesis is a prerequisite. The present study might provide a way to overcome the incomplete maturation of differentiated myogenic cells, through manipulation of RhoA/ROCK signalling with Y27632. Fine-tuning of Y27632 concentrations and exposure times will be essential to generate contractile myofibres without introducing exogenous DNA into the cells to force expression of transcription factors.

Finally, a significant translational consequence of the present study is seen from our recent studies on the role of *Nfix* in muscular dystrophies (Rossi et al., 2017a). Silencing of *Nfix* in adult skeletal muscle appears to be a promising approach for ameliorating dystrophic phenotypes, and for slowing down the progression of these pathologies. In light of this, the demonstration that *Nfix* expression is also ERK dependent in postnatal muscle stem cells provides the basis for future therapeutic approaches for muscular dystrophies, for which a medical cure is still needed.

## MATERIALS AND METHODS

### Animal work

All mice were kept under pathogen-free conditions with a 12 h/12 h light/dark cycle. All of the procedures on animals conformed to Italian law (D. Lgs n. 2014/26, as the implementation of 2010/63/UE) and were approved by the University of Milan Animal Welfare Body and by the Italian Ministry of Health.

Female mice were mated with males (2:1) and examined every morning for copulatory plugs. The day on which a vaginal plug was seen was designated as gestation day 0.5 (E0.5). All the female mice used for the experiments were at least 7 weeks old. For the *in vivo* evaluation of the effects of PD98059, pregnant mice at day 15.5 of gestation were injected with vehicle (dimethylsulfoxide) or 10 mg/kg PD98059 into the caudal vein.

The following mouse lines were used: *Myf5<sup>GFP-P/+</sup>* (Kassar-Duchossoy et al., 2004), *Tg:MLC1f-Nfix2*, *Nfix*-null (obtained from Prof. Richard M. Gronostajski, University of Buffalo, NY, USA) (Campbell et al., 2008) and wild-type CD1 mice (Charles River). The genotyping strategies were as previously published (Kassar-Duchossoy et al., 2004; Messina et al., 2010; Campbell et al., 2008).

### Cell isolation and culture

*Myf5<sup>GFP-P/+</sup>* embryonic muscle was isolated at E12.5 and foetal muscles at E16.5. These were mechanically and enzymatically digested for 30 min at 37°C under agitation with 1.5 mg/ml dispase (Gibco), 0.15 mg/ml collagenase (Sigma) and 0.1 mg/ml DNase I (Sigma), as previously described (Biressi et al., 2007b). The dissociated cells were filtered and collected in Dulbecco's modified Eagle's medium (DMEM) with high-glucose (EuroClone), 20% foetal bovine serum (EuroClone), 2 mM EDTA and 20 mM HEPES. The green fluorescent protein (GFP)-positive myoblasts were sorted (BD FACSAria) and cultured in DMEM high-glucose (EuroClone), 20% horse serum (EuroClone), 2 mM L-glutamine (Sigma-Aldrich), 100 IU/ml penicillin and 100 mg/ml streptomycin (Euroclone). The unpurified embryonic and foetal myoblasts, and the juvenile MuSCs isolated from wild-type postnatal muscle at postnatal day (P) 10, were obtained using the same enzymatic and mechanical procedures used for the *Myf5<sup>GFP-P/+</sup>* myoblasts, and the cells obtained after the digestions were plated onto plastic dishes to allow attachment of the fibroblasts. The non-adherent cells were collected and incubated at 37°C in 20% horse serum in DMEM (EuroClone), in collagen-coated plates. Differentiation was induced by decreasing the horse serum from 20% to 2%. The embryonic myoblasts and juvenile MuSCs were treated daily with 10 µg/ml of the ROCK inhibitor Y27632 (Calbiochem), while the foetal and juvenile MuSCs were treated overnight with 50 µM of the ERK antagonist PD98059 (Cell Signalling). Control cells were treated with vehicle only (dimethylsulfoxide).

### Plasmid and lentivirus production

The following plasmids were used: pCH-Nfix2, pCH-HA (Messina et al., 2010); pLentiHA-NfiEngr, pLentiHA-Engr (Messina et al., 2010); scrambled (Sigma-Aldrich) and shJunB plasmids (SHCLNG-NM\_008416, Sigma-Aldrich); and PGK-RHOV14, pcDNA3.1X-JunB or pcDNA3.1X as controls. The pcDNA3.1X-JunB plasmid was obtained by subcloning the JunB cDNA (kindly provided by Milena Grossi, Sapienza University of Rome, Italy) into the pcDNA3.1X vector (ThermoFisher). The PGK-RHOV14 plasmid was produced by cloning the cDNA of RhoA with a single point replacement (glycine with valine) at position 14 (RHOV14; kindly provided by Germana Falcone, Consiglio Nazionale delle Ricerche, Rome), in the PGK-GFP vector.

Viral particles were prepared through co-transfection of the packaging plasmids (16.25 µg pMDLg/p; 9 µg pCMV-VSVG; 6.25 µg pRSV-REV) together with each of the following lenti-plasmids: shJunB, pLentiHA-Nfix2, PGK-RHOV14 and the respective controls (i.e. scrambled, pLentiHA and PGK). Transfection was performed in HEK293T cells using the calcium phosphate transfection method. The viral particles were collected 40 h after transfection, and concentrated (Lenti-X concentrator; Clontech), in phosphate-buffered saline (PBS). The concentrated viral particles were stored at -80°C until use.

### Cell transfection and transduction

For the transfection experiments, the embryonic or foetal myoblasts were cultured to a confluency of 70% to 80% and transfected following the Lipofectamine LTX (Invitrogen) transfection protocol. The myoblasts were harvested 48 h after transfection. Transduction of foetal myoblasts was performed by addition of the viral preparation to the cultured cells at a multiplicity of infection of 10. After an overnight incubation, the medium was changed and the cells were then maintained in culture for 72 h to allow their differentiation.

### Immunofluorescence of cultured cells

Cell cultures were fixed for 10 min at 4°C with 4% paraformaldehyde in PBS, and were then permeabilised with 0.2% Triton X-100 (Sigma-Aldrich), 1% bovine serum albumin (BSA; Sigma-Aldrich) in PBS, for 30 min at room temperature. After permeabilisation, the cells were treated with a blocking solution (10% goat serum; Sigma-Aldrich) for 45 min at room temperature, and then incubated overnight at 4°C with the primary antibodies diluted in PBS. The primary antibodies used were: rabbit anti-Nfix (1:200; Novus Biologicals; NBP2-15039); mouse anti-JunB (1:100; SantaCruz Biotechnology; C-11); mouse anti-total MyHC [hybridoma MF20; 1:2; Developmental Studies Hybridoma Bank (DSHB)]; or rabbit anti-cleaved caspase 3 (1:300; Cell Signalling; D175). After two washes with PBS, 1% BSA and 0.2% Triton, the samples were incubated for 45 min at room temperature with the secondary antibodies (1:250; Jackson Laboratory): goat anti-mouse 594, 92278; goat anti-rabbit 488, 111-545-003 and Hoechst (1:500; Sigma-Aldrich). Finally, the cells were washed twice with 0.2% Triton in PBS and mounted with Fluorescence Mounting Medium (Dako). Images were acquired with a fluorescence microscope (DMI6000B; Leica) equipped with a digital camera (DFC365FX; Leica), and were merged as necessary using Photoshop. Cell counting and evaluation of myotube area were performed using ImageJ. For EdU (5-ethynyl-2'-deoxyuridine) assays, cells were treated for 2 h with 10 µM of EdU solution. After cell fixation and permeabilisation, the detection of EdU was performed following the manufacturer's instructions for the ClickIT Plus EdU Alexa Fluor 647 Imaging Kit (C10640). Conversely, cell cultures were incubated with BrdU (50 µM) in PBS for 1 h at 37°C in 5% CO<sub>2</sub> (light off). After two washes with PBS, cells were fixed with 95% ethanol/5% acetic acid 5% for 20 min at room temperature. Then HCl 1.5 M was added for 10 min at room temperature. After two washes with PBS, the cells were permeabilised with 0.25% Triton X-100 (Sigma-Aldrich) for 5 min at room temperature then incubated with the Amersham monoclonal antibody anti-BrdU (GE Healthcare, RPN202) for 1 h at 4°C. After two washes with 1×PBS, 0.25% Triton in PBS was added to cells for 5 min at room temperature. Cells were then incubated with the secondary antibody goat anti-mouse FITC (Alexa Fluor 488 nm, 92589, 1:250, Jackson ImmunoResearch) and Hoechst (1:500; Sigma-Aldrich) for 30 min at room temperature. Finally, the cells were washed twice with PBS and mounted with Fluorescence Mounting Medium (Dako). All the cell counting was performed using ImageJ; statistical analyses were performed with Graphpad.

### Immunofluorescence on sections

E16.5 fetuses were fixed overnight with 4% paraformaldehyde solution. After two washes with PBS, the samples were sequentially incubated in PBS supplemented with 7.5%, 15% and 30% of sucrose until completely dehydrated. Foetuses were embed in OCT, frozen in nitrogen-chilled isopentane and kept at -80°C. The sections were prepared at 7 µm and permeabilised in 1% BSA, 0.2% Triton X-100 in PBS for 30 min at room temperature. The antigens were unmasked by incubating the samples in citrate-based solution [10 mM sodium citrate (pH 6.0) for 20 min at 95-100°C]. The slides were allowed to cool at room temperature and incubated for 1 h with 10% goat serum in PBS. The incubation with primary antibody was performed overnight at 4°C using: rabbit anti-Nfix (1:200, Novus Biologicals; NBP2-15039); mouse anti-total MyHC or anti-Pax7 (hybridoma; 1:2; DSHB); rabbit anti-laminin (1:300, Sigma-Aldrich; L9393). After incubation, the samples were washed and incubated with secondary antibodies (goat anti-mouse 594, 92278; goat anti-rabbit 488, 111-545-003; 1:250, Jackson ImmunoResearch) and Hoechst

(1:500; Sigma-Aldrich; 861405) for 45 min at room temperature. Finally, the samples were washed in PBS 0.2% Triton X-100 and mounted, and fluorescent immunolabelling was recorded with a DM6000 Leica microscope. Measurement of cross-sectional area (CSA) and cell counting were performed with ImageJ.

### RNA extraction, retrotranscription and real-time qPCR

The extraction of total RNA from cultured cells and from freshly isolated myoblasts was achieved using kits (NucleoSpin RNA XS; Macherey-Nagel). After quantification of the RNA with a photometer (NanoPhotometer; Implen), 0.5 µg total RNA was retrotranscribed (iScript Reverse Transcription Supermix; Bio-Rad). The cDNA obtained was diluted 1:10 in sterile water and 5 µl of the diluted cDNA was used for real-time qPCR. The real-time qPCR was performed using SYBR Green Supermix (Bio-Rad). Relative mRNA expression levels were normalised on GAPDH expression levels. The primers used are listed in Table S1.

### Protein extraction and western blotting

Protein extracts were obtained from cultured myoblasts lysed using RIPA buffer [10 mM Tris-HCl (pH 8.0), 1 mM EDTA, 1% Triton-X, 0.1% sodium deoxycholate, 0.1% sodium dodecylsulphate (SDS), 150 mM NaCl, in deionised water] for 30 min on ice, and total protein extracts from embryonic and foetal muscle were obtained from homogenised tissues in tissue extraction buffer (50 mM Tris-HCl, 1 mM EDTA, 1% Triton-X, 150 mM NaCl). Both RIPA and the tissue extraction buffer were supplemented with protease and phosphatase inhibitors. After lysis, the samples were centrifuged at 11,000 g for 10 min at 4°C, and the supernatants were collected for protein quantification (DC Protein Assays; Bio-Rad).

For western blotting, 30 µg protein of each extract was denatured at 95°C for 5 min using SDS PAGE sample-loading buffer [100 mM Tris (pH 6.8), 4% SDS, 0.2% bromophenol blue, 20% glycerol, 10 mM dithiothreitol] and loaded onto 8%–12% SDS acrylamide gels. After electrophoresis, the protein was blotted onto nitrocellulose membranes (Protran nitrocellulose transfer membrane; Whatman), which was blocked for 1 h with 5% milk in Tris-buffered saline plus 0.02% Tween20 (Sigma-Aldrich).

The membranes were incubated with the primary antibodies overnight at 4°C under agitation, using the following conditions: rabbit anti-Nfix (1:1000; Novus Biologicals, NBP2-15039), rabbit anti-JunB (1:500; SantaCruz Biotechnology, 210), mouse anti-vinculin (1:2500; Sigma-Aldrich), mouse anti-slow MyHC (hybridoma Bad5; 1:2; DSHB); mouse anti-total MyHC (hybridoma MF20; 1:5; DSHB), rabbit anti-MYPT1 phosphorylated in Thr696 (1:500; SantaCruz Biotechnology, sc-17556-R), rabbit anti-Tot MYPT1 (1:500; SantaCruz Biotechnology, H-130), rabbit anti-pERK (1:1000; SantaCruz Biotechnology, sc-16982-R), mouse anti-Tot ERK (1:500; SantaCruz Biotechnology, sc-135900), mouse anti-Pax7 (hybridoma; 1:5; DSHB), mouse anti-Myogenin (hybridoma; 1:5; DSHB), mouse anti-caspase 9 (1:1000; Cell Signalling Technology, 9508), rabbit anti-caspase 3 (1:1000; Cell Signalling Technology, 9662) and mouse anti-GAPDH (1:5000; Sigma-Aldrich). After incubation with the primary antibodies, the membranes were washed and incubated with the secondary antibodies (1:10,000; IgG-HRP; Bio-Rad) for 40 min at room temperature, and then washed again. The bands were revealed using ECL detection reagent (ThermoFisher), with images acquired using the ChemiDoc MP system (Bio-Rad). The Image Lab software was used to measure and quantify the bands of independent western blot experiments. The obtained absolute quantity was compared with the reference band and expressed in the graphs as normalised volume (Norm. Vol. Int.). All the values are presented as mean±s.d.

### Chromatin immunoprecipitation assays

The ChIP protocol was performed on unpurified foetal differentiated myoblasts (E16.5) using 5×10<sup>6</sup> cells for each immunoprecipitation. Foetal myotubes were fixed with 1% formaldehyde (Sigma-Aldrich) in high-glucose DMEM for 10 min at room temperature. The fixation was quenched with 125 mM glycine (Sigma-Aldrich) in PBS for 10 min at room temperature. The cells were rinsed with ice-cold PBS, harvested and

centrifuged at 2500 g for 10 min at 4°C. The cell pellets were lysed and sonicated (Bioruptor sonicator; Diagenode) for 15 min, with repeated cycles of 30 s sonication/30 s rest. The sonicated suspensions were centrifuged at 14,000 g for 10 min at 4°C, and the supernatants were stored in aliquots at –80°C. Chromatin was precleared with Protein G Sepharose (Amersham) and rabbit serum, for 2 h at 4°C on a rotating platform, and the Protein G Sepharose was blocked overnight with 10 mg/ml BSA and 1 mg/ml salmon sperm (Sigma-Aldrich). After preclearing, the chromatin was incubated overnight at 4°C with 5 µg antibody: rabbit anti-Nfix (Novus Biologicals, NBP2-15039), mouse anti-JunB (SantaCruz Biotechnology, C-11) and normal rabbit IgG (SantaCruz Biotechnology). The following day, the blocked Protein G Sepharose was washed and added to the chromatin incubated with the antibodies, for 3 h under rotation at 4°C. After incubation, the Protein G Sepharose was spun down and repeatedly washed. Elution was performed overnight at 65°C with 10 mg RNase (Sigma-Aldrich) and 200 mM NaCl (Sigma-Aldrich) to reverse the crosslinking. After treatment with 20 µg proteinase K (Sigma-Aldrich), the DNA was purified with phenol/chloroform. The DNA obtained was analysed using real-time qPCR, and the data were plotted as fold-enrichment with respect to the IgG sample. The primers used are listed in Table S1.

### Pull-down assays

Active Rho Pull-Down and Detection kits (ThermoScientific) were used with 600 µg cell lysate obtained from unpurified myoblasts (E12.5, E14.5 and E16.5) following the manufacturer instructions.

### Statistical analysis

Graphs were constructed and Student's *t*-tests performed using GraphPad Prism 6.0e. The statistics are reported in the text as mean±s.d. (*n*=5). CSA distribution is expressed as mean±whiskers from minimum to maximum. Statistical significance was analysed using an unpaired two-tailed Student's *t*-tests (homoscedastic): \**P*<0.1; \*\**P*<0.05; \*\*\**P*<0.01.

### Acknowledgements

We thank M. Grossi for the JunB plasmid, and G. Maroli, G. Cossu and G. Rossi for helpful discussions. We are also grateful to R. Gronostajski for the kind exchange of information and animal models.

### Competing interests

The authors declare no competing or financial interests.

### Author contributions

Conceptualization: V.T., G. Messina; Methodology: V.T., G.A., G. Mura, C.B., E.C., S.M., G.L.C.; Validation: G.A., G. Mura, V.T.; Formal analysis: V.T.; Investigation: V.T., G.A., G. Mura, C.B., E.C., S.M.; Resources: G. Messina; Data curation: V.T.; Writing - original draft: V.T.; Writing - review & editing: S.T., F.R., G. Messina; Supervision: G. Messina; Project administration: G. Messina; Funding acquisition: G. Messina.

### Funding

This study was funded by the European Research Council, ERC StG2011 (RegenerationNfix 280611). F.R. acknowledges support from the Association Française contre les Myopathies via TRANSLAMUSCLE (project 19507). S.T. acknowledges support from the Institut Pasteur and the Agence Nationale de la Recherche (Laboratoire d'Excellence Revive, ANR-10-LABX-73).

### Supplementary information

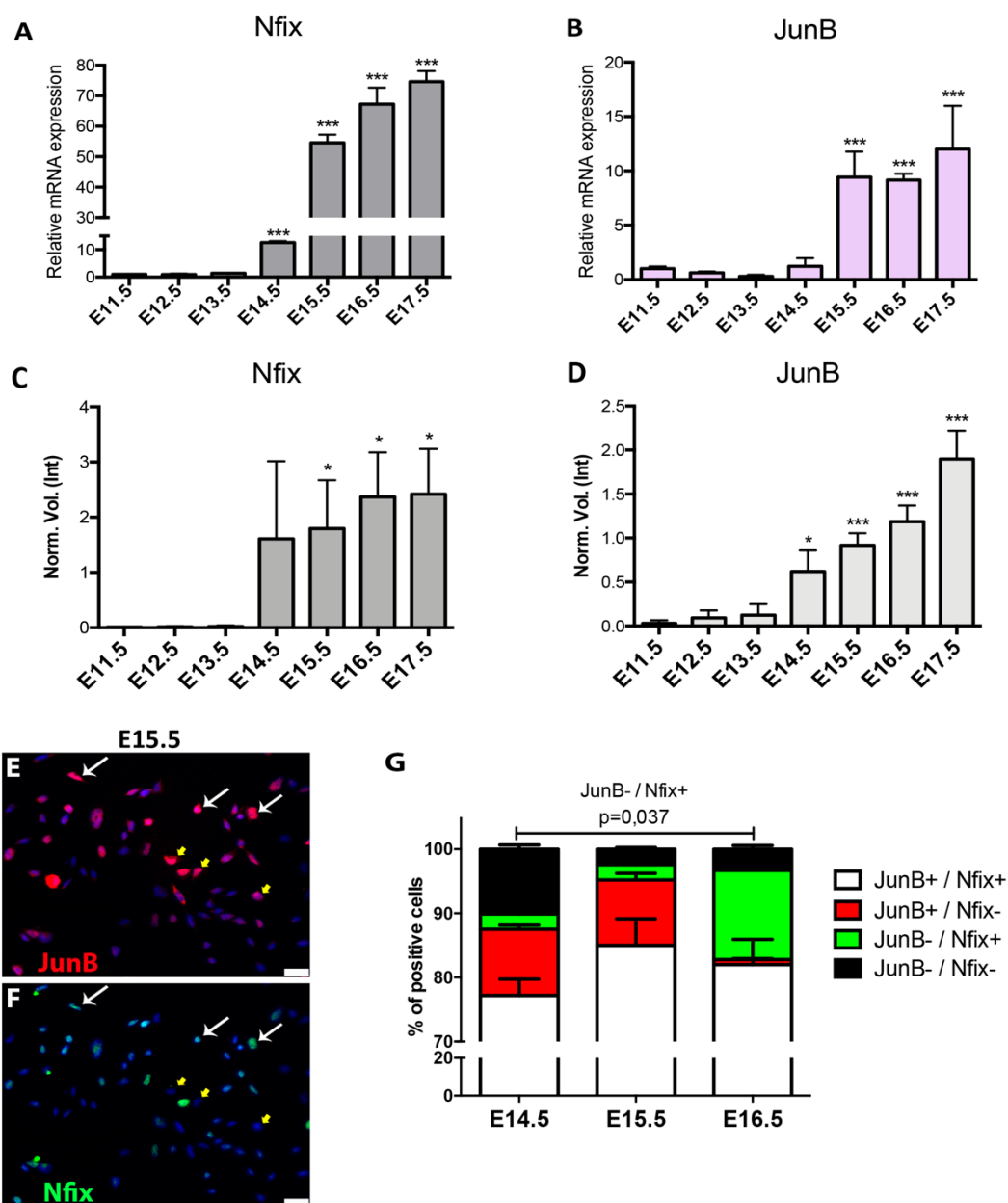
Supplementary information available online at <http://dev.biologists.org/lookup/doi/10.1242/dev.163956.supplemental>

### References

- Alonso-Martin, S., Rochat, A., Mademtoglou, D., Morais, J., de Reyniès, A., Auradé, F., Chang, T. H.-T., Zammit, P. S. and Relaix, F. (2016). Gene expression profiling of muscle stem cells identifies novel regulators of postnatal myogenesis. *Front. Cell. Dev. Biol.* **4**, 58.
- Amano, M., Ito, M., Kimura, K., Fukata, Y., Chihara, K., Nakano, T., Matsuura, Y. and Kaibuchi, K. (1996). Phosphorylation and activation of myosin by Rho-associated kinase (Rho-kinase). *J. Biol. Chem.* **271**, 20246–20249.
- An, C.-I., Dong, Y. and Hagiwara, N. (2011). Genome-wide mapping of Sox6 binding sites in skeletal muscle reveals both direct and indirect regulation of muscle terminal differentiation by Sox6. *BMC Dev. Biol.* **11**, 59.

- Bachurski, C. J., Yang, G. H., Currier, T. A., Gronostajski, R. M. and Hong, D. (2003). Nuclear factor I/thyroid transcription factor 1 interactions modulate surfactant protein C transcription. *Mol. Cell. Biol.* **23**, 9014-9024.
- Biressi, S., Molinaro, M. and Cossu, G. (2007a). Cellular heterogeneity during vertebrate skeletal muscle development. *Dev. Biol.* **308**, 281-293.
- Biressi, S., Tagliafico, E., Lamorte, G., Monteverde, S., Tenedini, E., Roncaglia, E., Ferrari, S., Ferrari, S., Cusella-De Angelis, M. G., Tajbakhsh, S. et al. (2007b). Intrinsic phenotypic diversity of embryonic and fetal myoblasts is revealed by genome-wide gene expression analysis on purified cells. *Dev. Biol.* **304**, 633-651.
- Campbell, C. E., Piper, M., Plachez, C., Yeh, Y.-T., Baizer, J. S., Osinski, J. M., Litwack, E. D., Richards, L. J. and Gronostajski, R. M. (2008). The transcription factor Nfix is essential for normal brain development. *BMC Dev. Biol.* **8**, 52.
- Castellani, L., Salvati, E., Alemà, S. and Falcone, G. (2006). Fine regulation of RhoA and Rock is required for skeletal muscle differentiation. *J. Biol. Chem.* **281**, 15249-15257.
- Chal, J. and Pourquie, O. (2017). Making muscle: skeletal myogenesis in vivo and in vitro. *Development* **144**, 2104-2122.
- Chal, J., Oginuma, M., Al Tanoury, Z., Gobert, B., Sumara, O., Hick, A., Bousson, F., Zidouni, Y., Mursch, C., Moncuquet, P. et al. (2015). Differentiation of pluripotent stem cells to muscle fiber to model Duchenne muscular dystrophy. *Nat. Biotechnol.* **33**, 962-969.
- Chapman, V. M., Miller, D. R., Armstrong, D. and Caskey, C. T. (1989). Recovery of induced mutations for X chromosome-linked muscular dystrophy in mice. *Proc. Natl. Acad. Sci. USA* **86**, 1292-1296.
- Chinenov, Y. and Kerppola, T. K. (2001). Close encounters of many kinds: Fos-Jun interactions that mediate transcription regulatory specificity. *Oncogene* **20**, 2438-2452.
- Coque, E., Raoul, C. and Bowerman, M. (2014). ROCK inhibition as a therapy for spinal muscular atrophy: understanding the repercussions on multiple cellular targets. *Front. Neurosci.* **8**, 271.
- Duclos, F., Straub, V., Moore, S. A., Venzke, D. P., Hrstka, R. F., Crosbie, R. H., Durbeej, M., Lebakken, C. S., Ettinger, A. J., van der Meulen, J. et al. (1998). Progressive muscular dystrophy in alpha-sarcoglycan-deficient mice. *J. Cell Biol.* **142**, 1461-1471.
- Eferl, R. and Wagner, E. F. (2003). AP-1: a double-edged sword in tumorigenesis. *Nat. Rev. Cancer* **3**, 859-868.
- Gronostajski, R. M. (2000). Roles of the NF1/CTF gene family in transcription and development. *Gene* **249**, 31-45.
- Haddad, F. and Adams, G. R. (2004). Inhibition of MAP/ERK kinase prevents IGF-I-induced hypertrophy in rat muscles. *J. Appl. Physiol.* **96**, 203-210.
- Hutcheson, D. A., Zhao, J., Merrell, A., Haldar, M. and Kardon, G. (2009). Embryonic and fetal limb myogenic cells are derived from developmentally distinct progenitors and have different requirements for beta-catenin. *Genes Dev.* **23**, 997-1013.
- Jiang, P., Song, J., Gu, G., Slonimsky, E., Li, E. and Rosenthal, N. (2002). Targeted deletion of the MLC1f/3f downstream enhancer results in precocious MLC expression and mesoderm ablation. *Dev. Biol.* **243**, 281-293.
- Kassar-Duchossoy, L., Gayraud-Morel, B., Gomès, D., Rocancourt, D., Buckingham, M., Shinin, V. and Tajbakhsh, S. (2004). Mrf4 determines skeletal muscle identity in Myf5:Myod double-mutant mice. *Nature* **431**, 466-471.
- Khatiwala, C. B., Kim, P. D., Peyton, S. R. and Putnam, A. J. (2009). ECM compliance regulates osteogenesis by influencing MAPK signaling downstream of RhoA and ROCK. *J. Bone Miner. Res.* **24**, 886-898.
- Kimura, K., Ito, M., Amano, M., Chihara, K., Fukata, Y., Nakafuku, M., Yamamori, B., Feng, J., Nakano, T., Okawa, K. et al. (1996). Regulation of myosin phosphatase by Rho and Rho-associated kinase (Rho-kinase). *Science* **273**, 245-248.
- Li, F., Jiang, Q., Shi, K. J., Luo, H., Yang, Y. and Xu, C. M. (2013). RhoA modulates functional and physical interaction between ROCK1 and Erk1/2 in selenite-induced apoptosis of leukaemia cells. *Cell Death Dis.* **4**, e708.
- Mathew, S. J., Hansen, J. M., Merrell, A. J., Murphy, M. M., Lawson, J. A., Hutcheson, D. A., Hansen, M. S., Angus-Hill, M. and Kardon, G. (2011). Connective tissue fibroblasts and Tcf4 regulate myogenesis. *Development* **138**, 371-384.
- Messina, G., Biressi, S., Monteverde, S., Magli, A., Cassano, M., Perani, L., Roncaglia, E., Tagliafico, E., Starnes, L., Campbell, C. E. et al. (2010). Nfix regulates fetal-specific transcription in developing skeletal muscle. *Cell* **140**, 554-566.
- Mourikis, P., Gopalakrishnan, S., Sambasivan, R. and Tajbakhsh, S. (2012). Cell-autonomous Notch activity maintains the temporal specification potential of skeletal muscle stem cells. *Development* **139**, 4536-4548.
- Murányi, A., Derkach, D., Erdödi, F., Kiss, A., Ito, M. and Hartshorne, D. J. (2005). Phosphorylation of Thr695 and Thr850 on the myosin phosphatase target subunit: inhibitory effects and occurrence in A7r5 cells. *FEBS Lett.* **579**, 6611-6615.
- Nishiyama, T., Kii, I. and Kudo, A. (2004). Inactivation of Rho/ROCK signaling is crucial for the nuclear accumulation of FKHR and myoblast fusion. *J. Biol. Chem.* **279**, 47311-47319.
- Pelosi, M., Marampon, F., Zani, B. M., Prudente, S., Perlas, E., Caputo, V., Cianetti, L., Berno, V., Narumiya, S., Kang, S. W. et al. (2007). ROCK2 and its alternatively spliced isoform ROCK2m positively control the maturation of the myogenic program. *Mol. Cell. Biol.* **27**, 6163-6176.
- Pistocchi, A., Gaudenzi, G., Foglia, E., Monteverde, S., Moreno-Fortuny, A., Pianca, A., Cossu, G., Cotelli, F. and Messina, G. (2013). Conserved and divergent functions of Nfix in skeletal muscle development during vertebrate evolution. *Development* **140**, 1528-1536.
- Raffaello, A., Milan, G., Masiero, E., Carnio, S., Lee, D., Lanfranchi, G., Goldberg, A. L. and Sandri, M. (2010). JunB transcription factor maintains skeletal muscle mass and promotes hypertrophy. *J. Cell Biol.* **191**, 101-113.
- Rossi, G., Antonini, S., Bonfanti, C., Monteverde, S., Vezzali, C., Tajbakhsh, S., Cossu, G. and Messina, G. (2016). Nfix regulates temporal progression of muscle regeneration through modulation of myostatin expression. *Cell Rep.* **14**, 2238-2249.
- Rossi, G., Bonfanti, C., Antonini, S., Bastoni, M., Monteverde, S., Innocenzi, A., Saclier, M., Taglietti, V. and Messina, G. (2017a). Silencing Nfix rescues muscular dystrophy by delaying muscle regeneration. *Nat. Commun.* **8**, 1055.
- Rossi, G., Taglietti, V. and Messina, G. (2017b). Targeting Nfix to fix muscular dystrophies. *Cell Stress* **2**, 17-19.
- Schiaffino, S. and Reggiani, C. (2011). Fiber types in mammalian skeletal muscles. *Physiol. Rev.* **91**, 1447-1531.
- Seko, T., Ito, M., Kureishi, Y., Okamoto, R., Moriki, N., Onishi, K., Isaka, N., Hartshorne, D. J. and Nakano, T. (2003). Activation of RhoA and inhibition of myosin phosphatase as important components in hypertension in vascular smooth muscle. *Circ. Res.* **92**, 411-418.
- Shi, H., Scheffler, J. M., Zeng, C., Pleitner, J. M., Hannon, K. M., Grant, A. L. and Gerrard, D. E. (2009). Mitogen-activated protein kinase signaling is necessary for the maintenance of skeletal muscle mass. *Am. J. Physiol. Cell Physiol.* **296**, C1040-C1048.
- Taglietti, V., Maroli, G., Cermenati, S., Monteverde, S., Ferrante, A., Rossi, G., Cossu, G., Beltrame, M. and Messina, G. (2016). Nfix induces a switch in Sox6 transcriptional activity to regulate MyHC-I expression in fetal muscle. *Cell Rep* **17**, 2354-2366.
- Uehata, M., Ishizaki, T., Satoh, H., Ono, T., Kawahara, T., Morishita, T., Tamakawa, H., Yamagami, K., Inui, J., Maekawa, M. et al. (1997). Calcium sensitization of smooth muscle mediated by a Rho-associated protein kinase in hypertension. *Nature* **389**, 990-994.
- Zuckerbraun, B. S., Shapiro, R. A., Billiar, T. R. and Tzeng, E. (2003). RhoA influences the nuclear localization of extracellular signal-regulated kinases to modulate p21Waf1/Cip1 expression. *Circulation* **108**, 876-881.

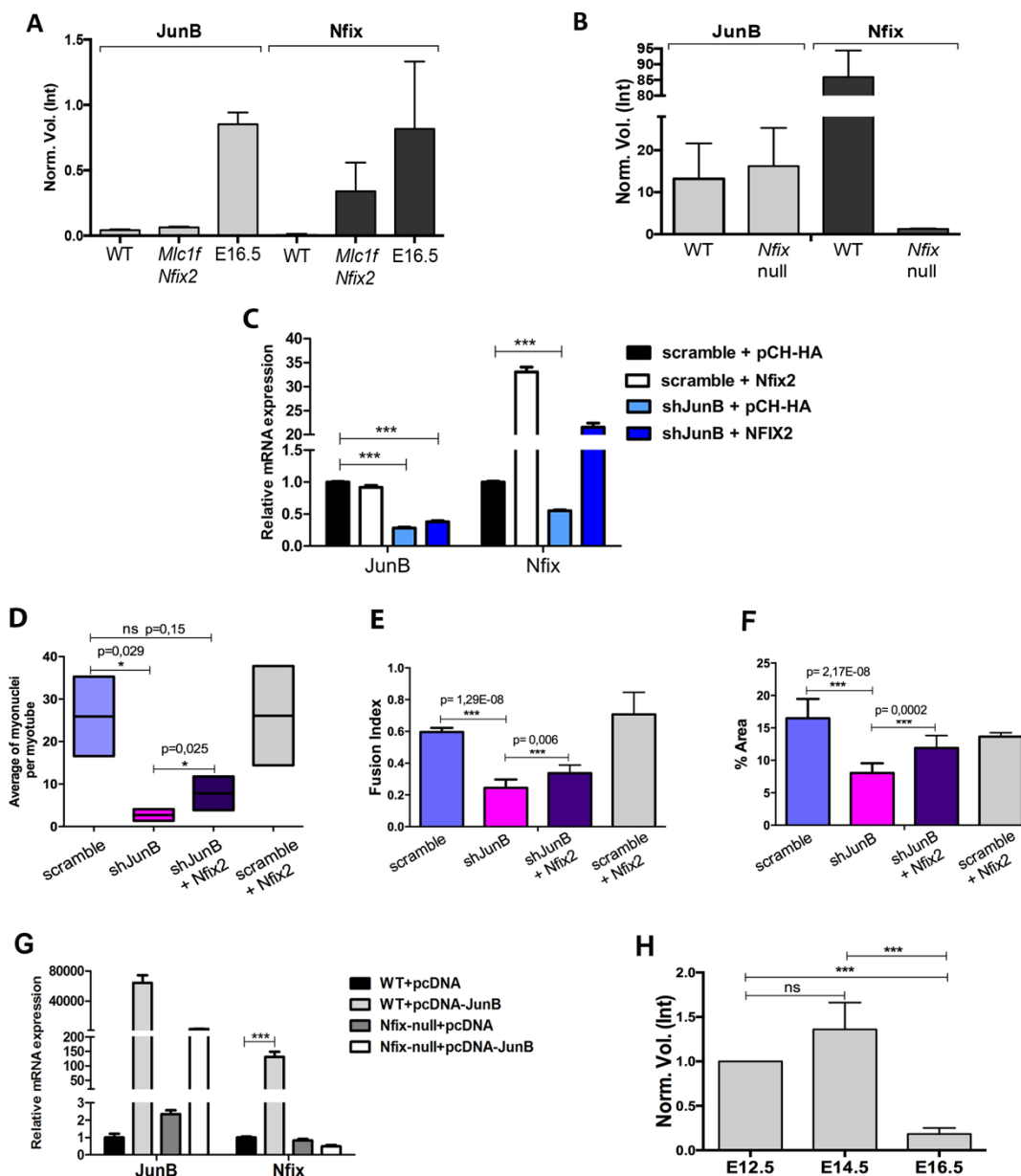
## Supplementary Information



**Supplementary Figure 1. JunB and Nfix are co-expressed in foetal myoblasts, with JunB earlier expressed than Nfix**

(A-B) qRT-PCR analysis on purified *Myf5*<sup>GFP-P/+</sup> myoblasts dissected from E11.5 up to E17.5 muscles, showing the expression profile of Nfix (A) and JunB (B) at different developmental stages. The statistical analyses are compared to E11.5 sample (\*\*\*) $p < 0.005$ ;  $n = 5$ ). (C, D) Densitometry analysis of Nfix (C) and JunB (D), related to

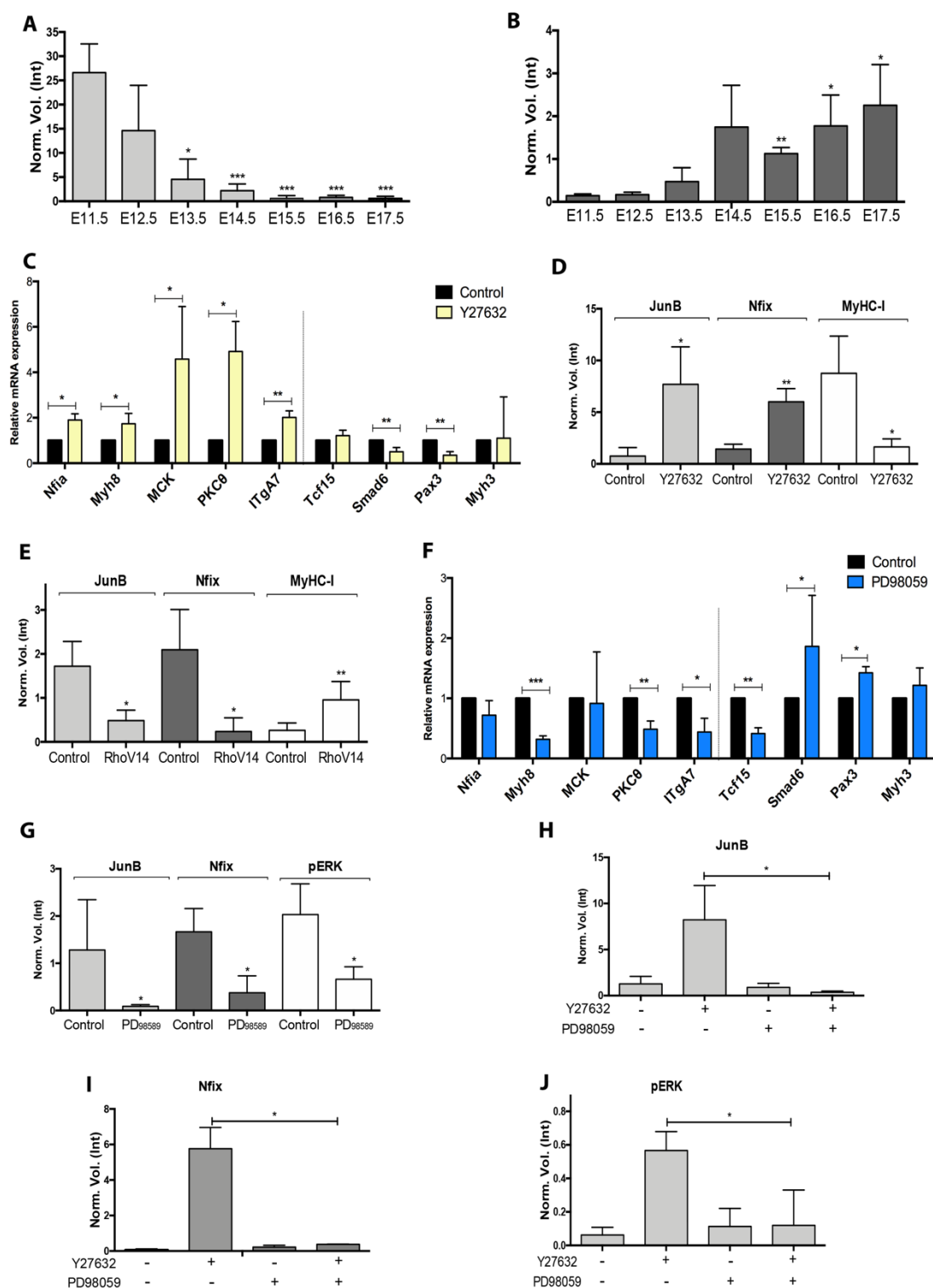
Western blot showed in Fig. 1A. The statistical analyses were performed comparing all the results to E11.5 (\* $p < 0.05$ ;  $n = 5$ ; \*\*\* $p < 0.005$ ;  $n = 5$ ). **(E-F)** Immunofluorescence for JunB (red) and Nfix (green) on freshly isolated Myf5<sup>GFP-P/+</sup>-purified myoblasts at E15.5. Nuclei were counterstained with Hoechst. White arrows indicate myoblasts coexpressing JunB and Nfix, while yellow arrows indicate myoblasts expressing JunB but not Nfix. Scale bars: 25  $\mu\text{m}$ . **(G)** Graph showing the percentage of JunB<sup>+</sup>/Nfix<sup>+</sup> (white bar), JunB<sup>+</sup>/Nfix<sup>-</sup> (red), JunB<sup>-</sup>/Nfix<sup>+</sup> (green) and JunB<sup>-</sup>/Nfix<sup>-</sup> (black). Percentages are calculated on the total number of nuclei (\* $p < 0.05$ ;  $n = 5$ ).



## Supplementary Figure 2. Silencing of JunB impairs the differentiation of foetal myoblasts

(A) Graphs for densitometric quantification of JunB and Nfix expression normalized against housekeeping protein Vinculin, respectively related to Fig. 2B (A) and Fig.2D (B). (C) qRT-PCR for JunB and Nfix on foetal myoblasts (E16.5) following the transduction with scramble or shJunB vector and with control or Nfix2-over-expressing vector. \*\*\* $p < 0.005$ ;  $n = 5$ . (D) Average of myonuclei per myotubes of foetal myoblasts,

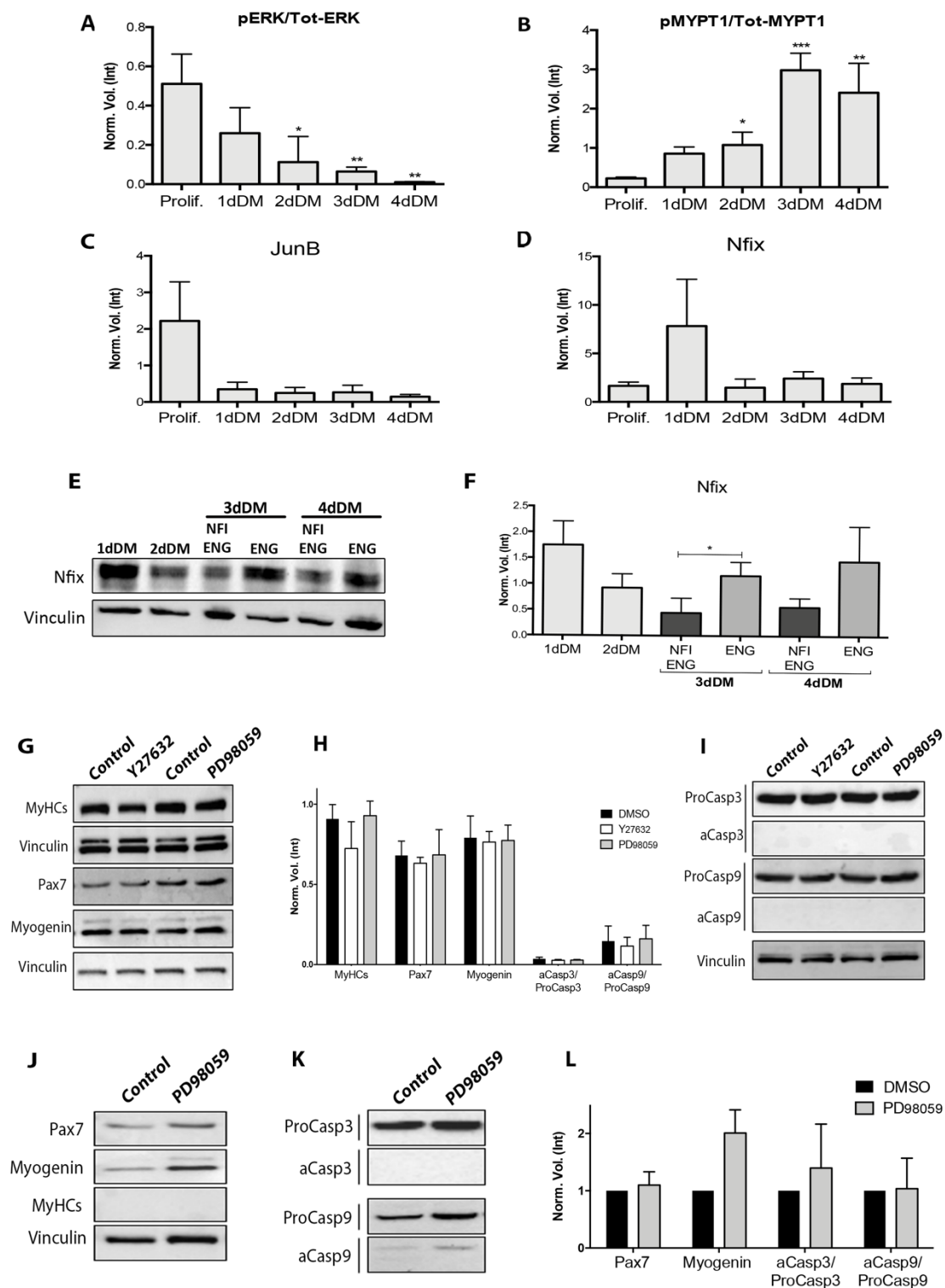
transduced with scramble or shJunB vector and with control or Nfix2-over-expressing vector, and induced to the terminal differentiation (\* $p < 0.05$ ;  $n = 5$ ). **(E)** Calculation of the fusion index as the ratio of the number of nuclei inside myotubes to the number of total nuclei of control (\*\* $p < 0.005$ ;  $n = 5$ ). **(F)** Quantification of MyHCs positive area (MF20) using image analysis software (\*\* $p < 0.005$ ;  $n = 5$ ). **(G)** qRT-PCR on wild-type (WT) and *Nfix*-null embryonic myoblasts (E12.5), transfected with JunB-overexpressing vector or with a control vector (pcDNA). (\*\* $p < 0.005$ ;  $n = 5$ ). **(H)** Quantitative densitometry of active Rho GTPases normalised according to the ratio between total Rho GTPases and  $\beta$ -tubulin. (\*\*\*,  $p < 0.001$ ;  $n = 5$ ).



**Supplementary Figure 3. Analysis of embryonic and foetal specific genes and protein levels upon ROCK and ERK kinase modulation.**

(A) Densitometry quantification of the ratio of pMYPT1 on Tot-MYPT1, linked to Fig.4B. The statistical analyses are compared to E11.5 (\* $p < 0.05$ ;  $n = 5$ ; \*\*\* $p < 0.005$ ;

n=5). **(B)** Densitometric quantification of the ratio pERK/Tot-ERK, related to Fig. 4C. The statistical analyses are compared to E11.5 (\*,  $p < 0.1$ ; \*\*,  $p < 0.05$ ; n=5). **(C)** qRT-PCR analysis on embryonic differentiated myotubes (E12.5) treated with vehicle (control) or with Y27632 of embryonic genes: *Tcf15*, *Smad6*, *Pax3* and *Myh3* (right part). The levels of expression of foetal specific genes (*Nfia*, *Myh8*, *MCK*, *PKC $\theta$*  and *ITgA7*) were represented on the left side of the graph (\*,  $p < 0.1$ ; \*\*,  $p < 0.05$ ; n=5). **(D)** Densitometric quantification of Western blots of JunB, Nfix and MyHC-I of embryonic myoblast treated with Y27632 (related to Fig. 5B) (\*,  $p < 0.1$ ; \*\*,  $p < 0.05$ ; n=5). **(E)** Quantification of the densitometry data from Western blot showed in Fig. 5D on fetal myoblasts expressing RhoV14 or a control vector (\*,  $p < 0.1$ ; \*\*,  $p < 0.05$ ; n=5). **(F)** qRT-PCR analysis on foetal myoblasts (E16.5) treated with vehicle (control) or with PD98059 of embryonic (*Tcf15*, *Smad6*, *Pax3* and *Myh3* - right part) and foetal (*Nfia*, *Myh8*, *MCK*, *PKC $\theta$*  and *ITgA7* - left part) genes (\*,  $p < 0.1$ ; \*\*,  $p < 0.05$ ; \*\*\*,  $p < 0.01$ ; n=5). **(G)** Densitometric quantification of Western blots, related to Fig. 5K, for JunB, Nfix and pERK, expressed as a ratio of pERK on Tot-ERK, upon PD98059 treatment of fetal myoblasts (\*,  $p < 0.1$ ; n=5). **(H-J)** Densitometric quantification of Western blot in Fig. 5L of JunB (H), Nfix (I) and pERK (J), as ration of pERK on Tot-ERK upon Y27632 and/or PD98059 treatment of embryonic myoblasts (\*,  $p < 0.1$ ; n=5).



### Supplementary Figure 4. Protein expression analysis on juvenile MuSCs.

(A-D) Densitometric quantification of Western blot in Fig.7A for pERK/Tot-ERK (A), Pmypt1/Tot-MYPT1 (B), JunB (C) and Nfix (D) on juvenile MuSCs in proliferating

conditions (Prolif.) or during differentiation (day in differentiation medium; dDM). Each sample is compared to E11.5 for the statistical analysis (\*,  $p < 0.1$ ; \*\*,  $p < 0.05$ ; \*\*\*,  $p < 0.01$ ;  $n=5$ ). **(E-F)** Western blot following transfection with dominant-negative NFI-engrailed (NFI-ENG) or engrailed domain (ENG), Nfix during differentiation (3, 4dDM) (E), and its related densitometric quantification (F). Vinculin is used as housekeeping control (\*,  $p < 0.1$ ;  $n=5$ ). **(G-H)** Western blot on juvenile MuSCs treated with PD98059 or Y27632 until the differentiation, showing Pax7, Myogenin, sarcomeric Myosins (MyHCs) (G), and their relative densitometric analysis (H). Vinculin is used as housekeeping control. **(I)** Western blot on juvenile MuSCs treated with PD98059 or Y27632, showing Caspase3 (total Caspase3 or ProCasp3; active Caspase3 or aCasp3) and Caspase9 (total Caspase9 or ProCasp9; active Caspase9 or aCasp9) until the differentiation. Vinculin was used to normalise the amount of protein. **(J-K)** Western blot assay on proliferating juvenile MuSCs, treated over-night with PD98059, for Pax7, Myogenin (J) and active Caspase3 and 9 (aCasp3 and aCasp9) (K). **(L)** Densitometric quantification of Western blots on proliferative satellite cells treated with vehicle or PD98059, showing Pax7, Myogenin, the ratio of aCasp3 on total Caspase3 (ProCasp3) and the ratio of aCasp9 on ProCasp9.

**Table S1.** Primers used in this study

Primer Name	Primer sequence	Usage	Reference
<i>Nfix</i> (Fw) <i>Nfix</i> (Rev)	CACTGGGGCGACTTGTAGAG AGGCTGACAAGGTGTGGC	<i>qRT-PCR</i>	Mourikis et al., 2012
<i>JunB</i> (Fw) <i>JunB</i> (Rev)	CCTGTGTCCCCATCAACAT CAGCCTTGAGTGTCTTCACCT	<i>qRT-PCR</i>	
<i>MyHC-I</i> (Fw) <i>MyHC-I</i> (Rev)	AGGGCGACCTCAACGAGAT CAGCAGACTCTGGAGGCTCTT	<i>qRT-PCR</i>	Mathew et al., 2011
<i>MyHC-emb</i> (Fw) <i>MyHC-emb</i> (Rev)	GCAAAGACCCGTGACTTCACCTCTAG GCATGTGAAAAGTGATACGTGG	<i>qRT-PCR</i>	Mathew et al., 2011
<i>Eno3</i> (Fw) <i>Eno3</i> (Rev)	TTCTACCGCAACGGCAAGTA GACCTTCAGGAGCAGGCAAT	<i>qRT-PCR</i>	
<i>Myogenin</i> (Fw) <i>Myogenin</i> (Rev)	CTGGGGACCCCTGAGCATTG ATCGCGCTCCTCTGTTGA	<i>qRT-PCR</i>	
<i>RhoA</i> (Fw) <i>RhoA</i> (Rev)	AGCTTGTGGTAAGACATGCTTG GTGTCCATAAAGCCAACCTCTAC	<i>qRT-PCR</i>	
<i>Gapdh</i> (Fw) <i>Gapdh</i> (Rev)	GGCATGGACTGTGGTCATGA TTCACCACCATGGAGAAGGC	<i>qRT-PCR</i>	
<i>Tcf15</i> (Fw) <i>Tcf15</i> (Rev)	GCAGCTGCTTGAAAGTGAG CGGTCCTTACACAACGCAGG	<i>qRT-PCR</i>	
<i>Pax3</i> (Fw) <i>Pax3</i> (Rev)	GGGAACTGGAGGCATGTTTA GTTTTCCGTCCCAGCAATTA	<i>qRT-PCR</i>	
<i>Smad6</i> (Fw) <i>Smad6</i> (Rev)	ATCACCTCCTGCCCTGT CTGGGGTGGTGTCTCTGG	<i>qRT-PCR</i>	
<i>PKC<math>\delta</math></i> or <i>Prkcq</i> (Fw) <i>PKC<math>\delta</math></i> or <i>Prkcq</i> (Rev)	ATGGACAACCCCTTCTACCC GCGGATGTCTCCTCTCACTC	<i>qRT-PCR</i>	
<i>ITGA7</i> (Fw) <i>ITGA7</i> (Rev)	GGCTGGGCTGTTAGTCCTG ATGGGCTCGGTGATAGTTGGT	<i>qRT-PCR</i>	
<i>MCK</i> or <i>Ckm</i> (Fw) <i>MCK</i> or <i>Ckm</i> (Rev)	TTCCTTGTGTGGGTGAACGA TTTTCCAGCTTCTTCTCCATC	<i>qRT-PCR</i>	
<i>NfiA</i> (Fw) <i>NfiA</i> (Rev)	TGGCATACTTTGTACATGCAGC ACCTGATGTGACAAAGCTGTCC	<i>qRT-PCR</i>	
<i>Myh8</i> (Fw) <i>Myh8</i> (Rev)	GTCACGCAATGCAGAAGAGA CAGGTCCTTCACCGTCTGTT	<i>qRT-PCR</i>	
<i>MyHC-2b promoter</i> (Fw) <i>MyHC-2b promoter</i> (Rev)	GAGGTCCGTAGTCAGTCTCTTTT TACCCCAAGTGTTAGGCTCA	<i>ChIP</i> <i>qRT-PCR</i>	Raffaello et al., 2010
<i>Nfix promoter -1400bp</i> (Fw) <i>Nfix promoter -1400bp</i> (Rev)	ACACTAGGATTGAGGAAGACTTAGA CAAGGCCTTCTGGGGCTC	<i>ChIP</i> <i>qRT-PCR</i>	
<i>Nfix promoter -200bp</i> (Fw) <i>Nfix promoter -200bp</i> (Rev)	TTGAGAATCCACCCAAGCCC AAGCCAACGCCTGATTCTGA	<i>ChIP</i> <i>qRT-PCR</i>	
<i>Nfix promoter -1000bp</i> (Fw) <i>Nfix promoter -1000bp</i> (Rev)	CAAAGAGGCATCCACTTGACAG GTTTTTGGTVTCCAACCTGCCG	<i>ChIP</i> <i>qRT-PCR</i>	
<i>Intergenic</i> (Fw) <i>Intergenic</i> (Rev)	TCGGACCGGAGTGTTAGGAA ACCCTGGAGTCTCAGCATCG	<i>ChIP</i> <i>qRT-PCR</i>	An et al., 2011

ARTICLE

Open Access

# Nutritional intervention with cyanidin hinders the progression of muscular dystrophy

Marielle Saclier<sup>1</sup>, Chiara Bonfanti<sup>1</sup>, Stefania Antonini<sup>1</sup>, Giuseppe Angelini<sup>1</sup>, Giada Mura<sup>1</sup>, Federica Zanaglio<sup>1</sup>, Valentina Taglietti<sup>1</sup>, Vanina Romanello<sup>2</sup>, Marco Sandri<sup>2</sup>, Chiara Tonelli<sup>1</sup>, Katia Petroni<sup>1</sup>, Marco Cassano<sup>1</sup> and Graziella Messina<sup>1</sup>

## Abstract

Muscular Dystrophies are severe genetic diseases due to mutations in structural genes, characterized by progressive muscle wasting that compromises patients' mobility and respiratory functions. Literature underlined oxidative stress and inflammation as key drivers of these pathologies. Interestingly among different myofiber classes, type I fibers display a milder dystrophic phenotype showing increased oxidative metabolism. This work shows the benefits of a cyanidin-enriched diet, that promotes muscle fiber-type switch and reduced inflammation in dystrophic *alpha-sarcoglyan* (*Sgca*) null mice having, as a net outcome, morphological and functional rescue. Notably, this benefit is achieved also when the diet is administered in dystrophic animals when the signs of the disease are seriously evident. Our work provides compelling evidence that a cyanidin-rich diet strongly delays the progression of muscular dystrophies, paving the way for a combinatorial approach where nutritional-based reduction of muscle inflammation and oxidative stress facilitate the successful perspectives of definitive treatments.

## Introduction

Muscular dystrophies (MDs) are a group of heterogeneous genetic diseases, characterized by wasting of skeletal muscle tissue, which over time compromises patient mobility and, in the most severe cases, respiratory and cardiac functionality leading to premature death<sup>1,2</sup>. In many cases, the mutations affect one or more proteins that cluster in the dystrophin-glycoprotein complex (DGC) located on the sarcolemma of the myofibers and links it to the basal lamina. This complex connects myofibers to the extracellular matrix, and its role is essential for fiber integrity and cell signaling during contraction. The mutations result in the disassembly and/or a malfunction of the entire DGC, which leads to increased fragility of sarcolemma and

myofibers death. Damaged and dead fibers can be replaced by satellite cells (SCs), the adult stem cells of skeletal muscle tissue. In this pathologic scenario, since SCs share the same mutation as well as the damaged myofibers, they differentiate in fragile myofibers, leading to a loop of degeneration and regeneration<sup>2</sup>. In time, the population of SCs is exhausted and the damaged muscle is replaced by connective and adipose tissue, impairing the physiological function of muscle tissue<sup>1-3</sup>. Despite the molecular mechanisms behind MDs are partially known, this class of diseases is one of the most difficult to treat. Indeed, although several clinical trials have been carried on, MDs are still orphan diseases<sup>4</sup>.

Skeletal muscle is the most abundant tissue in the human body and it is composed of large multinucleated fibers, whose nuclei cannot divide. Consequently, any cell or gene replacement strategy must restore proper gene expression in hundreds of millions of post-mitotic nuclei, which are embedded in a highly structured cytoplasm and surrounded by a thick basal lamina. It is therefore evident that, although caused by a single gene defect, this group of

Correspondence: Graziella Messina ([graziella.messina@unimi.it](mailto:graziella.messina@unimi.it))

<sup>1</sup>Department of Biosciences, University of Milan, via Celoria 26, 20133 Milan, Italy

<sup>2</sup>Venetian Institute of Molecular Medicine (VIMM), Department of Biomedical Sciences, University of Padova, Padova, Italy

These authors contributed equally: Katia Petroni, Marco Cassano, Graziella Messina

Edited by S. Inoue

© The Author(s) 2020



**Open Access** This article is licensed under a Creative Commons Attribution 4.0 International License, which permits use, sharing, adaptation, distribution and reproduction in any medium or format, as long as you give appropriate credit to the original author(s) and the source, provide a link to the Creative Commons licence, and indicate if changes were made. The images or other third party material in this article are included in the article's Creative Commons licence, unless indicated otherwise in a credit line to the material. If material is not included in the article's Creative Commons licence and your intended use is not permitted by statutory regulation or exceeds the permitted use, you will need to obtain permission directly from the copyright holder. To view a copy of this licence, visit <http://creativecommons.org/licenses/by/4.0/>.

pathologies could be considered as multifactorial: misregulation of associated sarcoplasmic proteins, severe chronic inflammation and consequent macrophage infiltration resulting in fibrosis. Among the different approaches, many efforts are directed to slow down the progression of the disease to counteract progressive degeneration and to improve patients' quality life<sup>5</sup>. Several pieces of evidence showed that oxidative stress and accumulation of reactive oxygen species (ROS) strongly contribute to aggravate the dystrophic pathology<sup>6,7</sup>. One of the considered strategies is to use antioxidant molecules to counteract the oxidative stress generated by muscle contraction and degeneration<sup>6–13</sup>.

Another important aspect of MD progression is chronic inflammation, as the secretion of several cytokines recalls macrophages, essential players in acute muscle regeneration. However, in a chronic myopathic context, this population establishes a sustained inflammatory milieu worsening the dystrophic phenotype<sup>14,15</sup>.

Anthocyanins are a subclass of flavonoids found in pigmented plants, widely recognized for their anti-inflammatory and antioxidant properties<sup>16,17</sup>. Preventive effects of dietary anthocyanins have been described in epidemiological and preclinical studies, indicating health-promoting properties against cardiovascular disease, cancer, and neurodegenerative diseases<sup>16,18</sup>. More than 700 different anthocyanins have been reported in nature, each identified by specific glycosylation, methylation, and acylation of the aglycones anthocyanidins (i.e., cyanidin, delphinidin, malvidin, pelargonidin, peonidin, and petunidin)<sup>17</sup>. Anthocyanin-rich corn mainly contains cyanidin 3-glucoside and its acylated derivatives<sup>19</sup>. Dietary intake of cyanidin 3-glucoside from anthocyanin-rich corn reduced myocardial injury upon ischemia-reperfusion and against cardiotoxic effects induced by Doxorubicin, an anthracycline widely used as chemotherapeutic drug against a variety of cancer types<sup>20,21</sup>.

In this study, we produce evidence that dietary intake of cyanidin 3-glucoside (here referred to as cyanidin), an anthocyanin from purple corn<sup>21</sup>, is beneficial for treating MD pathologies. We indeed provide significant results that cyanidin-enriched diet (Red diet, RD) supplied to the dystrophic *alpha-sarcoglycan* null mouse model<sup>22</sup> either at weaning or adulthood, when the signs of the disease are already present, improves the morphological and functional recovery of the pathologic phenotype. Additionally, we suggest that cyanidin supplementation promotes mitochondrial biogenesis which in turn preserves muscle function.

## Results

### Cyanidin-enriched diet ameliorates the histopathological condition of dystrophic muscles

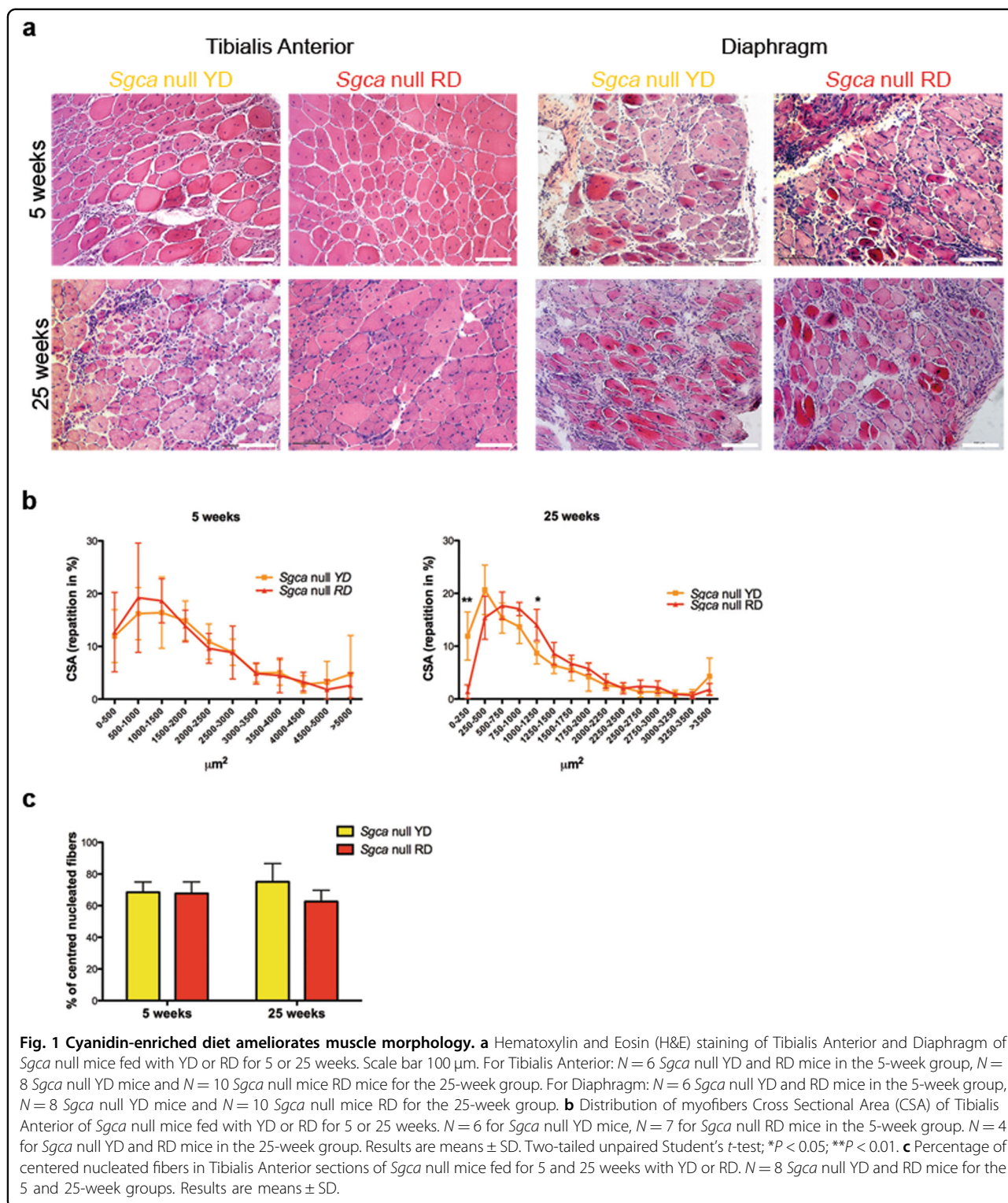
To establish whether cyanidin supplementation could affect the onset and progression of dystrophic conditions,

we fed *Sgca* null mice at weaning with a cyanidin-enriched diet either for 5 or 25 weeks, to evaluate, respectively, the short and long-term nutritional benefits. As a control, we also provide *Sgca* null and wild-type mice (WT) with a cyanidin-free diet isogenic to RD, referred to as Yellow diet (YD) (Fig. S1a). The *Sgca* null mouse model<sup>22</sup> was chosen considering its severity that makes it resemble the human Duchenne Muscular Dystrophy (DMD) pathology with respect to the usually studied *mdx* mouse.

First, to evaluate whether the two diets do not influence the normal growth and development of the mouse model, we analyzed the food intake and the body weight for 5-week post weaning in *Sgca* null mice. Compared to *Sgca* null mice fed with a standard diet, we did not observe differences in both parameters (Fig. S1b and not shown). Then, we analyzed muscle histology through Hematoxylin and Eosin staining on *Tibialis anterior* (TA) and diaphragm sections. While dystrophic mice fed with control YD for 5-week display the first signs of muscle degeneration with inflammatory infiltrates and necrotic areas that progressively degenerate, RD-fed *Sgca* null mice appeared with an improved morphology of muscle tissue, with less infiltrates yet at 5-week-time point (Fig. 1a, top panels). At 25-week-time point, RD-fed *Sgca* null mice show preserved muscle morphology with reduced necrosis and cellular infiltrates when compared with YD-fed counterpart (Fig. 1a, bottom panels). Consistently, the measurement of fiber size distribution (Cross-Sectional Area, CSA) in TA sections confirmed the cyanidin-induced morphological ameliorations at 25 weeks in RD-fed dystrophic mice with increased calibre homogeneity compared with the YD-fed counterpart (Fig. 1b). The analysis of centrally nucleated myofibers, as an index of muscle regeneration, did not show any significant difference between YD- and RD-fed animals, indicating that cyanidin supplementation does not affect the regeneration process (Fig. 1c).

Collagen deposits are hallmarks of myopathy in MDs and compromise patients' mobility by replacing muscle tissue upon chronic inflammatory cues<sup>23</sup>. To establish whether cyanidin-dietary enrichment might impact on collagen deposits, we performed Milligan's trichrome staining on TA and diaphragm of YD- and RD-fed *Sgca* null animals. As shown in Fig. 2a, while YD-fed dystrophic muscles accumulate abundant extracellular matrix deposits particularly at 25 weeks, the TA and diaphragm muscles of RD-fed animals exhibit a prolonged reduction of extracellular matrix deposition at both time points analyzed.

To strengthen these observations, we quantified the fluorescent positive area of TA sections stained for collagen I (Fig. 2b) revealing a drastic reduction of its deposition in RD- vs. YD-fed dystrophic mice both at 5 and 25 weeks from the diet regimen (Fig. S1c).



Inflammation accelerates the clinical progression of MDs and this is mainly accounted for by muscle-infiltrating macrophages that engender a chronic inflammatory milieu<sup>24</sup>. To assess the macrophage infiltration

status, we FAC-sorted CD64<sup>+</sup> cells from hind-limb muscle lysates of *Sgca* null mice fed with either YD or RD. As shown in Fig. 2c, the total macrophage population significantly drop in the muscle of dystrophic mice following cyanidin dietary

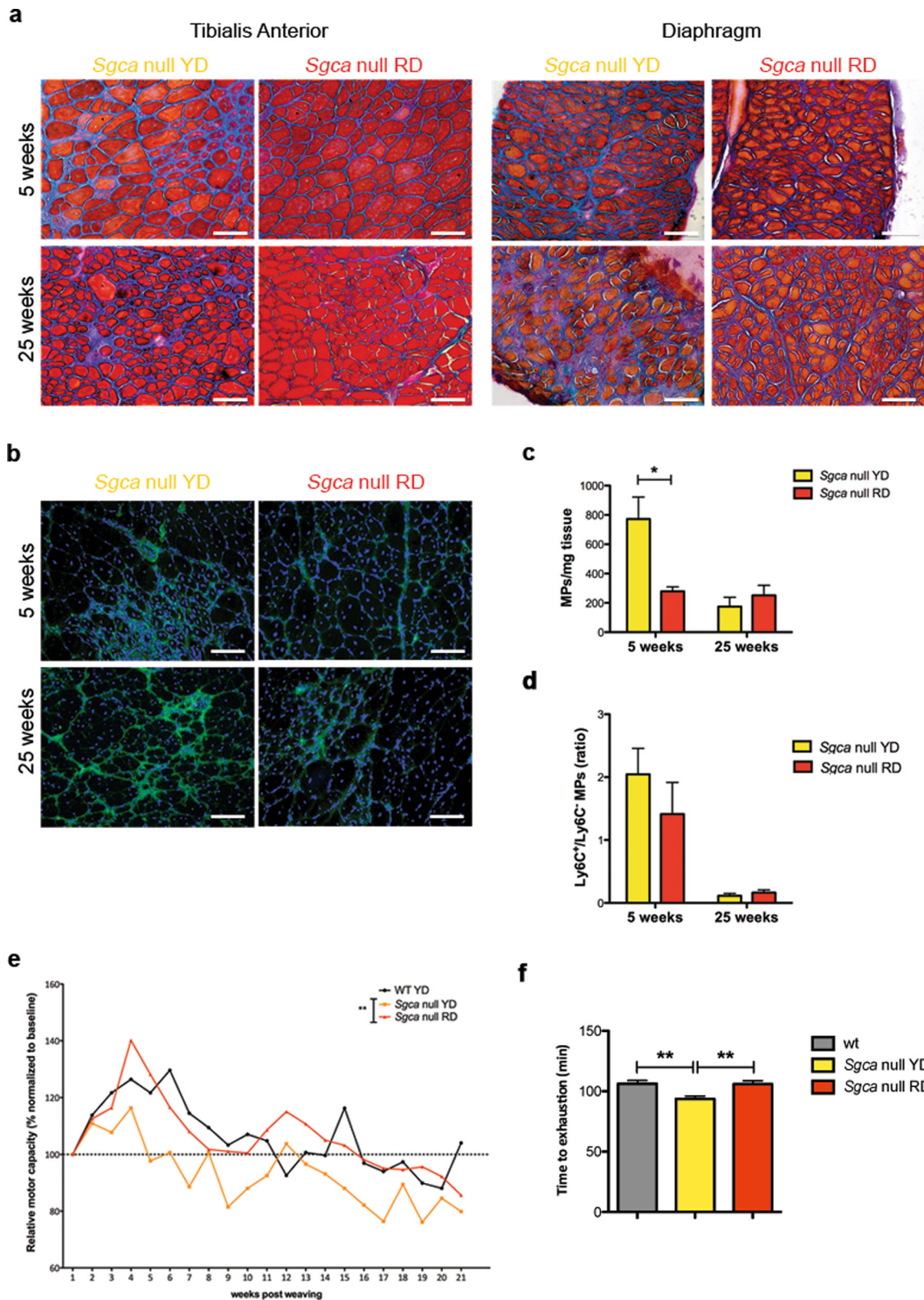


**Fig. 2** (See legend on next page.)

(see figure on previous page)

**Fig. 2 Cyanidin-enriched diet decreases collagen I deposition, macrophages infiltration and rescue muscle performance.** **a** Milligan's Trichrome staining of Tibialis Anterior and Diaphragm of *Sgca* null mice fed with YD or RD for 5 or 25 weeks. Scale bar 100  $\mu$ m. For Tibialis Anterior:  $N = 6$  *Sgca* null YD and RD mice in the 5-week group,  $N = 8$  *Sgca* null YD mice and  $N = 10$  *Sgca* null RD mice for the 25-week group. For Diaphragm:  $N = 6$  *Sgca* null YD and RD mice in the 5-week group,  $N = 8$  *Sgca* null YD mice and  $N = 10$  *Sgca* null RD mice for the 25-week group. **b** Collagen I Immunofluorescence (green) and nuclei (blue) in Tibialis Anterior sections of *Sgca* null mice fed for 5 and 25 weeks with YD or RD. Scale bar 100  $\mu$ m.  $N = 4$  *Sgca* null YD and RD mice in the 5-week group.  $N = 5$  *Sgca* null YD and RD mice in the 25-week group. **c** Number of MPs from total hind limb lysates of *Sgca* null mice fed with YD or RD for 5 or 25 weeks. Results are means  $\pm$  SD; Two-tailed unpaired Student's *t*-test; \* $P < 0.05$ .  $N = 6$  for *Sgca* null YD mice and  $N = 5$  for *Sgca* null RD mice in 5-week group.  $N = 4$  for *Sgca* null YD mice and  $N = 3$  for *Sgca* null RD mice in 25-week group. **d** Ratio between LyC6<sup>+</sup> and LyC6<sup>-</sup> MPs from total hind limb lysate of *Sgca* null mice fed with YD or RD for 5 and 25 weeks.  $N = 6$  for *Sgca* null YD mice and  $N = 5$  for *Sgca* null RD mice in 5-week group.  $N = 4$  for *Sgca* null YD mice and  $N = 3$  for *Sgca* null RD mice in 25-week group. Results are means  $\pm$  SD; Two-tailed unpaired Student's *t*-test. **e, f** Treadmill test (time to exhaustion) over time and **f** the total average of the measurements of WT mice fed with YD and *Sgca* null mice fed with YD or RD.  $N = 3$  WT mice,  $N = 4$  *Sgca* null YD and RD mice. Results are means  $\pm$  SD; Two-tailed unpaired Student's *t*-test; \*\* $P < 0.01$ .

enrichment. However, the ratio of pro-inflammatory to anti-inflammatory macrophage sub-populations (CD64<sup>+</sup>-Ly6C<sup>+</sup> and CD64<sup>+</sup>-Ly6C<sup>-</sup>, respectively) was not significantly affected by the diet at both time points (Fig. 2d). These observations suggest that cyanidin may facilitate an anti-inflammatory effect within the muscle environment, which is independent by macrophage phenotype.

Progressive reduction of muscle performance mainly characterizes MDs, thus we sought to investigate whether the cyanidin-enriched diet may beneficially impact this condition in *Sgca* null mice with the treadmill test. As an index of performance, animals after 5 weeks supplied with RD or YD were measured in terms of time to exhaustion over the following 15 weeks maintaining the dietary protocol. Cyanidin supplementation was sufficient to promote significant and prolonged muscle endurance of dystrophic animals compared to their control YD-fed littermates (Fig. 2e, f). Notably, the performance of *Sgca* null mice fed with the RD was comparable to the WT group.

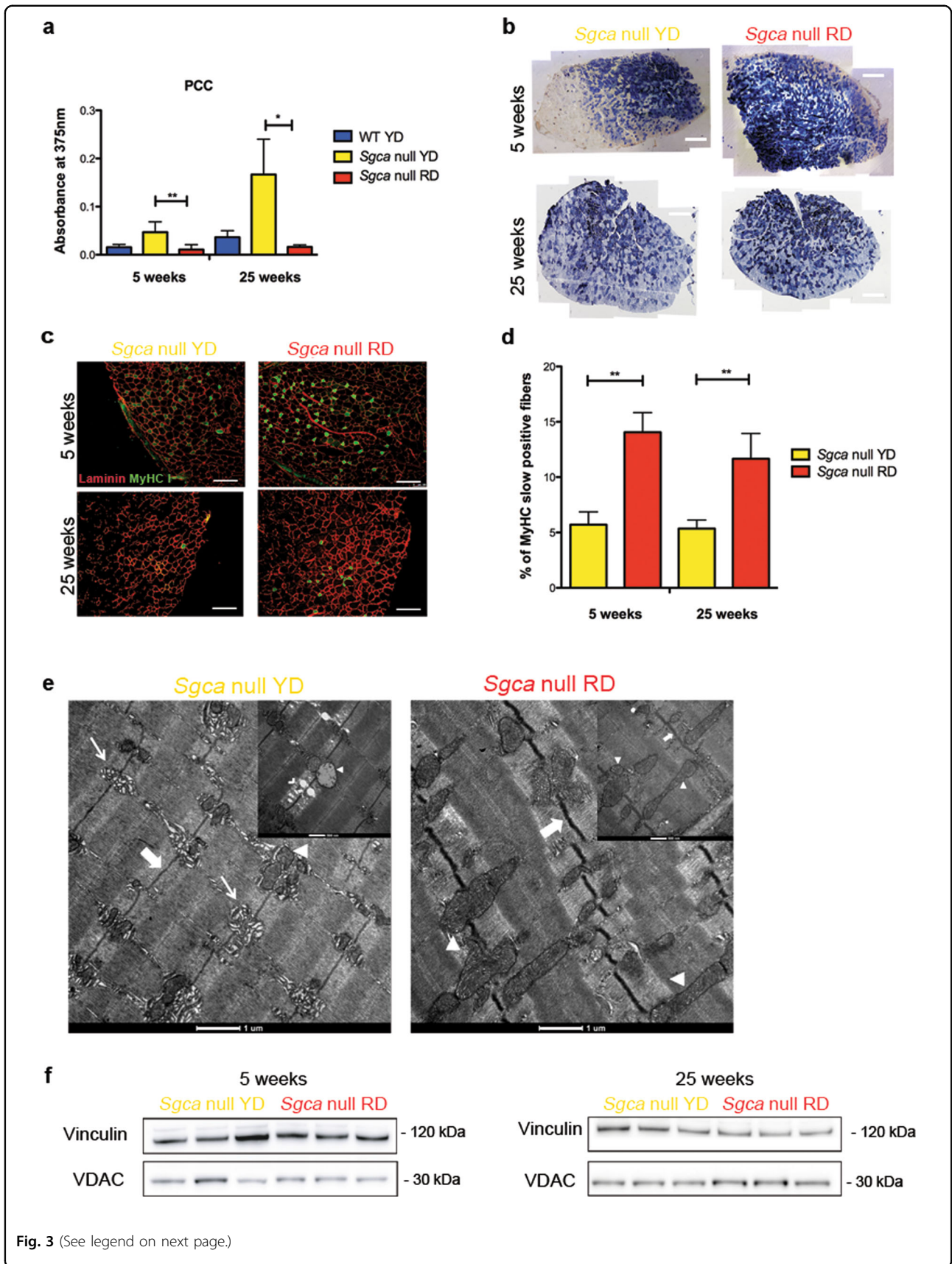
#### The cyanidin-enriched diet promotes a shift towards an oxidative metabolism

To dissect the molecular dynamics modulated by cyanidin, we assessed its anti-oxidant ability by measuring the index of protein oxidation<sup>25,26</sup>, calculated as protein carbonylation content (PCC) from quadriceps protein extracts of both RD- and YD-fed *Sgca* null mice. As shown in Fig. 3a, YD-fed dystrophic animals progressively accumulate higher PCC compared to the RD-fed counterpart. Interestingly, the latter reached levels of PCC as low as the WT conditions. The remarkable drop of PCC in RD-fed animals might represent the synergistic outcome of increased oxidative metabolism and mitochondrial activity<sup>27</sup>. Based on this evidence, we performed succinate dehydrogenase (SDH) staining on TA sections from *Sgca* null mice following YD or RD supplementation. SDH staining is an enzymatic assay able to stain fibers with oxidative metabolism owing to their mitochondrial SDH activity. The outcomes confirmed an increased number of oxidative fibers in the TA of *Sgca* null mice fed with RD compared to their YD-fed littermates (Fig. 3b).

It has been described both in dystrophic murine models and in patients that muscle fibers expressing high levels of myosin heavy chain isoform I (MyHC I) are preserved from MD progression as a consequence of their stronger antioxidant capacity<sup>24,28</sup>. The immunostaining for MyHC I<sup>+</sup> slow-twitching muscle fibers in the TA sections of RD-fed animals corroborates both the metabolic and the muscle fiber phenotype switch induced by this nutraceutical approach (Fig. 3c). The quantification indeed confirmed a significant shift towards an oxidative muscle metabolism following short- and long-term cyanidin supplementation (Fig. 3d). To follow-up on these findings, we parse the ultrastructure of *Extensor Digitorum longus* (EDL) muscle fibers in *Sgca* null mice fed with or without cyanidin for 12 weeks. Low magnification-electron microscopy analysis highlighted structural abnormalities in terms of sarcomere organization, mitochondria appearance, and distribution in YD-fed dystrophic mice (Fig. 3e and S1e). Conversely, RD-fed dystrophic mice presented with a healthier sarcomeric organization and increased mitochondrial amount, whereas only YD-fed dystrophic mice were characterized by aberrantly extended regions of endoplasmic reticulum, as a condition of sarcoplasmic stress. While disease progression causes flawed mitochondria and selective loss of the thin filaments, cyanidin supplementation was sufficient to improve mitochondrial number and morphology, encompassed by the preservation of sarcomere structure at thin filaments. Interestingly, RD-fed *Sgca* null animals show a thicker Z line as a key feature of MyHC I<sup>+</sup> fibers<sup>27</sup>, confirming the data observed from the MyHC immunostaining. Consistent with electron microscopy, the mitochondrial mass, revealed by VDAC, was increased in muscles from 25-week-RD-fed mice (Fig. 3f and S1f).

#### A cyanidin-enriched diet ameliorates the late-stage dystrophic phenotype

Sclerosis and inflammatory infiltrates characterize advanced stages of MD and hamper the prospective successful outcome of cell and gene delivery protocols, precluding the treatment for a large portion of dystrophic



(see figure on previous page)

**Fig. 3 Cyanidin-enriched diet promotes a shift to a more oxidative fiber metabolism.** **a** Quantification of protein carbonylation content (PCC) from protein lysate of WT, *Sgca* null YD or RD mice fed for 5 or 25 weeks.  $N = 4$  WT YD,  $N = 4$  *Sgca* null YD mice and  $N = 3$  *Sgca* null RD mice fed for 5 weeks. For the 25-week group,  $N = 4$  *Sgca* WT YD,  $N = 3$  *Sgca* null YD mice and  $N = 3$  *Sgca* null RD mice. Results are means  $\pm$  SD; Two-tailed unpaired Student's *t*-test; \* $P < 0.05$ ; \*\* $P < 0.01$ . **b** SDH on Tibialis Anterior muscle section *Sgca* null YD or RD mice fed for 5 or 25 weeks. Scale bar 500  $\mu$ m.  $N = 6$  *Sgca* null YD and 5 *Sgca* null RD mice fed for 5 weeks. For the 25 weeks, group  $N = 6$  *Sgca* null YD and RD mice. **c** MyHC I positive fibers (green) and laminin (red) Immunofluorescence of Tibialis Anterior sections of *Sgca* null mice fed with YD or RD for 5 or 25 weeks. Scale bar 200  $\mu$ m.  $N = 3$  for *Sgca* null YD and RD mice in the 5-week group.  $N = 3$  for *Sgca* null YD mice and  $N = 4$  for *Sgca* null mice RD in the 25-week group. **d** Quantification of MyHC I positive fibers in Tibialis Anterior muscles of *Sgca* null mice fed with YD or RD for 5 or 25 weeks.  $N = 3$  for *Sgca* null YD and RD mice in the 5-week group.  $N = 3$  for *Sgca* null YD mice and  $N = 4$  for *Sgca* null mice RD in the 25-week group. Results are means  $\pm$  SD; Two-tailed unpaired Student's *t*-test; \*\* $P < 0.01$ . **e** Ultrastructure of EDL of *Sgca* null mice fed with YD or RD. At low magnifications (scale bar 1  $\mu$ m) the endoplasmic reticulum (narrow arrow), the Z line (thick arrow) and mitochondria (triangle) are underlined. At higher magnifications (scale bar 500 nm), degradation sites of thin filament (arrowhead) are visible. **f** Western Blot of VDAC expression in *Sgca* null mice YD or RD mice fed for 5 or 25 weeks. Vinculin was used to normalize.  $N = 3$  for *Sgca* null YD mice and  $N = 3$  for *Sgca* null RD mice in 5 and 25 groups.

patients. In a therapeutic framework, we tested whether cyanidin offers remarkable benefits even when supplied at later stages of the disease, as this situation more likely represents the realistic clinical setting. In this protocol, the RD or the cyanidin-mock equivalent YD was supplied for 5 weeks to 15-weeks-old *Sgca* null mice (Fig. S1d), yet when early signs of dystrophy arise<sup>22</sup>. Hematoxylin and Eosin staining on TA and diaphragm muscles of RD-fed *Sgca* null mice revealed remarkable amelioration of muscle organization and morphology that appears more preserved and with less cell infiltrates (Fig. 4a, upper panels). Trichrome staining on TA and diaphragm sections also showed a decrease in extracellular matrix deposits when RD is supplied, at variance with *Sgca* null mice fed with the control diet (Fig. 4a, bottom panels). The diet-induced benefit on fibrotic degeneration was further consolidated by quantifying the fluorescent positive area of TA sections stained for collagen I (Fig. 4b), to reveal a considerable drop of its deposition in RD- vs. YD-fed dystrophic mice (Fig. 4c).

To parse the inflammatory milieu, we quantified the number of F4/80<sup>+</sup> macrophages in TA sections from YD- versus RD-fed *Sgca* null mice, revealing less macrophage infiltration in *Sgca* null mice upon cyanidin supplementation (Fig. 4d).

The homogenous fiber calibre distribution observed in RD- vs YD-fed dystrophic mice corroborates our previous results (Fig. 4e). Similarly to what has been observed at weaning (Fig. 3b), *Sgca* null animals fed with the RD at 5-weeks old shifted towards an oxidative fiber metabolism as from the SDH activity assay (Fig. 4f).

## Discussion

MDs represent a heterogeneous group of inherited pathologies, some are life-threatening conditions while others are still lacking a definitive therapy. The pathological hallmark consists of muscle degeneration loops followed by unsuccessful regeneration attempts to repair the damaged tissue. As a net outcome of this iteration, SC pool's exhaustion initiates the progressive replacement of

muscle by connective and adipose tissue, which compromise functionality and lead to the loss of ambulation at childhood and ultimately to premature death.

It is widely acknowledged that mitochondrial dysfunction and cellular energy perturbations serve as complementary mechanisms hastening muscle degradation. Indeed, dystrophic muscle is associated with a decrease in muscle mitochondrial content<sup>29,30</sup>. Previous studies reported the dystrophic muscle fibers to be intrinsically susceptible to oxidative stress, which emerges as the ground state underpinning pathology progression<sup>7,31</sup>. However, the mechanistic dynamics governing this phenomenon within the muscle milieu have been poorly characterized.

Proper nutrition, assumed as the optimal intake of bioactive compounds might be at the basis of innovative adjuvant therapies in patients with states of chronic muscle wasting<sup>32</sup>. As such, nutraceuticals aimed to target the metabolic reprogramming, are paving the way for auxiliary protocols in the treatment of MDs. For instance, specific aminoacidic formulation facilitates blood and oxygen supplies to the female *mdx* mice thus mitigating disease progression<sup>33</sup>.

Importantly, the expectations about the potential impact of nutraceutical options in the treatment of MDs must be realistic and far to presume they could reverse very advanced stages such as loss of ambulation. However, the implementation of these treatments could act as a disease modifier that hinders the pathological course, having beneficial effects on patients' healthspan and increasing their eligibility for curative options.

In this study, we show that a cyanidin-enriched diet delay the pathological onset and improve muscle performance in a pre-clinical model of MD. Among the wide portfolio of animal models, we focused on the *Sgca* null dystrophic mouse, since it presents with severe degenerative myopathy very similar to Duchenne human patients since the early life stage<sup>22</sup>. We demonstrated the nutritional benefits of cyanidin supplementation in the

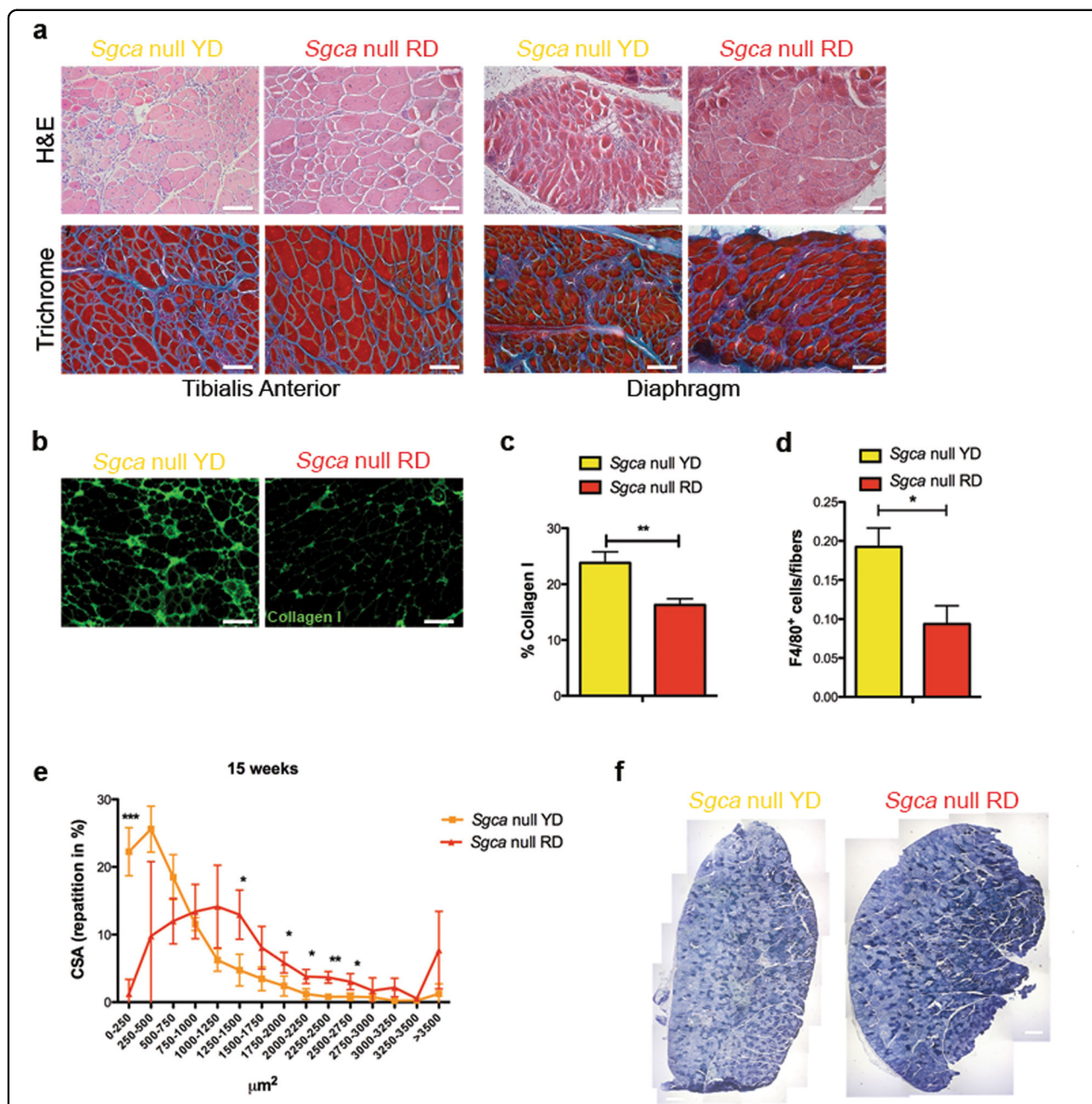


**Fig. 4** Cyanidin-enriched diet ameliorates dystrophic phenotype also in already compromised *Sgca*-null mice. **a** Hematoxylin and eosin (H&E) and Milligan’s Trichrome staining on Tibialis Anterior and Diaphragm muscles of 5-week-old *Sgca* null mice fed with YD or RD for 15 weeks. Scale bar 100 μm. *N* = 3 *Sgca* null YD mice and *N* = 3 *Sgca* null RD mice. **b** Collagen I Immunofluorescence (green) and nuclei (blue) in Tibialis Anterior sections of 5-week-old *Sgca* null mice fed with YD or RD for 15 weeks. Scale bar 100 μm. *N* = 4 *Sgca* null YD mice and *N* = 4 *Sgca* null RD mice. **c** Quantification of Collagen I<sup>+</sup> positive area in Tibialis Anterior sections of 5-week-old mice fed with YD or RD for 15 weeks. *N* = 3 *Sgca* null YD and RD mice. Results are means ± SD; Two-tailed unpaired Student’s *t*-test; \*\**P* < 0.01. **d** Quantification of F4/80<sup>+</sup> macrophages per myofibers in Tibialis Anterior sections of 5-week-old mice fed with YD or RD for 15 weeks. *N* = 3 *Sgca* null YD and RD mice. Results are means ± SD; Two-tailed unpaired Student’s *t*-test; \**P* < 0.05. **e** Distribution of myofibers Cross Sectional Area (CSA) of Tibialis Anterior of 5-week-old *Sgca* null mice fed with YD or RD for 15 weeks. *N* = 3 for *Sgca* null YD and RD mice. Results are means ± SD of at least three independent experiments; Two-tailed unpaired Student’s *t*-test; \**P* < 0.05. **f** SDH staining on Tibialis Anterior muscle section of 5-week-old *Sgca* null mice fed with YD or RD for 15 weeks. Scale bar 100 μm. *N* = 3 for *Sgca* null YD and RD mice. Results are means ± SD; Anova test was used. \*\**P* < 0.01; \*\*\**P* < 0.001.

disease progression of *Sgca* null mice, inducing important ameliorations both in terms of tissue morphology and muscle performance.

State-of-the-art knowledge recognizes slow-twitching fibers, with a prevalent oxidative metabolism, more prone to resist MD degeneration when compared to the glycolytic fast-twitching fibers<sup>20</sup>. Among others, our previous studies remarked the relevance for an oxidative fiber-type metabolism together with the expression of MyHC I isoform in both preserving muscular architecture and delaying the signs of the dystrophic progression<sup>24,28,34</sup>. Here, dietary supplementation with cyanidin promotes a metabolic shift towards oxidative muscle fibers and enhanced mitochondrial biogenesis, and ultimately, shield against the pathology progression.

Macrophages act as a cellular cornerstone playing both pro- and anti-inflammatory roles during muscle recovery. Chronic muscle injury, a key feature of dystrophic setting, provokes macrophage infiltrations which participate in the worsening of the disease and preventing macrophage infiltration improves dystrophic muscle<sup>6,35</sup>. We observed a remarkable reduction of macrophage infiltration when *Sgca* null mice were assigned to a diet supplemented with a cyanidin-rich preparation.

The safety and toxicological concerns about anthocyanins consumption in humans are remarkably low. There are no reports about adverse health effects associated with the consumption of anthocyanins at the usual dietary intake levels. Although most anthocyanins have reduced bioavailability, the cyanidin-3-glucoside (used in our study) ranks among the more stable with a relatively low-dose threshold to produce its protective results against oxidative stress both in vitro and in vivo<sup>36,37</sup>.

The health-caring effect of anthocyanins has been successfully proven against cardiovascular diseases, where 5-week-regimen with a purple corn diet was sufficient to protect from ischemic injury or to prevent the cardiotoxic effects of doxorubicin (Dox), a chemotherapeutic agent used for the treatment of breast cancer<sup>20,21</sup>. Currently, trial intervention in breast cancer-bearing patients undergoing radiotherapy is testing the beneficial effect of the administration of a product enriched in anthocyanins on the inflammatory response to radiation and on its consequent skin toxicity, as well as on systemic low-grade inflammation reaction<sup>38</sup>.

Our findings leverage the nutritional benefits of cyanidin in a model of chronic muscle condition where oxidative stress and inflammation trigger progressive tissue wasting and drive the detrimental outcomes of the pathology. In a dystrophic context, we provide compelling evidence that either short- or long-term supplementation of cyanidin, administered when the disease is either still pre-symptomatic (at weaning) or advanced, preserves muscle functionality thanks to its bivalent nature of anti-

oxidant and anti-inflammatory agent. To our knowledge, this feature renders cyanidin unique among other dietary antioxidants, such as Resveratrol or Sulphoraphane<sup>6,13</sup>. The inflammatory healing effects of anthocyanins have been previously observed in models of systemic inflammation, such as hepatic swelling, chronic pain conditions and recently obesity-associated inflammation<sup>39,40</sup>.

The modulation of fiber-type specificity coupled with a balance towards slow-twitch oxidative fibers provides a synergic protective mechanism prompted by the cyanidin-enriched diet, triggering the endogenous anti-oxidant response.

The biological significance of our findings entails extensive therapeutic implication since it reveals how nutritional-based intervention, intended to mitigate the cross-talk between oxidative stress and inflammatory cues, hamper the progression of MD.

The current study identifies cyanidin as a first-in-class natural compound that alleviates the progression of a degenerative genetic disease upon dietary consumption, representing an adjuvant nutritional-based intervention for MDs. Based on its documented potential to hinder dystrophic signs even at the advanced stage, when patients become ineligible for primary interventions such as gene- or cell-based protocols, cyanidin dietary supplementation may restore muscle conditions amenable to definitive therapeutic treatments, raising the likelihood of successful outcomes.

While experimental interventions aimed to correct the genetic cause of MDs still represent the mainstay therapeutic option, our findings advocate that nutraceutical supplementation with cyanidin holds promise as an auxiliary strategy in humans to target the multiple metabolic abnormalities of MDs and maintain functional muscle mass, further warranting successful clinical perspectives to an extended cohort of dystrophic patients.

## Methods

### Maize production

Maize genotypes were originally in W22 background, homozygous dominant for the *a1*, *a2*, *c1*, *c2*, *bz1* and *bz2* genes, homozygous recessive for the *r1* gene and different *b1 pl1* constitution. To obtain cyanidin-rich and cyanidin-free corn with an isogenic background, a maize cyanidin-rich hybrid was used carrying the *B1* and *Pl1* alleles (Red diet, RD), which confer purple pigmentation in seed pericarp and all plant tissues<sup>41–44</sup>. Plant and seed tissues carrying *b1 pl1* alleles are cyanidin-free (Yellow diet, YD). To obtain ears with a high production of kernels, the homozygous inbred line *B1 Pl1* W22 and the *b1 pl1* W22 inbred line were crossed to a *b1 pl1* B73 inbred line and the F1 progeny seeds were used to produce two synthetic populations differing only in *b1 pl1* constitution<sup>21</sup>.

### Mouse model

All mice were kept in pathogen-free conditions with 12–12 h light-dark cycle. All the procedures on animals were conformed to Italian law (D. Lgs n 2014/26, implementation of the 2010/63/UE) and approved by the University of Milan Animal Welfare Body and by the Italian Ministry of Health. The genotyping strategies have been published in the animal reference. *Sgca* null mice were previously described in Duclos et al.<sup>22</sup> At 3 weeks of age, *Sgca* null mice were randomly divided into two groups: one fed with the control cyanidin-free diet (YD) and the other one fed with the cyanidin-enriched diet (RD). Diets were supplied ad libitum for 5 or 25 weeks. Both male and female mice were used indiscriminately. To check the effects of the cyanidin-enriched diet on mice in adulthood, we also supplied the diets in *Sgca* null animals at 5 weeks of age for 15 weeks.

### Haematoxylin and eosin and Milligan's trichrome

Haematoxylin and eosin staining was performed on 7  $\mu$ m-thick cryosections fixed with 4% paraformaldehyde for 10 min at 4 °C. The staining was performed according to standard protocols. For Milligan's trichrome staining, sections were fixed for 1 h with Bouin's fixative (Sigma-Aldrich) and rinsed for 1 h under running water. Sections were then rapidly dehydrated to 95% EtOH in graded ethanol solutions, successively passed in 3% potassium dichromate (Sigma-Aldrich) for 5 min, rapidly washed in distilled water, stained with 0.1% acid fuchsin (Sigma-Aldrich) for 30 s, washed again in distilled water, passed in 1% phosphomolybdic acid (Sigma-Aldrich) for 3 min, stained with Orange G (2% in 1% phosphomolybdic acid) (Sigma-Aldrich) for 5 min, rinsed in distilled water, passed in 1% acetic acid (VWR) for 2 min, stained with 1% Fast Green for 5 min (Sigma-Aldrich), passed in 1% acetic acid for 3 min, rapidly dehydrated to 100% EtOH and passed in Xylene before mounting with Eukitt (Bio-Optica).

### SDH staining

For SDH staining, freshly cut 7  $\mu$ m-thick cryosections of *Tibialis anterior* were used. Sections were incubated in SDH incubating solution (1 tablet of nitroblue tetrazolium dissolved in 0.1 M sodium succinate-0.1 M phosphate buffer pH7.4, all from Sigma-Aldrich) for 1 h at 37 °C, rinsed in distilled water, rapidly passed in 30%, 60%, 30% Acetone (VWR), and rinsed again in distilled water. Sections were then rapidly dehydrated in graded EtOH solutions, cleared in Xylene and mounted with Eukitt mounting medium.

### Treadmill test

For Treadmill test functional assay, 3-week-old *Sgca* null mice were fed for 5 weeks with RD or YD diet and WT with YD diet, as control. Mice were trained three times once a week before recording the performance.

Treadmill test was therefore performed starting from 8-week-old mice, once a week for 15 weeks. The test was conducted on a treadmill (Bioseb) with a 10% incline, starting from a speed of 6 cm/s and increasing it by 2 cm/s every 2 min. For each test, the time to exhaustion of each mouse was measured.

### Protein extraction and Western Blot

Western blot was performed on protein extracts from muscles homogenized in Tissue Buffer (150 mM Tris-HCl, pH 7.5; 1 mM EDTA, 1% Triton, 150 mM NaCl, all from Sigma-Aldrich) for 30 s, followed by lysis on ice for 30 min and by centrifugation at 10000 rpm at 4 °C to pellet cell debris. The supernatant was quantified using DC Protein Assay (Biorad), and 30–50  $\mu$ g of total protein extracts were loaded for each sample. Images were acquired using Chemidoc ImageLab software (Biorad). The following antibodies and dilutions were used: rabbit anti-VDAC1 (1:10,000, Cell Signaling), mouse anti-Vinculin (1:2500, Sigma-Aldrich).

### Protein carbonylation content (PCC)

The level of oxidative stress in quadriceps protein extracts was quantified by measuring protein carbonylation. Carbonyl groups were derivatized into their DNP adducts using 2,4-Dinitrophenylhydrazine (DNPH)<sup>25</sup>. Quadriceps muscles were homogenized in tissue buffer adding 1 mM DTT. After protein quantification 50  $\mu$ g of protein was derivatized with the same volume of DNPH (10 mM in 2 M HCl, Sigma-Aldrich) for 1 h in the dark at RT. Afterward, to precipitate carbonylated protein and stop the derivatization reaction a solution 30% of trichloroacetic acid (TCA, Sigma-Aldrich) was added and sample incubated for 15 min on ice. Then, samples were centrifuged at 15,000  $\times g$  for 15 min at 4 °C. After removing the supernatant, each pellet was washed three times with a solution of ethanol-ethyl acetate (1:1) to remove the excess of DNPH, then the pellet was solubilized in 1 mL of guanidine (6 M, Sigma-Aldrich) and incubated for 30 min at 37 °C. The content of carbonylated protein was measured by a spectrophotometer at 370 nm (Janway).

### Immunofluorescence

Immunofluorescence was performed on 7- $\mu$ m cryosections. Slices were fixed for 10 min at 4 °C with 4%PFA, washed twice in PBS and permeabilized with a solution containing 1%BSA (Sigma-Aldrich) and 0.2% Triton X-100 (Sigma-Aldrich) in PBS, for 30 min at room temperature. After blocking for 30 min with 10% donkey serum, slices were incubated O/N with primary antibodies in PBS-1.5% donkey serum. The day after, two washes in PBS-1%BSA-0.2%Triton X-100 were performed and samples were incubated for 45 min at room temperature with secondary antibodies and Hoechst (1:500, Sigma-

Aldrich). The excess of antibody was washed twice in PBS-0.2% Triton X-100 before mounting with Fluorescence Mounting Medium (Dako). The following antibodies and dilutions were used: goat anti-Collagen I (1:200, Southern Biotech), donkey anti-goat 488 (1:250, Jackson Lab).

F4/80 immunofluorescence was performed on cryosections of Tibialis Anterior. Samples were permeabilized for 10 min at RT in a solution of PBS-0.5% Triton X-100 (Sigma-Aldrich), then washed three times in PBS. After blocking for 30 min with a solution of PBS-3% BSA (Sigma-Aldrich), slices were washed twice with PBS and incubated O/N with primary antibodies anti-F4/80 (rat, 1:400, Novus) and anti-laminin (rabbit, 1:300 Sigma-Aldrich) in PBS. The day after, three washes in PBS were performed and samples were incubated for 45 min at room temperature with secondary antibodies and Hoechst (1:500, Sigma-Aldrich). The excess of antibody was washed five times in PBS before mounting with Fluorescence Mounting Medium (Dako). F4/80 positive cells were normalized on the total number of fibers in the picture.

For slow Myosin heavy chain (MyHC I) immunostaining, cryosections were retrieved in a Na-citrate solution (10 mM pH 6) for 30 min in a steamer machine. Once equilibrated the section at RT, slices were washed twice with PBS for 10 min and then incubated with the primary antibody mouse anti-MyHC I 1:1000 (Sigma-Aldrich) and rabbit anti-laminin 1:300 (Sigma-Aldrich) O/N at 4 °C. Fibers positive for MyHC I were normalized on the total number of myofibers.

#### Transmission electron microscopy (TEM)

For TEM, EDL muscles were dissected from sacrificed animals, pinned on a Sylgard dish, fixed at room temperature with 3.5% glutaraldehyde in 0.1 M NaCaCO buffer (pH 7.4), and stored in the fixative at 4 °C. Fixed muscles were then post-fixed in a mixture of 2% OsO<sub>4</sub> and 0.8% K<sub>3</sub>Fe(CN)<sub>6</sub> for 1–2 h, rinsed with 0.1 M sodium cacodylate buffer with 75 mM CaCl<sub>2</sub>, en-block stained with saturated uranyl acetate, and embedded for EM in epoxy resin (Epon 812) as in ref. <sup>45</sup>. Ultrathin sections (~40 nm) were cut in a Leica Ultracut R microtome (Leica Microsystem, Austria) using a Diatome diamond knife (Diatome Ltd. CH-2501 Biel, Switzerland) and examined at 60 kV after double- with uranyl acetate and lead citrate, with a FP 505 Morgagni Series 268D electron microscope (FEI Company, Brno, Czech Republic), equipped with Megaview III digital camera (Munster, Germany) and Soft Imaging System (Germany).

#### Macrophages isolation from skeletal muscle

Skeletal Muscles collected from hind limb were minced and digested enzymatically and mechanically in a single cell suspension with 0.2% of Collagenase B (Roche) in

RPMI medium (Lonza) for 1 h and 30 min in a water bath at 37 °C under agitation. After filtration with cell strainers (70 and 40 μm, Grainer) and centrifugation at 272 × *g* for 10 min at 4 °C, the single cell suspension was resuspended in sterile PBS-0.5% BSA (Genespin)-2 mM EDTA (Sigma-Aldrich) and incubated with anti-CD45 antibody conjugated with magnetic beads (Miltenyi Biotech) for 30 min at 4 °C. Cells were then washed with PBS-0.5% BSA (Genespin)-2 mM EDTA (Sigma-Aldrich) and CD45<sup>+</sup> cell isolation was performed by using magnetic columns (Miltenyi, Biotech) according to manufacturer instructions. After Fc blocking (Fc Buffer, Miltenyi Biotech), the fraction of CD45<sup>+</sup> cells was incubated with Ly6C-PE antibody (eBioscience), to discriminate pro-inflammatory (Ly6C<sup>+</sup>) from anti-inflammatory macrophages (Ly6C<sup>-</sup>), and with CD64-APC antibody (BD Bioscience) to discriminate neutrophils from macrophages. Cell sorting experiments were then performed using a FACSaria II (BD Bioscience). Diva software (BD Pharmingen, San Diego, CA) was used for data acquisition and analysis.

#### Image acquisition

Images were acquired with an inverted microscope (Leica-DMI6000B) equipped with Leica DFC365FX and DFC400 cameras. The Leica Application Suite software was used for acquisition while Photoshop was used to generate merged images.

#### Measurement of myofiber CSA and Collagen I quantification

Measurement myofiber CSA was performed on Tibialis Anterior muscle sections using Image J software. Collagen I quantification was performed using a Macro in ImageJ to identify and quantify Collagen I positive areas.

#### Statistics

All data shown in the graphs are expressed as mean ± SD, apart from graphs showing CSA distributions, which are expressed as mean ± whiskers from min to max. Statistical analysis between two columns was performed using two-tailed unpaired Student's *t*-test, whereas data containing more than two experimental groups were analyzed with one-way ANOVA followed by Bonferroni's test. \**P* < 0.05; \*\**P* < 0.01; \*\*\**P* < 0.001; confidence intervals 95%, alpha level 0.05.

#### Acknowledgements

We thank Pura Muñoz and Giuseppina Caretti for the kind exchange of information and helpful discussion. We are also grateful to Prof. Andrea Binelli and Dr. Camilla Della Torre for the technical assistance in the PCC assay. This work was funded by the European Community, ERC StG2011 to G.M. (RegenerationNfx 280611) and FP7 ATHENA to C.T. (Grant Agreement 245121).

#### Author contributions

M. Saclier and C.B. designed and performed all the experiments with the assistance of S.A. V.T., V.R., G.A., G. Mura, F.Z. C.T., and K.P. supplied the different

diets and participated to the development of the work. M. Sandri performed the TEM analysis. G. Messina supervised the work and wrote the paper together with M.C. All authors discussed the results and commented on the manuscript.

#### Conflict of interest

The authors declare that they have no conflict of interest.

#### Publisher's note

Springer Nature remains neutral with regard to jurisdictional claims in published maps and institutional affiliations.

**Supplementary Information** accompanies this paper at (<https://doi.org/10.1038/s41419-020-2332-4>).

Received: 19 November 2019 Revised: 3 February 2020 Accepted: 4 February 2020

Published online: 18 February 2020

#### References

- Mercuri, E. & Muntoni, F. Muscular dystrophy: new challenges and review of the current clinical trials. *Curr. Opin. Pediatrics* **25**, 701–707 (2013).
- Emery, A. E. H. Muscular dystrophy into the new millennium. *Neuromuscul. Disord.* **12**, 343–349 (2002).
- Konieczny, P., Swiderski, K. & Chamberlain, J. S. Gene and cell-mediated therapies for muscular dystrophy. *Muscle Nerve* **47**, 649–663 (2013).
- Gee, P., Xu, H. & Hotta, A. Cellular Reprogramming, Genome Editing, and Alternative CRISPR Cas9 Technologies for Precise Gene Therapy of Duchenne Muscular Dystrophy. *Stem Cells Int.* **2017**, 8765154 (2017).
- Cossu, G. & Sampaolesi, M. New therapies for Duchenne muscular dystrophy: challenges, prospects and clinical trials. *Trends Mol. Med.* **13**, 520–526 (2007).
- Rando, T. A. Oxidative stress and the pathogenesis of muscular dystrophies. *Am. J. Phys. Med. Rehabilitation* **81**, S175–S186 (2002).
- Rando, Ta, Disatnik, M. H., Yu, Y. & Franco, a Muscle cells from mdx mice have an increased susceptibility to oxidative stress. *Neuromuscul. Disord.* **8**, 14–21 (1998).
- Hori, Y. S. et al. Resveratrol ameliorates muscular pathology in the dystrophic mdx mouse, a model for Duchenne muscular dystrophy. *J. Pharmacol. Exp. Ther.* **338**, 784–794 (2011).
- Kuno, A. et al. Resveratrol improves cardiomyopathy in dystrophin-deficient mice through sirt1 protein-mediated modulation of p300 protein. *J. Biol. Chem.* **288**, 5963–5972 (2013).
- Bhuiyan, M. I. H., Kim, J. Y., Ha, T. J., Kim, S. Y. & Cho, K. O. Anthocyanins extracted from black soybean seed coat protect primary cortical neurons against in vitro ischemia. *Biol. Pharm. Bull.* **35**, 999–1008 (2012).
- Ji, L. L. Modulation of skeletal muscle antioxidant defense by exercise: role of redox signaling. *Free Radic. Biol. Med.* **44**, 142–152 (2008).
- Perveen, S., Yang, J. S., Ha, T. J. & Yoon, S. H. Cyanidin-3-glucoside inhibits ATP-induced intracellular free Ca concentration, ROS formation and mitochondrial depolarization in PC12 cells. *Korean J. Physiol. Pharmacol.* **18**, 297–305 (2014).
- Sun, C. C. et al. Sulforaphane attenuates muscle inflammation in dystrophin-deficient mdx mice via NF-E2-related factor 2 (Nrf2)-mediated inhibition of NF- $\kappa$ B signaling pathway. *J. Biol. Chem.* **290**, 17784–17795 (2015).
- Haycock, J. W., Mac Neil, S. & Mantle, D. Differential protein oxidation in Duchenne and Becker muscular dystrophy. *Neuroreport* **9**, 2201–2207 (1998).
- Jackman, R. W., Cornwell, E. W., Wu, C. L. & Kandarian, S. C. Nuclear factor- $\kappa$ B signalling and transcriptional regulation in skeletal muscle atrophy. *Exp. Physiol.* **98**, 19–24 (2013).
- Pojer, E., Mattivi, F., Johnson, D. & Stockley, C. S. The case for anthocyanin consumption to promote human health: a review. *Compr. Rev. Food Sci. Food Saf.* **12**, 483–508 (2013).
- Wallace, T. C. & Giusti, M. M. Anthocyanins in health and disease. *Anthocyanins Health Dis.* <https://doi.org/10.1201/b15554> (2013).
- Tsuda, T. Dietary anthocyanin-rich plants: biochemical basis and recent progress in health benefits studies. *Mol. Nutr. Food Res.* **56**, 159–170 (2012).
- Pedreschi, R. & Cisneros-Zevallos, L. Phenolic profiles of Andean purple corn (*Zea mays* L.). *Food Chem.* **100**, 956–963 (2007).
- Toufeksian, M.-C. et al. Chronic dietary intake of plant-derived anthocyanins protects the rat heart against ischemia-reperfusion injury. *J. Nutr.* **138**, 747–752 (2008).
- Petroni, K. et al. Dietary cyanidin 3-glucoside from purple corn ameliorates doxorubicin-induced cardiotoxicity in mice. *Nutr. Metab. Cardiovasc. Dis.* **27**, 462–469 (2017).
- Duclos, F. et al. Progressive muscular dystrophy in alpha-sarcoglycan-deficient mice. *J. Cell Biol.* **142**, 1461–1471 (1998).
- Zanotti, S. et al. Anti-fibrotic effect of pirfenidone in muscle derived-fibroblasts from Duchenne muscular dystrophy patients. *Life Sci.* **145**, 127–136 (2016).
- Webster, C., Silberstein, L., Hays, A. P. & Blau, H. M. Fast muscle fibers are preferentially affected in Duchenne muscular dystrophy. *Cell* **52**, 503–513 (1988).
- Mecocci, P. et al. Oxidative damage to DNA in lymphocytes from AD patients. *Neurology* **51**, 1014–1017 (1998).
- Marin-Corral, J. et al. Redox balance and cellular inflammation in the diaphragm, limb muscles, and lungs of mechanically ventilated rats. *Anesthesiology* **112**, 384–394 (2010).
- Schiaffino, S. & Reggiani, C. Fiber types in mammalian skeletal muscles. *Physiol. Rev.* **91**, 1447–1531 (2011).
- Danieli-Betto, D. et al. Deficiency of alpha-sarcoglycan differently affects fast- and slow-twitch skeletal muscles. *Am. J. Physiol. Regul. Integr. Comp. Physiol.* **289**, R1328–R1337 (2005).
- Vila, M. C. et al. Mitochondria mediate cell membrane repair and contribute to Duchenne muscular dystrophy. *Cell Death Differ.* **24**, 330–342 (2017).
- Romanello, V. & Sandri, M. Mitochondrial quality control and muscle mass maintenance. *Front. Physiol.* **6**, 422 (2016).
- Bedard, K. & Krause, K. H. The NOX family of ROS-generating NADPH oxidases: physiology and pathophysiology. *Physiol. Rev.* **87**, 245–313 (2007).
- Speciale, A., Cimino, F., Saija, A., Canali, R. & Virgili, F. Bioavailability and molecular activities of anthocyanins as modulators of endothelial function. *Genes Nutr.* **9**, 404 (2014).
- Banfi, S. et al. Supplementation with a selective amino acid formula ameliorates muscular dystrophy in mdx mice. *Sci. Rep.* **8**, 14659 (2018).
- Rossi, G. et al. Silencing Nfix rescues muscular dystrophy by delaying muscle regeneration. *Nat. Commun.* **8**, 1055 (2017).
- Wehling, M., Spencer, M. J. & Tidball, J. G. A nitric oxide synthase transgene ameliorates muscular dystrophy in mdx mice. *J. Cell Biol.* **155**, 123–131 (2001).
- He, J. & Giusti, M. M. Anthocyanins: natural colorants with health-promoting properties. *Annu. Rev. Food Sci. Technol.* **1**, 163–187 (2010).
- Martin, M. A. et al. Protection of human HepG2 cells against oxidative stress by the flavonoid epicatechin. *Phyther. Res.* **24**, 503–509 (2010).
- Cerletti, C. et al. Dietary anthocyanins and health: data from FLORA and ATHENA EU projects. *Br. J. Clin. Pharmacol.* **83**, 103–106 (2017).
- Magni, G. et al. Purple corn extract as anti-allodynic treatment for trigeminal pain: role of microglia. *Front. Cell. Neurosci.* **12**, 378 (2018).
- Tomay, F. et al. Purple corn extract induces long-lasting reprogramming and M2 phenotypic switch of adipose tissue macrophages in obese mice. *J. Transl. Med.* **17**, 237 (2019).
- Radicella, J. P., Brown, D., Tolar, L. A. & Chandler, V. L. Allelic diversity of the maize B regulatory gene: different leader and promoter sequences of two B alleles determine distinct tissue specificities of anthocyanin production. *Genes Dev.* **6**, 2152–2164 (1992).
- Pilu, R. et al. pH-bol3, a complex allele of the anthocyanin regulatory pl1 locus that arose in a naturally occurring maize population. *Plant J.* **36**, 510–521 (2003).
- Pilu, R., Cassani, E., Sirizzotti, A., Petroni, K. & Tonelli, C. Effect of flavonoid pigments on the accumulation of fumonisin B1 in the maize kernel. *J. Appl. Genet.* **52**, 145–152 (2011).
- Petroni, K. & Tonelli, C. Recent advances on the regulation of anthocyanin synthesis in reproductive organs. *Plant Sci.* **181**, 219–229 (2011).
- Mammucari, C. et al. FoxO3 controls autophagy in skeletal muscle in vivo. *Cell Metab.* **6**, 458–471 (2007).